UNIVERSIDAD DE CHILE
Facultad de Medicina
Escuela de Postgrado
Programa de Grados Académicos

"Role of collagen chaperone HSP47 on the activation of endoplasmic reticulum stress sensor IRE1α"

Denisse Sepúlveda Alvarado

THESIS TO OBTAIN THE DEGREE OF
DOCTOR IN BIOMEDICAL SCIENCES

Thesis Director: Prof. Dr. Claudio Hetz
Thesis Co-Director: Dr. Diego Rojas Rivera

2018

UNIVERSIDAD DE CHILE

FACULTAD DE MEDICINA

ESCUELA DE POSTGRADO

INFORME DE APROBACION TESIS DE

DOCTORADO EN CIENCIAS BIOMEDICAS

Se informa a la Comisión de Grados Académicos de la Facultad de Medicina, que la Tesis de Doctorado en Ciencias Biomédicas presentada por la candidata

DENISSE SEPULVEDA ALVARADO

ha sido aprobada por la Comisión Informante de Tesis como requisito para optar al Grado de **Doctor en Ciencias Biomédicas** en Examen de Defensa de Tesis rendido el día 10 de enero de 2018.

Prof. Dr. Claudio Hetz
Director de Tesis
Laboratorio de estrés celular y biomedicina, Facultad de Medicina, Universidad de Chile

COMISION INFORMANTE DE TESIS

PROF. DRA. JIMENA SIERRALTA **PROF. DR. MARIO CHIONG**

PROF. DR. MAURICIO HENRÍQUEZ

Presidente Comisión de Examen

A mis padres Silvia y Danilo por permitir mi desarrollo en absoluta libertad,

a mis hermanas Melissa y Belén por acompañar e iluminar mi vida.

AGRADECIMIENTOS

Quiero agradecer en primer lugar a todos los miembro del Laboratorio liderado por mi tutor Dr. Claudio Hetz de la Facultad de Medicina de la Universidad de Chile, técnicos, administrativos, estudiantes e investigadores. En particular, a quienes comenzaron el proyecto interactoma Dr. Diego Rodríguez y Dr. Diego Rojas y a quienes me acompañaron científica y personalmente en este proceso, mi *team UPR*: Dr. Hery Urra, Dra. Estefanie Dufey, Dr.Philippe Pihán y Dr. Amado Carreras.

Agradezco a la comisión evaluadora: Dra. Jimena Sierralta, Dr. Mauricio Henríquez y Dr. Mario Chiong, por participar activa y constructivamente en el desarrollo de esta tesis doctoral.

Mis profundos agradecimientos a Cecilia Carter, secretaría del programa de doctorado en Ciencias Biomédicas, quien con su profesionalismo y carisma me apoyó en innumerables instancias.

Agradezco a todos los colaboradores de la publicación que esta tesis doctoral generó, en particular al Laboratorio de Dr. Kazuhiro Nagata por permitirme realizar una inolvidable estadía en la Universidad de Kyoto, Japón.

Finalmente, agradezco el financiamiento otorgado por Conicyt: Beca Doctorado Nacional, Beca Gastos operacionales y Beca Estadías en el extranjero, que permitió la realización de esta investigación.

1. INDEX.

2. TABLE OF FIGURES.

3. ABBREVIATIONS.

ATF4 : Activating Transcription Factor 4
ATF6 : Activating transcription factor 6
BAK : Bcl-2 homologous antagonist killer
BAX : Bcl-2-associated X
BI-1 : BAX inhibitor-1
BiP : Immunoglobulin binding protein
Blocs1: Biogenesis of lysosome-related organelles complex 1
BSA : Bovine serum albumin
bZIP : Basic Leucine Zipper Domain
CDA : Confined displacement analysis
cDNA : Complementary Deoxyribonucleic acid
CHOP: C/EBP-homologous protein
eIF2α : Eukaryotic Initiation Factor 2
ER : Endoplasmic reticulum
ERAD: ER-associated degradation
Erdj4 : Endoplasmic reticulum-localized DnaJ homologues 4
Erp57 : Endoplasmic reticulum protein 57
FBS : Fetal bovine serum
GFP : Green fluorescent protein
Grp94: Glucose-regulated protein 94
HEK : Human embryonic kidney
HPS47: Heat shock protein 47
HSP72: Heat shock protein 72
HSP90: Heat shock protein 90
Ig : Immunoglobulin
IP : Immunoprecipitation
IRE1α: Inositol-requiring enzyme 1
JNK : c-Jun N-terminal protein kinases
MEF : Mouse embryonic fibroblast
mRNAs: Messenger Ribonucleic acid
NF-κB: Nuclear factor kappa-light-chain-enhancer of activated B cells
PDI : Protein disulfide isomerase
PDIA6: Protein disulfide isomerase 6
PERK: Protein kinase RNA-like ER kinase
PP2A : Protein phosphatase 2A
RIDD : Regulated IRE1-dependent decay
S1P : Site 1 proteases
S2P : Site 2 proteases

sec61 :	Protein transport protein Sec61 subunit alpha isoform 1
shRNA:	Short hairpin Ribonucleic acid
siRNA :	Small interfering RNA
SPARC:	Secreted protein acidic and rich in cysteine
Tg :	Thapsigargin
Tm :	Tunicamycin
TRAF2:	TNF receptor-associated factor 2
UPR :	Unfolded Protein Response
WT :	Wild Type
XBP1 :	X-Box binding protein-1

4. RESUMEN.

Alteraciones en la homeostasis del retículo endoplasmático (RE) promueven la acumulación de proteínas mal plegadas en su lumen, una condición celular denominada estrés de RE. La adaptación al estrés de RE depende de la activación de la respuesta a proteínas mal plegadas (UPR: del inglés *unfolded protein response*). El sensor de estrés de RE, IRE1α, es una proteína transmembrana con actividad kinasa y endoribonucleasa. Bajo condiciones de estrés de RE, IRE1α promueve el procesamiento no convencional del ARNm de *Xbp1*, generando la expresión del factor de transcripción XBP1s, el cual regula la expresión de genes involucrados en el plegamiento proteico, secreción, control de calidad de proteínas, entre muchas otras funciones. Adicionalmente, bajo condiciones de estrés de RE, IRE1α degrada varios ARNms mediante un proceso conocido como decaimiento de RNA dependiente de IRE1α (RIDD: del inglés *regulated IRE1α -dependent RNA decay*). En ciertos sistemas bajo estrés de RE prolongado, la activación sostenida de IRE1α puede promover apoptosis en las células dañadas irreversiblemente. Por lo tanto, IRE1α controla la sobrevida celular bajo estrés de RE regulando el equilibrio entre señales adaptativas y pro-apoptóticas.

Los mecanismos subyacentes a la activación e inactivación de IRE1α no se conocen completamente, sin embargo, se ha descrito que IRE1α es regulado por la interacción con proteínas que modulan la amplitud de la actividad de IRE1α, a través de una plataforma de señalización conocida como UPRosoma. En nuestro laboratorio se realizaron estudios proteómicos con el objetivo de identificar nuevos componentes del UPRosoma en condiciones de estrés de RE. Mediante inmunoprecipitación de proteínas y espectrometría de masas se identificaron cuatro posibles reguladores de IRE1α que podrían modular su actividad RNasa. Usando esta aproximación experimental, se identificó a HSP47 como un putativo activador y regulador de la vía de señalización IRE1α/XBP1s. HSP47 es una

chaperona específica involucrada en el plegamiento de colágeno y se distribuye principalmente en el lumen del RE.

En esta tesis, nos propusimos estudiar el posible papel de HSP47 en la regulación de la actividad IRE1α. Específicamente, se evaluó el efecto de HSP47 en la activación de la vía de señalización IRE1α bajo condiciones de estrés ER, evaluando la cinética y amplitud de las respuestas de la vía IRE1α.

La caracterización celular y bioquímica utilizando estrategias de pérdida y ganancia de función, reveló que la expresión de HSP47 promueve la señalización de IRE1α. A nivel molecular, Hsp47 se une con alta afinidad al dominio luminal de IRE1α, desplazando al regulador negativo BiP del complejo y facilitando su activación. La regulación de la señalización de IRE1α mediante HSP47 es conservada en la evolución, ya que mediante la manipulación genética, se validaron estos hallazgos en modelos de mosca y ratón. HSP47 opera como un modulador positivo de la señalización de IRE1α, regulando el umbral de activación de la UPR en la sobrevida. En términos generales, los resultados de esta tesis demuestran una nueva función biológica de HSP47 como un componente de la UPR, lo que sugiere que la red de plegamiento en el RE integra la información sobre el estado de plegamiento de las proteínas para establecer un umbral de activación de la vía de IRE1α en la UPR. Considerando la complejidad de la vía IRE1α/XBP1s/RIDD en la sobrevida celular, es fundamental identificar los mecanismos moleculares implicados en la regulación de esta vía en condiciones de estrés RE.

5. ABSTRACT.

Alterations in the endoplasmic reticulum (ER) homeostasis results in the accumulation of misfolded/unfolded proteins in its lumen, a cellular condition referred to as ER stress. Adaptation to ER stress depends on the activation of the unfolded protein response (UPR). The ER stress sensor and UPR transducer inositol-requiring enzyme 1α (IRE1α) is a bifunctional kinase and endoribonuclease enzyme that upon activation catalyzes the unconventional splicing of the mRNA encoding the transcription factor X-box-binding protein 1 (XBP1). XBP1 spliced (XBP1s) mediates the upregulation of crucial UPR-related genes involved in folding, secretion and protein quality control, among other functions. In addition, under ER stress conditions, IRE1α degrades a subset of mRNAs through a process known as regulated IRE1α-dependent RNA decay (RIDD). Under prolonged ER stress, sustained activation of IRE1α, sensitizing irreversible damaged cells to undergo apoptosis. Therefore IRE1α controls cell fate under ER stress triggering adaptive and pro-apoptotic signals.

The mechanisms underlying IRE1α activation/inactivation are not fully understood, but it has been described that IRE1α is regulated by several proteins that interact and modulate the amplitude of IRE1α´s activity through a signaling platform known as the UPRosome. Proteomic studies were conducted in our lab in order to identify new components of the UPRosome coupled to IRE1α in ER stress conditions. Co-immunoprecipitation followed by mass spectrometry analysis was performed and four putative IRE1α regulators that could modulate the amplitude and kinetics of IRE1α RNAse activity on XBP1 were discovered. Through this analysis, we identified heat shock protein 47 (HSP47) as a putative activator of IRE1α/XBP1s signaling pathway. HSP47 is a specific chaperone involved in collagen folding located in the ER lumen.

In this thesis, we proposed to study the possible role of HSP47 in the regulation of IRE1α activity. Specifically, we studied the role of HSP47 on the activation of the IRE1α signaling pathway under ER stress.

Cellular and biochemical characterization, using gain and lose-function strategies, revealed that Hsp47 expression instigates IRE1α signaling. At the molecular level, Hsp47 directly binds with high affinity to the ER luminal domain of IRE1α, displacing the negative regulator BiP from the complex to facilitate its activation. The regulation of IRE1α signaling by Hsp47 is conserved in evolution, as validated using genetic manipulation in fly and mouse models. We conclude that Hsp47 operates as an adjustor IRE1α signaling, fine-tuning the threshold to engage an adaptive UPR. Overall, our results have uncovered a novel biological function of HSP47 as an adjustor of the UPR, suggesting that the ER folding network integrates information about the protein folding status at the ER to set the threshold for IRE1α activation. Considering the participation of the IRE1α axis on cell fate, it is crucial to identify the molecular mechanisms involved in the regulation of this pathway under ER stress conditions.

6. INTRODUCTION.

6.1 Endoplasmic reticulum homeostasis.

The maintenance of protein homeostasis or proteostasis is essential to sustain cell viability and function. In eukaryotic cells, protein folding and maturation occurs in the lumen of the endoplasmic reticulum (ER) and Golgi apparatus. Secretory proteins are synthesized by ribosomes attached to the ER membrane and then folded and modified by a large spectrum of chaperones and foldases. The ER is the main subcellular compartment involved in synthesis and folding of proteins that traffic through the secretory pathway [1].This cellular compartment maintains a reduced environment to facilitate the formation of disulfide bonds and protein complexes, in addition to mediate protein glycosylation [2]. Proteins correctly folded in the ER exit and traffic through the secretory pathway to their final destination at the extracellular matrix or plasma membrane. The rate of protein synthesis, folding and trafficking is regulated by an efficient “quality control mechanism” named calnexin-calreticulin cycle to ensure the correct folding of proteins before exit the ER [3]. If proteins are not properly folded, misfolded proteins are retained at the ER and then delivered to the cytosol for proteasomal degradation through the ER-associated degradation (ERAD) system [4].

Different physiological and pathological conditions can alter ER function and lead to the accumulation of unfolded or misfolded proteins in its lumen, altering global proteostasis, a cellular condition referred to as ‘‘ER stress” [5]. These alterations include the expression of disease-related mutant proteins, high secretory demands in the endocrine and exocrine cells, viral infection that overloads the ER with viral-encoded proteins, loss of calcium homeostasis that affects calcium-dependent chaperones, among others [6].

Upon ER stress, an adaptive mechanism is triggered to cope with unfolded proteins and restore ER homeostasis, known as the unfolded protein response

(UPR) [7]. The UPR transmits the information about the protein folding status in the ER lumen to the cytosol and nucleus to engage an adaptive response [6]. Initially, UPR signaling increases the biogenesis of the ER and Golgi apparatus thus enhancing the folding and quality control mechanisms and blocking protein translation. Conversely, if ER stress is chronic, the UPR signals through several mechanisms to promote cell death [8]. Thus, the UPR integrates the information regarding the duration and intensity of stress stimuli toward defining cell fate decisions to survive or enter into an apoptotic program [9].

6.2 Unfolded Protein Response.

In mammals, the ER stress is detected by at least three sensors located at the ER membrane, including protein kinase RNA-like ER kinase (PERK), activating transcription factor 6 α and β (ATF6), and inositol-requiring transmembrane kinase/endonucleases enzyme 1α and β (IRE1α and β) (Fig. 1) [7]. PERK is a type I transmembrane protein containing a luminal N-terminal domain involved in sensing misfolded protein status and a cytosolic C-terminal kinase domain. Upon ER stress, PERK activation occurs through a mechanism involving its dimerization/oligomerization and auto-transphosphorylation [10]. Activated PERK phosphorylates the eukaryotic translation initiation factor 2α (eIF2α) inhibiting global protein translation in order to reduce protein synthesis and decrease protein overload [11]. In addition, the phosphorylation of eIF2α selectively induces the translation of specific mRNAs containing short open reading frames in their 5′-untranslated regions such as the ATF4 mRNA. The induction of the transcription factor ATF4 upregulates the expression of genes involved in amino acid metabolism, antioxidant response, protein folding and the activation of apoptosis [12-14].

ATF6 is a type II glycoprotein that contains a single transmembrane domain. Under ER stress conditions, ATF6 translocates to the Golgi apparatus where it is processed by site-1 and site-2 proteases, releasing a cytosolic fragment of the

protein, named ATF6f [15-17]. ATF6f acts as a transcription factor regulating the expression of genes involved in ERAD and protein folding at the ER [15, 18].

Finally, the third UPR pathway, initiated by IRE1α is the most conserved branch of the UPR from yeast to higher eukaryotes [19]. IRE1α is formed by a luminal N-terminal domain that detect the misfolded proteins and a C-terminal domain that contains two enzymatic activities: serine/threonine protein kinase [20] and endoribonuclease (RNAse) [21]. Under ER stress conditions IRE1α dimerizes/oligomerizes and auto-transphosphorylates, leading to a conformational change that activates its RNAse domain [22-25]. Active IRE1α catalyzes the unconventional processing of the mRNA encoding the transcription factor X-Box binding protein-1 (XBP1), excising a 26-nucleotide intron that shifts the coding reading frame of its mRNA generating an active and stable transcription factor termed XBP1s [21, 26, 27]. XBP1s modulates the expression of genes involved in protein folding, ERAD, protein quality control and phospholipid synthesis [26, 28]. In summary, the UPR is a complex and dynamic signal transduction network that mediates the adaptation to ER stress or ultimately leads to cell death.

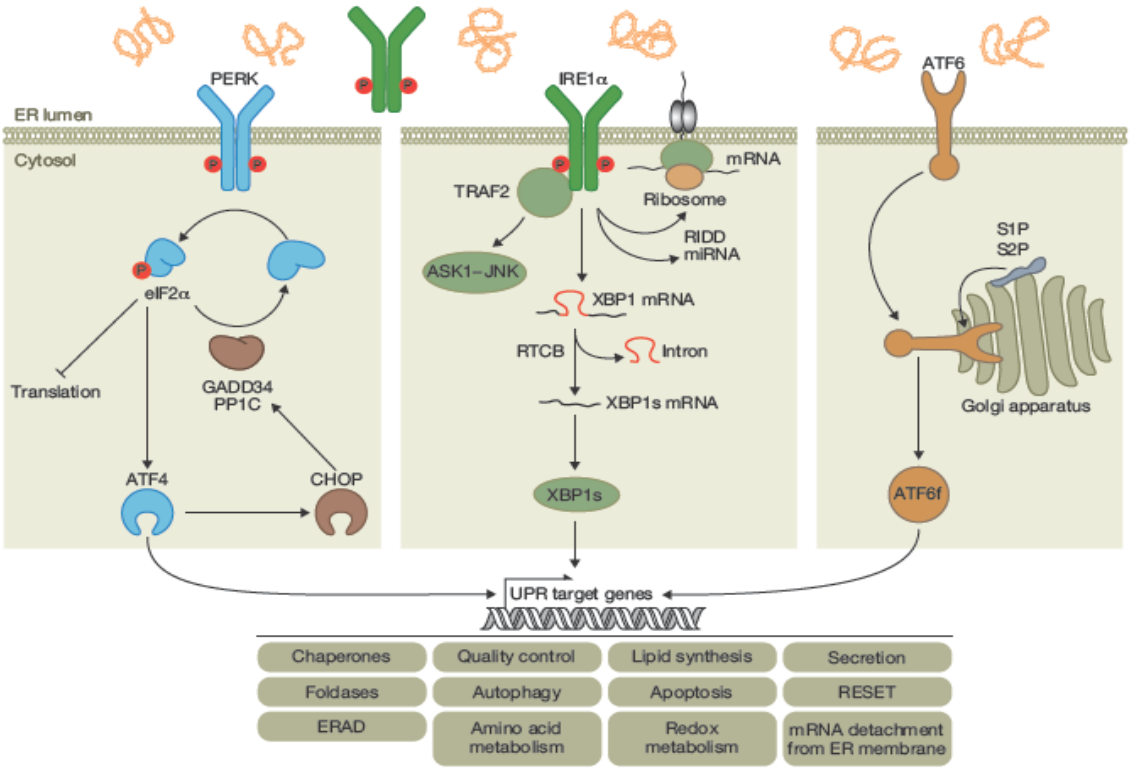

Modified from Hetz C, Chevet E. (2015) Nat Cell Biol

Figure 1. The three arms of unfolded protein response (UPR) in mammals. All three ER stress sensors (PERK, IRE1α, ATF6) are present in the ER membrane and initially activate signalling events that increase protein-folding capacity and reduce protein load on the ER. These transcriptional and translational outputs tend to re-establish protein-folding homeostasis in the ER and promote cell survival. **PERK** phosphorylates eIF2α, which in turn shuts down global translation and concomitantly increases the expression of the transcription factor ATF4. The latter induces the transcription of select genes whose functions are to restore proteostasis and of CHOP, itself inducing the transcription of GADD34, a regulatory subunit of PP1C. This creates a feedback mechanism leading to the dephosphorylation of eIF2α and translation is reinitiated. **IRE1α** signals through (i) the recruitment of TRAF2 leading the activation of the ASK1–JNK cascade and (ii) through its RNase via the splicing of *Xbp1* mRNA or the degradation of RNAs (RIDD activity), thereby regulating gene expression at transcriptional and post-transcriptional levels. Finally, following ER stress, **ATF6** is exported from the ER to the Golgi complex where it is cleaved by the proteases S1P and S2P, releasing its cytosolic domain which is a potent transcription factor. Together, UPR transcription factors determine cell fate by the regulation of distinct subsets of target genes toward recovery of ER homeostasis or the induction of apoptosis. The grey boxes illustrate the different functions of genes induced by the ER stress response.

6.3 IRE1α signaling.

As described above, the classic substrate for IRE1α RNAse activity is *Xbp*1 mRNA. However, IRE1α also degrades selected mRNAs and microRNAs through its RNAse activity, a phenomena known as Regulated IRE1α-Dependent RNA Decay (RIDD) [29] (Fig. 2). RIDD activity gradually increases with the intensity of ER stress [30] and this process depends on specific sequences contained in the target mRNAs [31]. The RIDD process is a conserved mechanism observed in mammals, yeast and plants [30, 32, 33]. Usually, the targets of RIDD are upregulated when IRE1α expression is decreased, even in absence of ER stress, suggesting a physiological role for this phenomenon [34-37]. Recent screening studies have demonstrated that the spectrum of mRNAs that are targets of RIDD involve mRNAs encoding for proteins localized in the nucleus and cytosol, microRNAs and ribosomal RNAs having an immediate impact on RNA stability and protein translation [38-40]. In addition, a recent report suggested that IRE1α dimers are optimal for RIDD activity, whereas larger oligomers are optimal for *Xbp1* mRNA splicing [41]. Conversely, other studies claim IRE1α oligomerization determines RIDD and cell death [29], therefore the molecular mechanism and physiological role of RIDD is still poorly understood. Despite these discrepancies, IRE1α and RIDD have been involved in several physiological processes such as the degradation of certain microRNAs linked to the regulation of apoptosis, cell migration, energy metabolism and inflammation [29, 39].

In addition to the RNAse activity, IRE1α can also control distinct signaling events that crosstalk with other classical stress pathways, such us the MAPK pathway. The cytosolic domain of IRE1α binds the adapter protein TNF receptor-associated factor 2 (TRAF2), promoting the activation of apoptosis-signal-regulating kinase 1 (ASK1) and the c-Jun-N-terminal kinase (JNK) pathways leading to cell death [42, 43]. In addition, IRE1α also modulates the activation of others "alarm pathways" including p38, ERK [44] and NF-kB [45]. In general, these signaling events are independent of XBP1 and have an impact on a wide range of

physiological processes, including apoptosis, autophagy, proliferation, metabolism, inflammation, among others.

Although irreversible ER stress triggers an apoptosis program involving a network of interrelated pathways [46], the mechanisms determining the transition from prosurvival to terminal UPR remains poorly defined. Sustained ER stress attenuates IRE1α signaling, ablating the adaptive activity of XBP1, which sensitizes cells to cell death [47, 48]. Moreover, in certain experimental systems overactivation of IRE1α results in apoptosis possibly mediated by changes in its oligomerization state and RIDD activity [49-52]. Thus, IRE1α is a central cell fate controller under ER stress, integrating signals about the intensity and duration of the insult, involving multiple checkpoints and setting up the threshold to induce an adaptive UPR or transit into a terminal proapoptotic program when ER proteostasis is irreversible altered (Fig. 3).

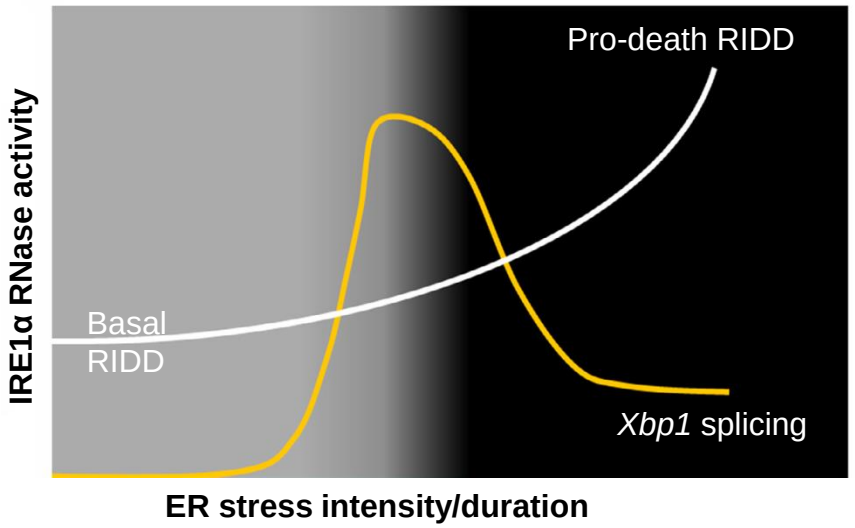

Maurel M (2014). Trends Biochem Sci

Figure 2. Schematic model of IREα RNAse activity. Representation of IRE1α- dependent decay of mRNA (RIDD) and *Xbp1* mRNA splicing activity under increasing ER stress intensity and/or duration. RIDD is constitutively active and its activity increases progressively with ER stress intensity and/or duration, leading to cell death, whereas *Xbp1* mRNA splicing is activated transiently on ER stress only during the adaptive/prosurvival phase.

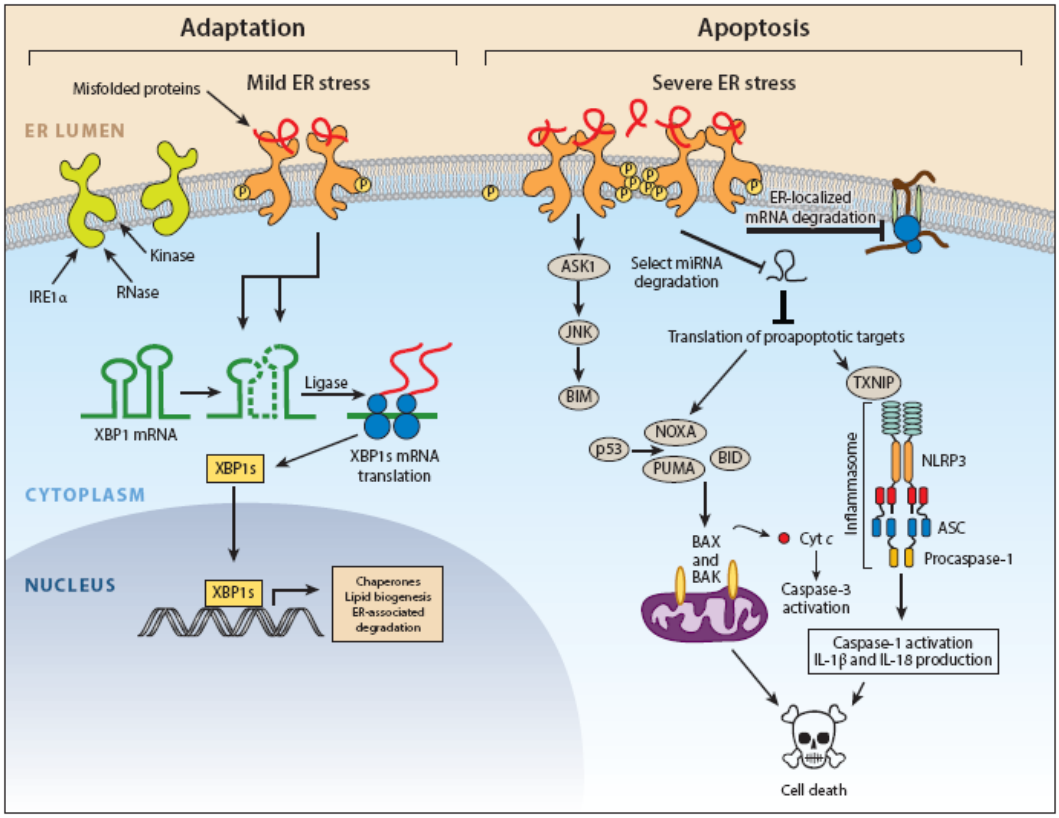

Oakes S., Papa F. (2015) Ann Rev Pathol Mech Dis

Figure 3. IRE1α activation and signaling on unfolded protein response.IRE1α is an endoplasmic reticulum (ER) transmembrane protein that becomes activated when misfolded proteins in the ER lumen bind to its luminal domains. The cytoplasmic tail of IRE1α has two enzymatic activities -serine/threonine kinase domain and an endoribonuclease (RNase) domain. Upon luminal binding of misfolded proteins, IRE1α's kinase becomes activated and *trans*-autophosphorylates multiple serine/threonine residues on the cytosolic tail. IRE1α phosphorylation leads to allosteric activation of the adjacent RNase. The consequences of IRE1α activation vary depending on the level of ER stress. In response to low levels of ER stress, IRE1α's RNase excises a 26-nt intron from the mRNA encoding the XBP1 (X-box protein 1) transcription factor to produce the homeostatic transcription factor XBP1s. XBP1s then translocates to the nucleus and induces transcription of many genes that augment ER size and function in an attempt to restore ER homeostasis. However, if ER stress is irremediable, IRE1α becomes hyperactivated and undergoes homo-oligomerization. Under sustained oligomerization, IRE1α's Rnase endonucleolytically degrades hundreds of ER-localized mRNAs containing an N-terminal signal sequence, which depletes ER cargo and protein-folding components to further worsen ER stress. Moreover, when hyperactivated, IRE1α's RNase directly cleaves select microRNAs that normally repress proapoptotic targets. In addition to signaling through RNA substrates, IRE1α oligomerization has been shown to induce activation or upregulation of a number of proinflammatory proteins, including the pro-oxidant protein TXNIP (thioredoxin-interacting protein), to activate the inflammasome and its Caspase-1-dependent prodeath pathway. Finally, sustained IRE1α oligomerization serves as an activation platform for ASK1 (apoptosis signal–regulating kinase) and its downstream target JNK (c-Jun NH2-terminal kinase). Phosphorylation by JNK has been reported to both activate proapoptotic BIM and inhibit antiapoptotic BCL-2. Once activated, BH3-only proteins such as BID and BIM disable mitochondrial protecting proteins (e.g., BCL-2, BCL-XL, MCL-1) and in some cases directly trigger the multidomain proapoptotic BAX and BAK proteins to permeabilize the outer mitochondrial membrane and release toxic mitochondrial proteins, such as cytochrome *c* (Cyt *c*), into the cytoplasm, where they lead to activation of downstream effector caspases (e.g., Caspase-3) and cell demise.

6.4 IRE1α regulation and the UPRosome.

The mechanism of activation of IRE1α has been primarily studied in yeast [53]. This model suggested that the binding of binding immunoglobulin protein (BiP), an ER-resident chaperone, to IRE1α retains the sensor in a monomeric and inactive state, thereby preventing its activation. Upon ER stress, BiP preferentially interacts with unfolded proteins, releasing its association with IRE1α luminal domain, enabling its dimerization [6, 22, 53, 54]. In this model, BiP is the actual sensor because of its ability to detect misfolded proteins, whereas IRE1α operates as a signal transducer protein. However, it has been proposed that a conserved region of luminal domain (cLD) of yeast IRE1p directly binds unfolded proteins [55]. The dimerization of cLD monomers creates a shared central groove that reminisces of the peptide binding domains of major histocompatibility complexes in its gross architecture [55]. Conserved amino acid side chains in IRE1p that face into the groove are shown to be important for UPR activation in that their mutation reduces the response in yeast [55]. In this model BiP binding to IRE1α would serve to desensitize IRE1α to low levels of stress and promotes its deactivation when favorable folding conditions are restored in the ER. BiP achieves these functions by sequestering inactive IRE1α molecules, thereby providing a barrier to oligomerization and activation [56]. Based on the previously studies, the luminal domain of yeast IRE1p senses the unfolded proteins via a two-step mechanism, namely dissociation of BiP and direct interaction with unfolded proteins. However, it has been unclear whether a similar mechanism is applicable to mammalian IRE1α since the same residues important in yeast to bind peptides are buried in mammals or not observed [57]. Evidence suggests that in contrast to yeast IRE1p, the regulation of mammalian IRE1α strongly depends on the dissociation of BiP [58]. Conversely, IRE1α is proposed to exist in three pools in dynamic equilibrium: i) a latent pool complexed with BiP, ii) a free inactive pool and iii) an active multimeric pool bound to unfolded luminal proteins [56]. Unfolded proteins in the ER lumen affect the equilibrium by pulling inactive IRE1α monomers into the active complex and competing with IRE1α for BiP. When the levels of unfolded proteins are low,

BiP sequesters IRE1α in an inactive complex, buffering the effects of small fluctuations in unfolded protein load [59]. More recently, a noncanonical interaction has been identified between the ATPase domain of BiP and the luminal domains of the UPR sensors IRE1α and PERK that dissociates when unfolded protein bind to the canonical substrate binding domain of BiP. Therefore, BiP has dual functions in the UPR, sensing unfolded proteins by canonical binding to substrates and transducing this event to noncanonical, signaling to IRE1α and PERK [60]. Overall, despite the central role of IRE1α as a master adjustor of ER proteostasis, the mechanisms connecting fluctuation in ER physiology and the engagement of the UPR remain poorly understood.

The integration of signaling pathways of the UPR is a key step to determine cell fate under stress. Evidence suggests the existence of fine-tuned differential regulation (activation and inactivation kinetics) of IRE1α activity that can impact the balance between survival and cell death under sustained ER stress. The kinetics of activation and attenuation of IRE1α signaling differs depending on the nature and duration of the stress stimuli and the cell type, suggesting the existence of regulatory mechanisms that modulate the UPR beyond the accumulation of misfolded proteins within the ER lumen [61].

The regulation of IRE1α has been explained by several mechanisms including, (i) structural changes in its luminal and cytosolic domains, (ii) post-translation modifications and (iii) the physical association with positive and negative regulators. This findings evidence a dynamic signaling platform that our laboratory has referred to as the “UPRosome” [62], in which many proteins assemble to modulate the amplitude of activation of IRE1α and downstream signaling pathways (Fig. 4).

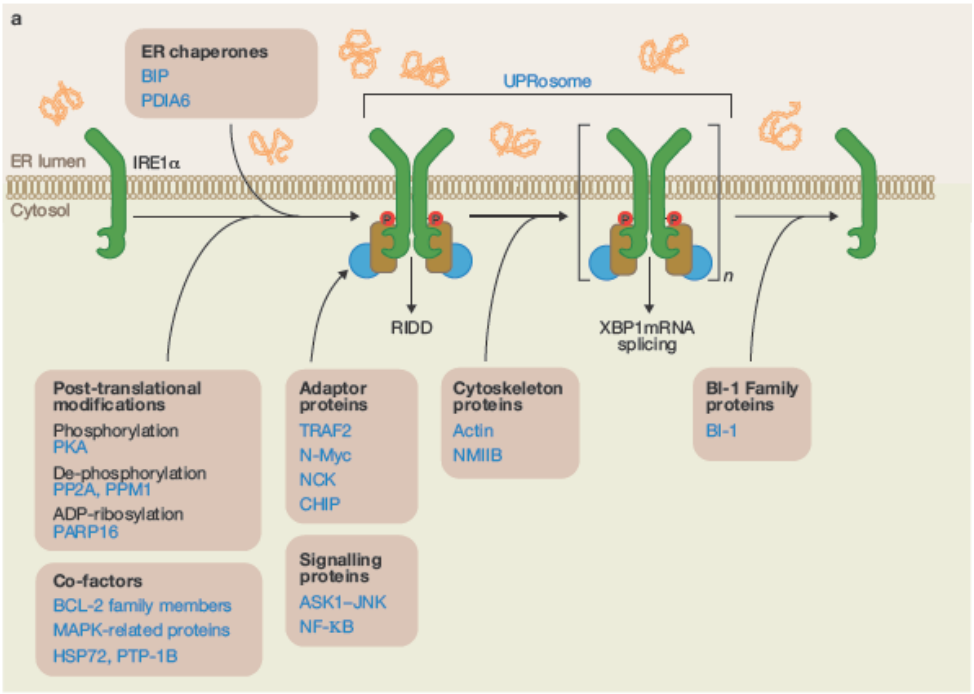

Hetz C, Chevet E. (2015) Nat Cell Biol

Figure 4. The UPRosome: IRE1α regulation. Fine-tuning ER stress signalling through protein–protein interactions and/or post-translational modifications. The activity of UPR stress sensors is regulated through the binding of co-factors and post-translational modifications that modulate the amplitude of their downstream signals and the kinetics of activation and attenuation. The assembly of distinct UPRosomes may also mediate the crosstalk of the UPR with other signalling pathways, and the control of novel stress-independent functions. Fine-tuning IRE1α signalling through the dissociation of ER chaperones in the activation phase, recruitment of the UPRosome that controls signalling outputs and inactivation phase

Our laboratory and others groups have described several proteins that act as positive and negative regulators of IRE1α that physically associate to the sensor including BAX inhibitor 1 (BI-1) [63], BAX/BAK [64], BIM/PUMA [65], PTP-1B [66], AIP1 [67] and among others (reviewed in [68]). Several additional components have been also reported [5], including the non-muscle myosin IIB and actin cytoskeleton, which controls the formation of the IRE1α oligomers [69]. Interestingly, a subset of proteins that have chaperone activity has been described to regulated IRE1α function, including PDIA6 [70, 71] and HSP72 [72] by the interaction with cytosolic domain of the sensor. In addition, BiP is the master inhibitor regulator by the interaction of luminal domain of IREα [22].

In addition, indirect evidence suggests that *Xbp1* mRNA splicing and RIDD activity may also be differentially modulated [38], adding an additional layer of complexity to the regulation of IRE1α. Under prolonged or chronic ER stress, IRE1α is inactivated by a mechanism that involves the dissolution of IRE1α clusters and its de-phosphorylation, leading to a decline of *Xbp1* mRNA splicing [73]. Our laboratory, has previously described that BI-1 is a central mediator of IRE1α attenuation, as demonstrated in different studies in cell culture and animal models of ER stress [63, 74-76]. Thus, IRE1α is fine-tuned by a dynamic mechanism through the assembling of distinct factors to the UPRosome, which potentially establishes a stress threshold to engage the UPR.

A proteomic study (Fig. 5a) was performed in our laboratory in order to identify new interactors of IRE1α. Using IRE1α knockout fibroblasts reconstituted with an HA-tagged IRE1α (IRE1α-HA) for its purification, we immunoprecipitated IRE1α at basal levels or in cells undergoing ER stress. Protein identification was conducted using mass spectrometry analysis in three independent experiments. This experimental approach led us to identify a large number of putative proteins that interacts with IRE1α and that potentially may modulate its enzymatic activities (unpublished data). More than 40 proteins were found, that are involved in several cellular processes such as DNA damage response, RNA processing, metabolism,

ER stress, regulation of cytoskeleton and protein folding. After bioinformatics analyses, the top 10 candidates were selected. Most of this candidates identified in IRE1α-containing complexes were present in both basal and ER stress conditions, whereas only four proteins were exclusively detected at resting conditions and two upon ER stress (Fig. 5b). A validation screening was performed with the list of top 10 interactors (Fig. 5b and Table 1), evaluating the effect of silencing these proteins using shRNAs in the activation of IRE1α evaluated by the *Xbp1* mRNA processing (Fig. 5c) and cell viability under ER stress (Fig. 5d). Interestingly, preliminary studies using loss- and gain-of-function in cellular models identified four putative modulators of the RNAse activity of IRE1α, including heat shock protein 47 (HSP47), the candidate that had the most robust effect on IREα activation (see thesis project).

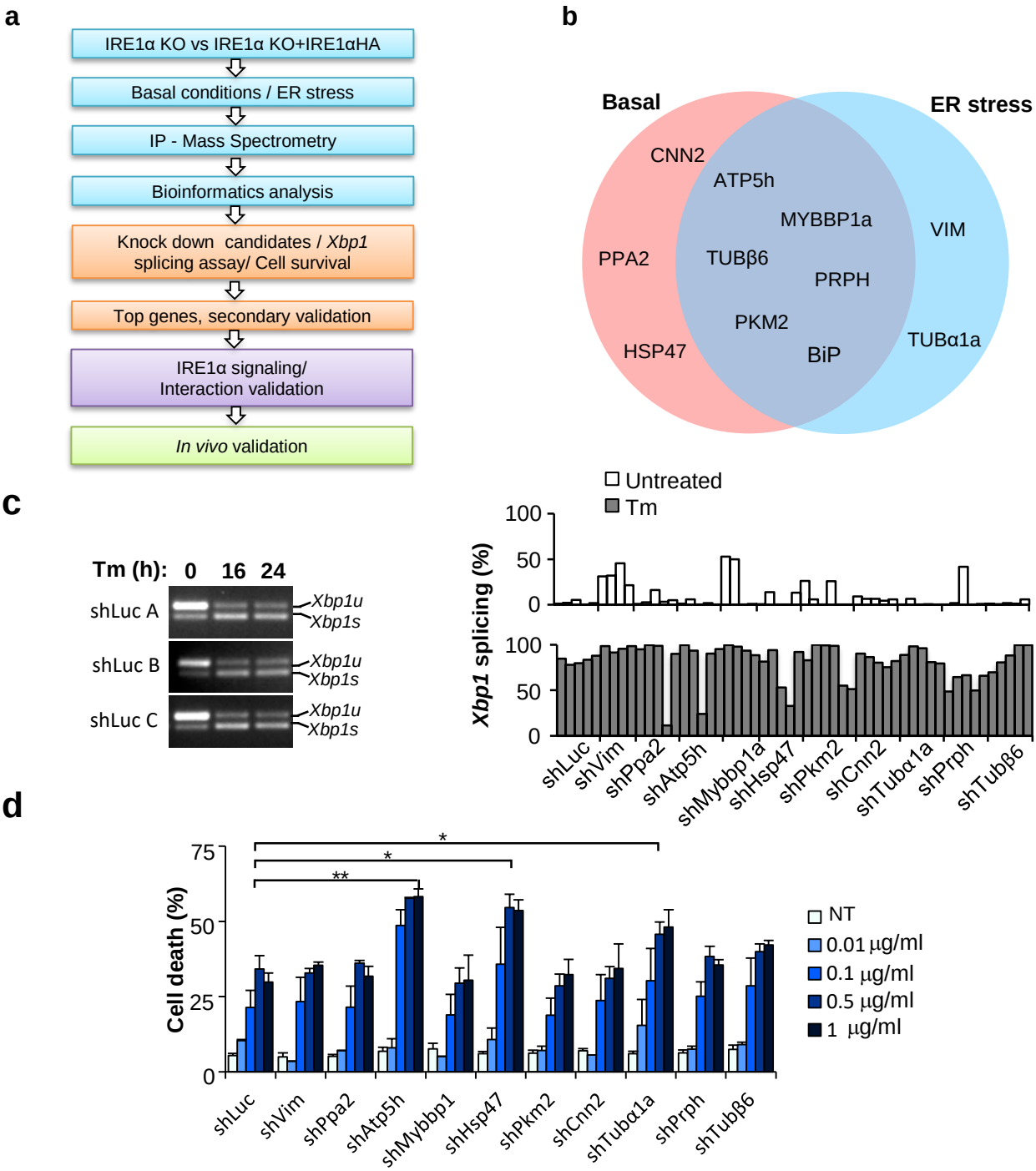

Figure 5. The interactome project: Functional screening for IRE1α interactors. (**a**) Strategy for the functional screening for IRE1α interactors. IRE1α knockout MEF cells were reconstituted using retrovirus coding for full length IRE1α -HA. Immunoprecipitation of HA-tagged IRE1α was performed at basal levels or in cells treated with 250 ng/mL of Tm for 6 h. Proteins present in complexes with purified IRE1α were then identified using mass spectrometry. Analysis was performed in three independent experiments (see summary of candidates and peptides detected in Table 1). (**b**) Representation of IRE1α associated proteins under basal, ER stress and the intersection of both conditions are shown. (**c**) The expression of ten IRE1α–binding candidates was knocked down by stably delivering the different pools of shRNA constructs for indicated genes. A primary functional screening was performed in cells treated with 10 ng/ml Tm for 24 h followed by the analysis of *Xbp1* mRNA splicing using RT-PCR. Densitometry analysis of the *Xbp1u* and *Xbp1s* amplicons was performed to calculate the levels of *Xbp1* mRNA splicing. Control MEFs cell lines were generated by transduction with lentiviruses carrying three different shRNAs against the luciferase gene (left panel). (**d**) Indicated shRNA cell lines were treated with increasing concentrations of Tm and cell death was evaluated after 24 h by propidium iodide staining and flow cytometry. When indicated statistical analysis was performed using ANOVA: *: $p < 0.05$, **: $p < 0.01$.

Protein ID	Protein	Peptide	Treatment	Function	Cellular localization
Q08093	Calponin-2, CNN2	CASQVGMTAPGTR SMQNWHQLENLSNFIK SWIEGLTGLSIGPDFQK LGTDKCDNSSMSLQMGYTQGANQSGQ VFGLGR GLQSGVDIGVK GPSYGLSAEVK TKGLQSGVDIGVK	Basal Conditions	Thin filament-associated protein that is implicated in the regulation and modulation of smooth muscle contraction. It is capable of binding to actin, calmodulin, troponin C and tropomyosin.	Extracellular exosome, focal adhesion, membrane, stress fiber.
D3Z636	Inorganic pyrophosphatase 2, PPA2	ILGTLALIDQSETDWK FKPGYLEATLNWFR		Catalyzes the hydrolysis of pyrophosphate to inorganic phosphate	Mitochondria
P19324	47 kDa heat shock protein, HSP47	STGLAFSLYQAMAK		Molecular chaperone essential for the correct folding of collagen. .	Endoplasmic reticulum, Cis-Golgi
Q3UMM1	Tubulin betha-6 chain, TUBβ6	SGPFGQLFRPDNFIFGQTGAGNNWAK FWEVISDEHGIDQAGGYVGDSALQLER	Basal conditions / ER stress	Subunit of tubulin, the major constituent of microtubules	Cytoplasm, cytoeskeleton
P52480	Pyruvate kinase, PKM2	KGDVVIVLTGWRPGSGFTNTMR GDLGIEIPAEK AGKPVICATQMLESMIK RFDEILEASDGIMVAR		Glycolytic enzyme that catalyzes the transfer of a phosphoryl group from phosphoenolpyruvate to ADP, generating ATP.	Cytoplasm, nucleus
P15331	Peripherin, PRPH.	MALDIEIATYR		Class-III intermediate filament protein.	Cytoplasm, cytoeskeleton
Q7TPV4	Myb-binding protein 1A, MYBBP1A	LYDLYWQAMR		Activate or repress transcription via interactions with sequence specific DNA-binding proteins.	Cytoplasm, nucleus, nucleolus
Q9DCX2	ATP synthase subunit d, ATP5h	LASLSEKPPAIDWAYYR		Subunit of mitochondrial membrane ATP synthase, that produces ATP from ADP in the presence of a proton gradient across the membrane.	Mitochondria
P20029	78 kDa glucose-regulated protein, GRP78,BIP	AKFEELNMDLFR TFAPEEISAMVLTK DAGTIAGLNVMR IEIESFFEGEDFSETLTR TFAPEEISAMVLTK		Involved in the correct folding of proteins, facilitating the assembly of multimeric protein complexes inside the endoplasmic reticulum	Endoplasmic reticulum lumen
P20152	Vimentin, VIM	MALDIEIATYR	ER stress	Class-III intermediate filaments attached to the nucleus, endoplasmic reticulum, and mitochondria.	Cytoplasm, cytoeskeleton
P68369	Tubulin alpha-1A chain, TUBα1A	AVFVDLEPTVIDEVR IHFPLATYAPVISAEK		Subunit of tubulin, the major constituent of microtubules.	Cytoplasm, cytoeskeleton

Table 1. Identification of putative IRE1α binding partners. IRE1α knockout MEF cells were reconstituted using retrovirus coding for full length IRE1α-HA. Immunoprecipitation of IRE1α-HA was done at basal conditions or in cells treated with 250 ng/mL of tunicamycin (Tm) for 6 h. Protein complexes were then analyzed using mass spectrometer. Analysis was performed in three independent experiments. Unique peptide sequences found are indicated, in addition to predicted protein function and cellular localization. Of note, one peptide corresponded for two putative protein candidates (PRPH and VIM).

6.5 Heat shock protein 47 (Hsp47).

Hsp47 protein belongs to the family of heat shock proteins (HSP), whose main feature is their regulation of the expression levels when cells are exposed to stress conditions. HSP have different physiological functions, acting as chaperones to assist protein folding, translocation and secretion of proteins, as well as the degradation of abnormal proteins [77].

Hsp47 is a glycoprotein [78] that operates as a specific chaperone for collagen production [79], assisting the transport of triple helix procollagen from the ER lumen to the cis-Golgi in a pH-dependent manner [80-82]. Hsp47 is not dependent on the ATP activity and interacts with several ER chaperones, such as PDI, Grp78 and Grp94 in order to function properly in the ER (Fig. 6) [82].

Since the early 90's, a group of researchers led by Dr. Nagata in Japan has characterized the potential role of the chaperone Hsp47 in the biosynthesis of procollagen, describing that this chaperone: (i) it prevents the formation of procollagen aggregates at the ER lumen, (ii) it prevents degradation of procollagen at the ER, (iii) it promotes quality control mechanisms of procollagen under conditions of cellular stress, and (iv) it is essential for the efficient secretion, processing and formation of collagen fibers [79]. Thus, the role of Hsp47 in normal physiology has been extensively studied in the context of collagen biology; however, the putative role of Hsp47 in ER stress responses is still unknown.

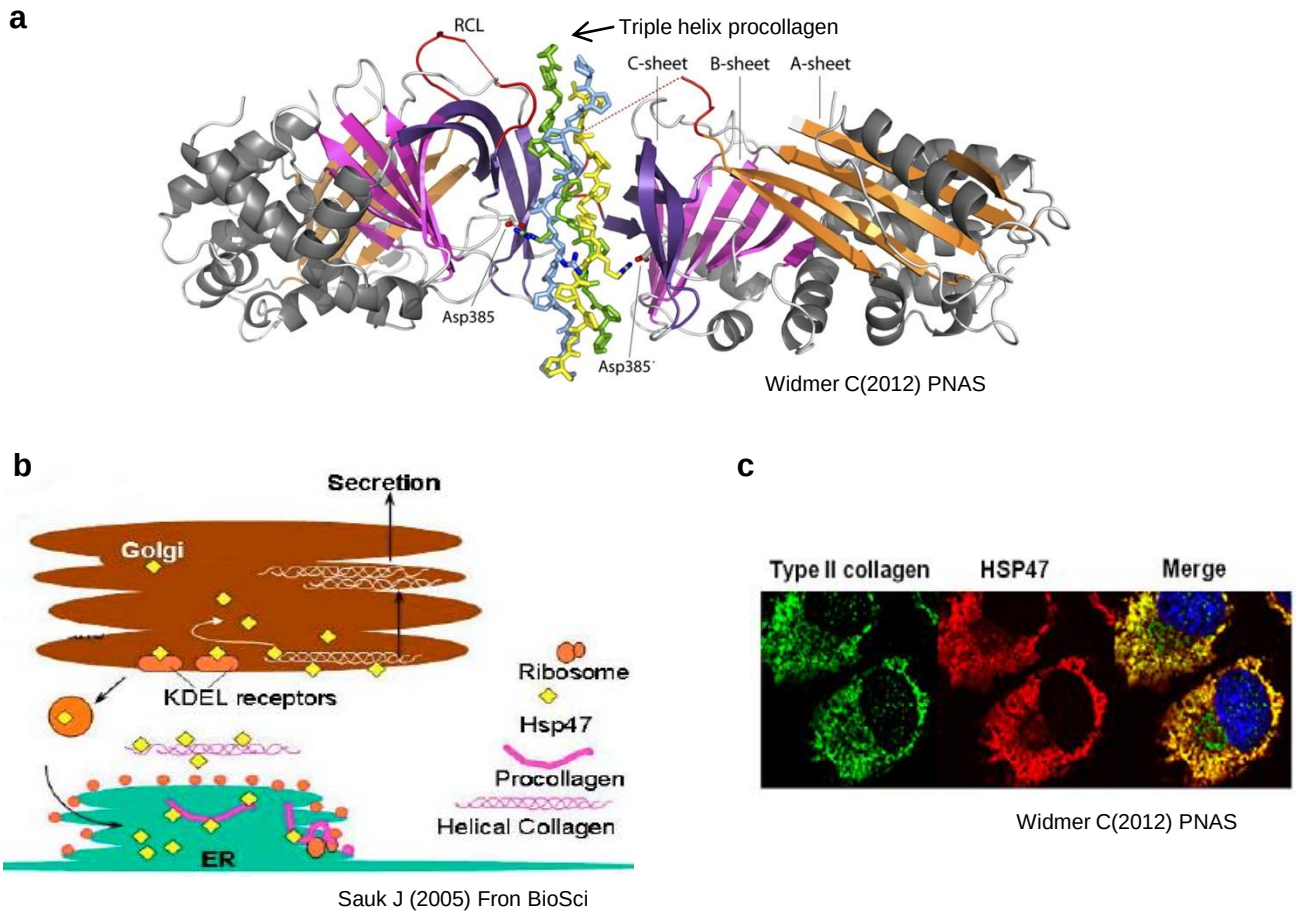

Figure 6. Structure, function and localization of Heat Shock Protein 47 (Hsp47). (**a**) Overall structure of the Hsp47 and collagen model peptides (CMP) complex. Hsp47 is shown in cartoon representation, and the CMP chains are depicted as sticks. α-Helices are drawn in gray. β-Sheet A is shown in orange, sheet B in magenta, and sheet C in violet. The segment corresponding to the reactive central loop (RCL) of inhibitory serpins is drawn in red. Asp385 is shown as sticks. The leading strand of the collagen triple helix is drawn in yellow, the middle strand in blue, and the trailing strand in green. (**b**) Schematic representation of Hsp47functions. Hsp47 is closely located with the translation and translocation of procollagen molecules. The continual association in the ER and cis-Golgi prevents aggregation and facilitates modification of collagen molecules. The persistent binding of Hsp47 to collagen prevents degradation of molecules prior to fibril formation. Dissociation of Hsp47 from collagen occurs beyond the cis-Golgi, where upon Hsp47 is recycled back to the ER. In epithelial tissues, some forms of malignancy and autoimmune connective tissue diseases Hsp47 is not recycled to the ER but is expressed on the cell surface. (**c**) Hsp47 localization. Primary chondrocyte of E18.5 embryos isolated from rib cartilage of control were maintained for 7 days. Localization of type II collagen and Hsp47 was analyzed by double staining immunofluorescence.

6.6 Chaperones and IRE1α regulation.

Until now, two regulators of IRE1α were identified at the ER lumen, including BiP and PDIA6. BiP binds to IRE1α at basal levels, keeping the sensor in inactive monomeric state [22]. On the other hand, PDIA6 modulates an IRE1α´s redox status [71, 83]. PDIA6 decreases IRE1α activity by direct interaction with cysteine 148 of the luminal domain of the sensor. This residue is oxidized when IRE1α is activated, so that binding of PDIA6 to IRE1α promotes the inactivation, without altering its initial activation [71]. In addition, another cytosolic HSP family member, HSP72 has been described, which modulates the IRE1α/XBP1 axis of the UPR. HSP72 expression increases *Xbp1* mRNA splicing and consequently increases the expression level of genes downstream of XBP1s as *Erdj4* and *Edem* [72]. Interestingly, evidence also suggests the formation of a stable complex between HSP72 and IRE1α cytosolic domain, suggesting a direct connection between cytosolic chaperones and response to ER stress [21].

In summary IRE1α signaling is fine-tuned by different chaperones at the ER, which has biological meaning since these proteins are specialized in detecting abnormally folded proteins. In this thesis we propose ER luminal chaperone HSP47 enhances IRE1α/XBP1/RIDD signaling. We propose that defining the composition of the UPRosome will allow us to understand how cells adapt to protein folding stress and to better define the contribution of the UPR to physiological and pathological processes involving protein misfolding.

Based on the evidence and the subcellular localization of HSP47, four important questions arise involving the activity of HSP47 into ER stress: i) Is HSP47 a possible modulator of IRE1α signaling? ii) Is the effect of HSP47 on IRE1α ER stress-dependent? iii) Is HSP47 regulating IRE1α through a direct interaction, affecting BiP binding? and iv) Does HSP47 regulate IRE1α signaling *in vivo*?

6.7 Highlights.

As a summary of the antecedents that will drive our working hypothesis, it is important to highlight the following aspects of the current state of the field that is relevant for this thesis:

1. IRE1α and XBP1s are essential components of the UPR involved in the adaptation to ER stress or the induction of apoptosis of irreversible-damaged cells.
2. IRE1α activity is controlled by different cofactors that modulate the kinetic and amplitude of its downstream responses (UPRosome).
3. The ER stress sensor IRE1α interacts with HSP47 (Co-immunoprecipitation).
4. HSP47 is a specific collagen chaperone and it is located at the ER lumen.
5. HSP47 overexpression correlates with increased synthesis and secretion of collagen.
6. Preliminary data indicates that HSP47 deficiency decrease *Xbp1* mRNA splicing levels and reduces cell viability under ER stress induced by tunicamycin.

The main objective of this thesis is to study the possible role of the chaperone HSP47 on IRE1α activation and function at different levels and the impact of this regulation to cell viability under ER stress.

7. HYPOTHESIS.

HSP47 increases IRE1α endoribonuclease activity by a direct interaction, promoting *Xbp1* mRNA processing and cell survival under ER stress conditions.

8. GENERAL AIM.

To determine the possible involvement of HSP47 on the activation of IRE1α under ER stress conditions.

9. SPECIFICS AIMS.

Specific aim 1. To determine the impact of HSP47 in the oligomerization and phosphorylation of IRE1α under ER stress conditions.

Specific aim 2. To evaluate the participation of HSP47 in the regulation of signaling pathways downstream of IRE1α and its impact to cell survival under ER stress conditions.

Specific aim 3. To study the interaction between IRE1α and HSP47 and its possible relation with BiP.

Specific aim 4. To study the significance of HSP47 in the modulation of IRE1α activity *in vivo*.

10. MATERIALS AND METHODS.

10.1 Reagents.

Tunicamycin and puromycin were purchased from Calbiochem (EMB Bioscience Inc). Phos-tag™ was purchased from Wako Pure Chemical Industries. Cell culture media, fetal bovine serum, and antibiotics were obtained from Life Technologies (Maryland, USA). All other reagents used here were from Sigma or the highest grade available.

10.2 Cell culture and treatments.

All MEFs used here were maintained in Dulbecco's modified Eagles medium supplemented with 5% fetal bovine serum, non-essential amino acids and grown at 37°X and 5% CO_2. pMSCV-Hygro retrovirus vector expressing IRE1α-HA were previously described in [65], where IRE1α contains two tandem HA sequences at the C-terminal domain and a precision enzyme site before the HA tag. A HIS tag was also included after the signal peptide at the N-terminal region. For Tm treatments, cells were incubated in 6-wells in 2 mL of culture media in the presence of described concentrations of Tm. COS-1 cells were maintained under standard tissue culture conditions, including 5% CO_2 with high humidity.

10.3 shRNA *production and virus transduction.*

We generated stable MEFs with reduced levels of Hsp47 mRNA using methods previously described [63, 65, 84, 85], with shRNA using the lentiviral expression vector pLKO.1. As control, an shRNA construct against the luciferase gene was employed. shRNA constructs were generated by the Broad Institute (Boston, MA, USA). In brief, HEK293T cells were co-transfected with lentiviral vectors in 6-well plates. Then, 48h after transfection, WT MEF cells were transduced for 48h using different M.O.I. of viruses. After transduction, we

generated shHsp47 MEF cell lines, which were selected for the resistance to puromycin (2 mg/mL).

10.4 RNA isolation, RT-PCR and real time qPCR.

Total RNA was extracted from cells and tissue using Trizol (Invitrogen, Carlsbad, CA, USA), and cDNA was synthesized with SuperScript III (Invitrogen) using random primers p(dN)6 (Roche). Quantitative real-time PCR reactions employing SYBRgreen fluorescent reagent and/or EvaGreen™ were performed in Stratagene Mx3000P system (Agilent Technologies, Santa Clara, CA 95051, United States). The relative amounts of mRNAs were calculated from the values of comparative threshold cycle by using *Actin* as control and *Rpl19* or *Rpl32* for RIDD in mouse or *D. melanogaster* samples, respectively. All Real time qPCR primers and methods for the *Xbp1* mRNA splicing assay used here were previously described [63, 65, 84]. For PstI splicing, PCR product that was digested by PstI to reveal a restriction site that is lost after IRE1α mediate the splicing of *Xbp1* mRNA [21]. For *Xbp1* mRNA splicing quantification, data from densitometric analysis was obtained using Image J software where the each time point analyzed was considering the addition of the spliced and unspliced *Xbp1* form as 100% and then we calculate the percentage of splicing to each time point [65].

10.5 Immunoprecipitation.

MEF cells stably transduced with retrovirus or lentivirus were prepared in CHAPS buffer (1% CHAPS, 100 mM KCl, 50 mM Tris [pH 7.5], 50 mM NaF, 1 mM Na_3VO_4, 250 mM PMSF, and protease inhibitors) or NP40 buffer (0.2% NP40, 150 mM NaCl, 50 mM Tris [pH 7.5], 5% Glicerol, Complete (Roche), PhosStop (Roche). Immunoprecipitation were performed as described [63, 65, 84].

10.6 IRE1α-NLD pulldown.

For pull-down experiments, COS-1 cells were transfected with the pED-IRE1-NLD-His6-KDEL mammalian expression vector and/or the human HSP47 pCAGGS mammalian expression vector, grown for 72 h, followed by treatment with 0.5 μM thapsigargin, 5 μg/mL tunicamycin or control conditions for 24 h. Transfected cells were harvested by washing with cold Tris-buffered saline followed by scraping into 1 mL cold lysis buffer (25 mM Tris-Cl, pH 8.0, 150 mM NaCl, 0.5% NP-40, and 0.5% sodium deoxycholate). The lysate was incubated on ice for 30 min followed by centrifugation to pellet insoluble material and the supernatant was incubated 4 h at 4°C with 100 μl of 10% slurry of Ni-NTA-Agarose beads (Qiagen). The beads were centrifuged briefly to pellet, and washed five times with 1 mL cold lysis buffer. The beads were pelleted, resuspended in 100 μl SDS-PAGE sample buffer, with 20 μl separated on SDS-PAGE (10% acrylamide), and followed by Western blot analysis using anti-HSP47, anti-BiP or anti-His antibodies.

10.7 Western blot analysis and phostag gels.

Western blot analysis was performed using standard conditions. [84]. In brief, cells were collected and homogenized in RIPA buffer (20 mM Tris pH 8.0, 150 mM NaCl, 0.1% SDS, 0.5% Triton X-100) containing a protease inhibitor cocktail (Roche, Basel, Switzerland) in presence of 50 mM NaF and 1 mM Na_3VO_4. Protein concentration was determined in all experiments by micro-BCA assay (Pierce, Rockford, IL), and 20-40 μg of total protein was loaded onto 8% SDS-PAGE minigels (Bio-Rad Laboratories, Hercules, CA) prior transfer onto PVDF membranes. Membranes were blocked using PBS, 0.1% Tween20 (PBST) containing 5% milk for 60 min at room temperature then probed overnight with primary antibodies. The following antibodies and dilutions were used: anti-HSP90 1:3000 (Santa Cruz, CA), anti-CHOP 1:2000 (Santa Cruz, CA), anti-HA 1:2000 (Roche, Basel, Switzerland), anti-BiP 1:10000 (Cell Signaling technology), Anti-V5

1:2000 (Invitrogen), Anti-HSP47 1:5000 (Enzo Lifesciences), Anti-HIS 1:2000 (Thermo Scientific). Detection of IRE1α phosphorylated form was performed using Phostag™ assay loading 15 μg of total protein into 4% SDS-PAGE minigels containing 50 μM of Phostag™ in presence of 25 mM of $MnCl_2$.

10.8 Purification of IRE1-NLD and HSP47 protein.

COS-1 cells were transfected with the pED-IRE1-NLD-His6-KDEL expression vector and purified by Ni-NTA-Agarose [86]. Briefly, COS-1 cells were transfected with IRE1-NLD expression vector, grown for 72 hours, harvested and lysed into a buffer containing 25 mM Tris-Cl, pH 8.0, 150 mM NaCl, 0.5% Nonidet P-40, and 0.5% sodium deoxycholate. Cell lysates were incubated on ice for 30 minutes and centrifuged at 20,000 g for 15 min, with the supernatant used for protein purification. Ni-NTA-Agarose chromatography was carried out using a buffer containing 50 mM Tris-Cl, pH 8.0, 300 mM NaCl, and 10 mM imidazole. The IRE1-NLD protein was eluted with 300 mM imidazole and concentrated. Human HSP47 was cloned into pET-21a containing a 6HIS tag for expression in LEMO21 *E. coli* cells. Transformed *E. coli* were grown at 37°C to an OD of 0.3-0.6 and induced with 1 mM IPTG at 37°C for 2 hours. Cells were harvested, crushed and the supernatant passed over a Ni-NTA-Agarose column using FPLC and eluted with 300 mM imidazole. Fractions were combined, concentrated and buffer exchanged for further purification using a Resource-Q column. Purified HSP47 protein was eluted using a high salt gradient, with fractions combined and concentrated. Purified proteins were buffer exchanged to the MST buffer system.

10.9 Surface Plasmon Resonance (SPR).

SPR technology was employed to monitor the interaction of HSP47 or BiP with purified IRE1α-NLD protein (BIACore T200, GE). For BIACore analysis of HSP47, BiP, PDIA6 or actinin interaction with IRE1α-NLD, the carboxymethylated

dextran (CMD) surface of a CM5 chip was activated using *N*-hydroxysuccinimide (NHS)/1-ethyl-3(3-dimethylaminopropyl)-carbodiimide hydrochloride (EDC). Purified IRE1α-NLD protein was diluted in 10 mM NaAc, pH 5 at a concentration of 1 µM and injected over the activated CM5 chip at a flow rate of 5 µl/min to a total of ~1.5 x 10^3 Response Units (RU) followed by the blocking solution of 1 M ethanolamine, pH 9. A reference lane with no protein coupled was also generated in order to subtract background interactions. The CM5 chip was normalized and prepared for kinetic analysis. HSP47 and BiP, PDIA6 and ACTININ controls were diluted in a buffer containing 10 mM Hepes, pH 7.4, 150 mM KCl, and 0.005% P20 at concentrations from 0 to 1 x 10^4 nM and passed over the sensor surface. The data were collected at 25°C at a flow rate of 30 µl/min. The experimental results were corrected against the control surface response to remove any refractive index deviations. Kinetic analyses were carried out with the BiaEvaluation software (GE) using a 1:1 Langmuir binding model and were performed in triplicate. Association and dissociation rates and affinity (K_D) were calculated for each experiment and averaged. The binding response signals in RUs were continuously recorded and presented graphically as a function of time.

10.10 MicroScale Thermophoresis (MST).

MST was carried out using a Monolith NT.115 instrument (NanoTemper Technologies GmbH). To evaluate HSP47 binding to IRE1-NLD, an increasing concentration of purified HSP47 protein (0-20000 nM) was incubated with 200 nM RED-labeled IRE1-NLD protein (NanoTemper Technologies GmbH; as per manufacturer's protocol). The reverse was also performed, with 200 nM RED-labeled HSP47 incubated with an increasing concentration of purified IRE1-NLD (0-10000 nM). To evaluate HSP47 competition with BiP binding to IRE1-NLD, an increasing concentration of BiP (0-10000 nM) was incubated with RED-labeled IRE1-NLD protein in the absence of HSP47 or with a constant concentration of 500 nM HSP47 included in the buffer. To evaluate IRE1-NLD dimerization ability in

vitro, 200 nM of RED-labeled IRE1-NLD was incubated with unlabeled IRE1-NLD (0-10000 nM) in the absence or presence of 500 nM HSP47. Experiments were carried out in a buffer containing 10 mM Hepes, pH 7.4, 125 mM KCl, 1 mM EGTA, 2 mM $CaCl_2$, 1 mM $MgCl_2$ and 0.005% P20. Experiments were done using hydrophobic capillaries and were performed independently more than three times. Data evaluation was performed using the Monolith software as well as Origin graphing software.

10.11 Immunofluorescence, Duolink assay and IRE1-GFP clustering.

IRE1α-HA and Hsp47 proteins were visualized by immunofluorescence. Cells were fixed for 30 min with 4% paraformaldehyde (PFA) and permeabilized 0.5% NP-40 in PBS containing 0.5% BSA (Bovine serum albumin) for 10 min. After blocking for 1 h with 10% FBS in PBS containing 0.5% BSA, cells were subsequently incubated with anti-HA and anti-Hsp47 antibodies overnight at 4°C. Cell were washed three times in PBS containing 0.5% BSA, and incubated with Alexa-conjugated secondary antibodies (Molecular Probes) for 1 h at 37°C. Nuclei were stained with Hoechst dye. Coverslips were mounted with Fluoromount G onto slides and images were acquired in Olympus FluoView FV1000 microscope with a 60x oil immersion objective. The Duolink assay was developed in *Ern1* null cells reconstituted with IRE1α-HA. Briefly, cells were fixed in PFA 4% (10 min a room temperature), permeabilized (NP40 0.5%-BSA 0.5% in PBS) and blocked for 1 h (BSA 0.5%-FBS 10% in PBS) and anti-HA (rabbit) and anti-HSP47 (mouse) primary antibodies were incubated overnight. After this point, all protocols were developed following manufacturer´s instructions, (Duolink®, Sigma-Aldrich). TREX293 IRE1-3F6HGFP cells [73] were transiently transfected with pcDNA3.1-HSP47-V5 or pcDNA3.1 as control. Twenty-four hours after transfection, cells were split and reseeded on 25-mm-diameter coverslips in DMEM with 5% FBS and treated with doxycycline (5 μg/mL) for 24 h to induce IRE1α-GFP expression, followed by the addition of 1 μg/mL Tm. Cells were fixed in PFA 4% for 2, 4 and 6

h, followed by incubation with a blocking solution [0.25% bovine serum albumin (BSA), 10% horse serum in PBS] for 10 min. Cells were permeabilized with 0.5% NP-40 in 0.25% BSA, 10% horse serum in PBS for 10 min at room temperature. Samples were incubated sequentially with primary antibodies (mouse anti-V5 1:500) and secondary antibody (goat anti-mouse Alexa Fluor 594, Life Technologies) for 60 min at room temperature. Nuclei were stained with 4′, 6-diamidino-2-phenylindole (DAPI). Images were acquired using an Olympus FluoView FV1000 confocal laser-scanning microscope. Image stacks were captured using a 63×/1.4 objective with constant parameters for all conditions of each type of experiment, guaranteeing that the image was not saturated and that image background was slightly above zero. Twenty different fields were analyzed with a total of 150 to 200 cells per group in three independent experiments. The numbers of IRE1α clusters and cluster size were quantified using ImageJ.

10.12 *Fly studies*

Flies were kept at 25°C on standard medium with a 12–12 dark-light cycle. The line Tub-Gal4/TM3-GFP was obtained from the Bloomington Drosophila Stock Center (Bloomington, In, USA). UAS-RNAi line was obtained from the Vienna Drosophila RNAi Center (VDRC): UAS-RNAi SRP2 (CG8137). For the RNAi experiments, males UAS-RNAi were crossed to females Tub-Gal4/TM3-GFP flies. Third instar GFP-positive larvae (not expressing the RNAi) were separated from GFP-negative larvae (expressing the RNAi) and fed separately with Tm or the vehicle (DMSO). After the treatments, total RNA was obtained from larvae using Trizol (Invitrogen, Carlsbad, CA, USA), and cDNA was synthesized with SuperScript III (Invitrogen). In survival experiments, 50 flies were fed with 25 μg/mL Tm or DMSO in instant Drosophila food (Carolina Biological Supply 2700 York Burlington, NC, USA). The total number of flies alive each 2-3 days was counted.

10.13 *Generation of Hsp47 conditional knockout mice*

A conditional Hsp47 knockout mice was generated by crossing Hsp47 floxed mice [87] with TTR-Cre inducible (liver-specific promoter) transgenic animals [88]. The Cre-loxP system was used to disrupt the Hsp47 gene in a tissue-specific manner using a transgenic mouse harboring a floxed Hsp47 gene in which the exon-6-containing region was flanked by loxP sites [87]. Exon 6 is the final exon that encodes approximately 24% of the amino acid sequence of Hsp47, including a region essential for binding to collagen and a poly(A) signal. Correct targeting by homologous recombination and germ line transmission was previously confirmed by southern blotting [87]. The TTR-Cre ind strain was acquired from Prof. Mireile Vasseur-Cognet. Animal experimentation protocols were approved by the Kyoto Sangyo University Committee for Animal Care and Welfare. Breeding homozygous Hsp47 floxed and TTR-Cre ind mice resulted in double-heterozygous animals. Then, animals were mated with Hsp47 floxed homozygous mice to obtain animals with the TTR–Cre ind transgene with two Hsp47 floxed alleles. Mice were used for experiments after backcrossing with C57BL/6 mice for at least seven generations. Routine mouse genotyping was performed by PCR. The following primer pairs were used for floxed Hsp47 alleles and the Cre transgene: 5´-GAGTGGGCTGAGCCCTCTCAAGAAAATCC-3´,5´-CTTCGGTCAGGCCCAGTCC TGCCAGATG-3´; and 5´-CTGCATTACCGGTCGATGCA-3´, 5´-ACGTTCACCGGC ATCAACGT-3´, respectively. Tamoxifen (Sigma T6548) was dissolved in sunflower oil/ethanol (10:1) mixture. 8 weeks old TTR-Cre ind/Hsp47 flox/flox mice or Hsp47 flox/flox mice were injected intraperitoneally for five consecutive days with 1 mg Tamoxifen or with sunflower oil (control) and sacrificed 1 week after the last injection. The liver and kidney were frozen at -80°C for biochemical analysis and the right major lobe of the liver was placed in a petri dish (on ice). The liver was washed in PBS to remove the blood and then, it was fixed in 4% paraformaldehyde for 72 h to histological analyses.

10.14 *Histological evaluation and TUNEL assay*

Liver tissue specimens were fixed in 10% buffered formalin, embedded in paraffin, sectioned (5 µm thick), stained with hematoxylin-eosin or Masson's trichrome, and then analyzed blindly by microscopy at high power magnification (x100, x200 or x400). Liver tissue specimens were embedded in paraffin and sectioned at 5 µm for processing by the TUNEL method using a commercial kit, using DAB peroxidase substrate (Roche Molecular Biochemicals, Meylan, France) and counterstained with hematoxylin. Specimens were evaluated by microscopy using a Zeiss PALM MicroBeam at high power magnification (x100) in a blinded manner. At least 10 random fields were counted for each TUNEL-stained tissue sample. Inflammatory infiltration sites were excluded from the quantification.

10.15 *Statistical analysis.*

When pertinent, results were statistically compared using One Way or Two Way ANOVA followed by a post hoc test (Bonferroni multiple comparison test), depending on the number of independent variables of the experiment. In all plots p values are show as indicated: * $p < 0.05$, ** $p < 0.01$, *** $p < 0.001$, **** $p < 0.0001$ and were considered significant. Ns = non-significant.

11. RESULTS.

11.1 Effect of the IRE1α interactors on UPR signaling outputs.

The global analysis of the proteomic screening identified 10 novel candidate proteins that differentially interact with IRE1α in a reproducible manner, in addition to the known interactor BiP (Fig. 5b-d). We performed a second validation and this approach lead us to select four candidates for further functional validation, three putative activators identified as the protein phosphatase A2 (Ppa2), the ER chaperone Heat Shock Protein 47 (Hsp47) and the mitochondrial ATPase 5h (Atp5h), in addition to one inhibitor of the pathway, cytoskeleton protein Tubulin α 1a (Tubα1a) (Unit of investigation, 2013). We performed a knockdown of Ppa2, Hsp47, Atp5h and Tubα1a by the stable delivery of a shRNA construct using lentiviral vectors. This led to a reduction of mRNA levels of candidates compared with control cells expressing a shRNA against luciferase mRNA (shLuc) as monitored by real time qPCR (Fig. 7e). We then monitored *Xbp1* mRNA splicing after treatment with the Tm (Fig. 7a). Similar results were obtained as the ones observed in the primary screening (Fig. 5c). After densitometric analyses of *Xbp1u* and *Xbp1s* products (Fig. 7b), we observed a significant decrease in *Xbp1* mRNA splicing in the knock down cells to Ppa2, Hsp47 and Atp5h, suggesting a role in IRE1α activation of these candidates. Conversely, Tubα1a deficiency increased *Xbp1* mRNA splicing, suggesting a putative role as inhibitor of IREα (Fig. 7b).

To control the UPR activation and determine the specificity over IRE1α regulation, we measured the levels of *Bip*, general marker of the ER stress and *Chop*, a target gene controlled by the PERK/ATF4 branch. From this analysis, targeting Pp2a, Atp5h and Hsp47 did not affect the upregulation of *Bip* (Fig. 7c) and *Chop* (Fig. 7d), whereas the knockdown of Tubα1a increased the expression of *Bip*, suggesting global alterations to ER physiology (Fig. 7c).

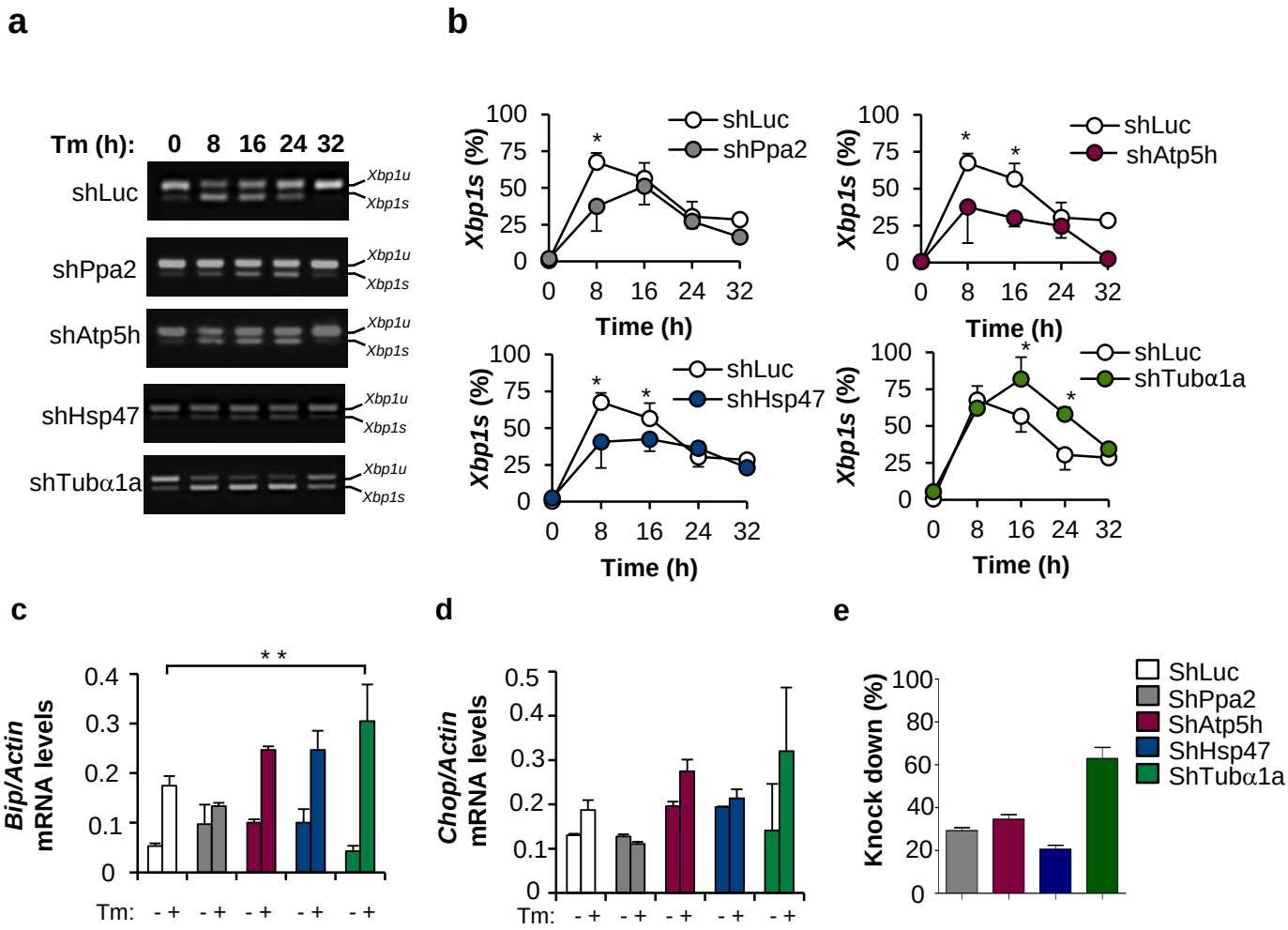

Figure 7. IRE1α interactors regulate IRE1α signaling outputs: loss of function. Secondary validation was performed in four top candidate genes based on the results obtained in the *Xbp1* mRNA splicing assay and cell viability experiments (See Fig. 5). **(a)** MEF cells stably expressing the indicated shRNA constructs were exposed to 10 ng/ml of Tm for indicated time points and the levels *Xbp1* mRNA splicing was evaluated by RT-PCR. Representative images of *Xbp1u* and *Xbp1s* bands in agarose gel are shown. **(b)** The percentage of *Xbp1* mRNA splicing was calculated by densitometric analysis of PCR fragments corresponding to the *Xbp1u* or *Xbp1s* forms (%*Xbp1s* = ((*Xbp1s*/(*Xbp1s* + *Xbp1u*))*100.. Data represents average and standard error of 4 independent experiments. **(c,d)** MEF cells stably expressing the indicated shRNA constructs were exposed to 10 ng/ml of Tm for 8 h and the mRNA levels of *Bip* **(c)** and *Chop* **(d)** were evaluated by real time qPCR. **(e)** The efficiency of the knockdown of indicated stable cell lines expressing specific shRNAs (shPpa2, shAtph5h, shHsp47, shTubα1a) was validated by real time qPCR. The average and standard error of three independent experiments are shown. Statistical analysis were performed using ANOVA. *: $p < 0.05$, **: $p < 0.01$.

To further validate the four selected IRE1α interactors, we performed gain-of-function experiments and assessed UPR signaling using different approaches. We stably expressed V5-tagged versions of human HSP47, TUBα1a, PPA2 and ATP5h in MEFs using retroviral transduction. First, we monitored protein expression using V5 antibodies (Fig. 8a). Then, we treated these cells with tunicamycin (Tm) and monitored *Xbp1* mRNA splicing in time-course experiments. We used an alternative and more sensitive *Xbp1* mRNA splicing assay based on PstI digestion of the *Xbp1u* products (Fig. 8b-c). In agreement with our previous results of loss of function model, the overexpression of PPA2, ATP5H and HSP47 enhanced the levels of *Xbp1* mRNA splicing, which was sustained over time (Fig. 8b). Unexpectedly, TUBα1a overexpression also resulted in sustained *Xbp1* mRNA splicing after 24 h of treatment (Fig. 8b). Virtually, the same results were obtained when we monitored *Xbp1* splicing using conventional assays (Fig. 9a). From these two experiments, we concluded that the overexpression of HSP47-V5 has a robust effect on the attenuation phase of the IRE1α activation (Fig. 8b and 9a).

To determine XBP1s transcriptional targets in these cells overexpressing putative IRE1α regulators, we measured the mRNA levels of *Edem1* and *Sec61*, two classical XBP1s-target genes [26]. Real time qPCR analysis revealed that the overexpression of all four candidates significantly enhanced the induction of *Edem1* (Fig. 9b) and *Sec61* (Fig. 9c) mRNA under ER stress, induced by Tm 10 ng/mL for 8 hours.

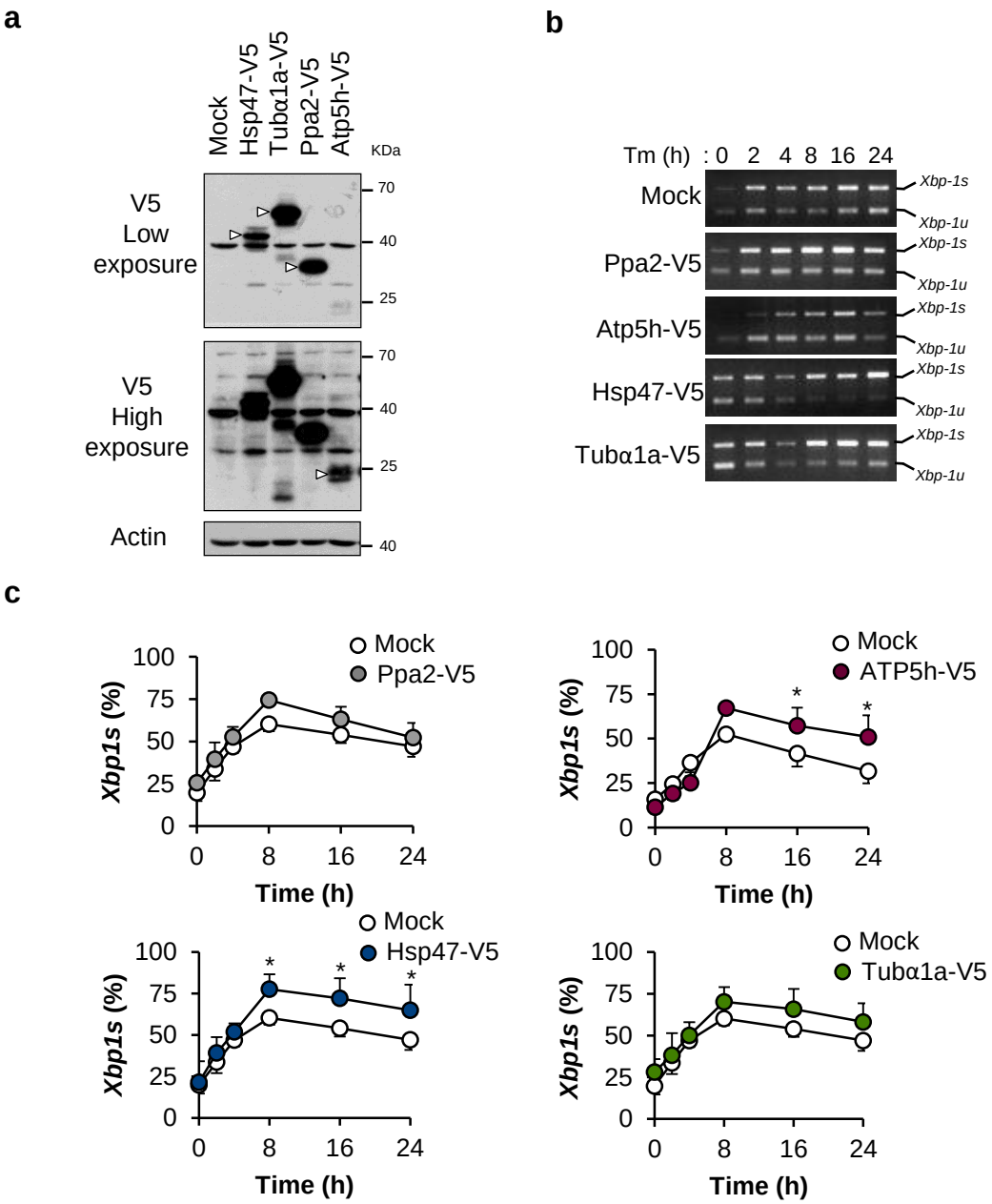

Figure 8. Gain-of-function experiments to assess the impact of IRE1α´s interactors on *Xbp1* mRNA splicing. (a) Wild type MEFs cells were stably transduced with retroviruses expressing a V5-tagged version of the full length human PPA2, ATP5h, HSP47 and TUBα1a proteins. Protein expression levels were assessed by Western blot analysis. White arrows indicate specific overexpression proteins and two exposure time of the V5 antibody signal are shown. Actin levels were monitored as loading control. **(b)** Cells were incubated with 10 ng/mL of Tm for indicated time points and *Xbp1* mRNA splicing was evaluated by total Xbp1 RT-PCR followed by PstI digestion. Spliced *Xbp1* mRNA is resistant to PstI digestion (upper band). **(c)** The percentage of *Xbp1* mRNA splicing was calculated after densitometric analysis of PCR fragments corresponding to *Xbp1u* or *Xbp1s* forms. Data represents average and standard error of 4 independent experiments. Statistical analysis was performed using ANOVA. *: $p < 0.05$.

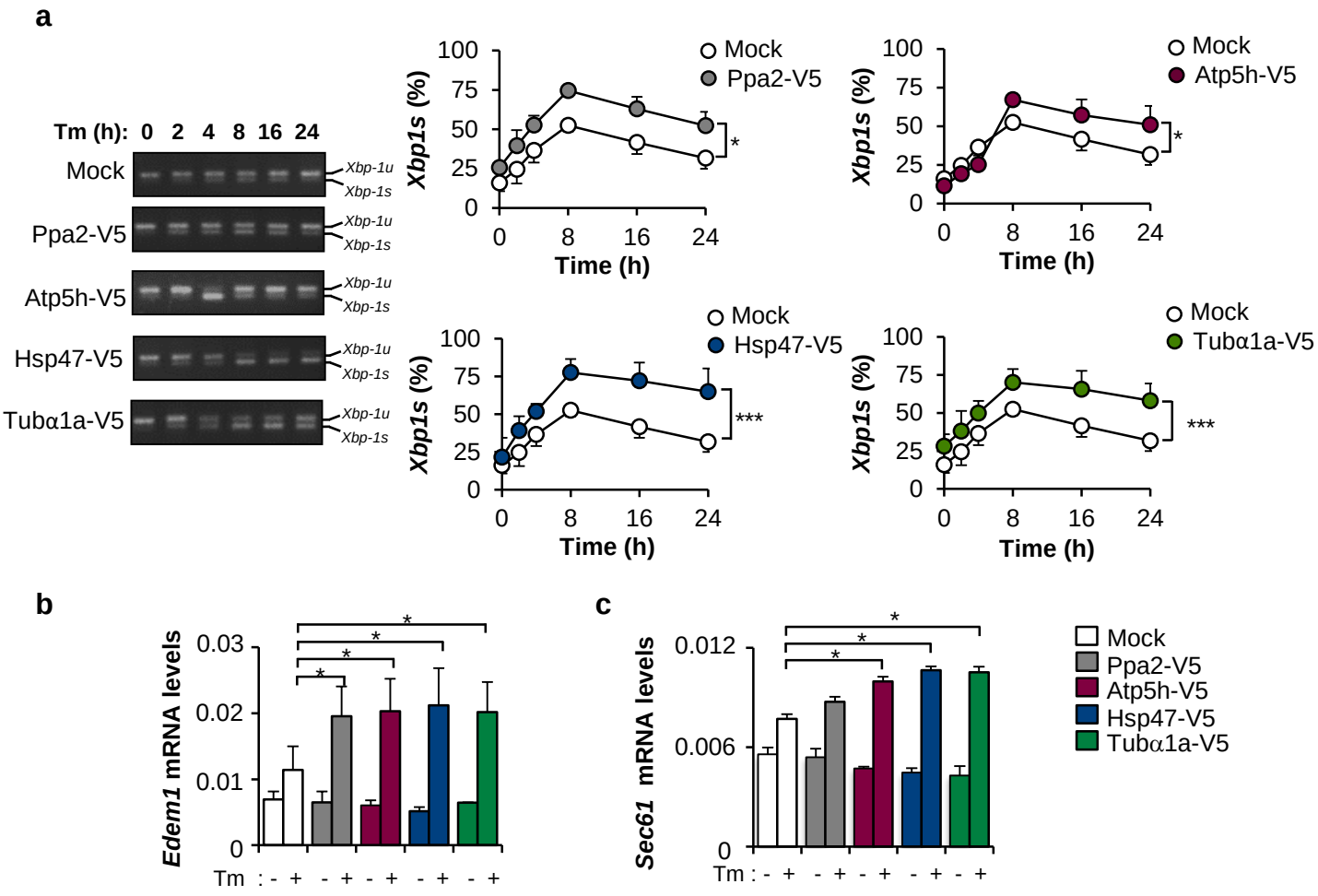

Figure 9. IRE1α´s interactors regulate IRE1α signaling outputs: *Xbp1* mRNA splicing levels and mRNA levels of Xbp1s targets. (a) MEFs stably expressing V5-tagged human PPA2, ATP5h, HSP47 or TUBα1a were incubated with 10 ng/mL of Tm for indicated time points and *Xbp1* mRNA splicing evaluated by RT-PCR. Representative images are shown (left panel). The percentage of *Xbp1* mRNA splicing was calculated after densitometric analysis of PCR fragments corresponding to the *Xbp1u* or *Xbp1s* forms (right panel). Data represents average and standard error of 4 independent experiments. **(b,c)** The mRNA levels of Xbp1s targets *Edem* (**b**) and *Sec61* (**c**) mRNA levels were evaluated by real time qPCR in cells treated with 10 ng/mL of Tm for 8 h. The average and standard error of three independent experiments are shown. Statistical analysis was performed using ANOVA. *: $p < 0.05$, **: $p < 0.01$, ***: $p < 0.001$.

We also measured RIDD activity as an additional output of the IRE1α activity in cells overexpressing the four candidate proteins. Since lower doses of Tm did not trigger any detectable RIDD as measured by real time qPCR (not shown), we increased the concentration of Tm to 100 ng/mL. Surprisingly, analysis of two canonical RIDD substrates, *Sparc* and *Blocs1*, indicated that the overexpression of HSP47-V5 or ATP5-V5 enhanced the decay of these two mRNAs whereas the expression of PP2A-V5 or TUBα1a-V5 did not affect RIDD (Fig. 10a and 10b) despite augmented *Xbp1* mRNA splicing. In contrast, the upregulation of the ATF4 target genes *Bip* and *Chop* was not altered in cells overexpressing PP2A-V5, ATP5H-V5, HSP47-V5 or TUBα1a-V5 (Fig. 10c and 10d), suggesting a specific regulation over IRE1α signaling. Based on the global analysis of our results, we decided to focus our further studies on assessing the contribution of Hsp47 to the regulation of IRE1α because it had the strongest effects on *Xbp1* mRNA splicing and RIDD and it is located in the ER. We performed a systematic approach to observe the kinetic of the Hsp47 contribution on IRE1α activation.

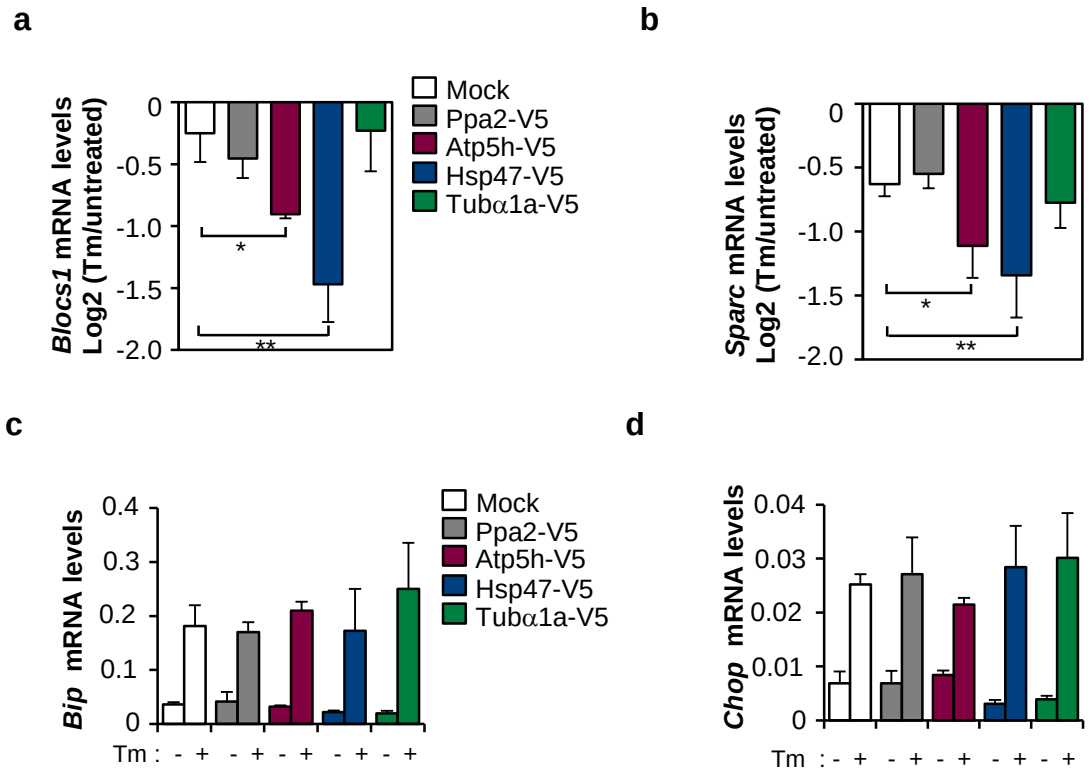

Figure 10. IRE1α´s interactors regulate IRE1α signaling outputs: Regulated IRE1 dependent decay (RIDD). MEFs cells stably overexpressing IRE1α´s interactors were treated with 100 ng/mL of Tm for 16 h and the decay of *Blocs1* **(a)** and *Sparc* **(b)** mRNA levels was monitored by real-time QPCR. Relative mRNA decay was normalized to the levels of *Rpl19* mRNA as a housekeeping gene. **(c,d)** MEF cells overexpressing the indicated IRE1α interactors were exposed to 10 ng/ml of Tm for 8 h and the mRNA levels of *Bip* **(a)** and *Chop* **(b)** were evaluated by real time qPCR. The average and standard error of three independent experiments are shown. Statistical analysis was performed using ANOVA. *: $p < 0.05$, **: $p < 0.01$.

11.2 HSP47 regulates IRE1α signaling outputs: *Xbp1* mRNA splicing and RIDD.

HSP47 deficiency reduces IRE1α/XBP1s signaling.

As part of the specific aim 1 and 2 of this thesis, we knockdown Hsp47 by the stable delivery of a shRNA construct using lentiviral vectors. This led a remarkable reduction of Hsp47 levels compared with control cells expressing a shRNA against luciferase mRNA (shLuc) as monitored by Western blot (Fig. 11a). Hsp47 deficiency decreased *Xbp1* mRNA splicing in cells treated with 10 ng/m of Tm, but did not change of the total levels of *Xbp1* mRNA evaluated by real-time PCR (Fig. 11c). This result confirmed our initial functional screening using four shRNAs for *Hsp47* (Figure 5) and the secondary validation (Fig. 7). In addition, we measured mRNA levels of some well-know XBP1s target genes. In correlation with the diminution of *Xbp1* mRNA splicing in cells Hsp47 deficient, *Edem1* and *Sec61* mRNA levels were also decreased after Tm treatment (Fig. 10d and 10e). As a control of ER stress induction, we evaluated the mRNA levels of UPR markers like *Bip* and *Chop*. As expected, we observed an increase in mRNA expression of UPR markers after tunicamycin treatment in both cell lines, but not significant differences were observed (Fig. 12a and 12b).

Additionally, RIDD activity was evaluated. *Blocs1* mRNA is a well-known RIDD target validated *in vitro* and *in vivo* under ER stress conditions [30, 34]. We observe a subtle decrease on RIDD of *Blocs1* mRNA in shHsp47 cells under treatment with 100 ng/mL of Tm after 16 and 24 hours (Fig. 12c).

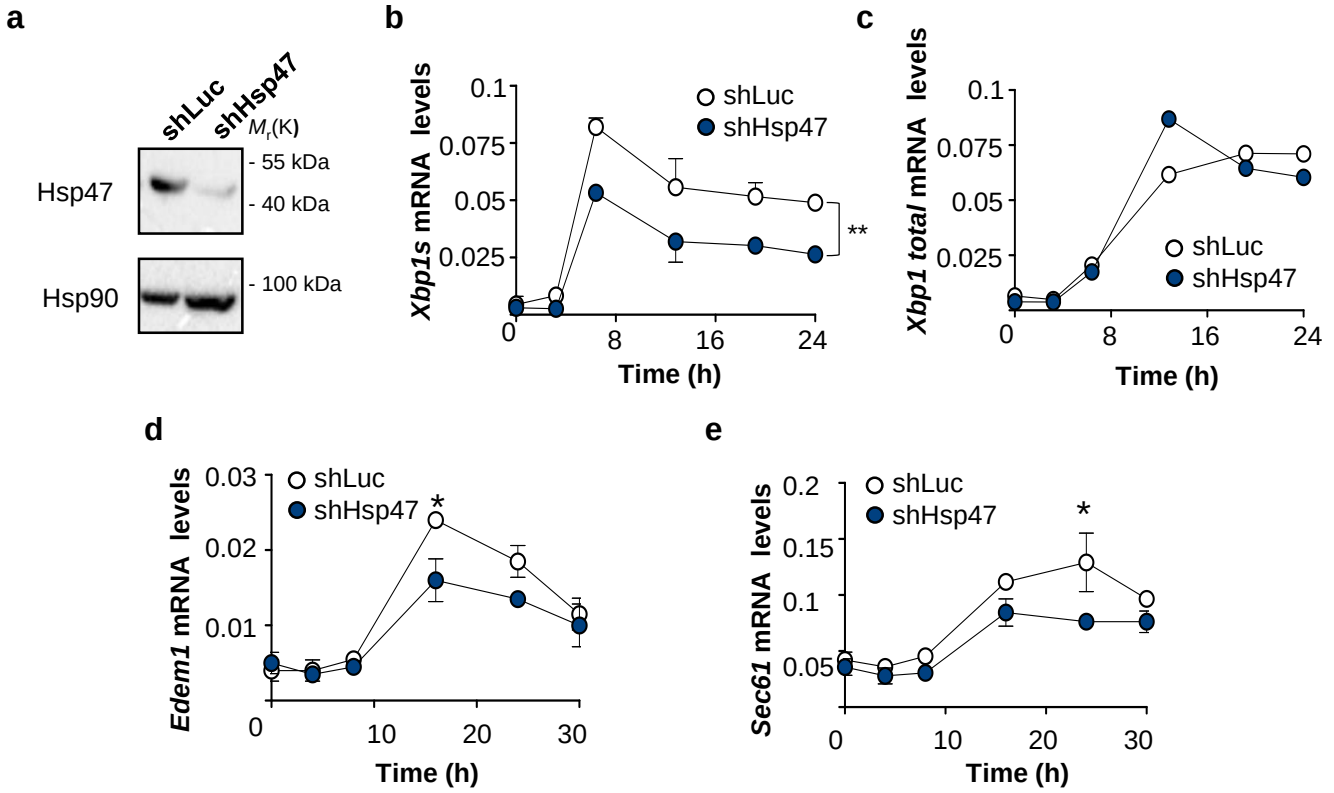

Figure 11. Hsp47 deficiency reduces *Xbp1* mRNA splicing. (a) MEFs wild type cells were stably transduced with lentiviruses expressing a short harpin (sh) RNA directed against the endogenous mouse *Hsp47* mRNA (shHsp47) or luciferase as a control (shLuc). The levels of Hsp47 were evaluated from total protein extracts by western blot, using a primary antibody that recognizes the endogenous Hsp47. Hsp90 levels were monitored as loading control in the same samples. shLuc and shHsp47 cell lines were treated with 10 ng/ml of Tm for 4, 8, 16 and 24 h and the mRNA levels of *Xbp1s* **(b)** and total *Xbp1* **(c)** were determined by real-time QPCR. **(c,d)** Cells were treated with 10 ng/ml of Tm for indicated time points and the levels of Xbp1s targets *Edem* (**c**) and *Sec61* (**d**) were evaluated by real time qPCR. Data represent the average and standard deviation of three independent experiments. Statistical analysis was performed using ANOVA. *: $p < 0.05$, **: $p < 0.01$.

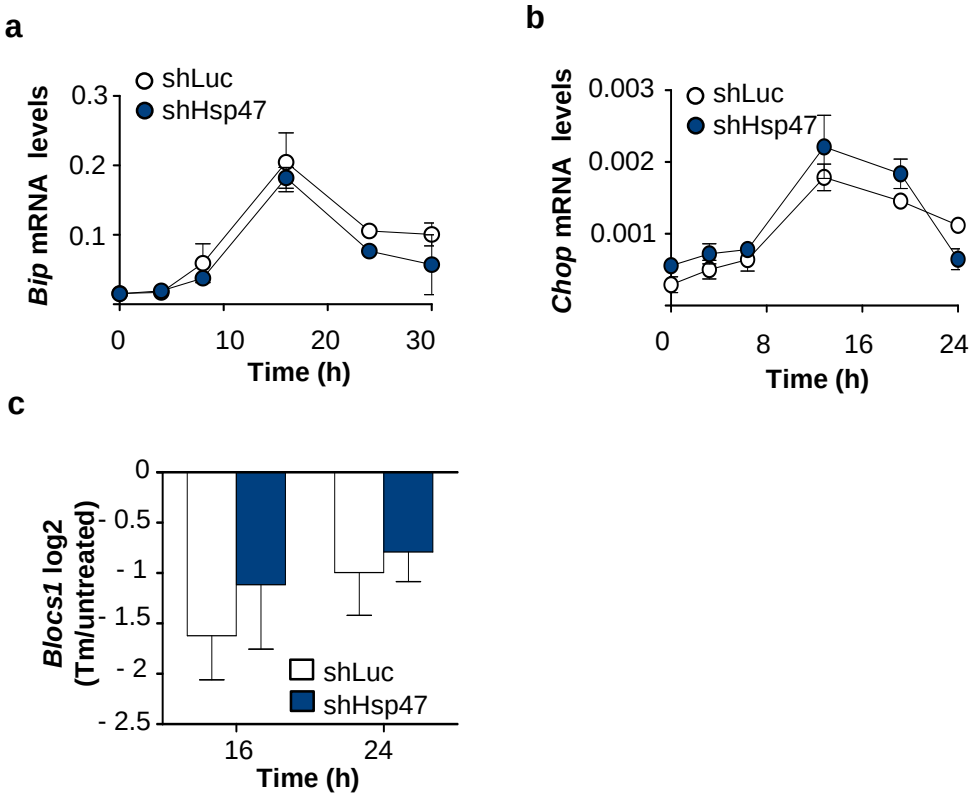

Figure 12. Hsp47 deficiency reduces RIDD. (a,b) MEF shLuc and shHsp47 cells were treated with 10 ng/ml of Tm for indicated time points and the mRNA levels of *Bip* **(a)** and *Chop* **(b)** , were evaluated by real-time PCR. (**c**) shLuc and shHsp47 cell were treated with 100 ng/ml of Tm for 16 and 24 h, and the mRNA decay of the IRE1α target *Blocs1* was monitored by real-time QPCR and normalized to the levels of *Rpl19* as a housekeeping gene. Values were normalized to the mRNA levels under untreated conditions. Bars represent the average and standard error of three independent experiments. Data represent the average and standard deviation of three independent experiments. Statistical analysis was performed using ANOVA.

Hsp47 overexpression enhances IRE1α/XBP1s signaling.

In parallel, we overexpressed Hsp47 with the stable delivery of Hsp47-V5 tagged construct using pMSCV retroviral vectors in MEFs cells (Fig. 13a). We assessed if HSP47 overexpression could impact on the RNAse activity of IRE1α by evaluating the splicing of *Xbp1* mRNA and RIDD upon Tm treatment. The results indicate that Hsp47-V5 overexpression increased the *Xbp1* mRNA splicing after treatment with 10 ng/mL of tunicamycin (Fig. 13b), but no changes of total levels of *Xbp1* mRNA were observed (Fig. 13c). Additionally, we measured mRNA levels of some well-known XBP1s target genes. In correlation with the augment of *Xbp1* mRNA splicing in Hsp47-V5 cells, *Edem1* and *Sec61* mRNA levels were also increased after Tm treatment (Fig. 13c and 13d). As a control of ER stress induction, we evaluated the mRNA levels of *Bip* and *Chop* and no differential mRNA expression of UPR markers were observed after Tm treatment in Hsp47-V5 and Mock cells (Fig. 14a and 14b). These results suggest that HSP47 specifically modulates IRE1α axis, because it does not produce changes in the expression of these general markers the UPR. Additionally, RIDD activity was evaluated. We observed an decreased of *Sparc* and *Blocs1* mRNA (Fig. 14c and 14d) in Hsp47-V5 cell lines under treatment with100 ng/mL of Tm after 16 and 24 hours suggesting an increase of the RIDD.

Taken together, in loss and gain of function experiments we have demonstrated that HSP47 increased RNAase activity of IRE1α under ER stress conditions.

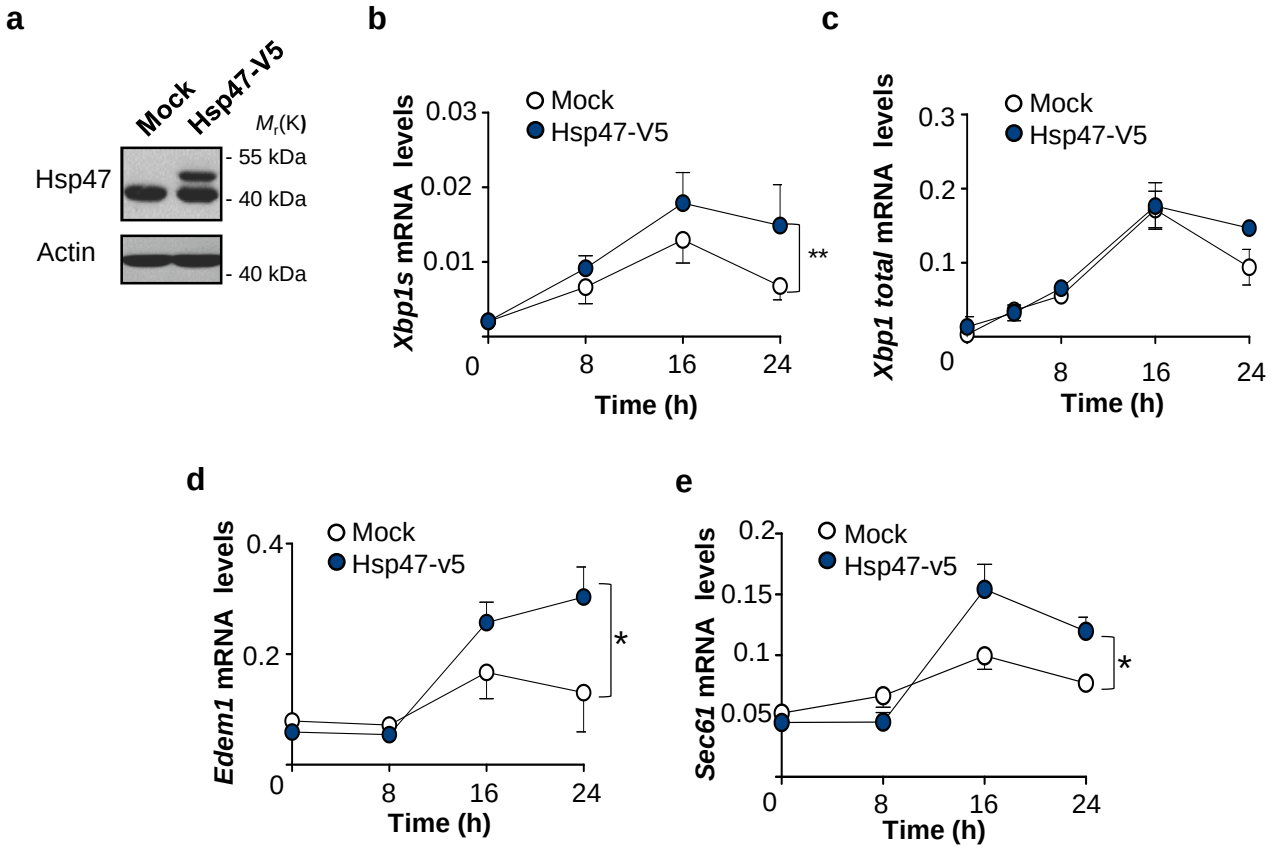

Figure 13. Hsp47 overexpression increase *Xbp1* mRNA splicing. MEF wild type cellls were stably transduced with retroviruses expressing the V5 tagged version of full-length HSP47 (HSP47-V5) or an empty vector as control (Mock). The levels of Hsp47 were evaluated from total protein extracts by Western blot, using a primary antibody that recognizes the endogenous Hsp47. Actin levels were monitored as loading control. Mock and Hsp47-V5 cell lines were treated with 10 ng/ml of Tm for indicated time points and mRNA levels of *Xbp1s* **(a)** total levels of *Xbp1* **(b)**, *Edem1* **(c)** and *Sec61* **(d)** were evaluated by real-time QPCR. Data represent the average and standard error of three independent experiments. Statistical analysis was performed using ANOVA. *: $p < 0.05$, **: $p < 0.01$.

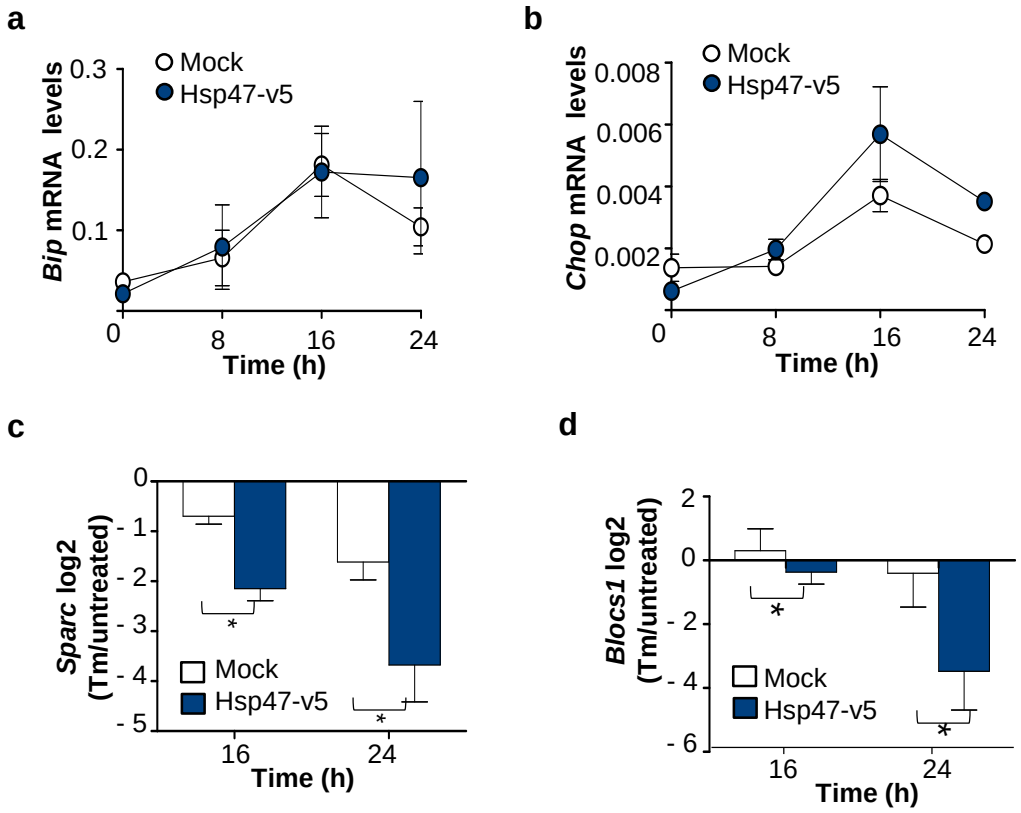

Figure 14. Hsp47 overexpression increase RIDD. MEFs WT were stably transduced with retroviruses expressing the V5 tagged version of full-length HSP47 (HSP47-V5). As control, cells were transduced with an empty vector (Mock). Mock and Hsp47-V5 cell lines were treated with 10 ng/ml of Tm for indicated time points and mRNA levels of *Bip* **(a)** and *Chop* **(b)**, were evaluated by real-time PCR. Mock and Hsp47-V5 cell lines were treated with 100 ng/ml of Tm for 16 and 24 h, and the mRNA decay of the IRE1α targets *Sparc* **(c)** and B*locs1* **(d)** was monitored by real-time PCR and normalized with respect to the levels of *Rpl19* as a housekeeping gene. Values were normalized with the mRNA levels under untreated conditions. All data represent the average and standard error of three independent experiments. Statistical analysis was performed using ANOVA. *: $p < 0.05$, **: $p < 0.01$.

11.3 Hsp47 modulates the activation of IRE1α: phosphorylation

The induction of *Xbp1* mRNA splicing is regulated at multiple levels [68], including ER stress sensing, IRE1α expression, IRE1α phosphorylation and oligomerization, in addition to the regulation of *Xbp1* mRNA possessing (i.e. RNAse activity, the RctB ligase or mRNA docking at the ER membrane). IRE1α activation involves its dimerization and phosphorylation, leading to a conformational change in the cytosolic region that engages the RNAse domain [23]. We used a Phostag assay to assess the phosphorylation status of IRE1α in MEFs. The treatment of Hsp47 silenced cells with Tm revealed a delay in the electrophoretic shift associated with its activation (Fig. 15a) suggesting a change in the phosphorylation status. In agreement with these results, overexpression of HSP47-V5 accelerated the activation process, reflected by an almost complete phosphorylation of IRE1α that was sustained over time (Fig. 15b). Importantly, total IRE1α levels were not significantly altered upon HSP47-V5 overexpression as determined using standard western blot analysis (Fig. 15b, bottom panel). These results suggest that HSP47 expression favored the phosphorylation of IRE1α-HA under ER stress conditions.

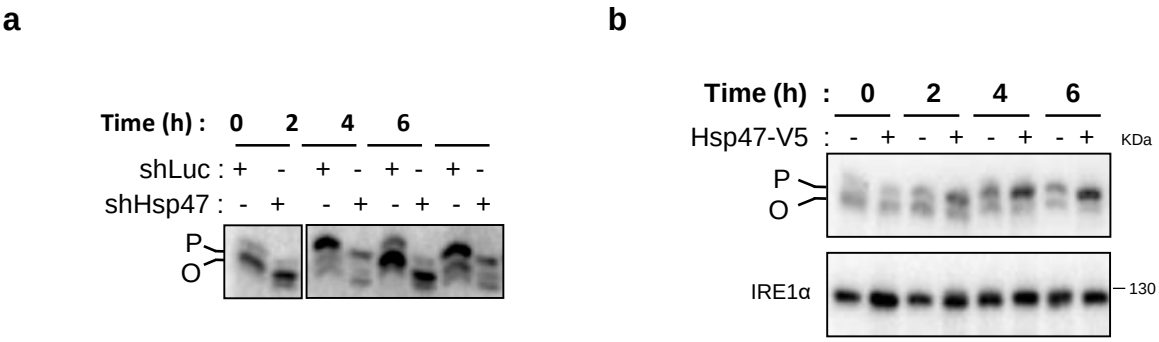

Figure 15. Hsp47 modulates the activation of IRE1α. (a) Stable knockdown cells for Hsp47 (shHsp47) and control cells (shLuc) in IRE1α-HA background were treated with 250 ng/ml of Tm for indicated time points and IRE1α phosphorylation levels were determined using the Phostag assay followed by Western blot analysis using anti-HA antibody. Upper band (P) represent phosphorylated IRE1α and bottom band (O) shown unphosphorylated IRE1α. **(b)** MEFs stably expressing Hsp47-V5 or empty vector (Mock) were treated with 250 ng/ml Tm for indicated time points and analyzed as described in (a). Total levels of IRE1α are also shown using standard western blot analysis.

11. 4 Hsp47 modulates the activation of IRE1α: oligomerization.

The dimerization and oligomerization of IRE1α into clusters of high molecular weight is associated with IRE1α phosphorylation and activity [73]. Therefore, we determined if HSP47 overexpression might impact IRE1α oligomerization. To this aim, we used a cellular system to visualize IRE1α oligomerization using the inducible expression of a GFP-tagged IRE1α protein in TREX cells (IRE1α-3F6H-GFP) [73] stably transduced with Mock or HPS47-V5 vector. The expression of IRE1α-GFP and HSP47-V5 were controlled by Western blot (Fig. 16a). To evaluate IRE1α oligomerization, both stable cell lines were platted and treated with 1 μg/mL of Tm for 4 h. Cells were fixed and visualized by confocal microscopy (Fig. 16b). As shown in figure 16b, we observed clustering of IRE1α in both cell lines treated with Tm. Visualization of GFP-positive foci revealed an increase in the number of IRE1α-GFP puncta in HSP47-V5 overexpressing cells after Tm treatment (Fig. 16b). Quantification of the number of IRE1α clusters per cell indicated a significant increase upon HSP47-V5 overexpression compared to control cells (Fig. 16c). Thus HSP47 generates changes in the IRE1α–GFP clustering. Taken together these results indicate that HSP47 expression increased the appearance of molecular events related to IRE1α activation in cells undergoing ER stress.

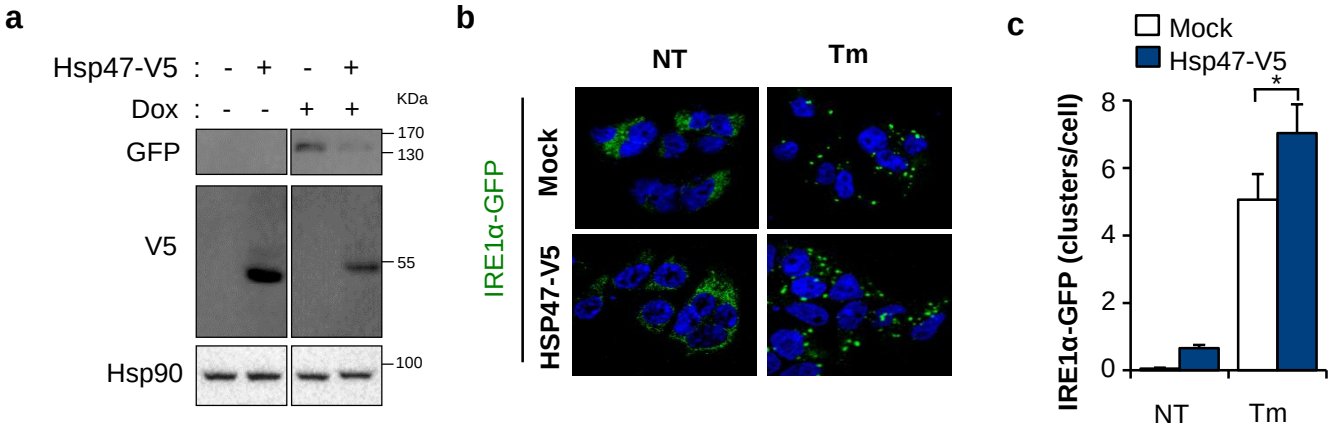

Figure 16. Hsp47 increases oligomerization the IRE1α. (a) TREX cells inducible expressing IRE1α-3F6H-GFP were stably transduced with retroviruses expressing the HSP47-V5. The levels of IRE1α-GFP and HSP47-V5 proteins were evaluated by western blot. Hsp90 levels were monitored as a loading control. **(b)** Cells were stably transduced with retroviruses expressing Hsp47-V5 or an empty vector (Mock) and treated with 1 μg/ml of Tm for 4 h. IRE1α-GFP cluster formation was visualized by confocal microscopy (upper panel). (**c**) Quantification of GFP-positive puncta per cell was performed using Image J software. Data represents the mean and standard error of three independent experiments. Statistical analysis was performed using ANOVA. *: $p < 0.05$

11.5 Hsp47 colocalizes with IRE1α.

According to our co-IP studies followed by spectrometry analysis, Hsp47 and IRE1α interact under basal conditions. In order to verify these findings we performed colocalization studies in order to evaluate the subcellular distribution of IRE1α and Hsp47 using immunofluorescence and confocal microscopy. Due to the lack of antibodies for IRE1α that work well in immunofluorescence, we performed this experiment using a stable cell line that expresses IRE1α-HA in a background of IRE1α null cells (Fig. 17a). As expected both proteins presented a reticular distribution, then we used a sensitive co-localization analysis using a confined displacement algorithm previously described to calculate the co-localization coefficients [89]. Quantification of Manders coefficient M1 and M2 indicated an average 0.32 and 0.35 index of co-localization respectively under basal conditions (Fig. 17b). The co-localization significantly decreased when cells are stimulated with 250 ng/mL of Tm for 6 hours. These results suggest that endogenous HSP47 co-localizes with IRE1α-HA on the perinuclear region at basal levels and this co-localization diminishes under ER stress.

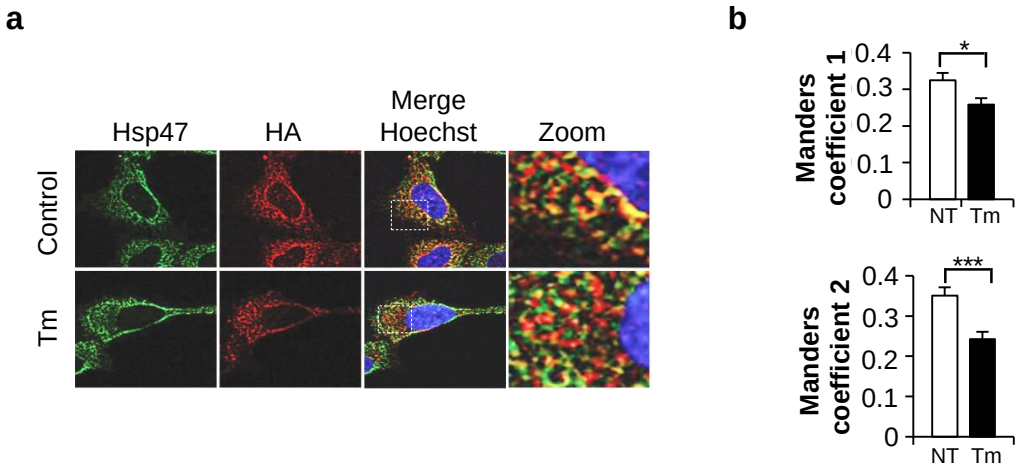

Figure 17. Hsp47 colocalizes with IRE1α. (**a**) Cells expressing IRE1α-HA were treated with 250 ng/mL of Tm for 6 h and then fixed. The distribution of endogenous Hsp47 and IRE1α-HA was assessed by indirect immunofluorescence (IF) and visualized using a confocal microscope. Nuclei were stained with Hoechst. (**b**) Images were deconvoluted and colocalization between Hsp47 and IRE1α-HA was calculated using Mander´s algorithm. Data show Manders coefficient 1 and 2. Data represents the average and standard error of three independent experiments. Statistical analysis was performed using ANOVA. *: $p < 0.05$, **: $p < 0.01$, ***: $p < 0.001$.

11. 6 Hsp47 interacts with IRE1α.

Then, we validated the physical interaction of endogenous Hsp47 with IRE1α on cells that expresses physiological levels of IRE1α. To this aim, we used IRE1α KO cells stably reconstituted with one copy of IRE1α-HA using a retroviral system. IRE1α-HA cells were treated or not with 250 ng/mL of Tm for 6 hours. After IP of HA-tagged IRE1α we assessed the possible co-immunoprecipitation of endogenous Hsp47. We observed that Hsp47 Co-IP with IRE1α at basal levels and this interaction is reduced when cells are exposed to Tm stimulus (Fig. 18a). Of note, similar results were observed in colocalization studies (Fig. 17). We were able to confirm the interaction between IRE1α-HA and HSP47 at basal levels whereas, in cells undergoing ER stress it a decrease in the interaction between IRE1α-HA and HSP47 was observed.

We moved forward to validate this interaction using an in situ proximal ligation assay (Duolink) in IRE1α KO cells reconstituted with IRE1α-HA to confirm if the interaction between IRE1α and HSP47 occurs. Fig. 18c shows representative images from cells treated or not with 250 ng/mL of Tm for 6 hours. As a control we used a knock down cell line for HSP47 that stably express a shRNA against *Hsp47* mRNA (Fig. 18b). We observed positive signals between anti-HA and anti-Hps47 antibodies suggesting protein interaction. The number of PLA puncta per cell decreased under Tm stimulus, validating the IP-mass experiments. Again, a positive interaction between Hsp47 and IRE1α was observed using this assay, a method that is predicted to have sensitivity for protein complexes in the range of 40 nm.

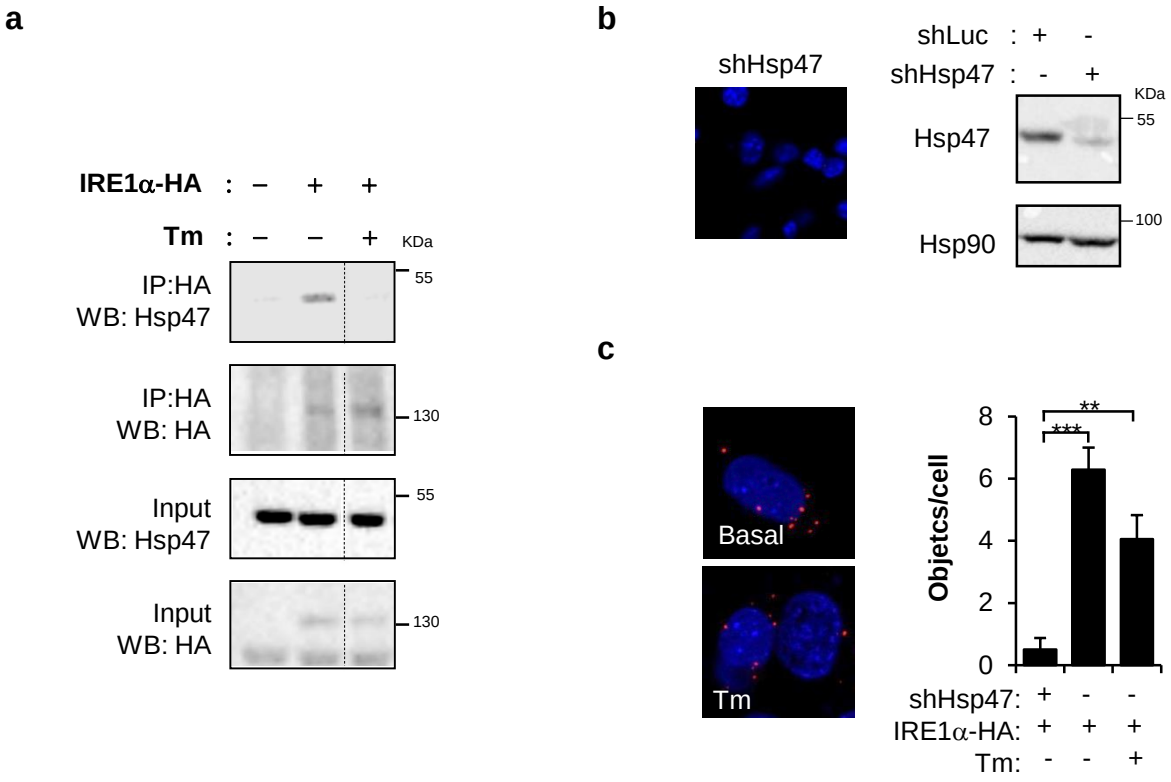

Figure 18. IRE1α interacts with Hsp47. (a) IRE1α deficient MEFs cells were stably transduced with retroviral expression vectors for IRE1α-HA or empty vector, and incubated for 6 h in presence or absence of 250 ng/ml of Tm. IRE1α-HA was immunoprecipitated followed by Western blot analysis of endogenous Hsp47. Total extracts (input) are shown as control. Dotted lines indicate splicing of images from the same gel and film exposure. **(b)** Cells shHsp47 were fixed in PFA 4%, permeabilized and blocked. The anti-HA (rabbit) and anti-Hsp47 (mouse) primary antibodies were incubated overnight and treated with Duolink® reagents to observe dots that represent the protein interaction in the range of 40 nm. Knockdown Hsp47 was confirmed in MEFs after western blot analysis. **(c)** IRE1α KO cells expressing IRE1α-HA were treated with 250 ng/mL of Tm by 6 h, fixed and endogenous Hsp47 and HA epitope were detected using Proximity Ligation assay (Duolink ®). As control, Hsp47 was knocked down using an shRNA. Confocal images were quantified using Image J software. Statistical analysis was performed using ANOVA. *: $p < 0.05$, **: $p < 0.01$, ***: $p < 0.001$.

11. 7 Hsp47 interacts with high affinity to the luminal domain of IRE1α.

Based on the subcellular distribution of Hsp47, we then performed immunoprecipitation experiments in cells expressing an IRE1α deletion mutant containing only the N-terminal luminal domain (NLD). To confirm that HSP47 binds to the ER luminal domain of IRE1α, we performed an IP using an anti-HA antibody in total lysate from MEFs IRE1α KO cells stably reconstituted with IRE1α–NLD-HA. After immunoprecipitation of HA-tagged NLD-IRE1α we assessed the possible co-immunoprecipitation with endogenous Hsp47 (Fig. 19a). Notably, a positive interaction was observed between the luminal domain of IRE1α and Hsp47. These results support an interaction between Hsp47 and IRE1α, restricted at the ER lumen.

To further validate this interaction, we also tested the interaction by pull-down assays in COS-1 cells transfected with vectors encoding the NLD of IRE1α fused with a poly-histidine sequence (His-IRE1α-NLD) and the human HSP47 pCAGGS mammalian expression vectors. Total lysates were incubated with Ni-NTA-Agarose beads (Qiagen) and the presence of Hsp47 was determined by WB. Again, a strong association between these two proteins was observed in three independents experiments (Fig. 19b).

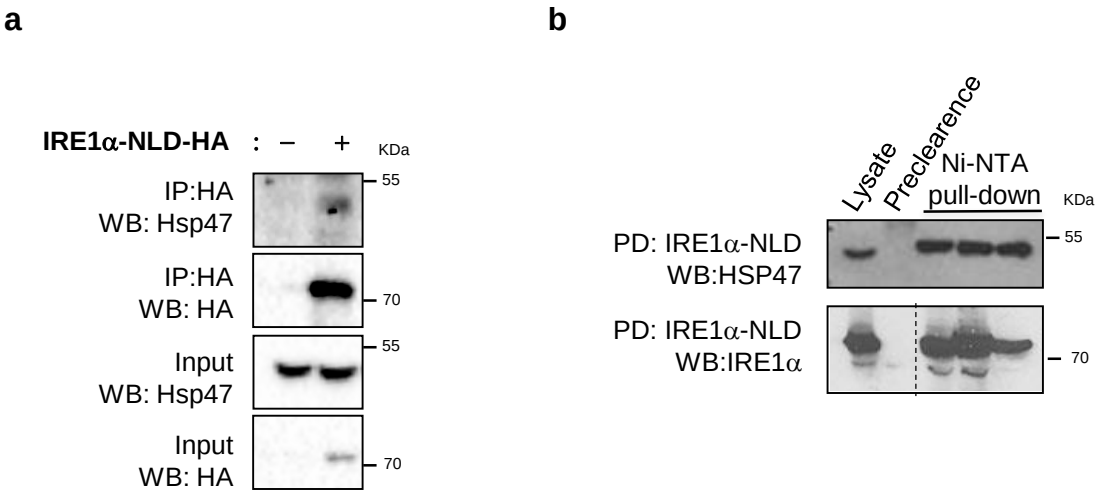

Figure 19. Hsp47 interacts with the luminal domain of IRE1α. (a) IRE1α KO cells were stably transduced with retrovirus expressing a deletion mutant of IRE1α-HA in the cytosolic region (IRE1α-NLD-HA). HA was immunoprecipitated followed by western blot analysis of Hsp47. Total extracts (input) are shown as control. **(b)** COS-1 cells were transiently transfected with a HIS-tagged version of the ER luminal domain of IRE1α (IRE1α-NLD) and the human HSP47 pCAGGS mammalian expression vector, followed by a pull-down with Ni-NTA-agarose beads. The presence of HSP47 was assessed by western blot analysis. Each lane represents an independent pull-down experiment. Dotted line indicates splicing of images from the same gel and film exposure.

All our results suggest the formation of a protein complex between IRE1α and Hsp47. In order to evaluate a direct interaction between these two proteins, in collaboration with Dr. Marek Michalak and his team from University of Alberta in Canada, we developed different biochemistry strategies to determine the physical interaction. To purify IRE1α-NLD (luminal domain of IRE1α) protein, from COS-1 cells transfected with the pED-IRE1-NLD-His6-KDEL. Human HSP47 was cloned into pET-21a containing a 6HIS tag for expression in LEMO21 *E. coli* cells and then purified using a Resource-Q column.

Surface plasmon resonance (SPR) technology was employed to monitor the interaction of purified HSP47 and IRE1α-NLD protein (BIACore T200, GE) (Fig. 20a). This approach is based on a chip that detects the weight that passes thought it, causing a change in refractive index of light. This technology is often used to validate protein interaction *in vitro*. Therefore, SPR BIACore analyses of HSP47 interaction with IRE1α-NLD was performed. The experimental results were corrected against the control surface response to remove any refractive index deviations. Kinetic analyses were carried out with the BiaEvaluation software (GE). Association and dissociation rates and affinity (KD) were calculated for each experiment and the average is shown in table 2.

In order to verify these findings, another biochemical approach was carried out named MicroScale Thermophoresis (MST) using a Monolith NT.115 instrument (NanoTemper Technologies GmbH) (Fig. 20b). In brief, if the two proteins interact, the water shells around the complex changes, causing the complex to move faster or slower when the solution is heated by a laser. This movement is monitored by one of the proteins labeled with a fluorescent tag (IRE1α-NLD has a red tag covalently linked). By this means, if there is an interaction, it is possible to detect the change in the height (fluorescence) of the curves. To evaluate HSP47 binding to IRE1α-NLD, an increasing concentration of purified HSP47 protein (0-10000 nM) was incubated with 200 nM RED-labeled IRE1-NLD protein. The reverse was also

performed, with 200 nM RED-labeled HSP47 incubated with an increasing concentration of purified IRE1α-NLD (0-10000 nM) (data not shown). Data evaluation was performed using the Monolith software as well as Origin graphing software. All MTS and SPR experiments were performed independently more than three times.

BiP and PDIA6 have been reported to bind to the luminal domain of IRE1α controlling its activation and inactivation process [7, 22, 60]. To determine if HSP47 directly interacts with IRE1α, we used the two sensitive *in vitro* binding assays described before. Calculation of the dissociation constant (KD) revealed a high affinity between HSP47 and IRE1α-NLD of 73.2 nM (Table 2). This data was further confirmed using surface plasmon resonance to determine the biophysical parameters of the interaction. The affinity detected between the two proteins was again in the nanomolar range (Table 2). We then compared the strength of the interaction between HSP47 and IRE1α-NLD with the affinity for BiP or PDIA6. In this experimental setting recombinant BiP associated with the luminal domain of IRE1α with a KD value of 39.7 nM, in the same range as recombinant HSP47. In contrast, PDIA6 displayed a lower binding affinity to IRE1α-NLD under the same experimental conditions (Table 2). Actinin was used as a negative control, which did not show any detectable binding to IRE1α-NLD (not shown). In summary, our combinatorial approaches suggest that HSP47 forms a complex with the luminal domain of IRE1α through a direct interaction.

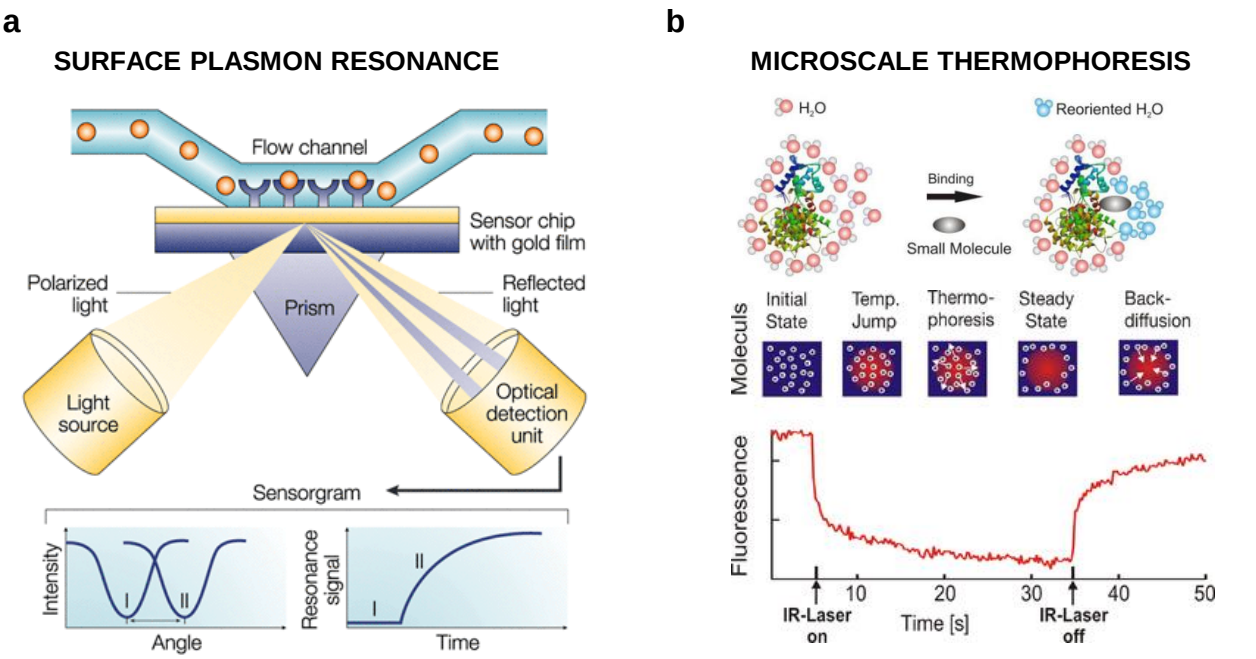

Cooper M. (2002). Nature Reviews Drug Discovery

Nature Reviews|Drug discovery

Figure 20. Surface plasmon resonance (SPR) and Microscale thermophoresis (MST). (**a**) SPR enables high sensitivity, label-free detection, real-time monitoring, low volume sample consumption, quantitative evaluation, and determination of kinetic rate constants. Furthermore, SPR is easy to perform and can be a cost-effective solution. Basic components of an instrument for SPR biosensing: A glass slide with a thin gold coating is mounted on a prism. Light passes through the prism and slide, reflects off the gold and passes back through the prism to a detector. Changes in reflectivity versus angle or wavelength give a signal that is proportional to the volume of biopolymer bound near the surface. A flow cell allows solutions above the gold surface to be rapidly changed. (**b**) MST is a powerful method to quantify biomolecular interactions. It measures the motion of molecules along microscopic temperature gradients and detects changes in their hydration shell, charge or size. Any change of the hydration shell of biomolecules due to changes in their primary, secondary, tertiary and/or quaternary structure affects the thermophoretic movement and is used to determine binding affinities with high accuracy and sensitivity. When performing a MST experiment, a microscopic temperature gradient is induced by an infrared laser, and the directed movement of molecules is detected and quantified using either covalently attached dyes, fluorescent fusion proteins or intrinsic tryptophan fluorescence. The applications range from small-molecule binding events to protein-protein interactions and interactions of multi-protein complexes.

	SPR			MTS
	Ka (1/Ms)	**Kd (1/s)**	**KD (nM)**	**KD (nM)**
BIP	$2.09 \times 10^{12} \pm 1.47 \times 10^{12}$	$7.75 \times 10^{4} \pm 5.46 \times 10^{4}$	39.7 ± 1.6	-
PDIA6	$4.29 \times 10^{3} \pm 5.48 \times 10^{1}$	$7.21 \times 10^{-4} \pm 3.53 \times 10^{-6}$	168 ± 1.6	-
HSP47	$5.74 \times 10^{3} \pm 5.18 \times 10^{2}$	$4.15 \times 10^{-4} \pm 3.15 \times 10^{-6}$	74.9 ± 7.33	73.2 ± 8.4

Ka: equilibrium association constant; Kd: equilibrium dissociation constant; KD: affinity constant; SPR: surface plasmon resonance; MTS: microscale thermophoresis

Table 2. HSP47 interacts with high affinity to the ER luminal domain of IRE1α. Surface plasmon resonance (SPR) or MicroScale thermophoresis (MST) were employed to monitor the interaction between recombinant HSP47 with purified IRE1α-NLD protein from COS-1 cells. For the SRP assay, binding affinity was also compared with the binding of recombinant BiP or PDIA6 to IRE1α-NLD. For SPR, experimental results were corrected against the control surface response to remove any refractive index deviations. Kinetic analyses were carried out with the BiaEvaluation software (GE) using a 1:1 Langmuir binding model and were performed in triplicate. Association and dissociation rates and affinity (KD) were calculated for each experiment and averaged.

11. 8 Hsp47 reduce the binding of BiP to the luminal domain of IRE1α.

BiP is a major adjustor of the UPR possibly by negatively controlling the activation of IRE1α [53], in addition to PERK and ATF6. Because Hsp47 enhances IRE1α oligomerization, we decided to explore its possible modulatory effects on the binding of BiP to the ER luminal domain to IRE1α. To test this hypothesis, we transiently expressed His-IRE1α-NLD in COS-1 cells followed by HIS pull-down and western blot analysis. Overexpression of HSP47 significantly reduced the association of BiP with His-IRE1α-NLD (Fig. 21a). In the same experiments, no effect of HSP47 overexpression were observed on the interaction between PDIA6 and the luminal domain of IRE1α (Fig. 21b). We confirmed the consequences of HSP47 on the binding of BiP to IRE1α in vitro using the MST. We incubated increasing concentrations of recombinant BiP (0 - 10^5 nM) with RED-labeled His-IRE1α-NLD (200 nM) in the presence or absence of recombinant HSP47 (500 nM). Using this approach we observed a strong reduction in the binding of BiP to the luminal domain of IRE1α when HSP47 was present (Fig. 21c).

We then tested the possible impact of HSP47 on the oligomerization status of IRE1α-NLD by *in vitro* binding assay. We incubated RED-labeled IRE1α-NLD with an increasing concentration of unlabeled-IRE1α-NLD (0 - 10^5 nM) in the presence or absence of recombinant HSP47 and performed MST. Unexpectedly, using this approach we observed increased dimerization/oligomerization of IRE1α-NLD in vitro only when HSP47 was present in the reaction (Fig. 22a). Importantly, under this experimental condition, RED-labeled-IRE1α-NLD did not oligomerize spontaneously when increasing concentration of IRE1α-NLD were added to the assay in the absence of purified HSP47 (Fig. 22b). Taken together, these results suggest that HSP47 regulates IRE1α activation by favoring the release of BiP from the complex and probably stabilizing the IRE1α dimerization/oligomerization.

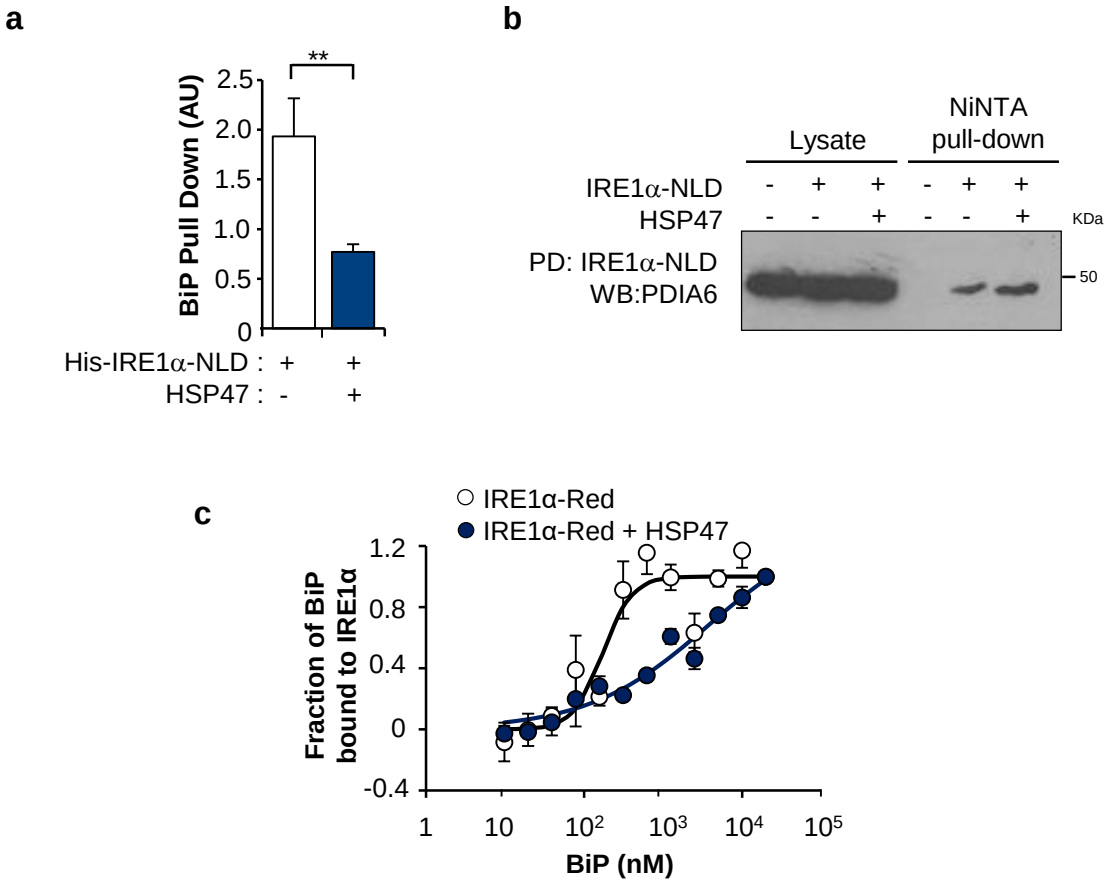

Figure 21. Hsp47 reduces the binding of BiP to the luminal domain of IRE1α. (**a**) COS-1 cells were transfected with His-tagged IRE1α-NLD expression vector in the presence or absence of an HSP47 expression vector. After 72 h cells were lysed and pulled-down using Ni-NTA-agarose beads. The presence of BiP in the complex was analyzed by Western blot and quantified. Normalization was performed with signal in total extracts and the amount of IRE1α pulled down. (**b**) Control experiment for pull-down assays: COS-1 cells were transiently transfected with a HIS-tagged version of the ER luminal domain of IRE1α (IRE1α-NLD-His6-KDEL) in the presence or absence of Hsp47 followed by a pull-down with Ni-NTA-agarose beads. The presence of PDIA6 was assessed in the pull-down using western blot analysis. (**c**) MicroScale thermophoresis (MST) were employed to monitor the interaction between recombinant BiP with purified IRE1α-NLD. Increasing concentrations of recombinant BiP protein (0-1 x 10^5 nM) was incubated with Red-labeled IRE1α-NLD protein in the presence or absence of 500 nM recombinant HSP47. MST was used to evaluate BiP binding to IRE1α-NLD.

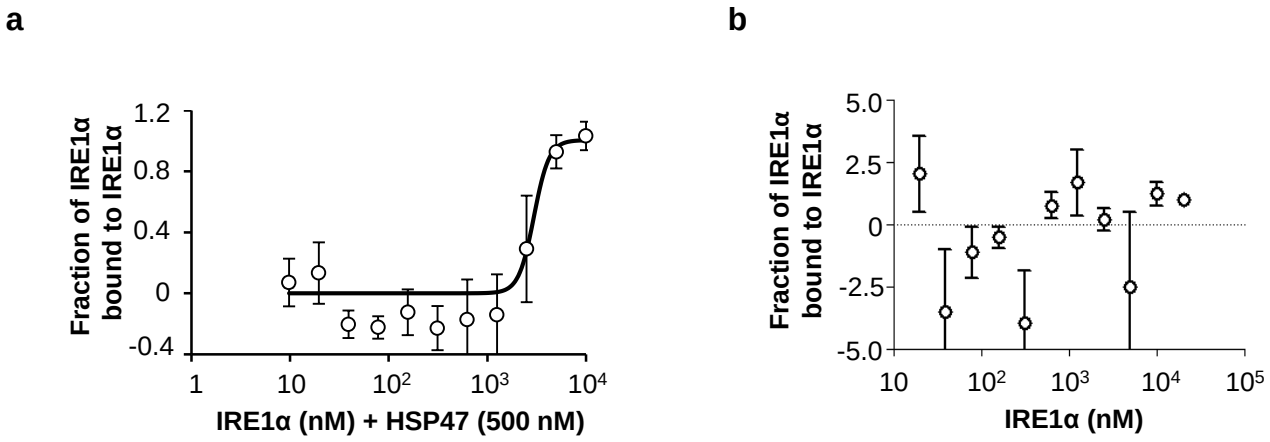

Figure 22. Hsp47 induces IRE1α dimerization/oligomerization. MicroScale thermophoresis (MST) was employed to monitor the interaction between IRE1α-NLD molecules. IRE1α-NLD-RED-labeled with an increasing concentration of unlabeled-IRE1α-NLD (0-10^5 nM) in the (**a**) presence or (**b**) absence of 500 nM of recombinant HSP47 and MST was used to evaluate IRE1α-NLD dimerization/oligomerization status. .

11.9 Hsp47 deficiency reduces IRE1α/XBP1 signaling and viability in *Drosophila Melanoganster*.

Because the UPR machinery is highly conserved in flies, this model has been widely used to investigate novel genes that participate in the ER stress response [90, 91]. We previously set up simple bioassays to trigger ER stress in vivo in *D. melanogaster* larvae to monitor UPR signaling, in addition to determine the survival of whole animals to the exposure of Tm [48, 84, 85]. *D. melanogaster* expresses collagen like-proteins and thus it is expected to contain an HSP47 homologue on its genome. Analysis of *D. melanogaster* DNA databases indicated the presence of a putative homologue of HSP47 in identified as CG8137 (here termed dHsp47; Fig. 24a and see sequence and secondary structure analysis in Fig. 25 and 26 respectively). We knocked down dHsp47 *in vivo* by expressing specific RNAi constructs using the UAS-GAL4 system under the control of a tubulin driver promoter to express in all tissues of larvae [92] (Fig. 23a), then males UAS-RNAi were crossed to females Tub-Gal4/TM3-GFP flies. Third instar GFP-positive larvae (not expressing the RNAi) were separated from GFP-negative larvae (expressing the RNAi) and fed separately with Tm or the vehicle (DMSO) to evaluate gene expression (Fig. 23b). This system led to 50% knockdown of *dHsp47* mRNA in fly larvae as measured by real time qPCR in total mRNA extract from third stage larvae (Fig. 24b).

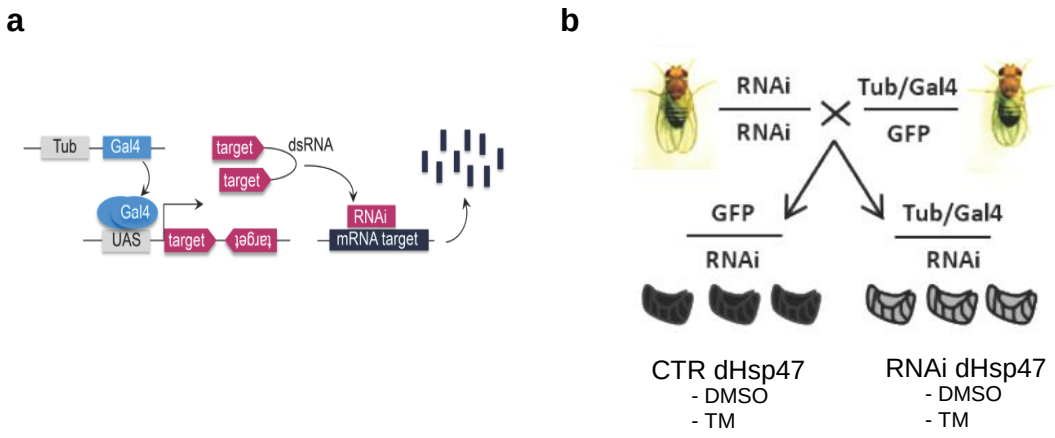

Figure 23. Experimental strategy in *Drosophila Melanogaster* model. The UPR machinery is highly conserved in flies and this model has been widely used to validate genes that control the UPR or apoptosis under ER stress [85]. (**a**) dHsp47 was knocked down *in vivo* by expressing specific RNAi constructs using the UAS-GAL4 system under the control of a tubulin driver promoter to express in all tissues of larvae. (**b**) Flies were kept at 25°C on standard medium with a 12–12 dark-light cycle. The line Tub-Gal4/TM3-GFP and UAS-RNAi SRP2 (CG8137) were obtained from Bloomington Drosophila Stock Center and VDRC (Vienaa Drosophila RNAi Center) respectively. For the RNAi experiments, males UAS-RNAi were crossed to females Tub-Gal4/TM3-GFP flies. Third instar GFP-positive larvae (not expressing the RNAi) were separated from GFP-negative larvae (expressing the RNAi) and fed separately with Tm or the vehicle (DMSO) to evaluate gene expression. In survival experiments, we used adult flies under basal or ER stress conditions.

a

Mammalian protein	HSP47
D. Melanogaster	
Symbol	CG8137
Name	Serpin 28F
Identity to H.s.(%)	27%
Similitude to H.s.(%)	47%

b

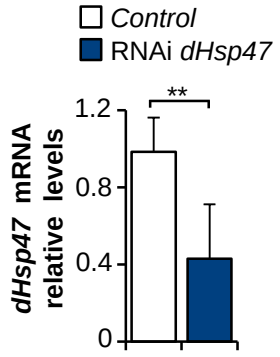

Figure 24. Downregulation of the putative homologue of Hsp47 in *D. melanogaster*. **(a)** Summary of the sequence analysis of the putative homologue of Hsp47 in *D. melanogaster* (dHsp47). **(b)** dHsp47 was knocked down *in vivo* (Experimental design Fig. 23) and the mRNA levels of *dHsp47* were monitored by real time qPCR from total extracts prepared from early third instar larvae. Mean and standard error is presented from three independent experiments. Statistical analysis was performed using ANOVA. **: $p < 0.01$.

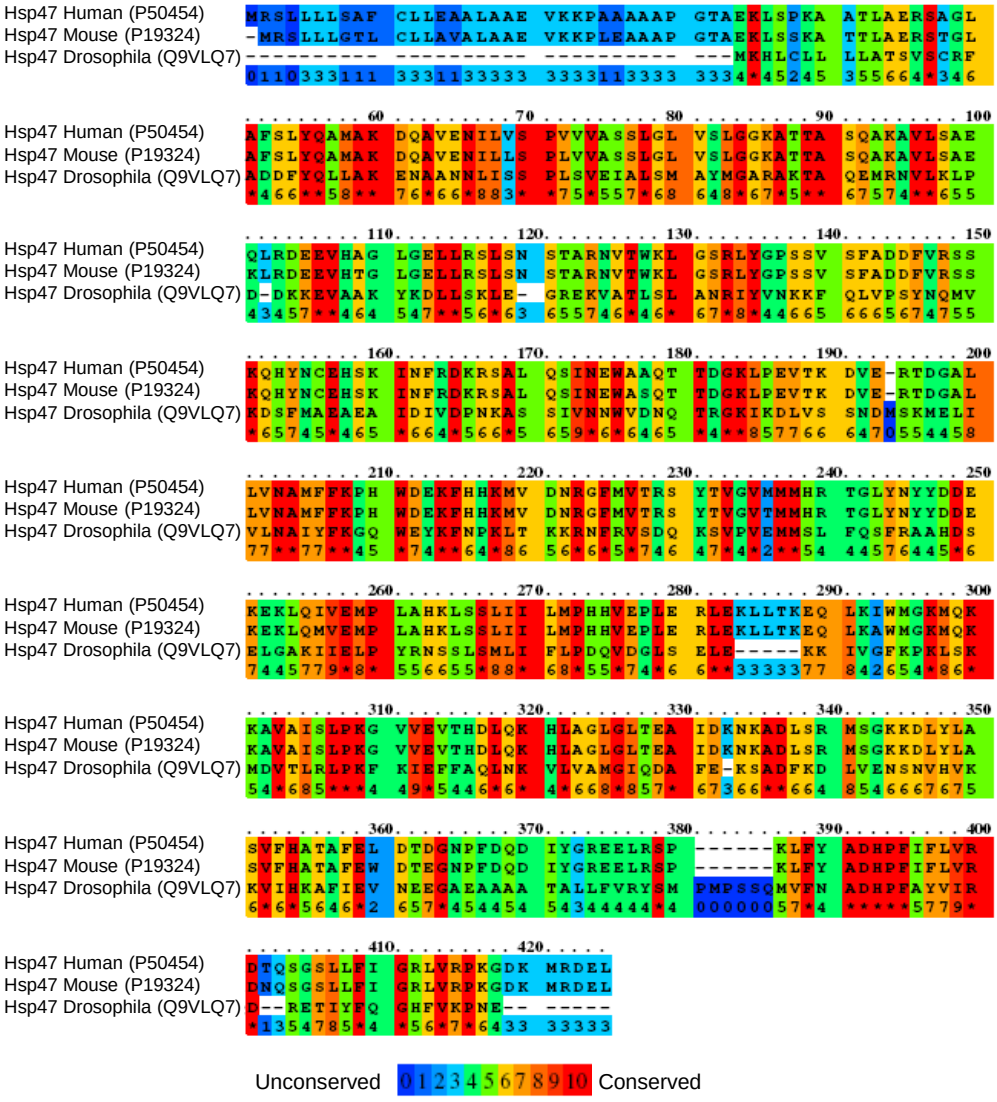

Figure 25. Identification of an HSP47 homologue in *D. melanogaster*. Aminoacid sequence alignment of Hsp47 from *H. sapiens*, *M. musculus* and *D. melanogaster* using PRALINE with BLOSUM62 scoring matrix. Color scale from unconserved (blue) to conserved (red) aminoacids.

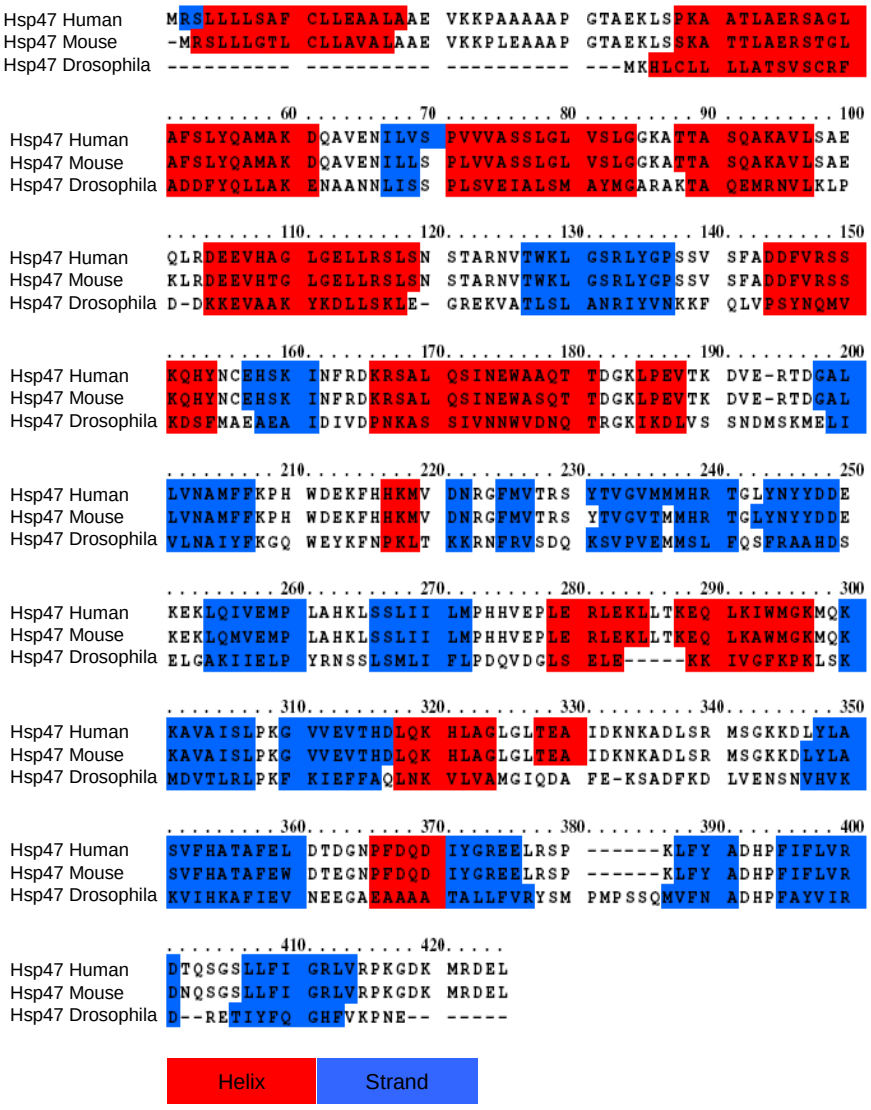

Figure 26. Identification of an HSP47 homologue in *D. melanogaster*. Predicted secondary structure alignment of Hsp47 from *H. sapiens*, *M. musculus* and *D. melanogaster* using PRALINE.

Then, we determined the consequences of down regulate dHsp47 on *dXbp1* mRNA splicing. To this aim, we exposed third stage larvae to Tm for 24 h. A significant reduction in the spliced form of *dXbp1* was observed upon reducing dHsp47 levels as assessed by conventional RT-PCR (Fig. 27a) or real time qPCR (Fig. 27b). We then performed time course experiments and confirmed that knocking down dHsp47 using RNAi had a dramatic effect on the activation of dIRE1α signaling (Fig. 27c). We also measured the expression levels of Heat Shock Cognate 3 chaperone (Hsc3), a target gene of dXBP1 [93]. Consistent with our previous results, an attenuated induction of Hsc3 mRNA was detected in dHsp47 RNAi larvae compared to control animals (Fig. 27d). We also monitored RIDD activity by quantifying the mRNA levels of *Sparc* and *Mys*, two dIRE1α substrates previously described in *D. melanogaster* [94, 95]. As shown, the decay of *Sparc* (Fig. 28a) and *Mys* (Fig.28b) mRNA levels was fully blocked by knocking down dHsp47, observing even the upregulation in dHsp47 deficient animals treated with Tm.

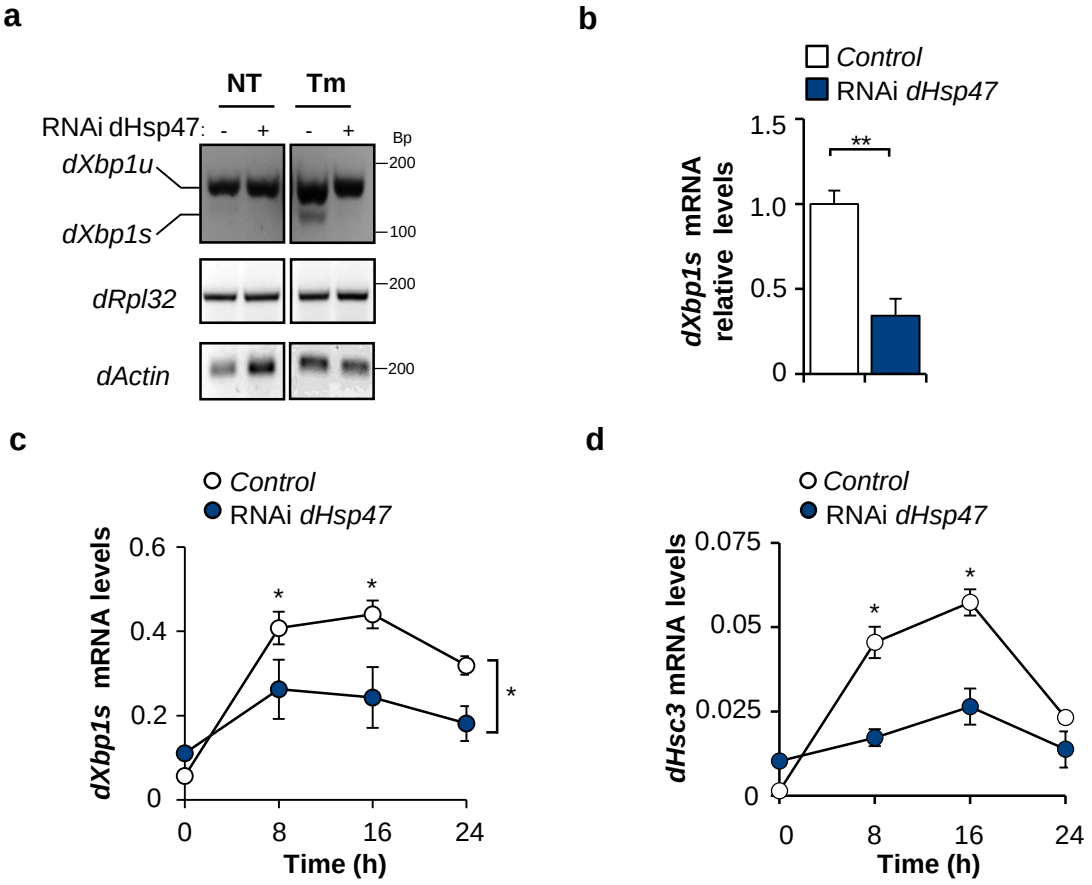

Figure 27. Hsp47 increases IRE1α signaling in *D. melanogaster*: *Xbp1* mRNA splicing. (a) Early third instar larvae of control and RNAi dHsp47 fly lines were grown under standard feeding conditions supplemented with 25 µg/mL of Tm. After 16 h larvae were collected and *dXbp1* mRNA splicing determined by RT-PCR. *dRpl32* and *dActin* were monitored as loading controls. **(b)** Early third instar larvae of control and dHsp47 RNAi fly lines were grown in the presence of 25 µg/mL of Tm for 8 h, and *dXbp1s* mRNA levels monitored by real time qPCR using cDNA prepared from total RNA extracts. Data was normalized to control and represents the mean and standard error for three independent experiments. **(c,d)** Animals were treated as described in (b). for indicated time points and the mRNA levels of *dXbp1s* **(c)** or *dHsc3* **(d)** were evaluated by real time qPCR. Data represents the mean and standard error of at least three independent experiments. Statistical analysis was performed using ANOVA. *: $p < 0.05$, **: $p < 0.01$.

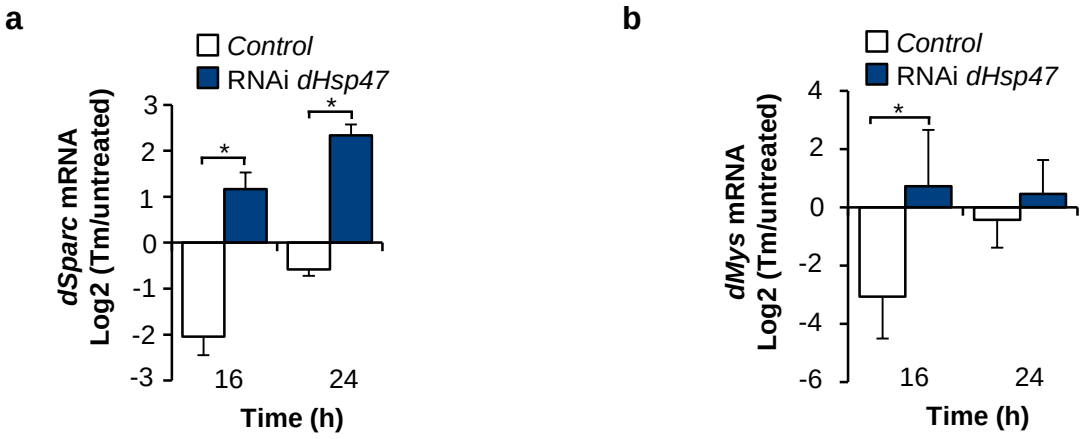

Figure 28. Inhibition Hsp47 expression decreases RIDD in *D. melanogaster*. (a, b) Early third instar larvae of control and RNAi dHsp47 fly lines were grown under standard feeding conditions supplemented with 25 µg/mL of Tm for 16 and 24 h, the mRNA levels of *dSparc* **(a)** and *dMys* **(b)** were evaluated by real time qPCR as previously described. Data was normalized to non-treated larvae and the mRNA of *dRpl32* was used as housekeeping gene. Data represents the mean and standard error for three independent experiments. Statistical analysis was performed using ANOVA. *: $p < 0.05$.

We then monitored the life span of adult *D. Melanogaster* exposed to 25 μg/mL Tm administered to lyophilized food or the equivalent concentration of DMSO. We quantified the number of dead flies over time after exposure to the ER stress-inducing agent (Fig. 29a). Remarkably, knocking down dHsp47 significantly reduced the survival of flies exposed to Tm (Fig. 29b). Importantly, at basal levels targeting dHsp47 did not result in spontaneous defects in animal survival (29c). In summary, these results suggest that dHsp47 controls IRE1α signaling *in vivo* in a fly model of ER stress, and influences the capacity of the whole animal to adapt and cope with alterations to ER proteostasis.

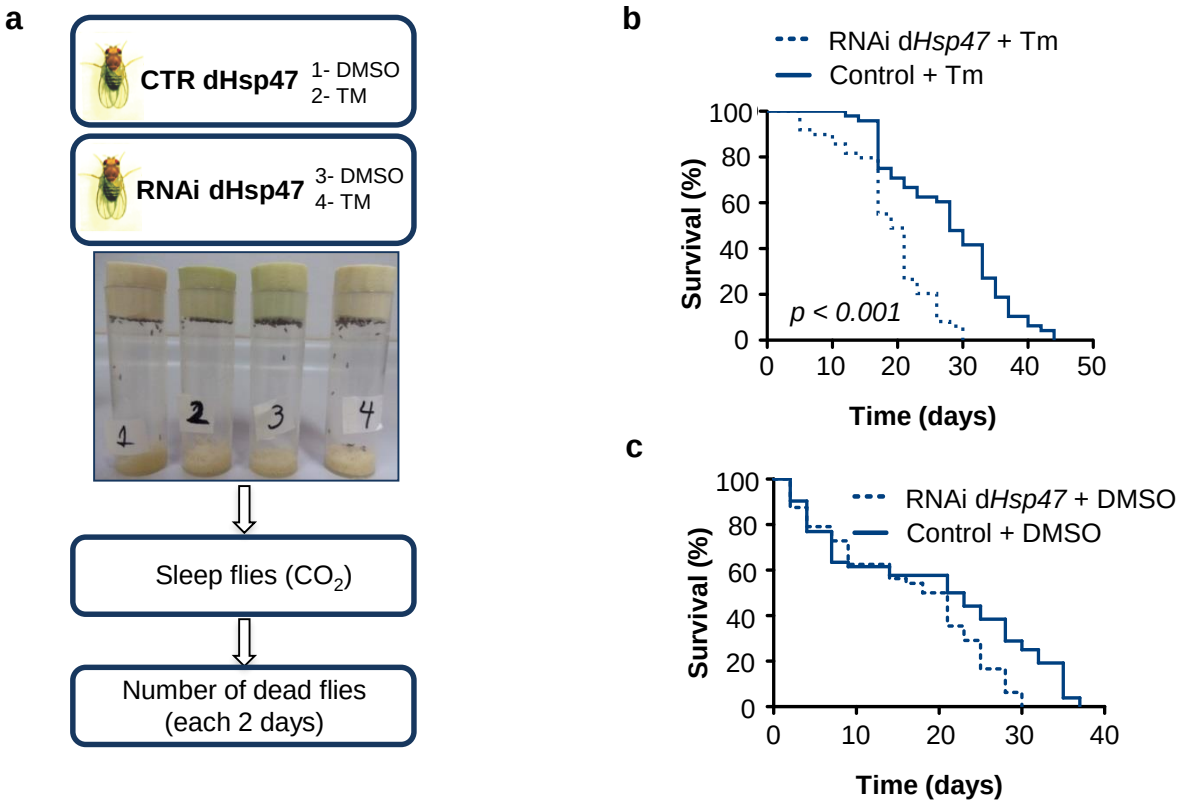

Figure 29. Inhibition Hsp47 expression decreases survival in *D. melanogaster*. (a) The life span of adult *D. Melanogaster* exposed to Tm administered to lyophilized food or the equivalent concentration of DMSO was monitored. We quantified the number of dead flies over time after exposure to the ER stress-inducing agent. **(b)** 50 control and 50 RNAi dHsp47 adult flies were grown in standard feeding conditions in presence of 25 µg/mL of Tm. **(c)** 50 control and 50 RNAi dHsp47 adult flies were grown in standard feeding conditions in presence of DMSO. The number of viable flies was calculated over time by counting dead flies.. Statistical analysis performed using the Kaplan-Meyer and log-rank (Mantel-cox) test.

11.10 Hsp47 regulates IRE1α signaling in a mouse model of ER stress.

A classical paradigm of ER stress in mammals is the injection of mice with a single dose of Tm, which triggers a strong UPR in the liver and kidney. We have previously used this model to dissect mechanisms underlying the activation and attenuation of IRE1α signaling [48, 64, 65]. We generated a conditional knockout (cKO) mouse model of Hsp47 in the liver using the Cre-LoxP system to delete exon 6 in hepatocytes with a tamoxifen-inducible system driven by the transthyretin promoter (TTR-Cre ind) (Fig. 30a). We treated adult animals with tamoxifen for five consecutive days and confirmed the deletion of Hsp47 in the liver using PCR of genomic DNA one week later (Fig. 30b). We calibrated the concentrations of Tm after intraperitoneal injection to avoid saturation of the *Xbp1* mRNA splicing assay and defined a concentration of 50 ng of Tm per gram of animal for injections. Kinetic analysis of IRE1α signaling in the liver revealed a transient induction of *Xbp1* mRNA splicing after Tm injection that was then attenuated over time. At 6 h post treatment almost full splicing was observed in both genotypes, whereas a clear reduction in the levels of splicing was observed in Hsp47cKO animals after 16 h of Tm treatment when compared to littermate control floxed mice (Fig. 31a). Quantification of these experiments indicated a significant attenuation of Xbp1 mRNA splicing in Hsp47cKO mice treated with Tm (Fig. 31b). The inhibitory effects of Hsp47 ablation were confirmed when *Xbp1s* mRNA levels were measured by real time qPCR (Fig. 31c). As an internal control for these experiments we analyzed the kidney of the same animals because of the lack of Hsp47 gene deletion in this organ by the TTR-Cre ind system. No effects were observed on the levels of *Xbp1s* in the kidney of Hsp47cKO mice (Fig. 31d), indicating that Tm treatments were equally effective in inducing an ER stress response in both experimental groups.

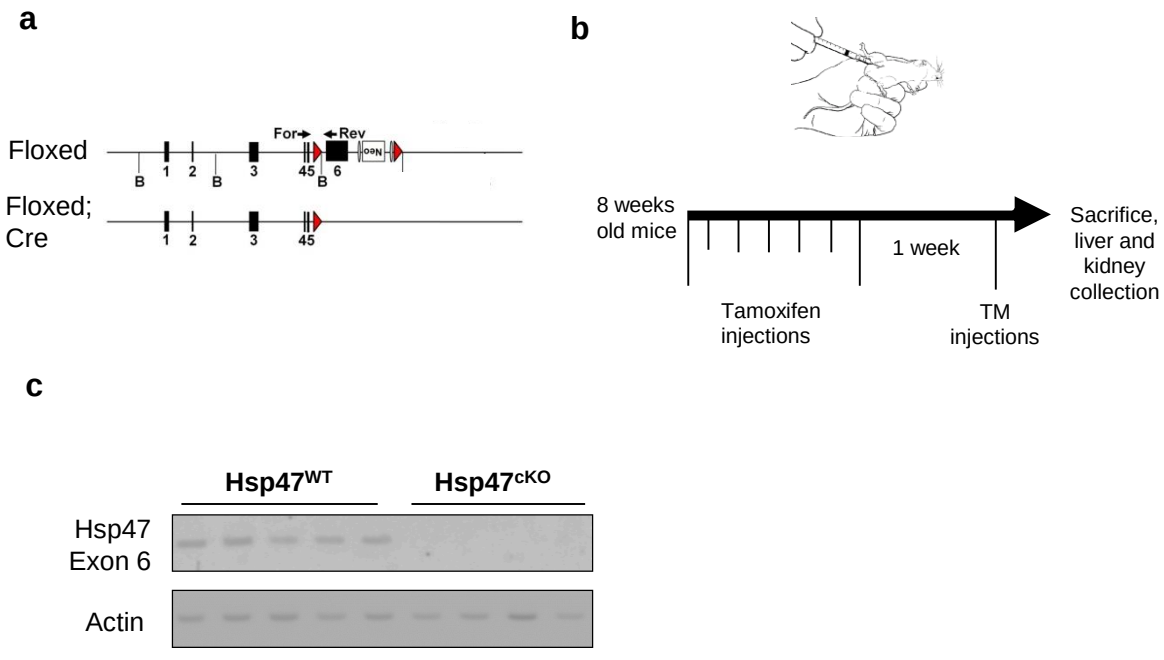

Figure 30. Conditional deficiency of Hsp47 in the liver mouse model. (**a**) Conditionally knockout (cKO) mice for the Hsp47 gene was generated in hepatocytes using LoxP system and a TTR-inducible Cre line. The Cre-loxP system was used to disrupt the Hsp47 gene in a tissue-specific manner using a transgenic mouse harboring a floxed Hsp47 gene in which the exon-6-containing region was flanked by loxP sites. Exon 6 is the final exon that encodes approximately 24% of the amino acid sequence of Hsp47, including a region essential for binding to collagen and a poly(A) signal. Breeding homozygous Hsp47 floxed and TTR-Cre ind mice resulted in double-heterozygous animals. Then, animals were mated with Hsp47 floxed homozygous mice to obtain animals with the TTR–Cre ind transgene with two Hsp47 floxed alleles. Mice were used for experiments after backcrossing with C57BL/6 mice for at least eight generations. (**b**) Experimental design: 8 weeks-old animals were injected intraperitoneally with 1 mg of tamoxifen for 5 consecutive days and 1 week later we performed TM injections for 6, 16 and 24 h. Finally, mice were sacrificed to extract liver and kidney to perform gen expression and histological analysis (**c**) Adult animals $Hsp47^{WT}$ and $Hsp47^{cKO}$ were treated with tamoxifen for five consecutive days and confirmed the deletion of Hsp47 in the liver using PCR of genomic DNA one week later. Actin was amplified as the internal control.

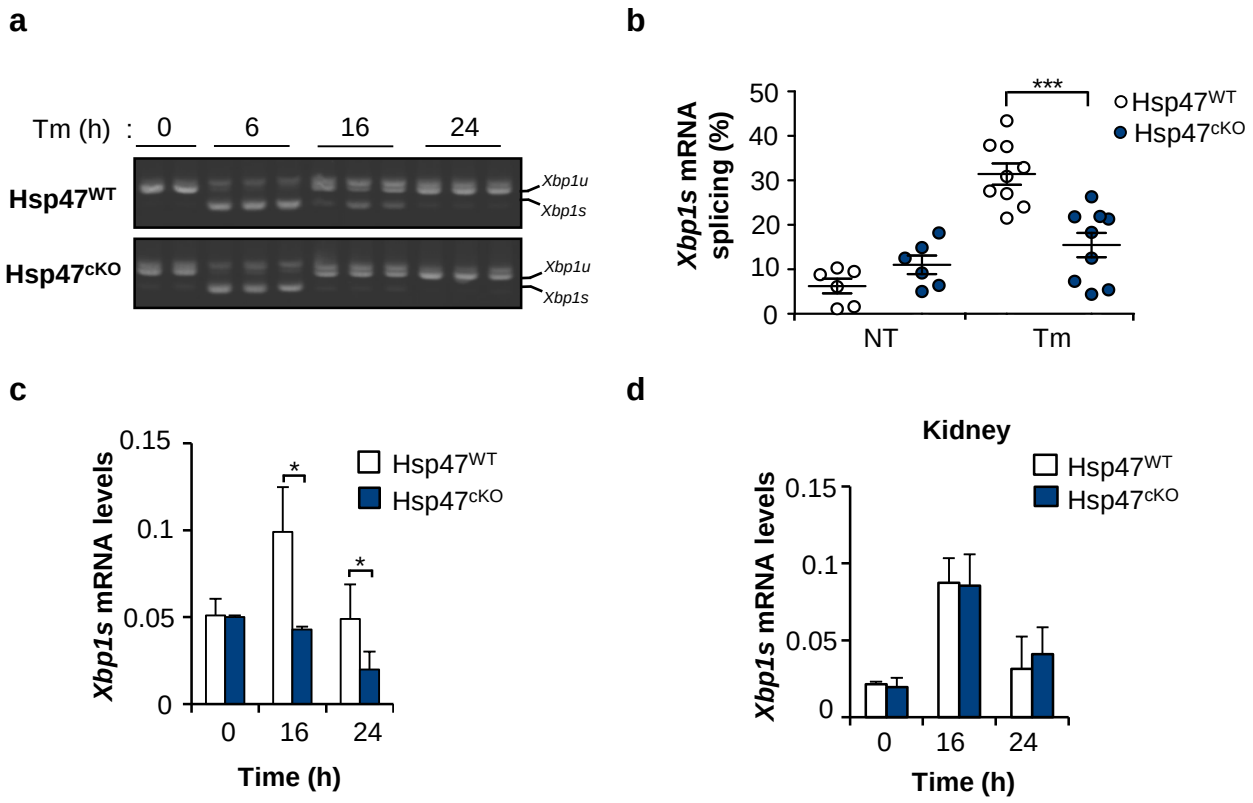

Figure 31. Conditional deficiency of Hsp47 in the liver mouse attenuates IRE1α signaling under ER stress *in vivo*: *Xbp1* mRNA splicing. (**a**) Hsp47WT or Hsp47cKO mice were injected with Tm (50 ng/g, i.p.) and sacrificed after 6, 16 and 24 h. The levels of *Xbp1* mRNA splicing was monitored by RT–PCR in total liver mRNA and normalized to *Actin* mRNA levels. Each lane represents the analysis of three independent animals. (**b**) The level of *Xbp1* mRNA splicing were quantified in the livers of animals described in b after 16 h of Tm injection. Expression of *Xbp1s* mRNA in (**c**) liver and (**d**) kidney was measured by real time qPCR. Data represents average and standard error (untreated animals, NT: n = 6; Tm treated mice: n = 9). When indicated statistical analysis was performed using ANOVA. *: $p < 0.05$, **: $p < 0.01$, ***: $p < 0.001$.

We also measured other downstream UPR signaling events in Hsp47cKO livers. Analysis of mRNA levels of *Edem1* (Fig. 32a) and *Blocs1* (Fig. 32c) indicated reduced IRE1α signaling upon Hsp47 deletion under ER stress conditions. In contrast, the upregulation of *Bip* was unaltered in Hsp47cKO animals injected with Tm (Fig. 32b). We then analyzed the extent of tissue damage triggered by Tm injections in control and Hsp47 deficient livers. Hematoxylin staining indicated slight signs of hepatocyte damage in Hsp47cKO mice in animals treated with Tm, associated with the appearance of enlarged cells and signs of inflammatory cell infiltration (Fig. 33a, see arrowhead). We also monitored the levels of apoptosis using the TUNEL assay. As expected the low concentration of Tm used to treat mice did not result in a clear induction of the apoptosis index in control animals (Fig. 33c). In contrast, a significant increase in the number of TUNEL-positive cells was observed in the liver of Hsp47cKO animals exposed to Tm (Fig. 33d).

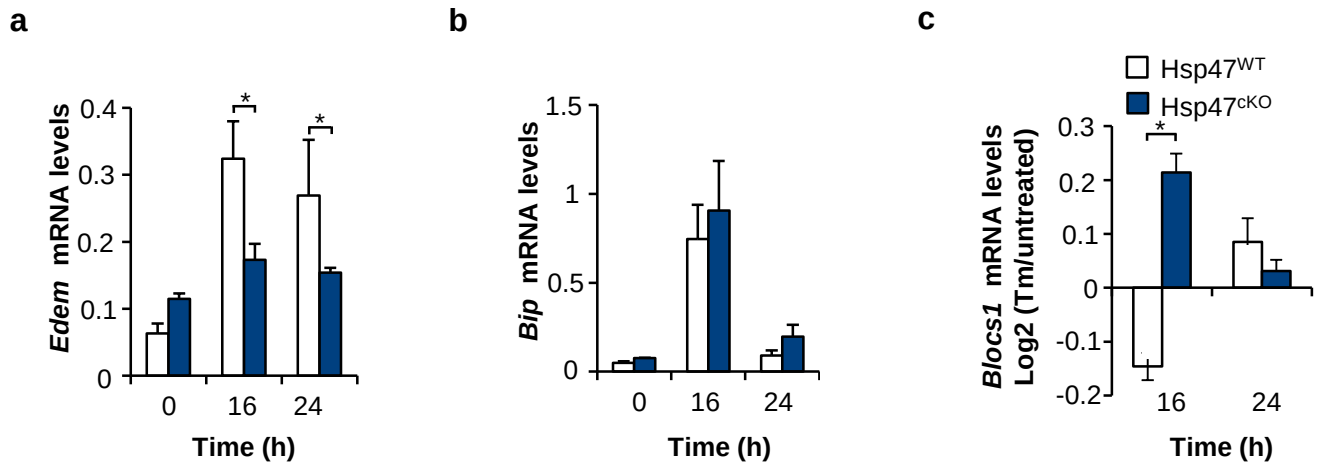

Figure 32. Conditional deficiency of Hsp47 in the liver mouse attenuates IRE1α signaling under ER stress i*n vivo*: Xbp1s targets and RIDD. Hsp47WT or Hsp47cKO mice were injected with Tm (50 ng/g, i.p.) and sacrificed. Expression of (**a**) *Edem* and (**b**) *Bip* mRNA was measured by real time qPCR in liver animals and normalized to *Actin* mRNA levels (**c**) The decay of *Blocs1* mRNA levels under ER stress was monitored in samples described in a. and b. by real time qPCR and normalized to *Rpl19* mRNA levels. Data represents average and standard error (untreated animals, NT: n = 6; Tm treated mice: n = 9). When indicated statistical analysis was performed using ANOVA. *: $p < 0.05$.

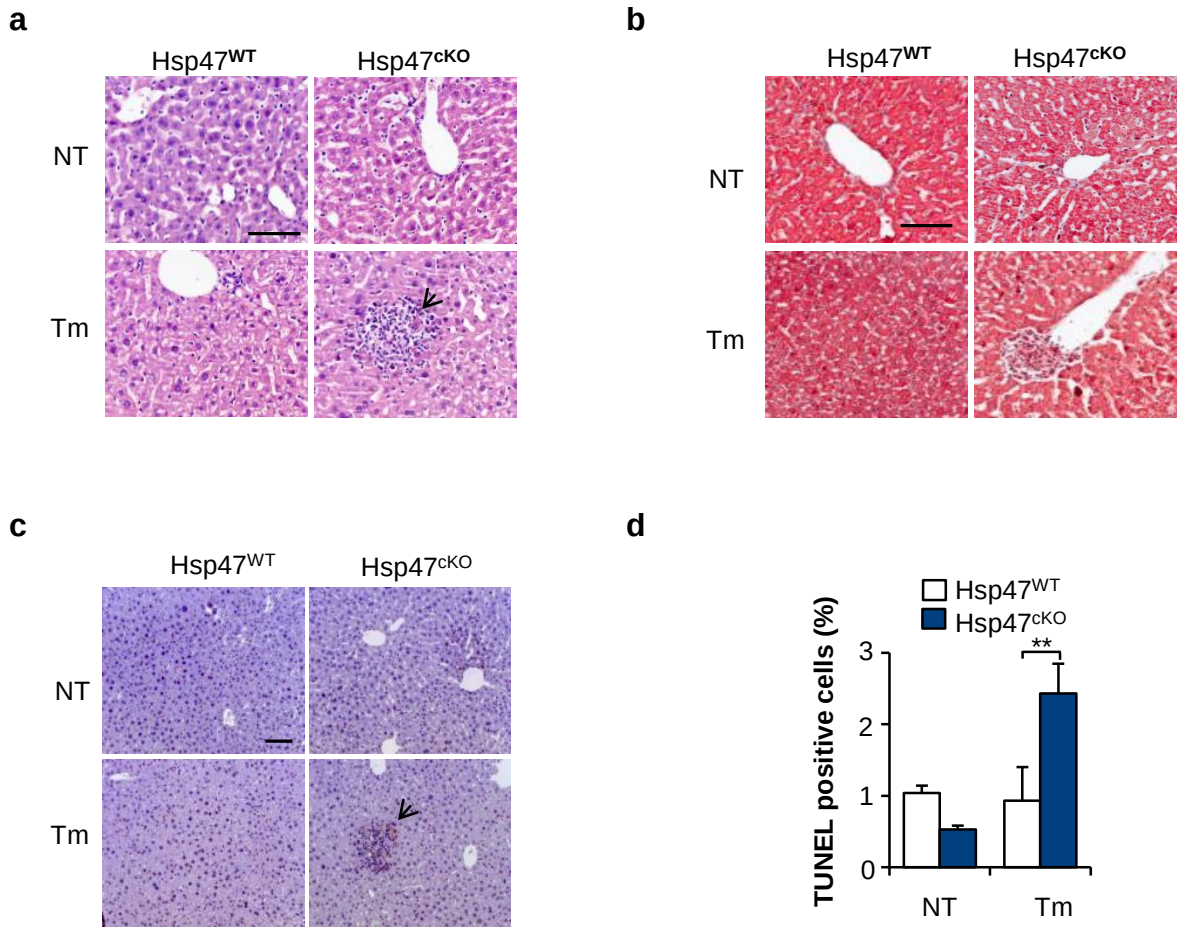

Figure 33. Evaluating tissue damage in conditional deficiency of Hsp47 in the liver mouse model. (**a**) Liver tissue from *Hsp47*^{WT} and *Hsp47*^{cKO} mice injected with 50 ng/g of Tm was fixed after 24 h of treatment, and stained with hematoxylin-eosin (magnification x400). Immune cell infiltration is indicated with an arrowhead. Scale bars, 100 μm. (**b**)) The possible occurrence of fibrosis was analyzed in the liver of Hsp47WT and Hsp47cKO mice after trichrome staining (untreated animals n = 2; Tm treated mice n = 3). Scale bars, 100 μm. (**c**) Apoptotic cells were quantified in samples described in a. with the TUNEL assay using DAB peroxidase substrate and counterstained with hematoxylin (**d**) Quantification of apoptotic cells described in c. Data represents the average and standard error of the analysis of 2 untreated animals and 3 Tm treated mice. Scale bars, 100 μm.

Hsp47 is the major chaperone involved in the folding and secretion of collagen and its deletion may generate deleterious effects to liver physiology. As control, we performed histological and biochemical analysis of the liver to assess several parameters associated with liver physiology and collagen production. Consistent with the short period after deletion used to analyze the animals, trichrome staining did not show evident collagen deposition at basal levels in Hsp47cKO mice or after ER stress stimulation (Figure 33b). Analysis of the mRNA levels of genes related to fibrosis including several collagen isoforms: *Col6α1* (Fig. 34a), *Col6α3* (Fig. 34b) and *Col1α1* (Fig.34c), *Acta2* (Fig. 34d) and the metalloproteinase inhibitor *Timp2* (Fig. 34e) revealed minor alterations under resting conditions and a slight enhancement in their expression in Hsp47 deficient livers after injection of Tm. Taken together, these results indicate that Hsp47 expression has a relevant function in modulating IRE1α signaling and the survival of hepatocytes against ER stress *in vivo*.

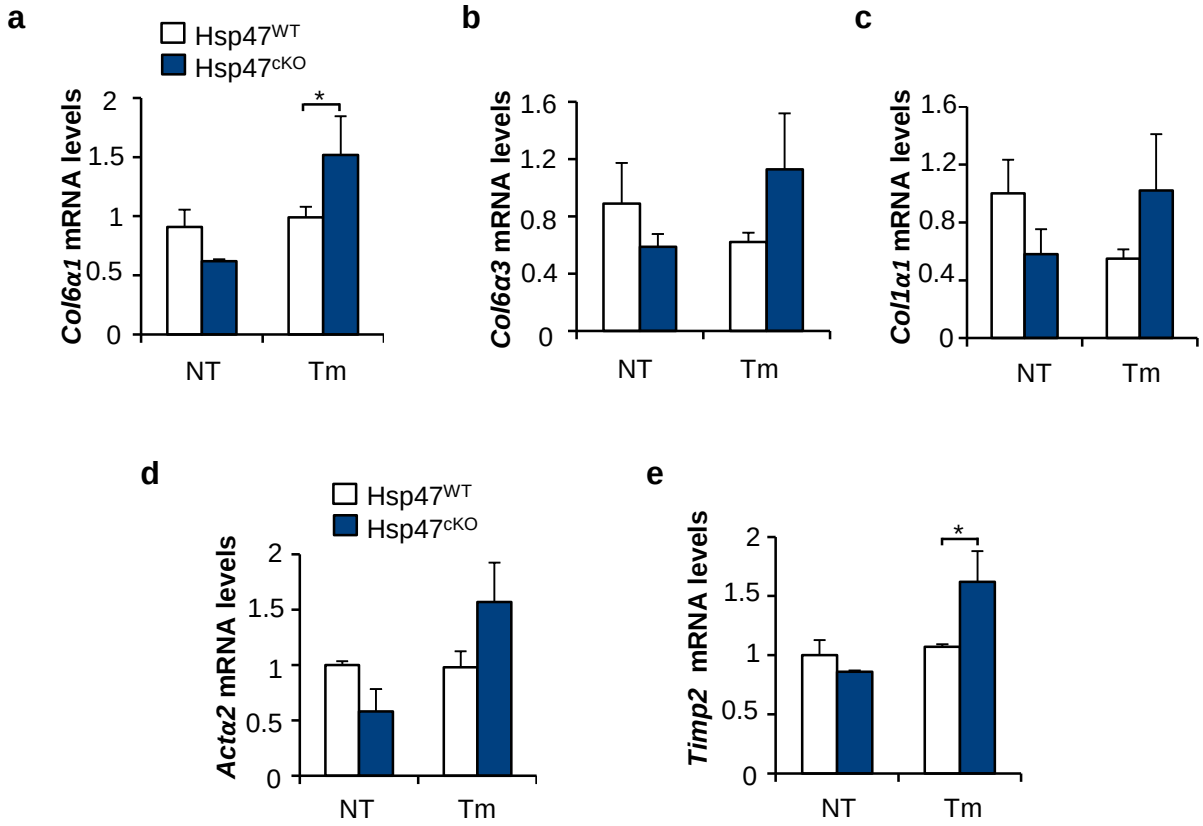

Figure 34. Evaluating fibrotic markers in conditional deficiency of Hsp47 in the liver mouse model. Hsp47WT or Hsp47cKO mice were injected with Tm (50 ng/g, i.p.) for 24 h and sacrificed. Total RNA was extracted from tissue using Trizol and cDNA was synthesized with SuperScript III. The expression levels of (**a**) *Col6α1*, (**b**) *Col6α3*, (**c**) *Col1α1*, (**d**) *Acta2* and (**e**) *Timp2* mRNAs were measured by real time qPCR and normalized to *β2-microglobulin* mRNA levels (untreated animals n = 2; Tm treated mice n = 3). When indicated statistical analysis was performed using ANOVA. *: $p < 0.05$.

12. DISCUSSION.

IRE1α initiates the most conserved signaling branch of the UPR, determining cell fate under ER stress. Although the biology of IRE1α has been extensively studied for the last two decades, the mechanisms mediating its regulation are poorly understood. ER stress is emerging as a driver of multiple pathological conditions, ranging from cancer, neurodegeneration, inflammation, and metabolic disorders among other diseases [96]. In this context, recent studies have demonstrated that targeting the activity of IRE1α with small molecules has important protective effects in various disease models [97, 98]. Notably, the physiological relevance of the UPR has greatly increased because of the discovery of multiple novel connections between IRE1α and various processes that are beyond protein folding stress, including energy control [99], inflammation [100], angiogenesis [101], synaptic function [102], and lipid metabolism [103]. Furthermore, studies in model organisms have added a new layer of control of global proteostasis at the level of whole organisms by the discovery of cell-nonautonomous UPR responses. This process is mediated by XBP1 and may engage IRE1α in the targeted tissue through signaling events [104], having a relevant impact in aging and healthspan [105], innate immunity [106] and global energy control [107]. Thus, understanding the molecular events controlling IRE1α activation is crucial to assess the connection between UPR signaling and cell physiology in various contexts.

IRE1α signaling enforces adaptive programs to mitigate ER stress or engage terminal UPR responses. XBP1s controls the expression of a vast spectrum of UPR genes involved in almost every aspect of the secretory pathway [28, 108, 109], whereas RIDD may have tissue specific and stimuli-dependent functions related to several processes [29]. Due to the implications of IRE1α in sustaining cell function under stress, a complex network of regulatory check points has evolved to tightly control the behavior of its signaling. The concept of the UPRosome has emerged to envision IRE1α as a scaffold where many components

assemble to fine-tune its activity [62]. The UPRosome may also serve as a platform to connect ER stress responses to other cellular processes through signaling cross talk. In the last years, a few IRE1α binding partners have been identified that modify biochemical aspects involved in its activation, including its phosphorylation status, oligomerization and the kinetics of activation/inactivation (reviewed in [68]). This concept has been also applied to other UPR mediators including ATF6 and PERK [68], indicating that the threshold of ER stress to engage the UPR and the amplitude of its downstream outputs depend on intrinsic and selective modifications at the level of the three main stress sensors. Identify the composition of the UPRosome will allow us understanding how cells adapt to protein folding stress and the contribution of UPR to physiological and pathological processes.

Here we have developed an effort to uncover novel IRE1α interactors and identified four candidates that differentially regulate Xbp1 mRNA splicing, RIDD and cell survival. From these hits, the ER chaperone Hsp47 had a significant effect over IRE1α activation. Unexpectedly, two of these four hits, PPA2 and ATP5h are localized to the mitochondria and were classified as IRE1α activators because their expression enhanced *Xbp1* mRNA splicing under ER stress. However, targeting PPA2 did not influence RIDD, suggesting a selective regulation of the RNAse domain. Although the mechanisms underlying the selectivity between these two outputs of IRE1α are unknown recent reports suggest that the RNAse domain may have distinct structural modes of action involving changes in its oligomerization status [41, 49, 110]. Further studies are needed to define how PPA2 and ATP5h expression affects UPR signaling. Of note, IRE1α has been recently reported to localize to ER-mitochondrial contact sites [111, 112] where the interaction between PPA2, ATP5h and IRE1α may occur. In the case of TUBα1a we obtained conflicting results where both gain- and loss-of function increased IRE1α signaling. Based on our results, we speculate that knocking down TUBα1a may have pleiotropic effects in the cell impacting the physiology of the ER, and increasing the susceptibility to ER stress, whereas its overexpression may reveal its true activity

in the UPR. Since available data indicates that the actin cytoskeleton and type-II myosin control the oligomerization status of IRE1α [69, 113], it may be feasible that TUBα1a overexpression selectively regulates *Xbp1* mRNA splicing. Importantly, we also obtained data demonstrating that knocking down the corresponding homologues of PPA2, ATP5h and TUBα1a in *D. melanogaster* has a clear influence over *dXbp1* mRNA splicing *in vivo*, in addition to affecting the survival of whole animals under ER stress conditions, fully recapitulating the phenotypes obtained in mouse cells (data no shown in the thesis, see annex: Supplementary Figure 6 of paper published on Molecular Cell: Sepulveda, Rojas-Rivera, Rodríguez 2018: Interactome screening identifies the ER luminal chaperone Hsp47 as a novel regulator of the unfolded protein response (UPR) transducer IRE1α).

Based on the global analysis of our results, we decided to focus our further studies on assessing the contribution of Hsp47 to the regulation of IRE1α because it had the strongest effects on *Xbp1* mRNA splicing and RIDD and it is located in the ER. Our results using knockdown and overexpressing cells support a positive role of HSP47 over IRE1α signaling under mild ER stress, enhancing *Xbp1* mRNA splicing and increasing the expression of XBP1s target genes. The RIDD activity was increased in HSP47 overexpressing cells. In mammalian cells, RIDD mRNA targets contain a cleavage site with a consensus sequence (CTGCAG) and a predicted secondary structure similar to the conserved IRE1α recognition stem−loop of the *Xbp1* mRNA [29, 31, 114]. This mechanism was originally reported to degrade mRNAs encoding proteins with signal peptide/transmembrane domains that would represent an additional challenge to the ER folding machinery under ER stress [30, 115]. By contrast, the described IRE1α RNAse-target metazoan RNAs encodes 64% ER-localized/secretory proteins and 36% cytosolic proteins [29]. However, the mechanisms involved in the IRE1α-dependent degradation of mRNAs encoding cytosolic proteins remain unclear. In the past few years, many studies performed in various model organisms have demonstrated that IRE1α has a basal RIDD activity that is necessary for maintaining ER homeostasis [29]. The basal RIDD activity is detectable without induction of *Xbp1*

mRNA splicing; or in other words, in the absence of ER stress. RIDD-dependent molecular mechanisms are involved in ER homeostasis maintenance [116, 117], but depending on the intensity of ER stress, triggering RIDD may also induce apoptosis since it can promote the degradation of ER resident proteins and de-repress Caspase-2 mRNA by the cleavage of miRNAs and others mRNAs [39]. In our results, the ER stress levels necessary to observe RIDD activity was tenfold higher than the concentration of Tm used to evaluate *Xbp1* mRNA splicing. It is necessary to analyze the expression of the JNK pathway to complement the results related with IRE1α outputs. We speculate that JNK is not activated in our system, because this pathway is engaged by high ER stress and lead to cell death [42, 43] and in our model, we used a low doses of Tm stressor (10 and 100 ng/mL) and we did not observed changes in the expression of other apoptotic marker as *Chop*.

In mammalian cells, a recent report showed that *Xbp1* mRNA splicing and RIDD activities are induced through two different IRE1α activation modes: pseudokinase and phos-photransfer, respectively [114]. Han and coworkers used an IRE1α mutant with an engineered nucleotide-binding pocket, allowing specific accommodation of an ATP-competitive inhibitor (NM-PPI) [114]. This system triggered allosteric activation of the IRE1α RNAse in the absence of phosphotransfer. Remarkably, NM-PPI treatment promoted *Xbp1* mRNA splicing, but not the degradation of RIDD targets. This finding raises the possibility that different IRE1α outputs can be triggered by different activating stimuli. A recent report suggested that IRE1α dimers are optimal for RIDD activity whereas larger oligomers are optimal for *Xbp1* mRNA splicing [41]. In contrast, KIRA6, an allosteric inhibitor of the RNAse domain of IRE1α that breaks the oligomers, showed that a decrease oligomerization is related to reduced RIDD activity [49].

Hsp47 is an ER resident glycoprotein that belongs to the family of heat shock proteins and operates as a specific chaperone for different types of collagen [77-79]. Hsp47 guides the trafficking of the triple helix of collagen into the Golgi

apparatus, operating as a quality control factor by interacting with TANGO1 [80-82, 131]. In contrast to BiP, the activity of Hsp47 is not dependent on ATP binding and forms large complexes with collagen together with other ER chaperones, including PDI, BiP and Grp94 [82, 118, 119]. Our results indicate that Hsp47 enhances IRE1α activation and its downstream signaling outputs under ER stress, associated with enhanced phosphorylation and oligomerization. We provided functional *in vivo* data supporting a conserved regulation of the UPR by Hsp47 in different species as demonstrated by genetic manipulation of fly and mouse models. At the molecular level, we were able to reconstitute the interaction between Hsp47 and IRE1α in a cell-free system using purified proteins. Hsp47 binds to the ER luminal domain of IRE1α, reducing the binding of BiP to the complex, which may contribute to promote IRE1α oligomerization or stabilize its active form (Fig. 35) under ER stress conditions. The association between Hsp47 and IRE1α is quickly enhanced upon ER stress, leading to a release of the protein after prolonged stimulation, suggesting a hit and run interaction (see annex: Figure 4d and 4e of paper Sepulveda, Rojas-Rivera, Rodríguez (2018): Interactome screening identifies the ER luminal chaperone Hsp47 as a novel regulator of the unfolded protein response (UPR) transducer IRE1α).

Based in our findings and previous evidence linking BiP and PDIA6 to the regulation of IRE1α, we speculate that a complex network of ER chaperons may operate as stress sentinels that converge into the activation of IRE1α to transduce signals about the protein folding status at the ER to the cytosol and nucleus to induce feedback mechanisms that sustain proteostasis. Since chaperons are specialized in the recognition of misfolded proteins of selected populations of clients, the fact that the ER stress sensing mechanism depends on the expression of different ER chaperones to control the buffering capacity of the UPR has biological significance.

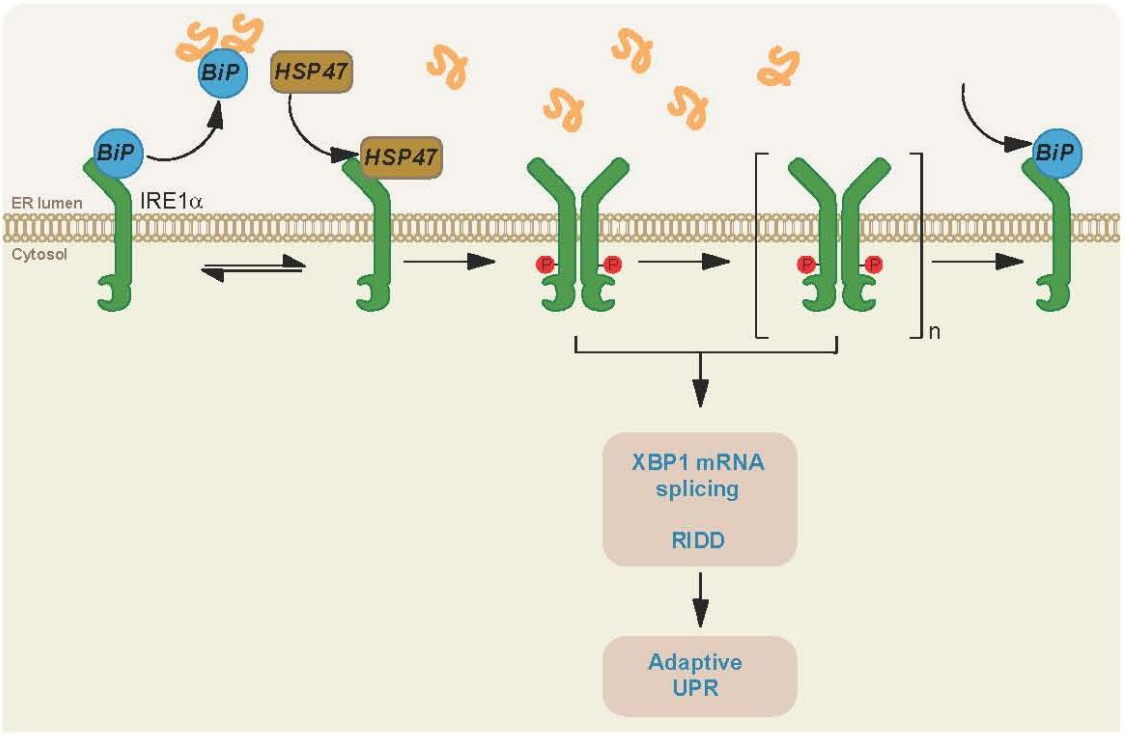

Figure 35. Model: Hsp47 enhances IRE1α activation. Under basal conditions IRE1α is maintained in a monomeric inactive state through its interaction with BiP. Accumulation of misfolded proteins at the ER triggers the dissociation of BiP from IRE1α, allowing its dimerization and autotransphosphorylation. This phenomena triggers a conformational change in the cytosolic region that engages the RNase domain, which catalyzes the splicing of the mRNA encoding the transcription factor XBP1, in addition to promote the selective degradation of specific mRNAs through RIDD, allowing the establishment of stress mitigation programs. The ER chaperone Hsp47 binds to IRE1α and enhances its activation in part through dissociation of BiP from the complex, which may facilitate IRE1α dimerization. This specific interaction does not affect the binding of other regulators to the ER luminal domain of IRE1 α, including PDIA6.

The proposed models underlying the activation of IRE1α in simple unicellular organisms and mammalian cells are divergent [53]. In yeast a direct recognition model has been proposed to mediate the sensing of misfolded proteins, whereas in mammals all UPR stress sensors are highly dependent on the expression of BiP to control their activation status. Hsp47 has evolved as a specialized chaperone for collagen [120, 121], a process that is also assisted by BiP and other ER chaperones [120, 122]. Importantly, collagen is one of the most abundant proteins in the cell reaching near 30% of the total proteome mass in certain cell types, and certainly represents a main ER client [120, 123]. Due to the relative high expression levels of collagens and their complex folding process [120, 122], we speculate that collagens may represent one of key proteins that unfold and accumulate under ER stress. In fact, complete deficiency of Hsp47 has been reported to result in ER stress-mediated apoptosis in various models [124, 125], engaging the activation of compensatory autophagy to eliminate misfolded collagen and sustain cell survival [126]. Thus, the molecular connection identified between Hsp47 and IRE1α in this study may represent a mechanism that adjusts the ER folding needs according to the production of collagen, where more collagen expression engages stronger IRE1α signals mediated by Hsp47. This model is supported by the observation that Hsp47 expression mirrors the levels of collagen in various experimental systems, suggesting a co-regulatory mechanism [78, 119, 127, 128]. In agreement with this idea, a recent study indicated that TANGO1, a central component involved in the trafficking of the collagen triple helix to the Golgi apparatus [132], is a direct target gene of XBP1s [133]. In addition, Hsp47 is a well-known ER stress-target gene [129, 130], indicating that one of the adaptive outputs of the UPR is the improvement of collagen biosynthesis. Interestingly, a canonical RIDD target in mammals is Colagen-6 [30], suggesting that under ER stress collagen levels may be rapidly reduced by the control of their mRNA stability. Interestingly, the levels of *Col6* mRNA were upregulated in the liver of Hsp47cKO animals. Since the establishment of the extracellular matrix and connective tissue is an important factor to sustain multicellular organization in

higher organisms, the dependency of mammalian and fly UPR on Hsp47 expression may have evolved as an adjustor of whole organismal proteostasis. It remains to be determined if collagen expression can also assist during UPR signaling. To address this, we are currently investigating the possible contribution of the IRE1α/Hsp47 axis to fibrosis, a condition driven by abnormal collagen deposition. Overall, the current study has uncovered a previously unanticipated point of control of IRE1α signaling, contributing to our understanding of how fluctuations in the ER folding capacity are monitored and adjusted to maintain proteostasis.

Based on the data presented in our PhD project we postulated the following hypothesis: “HSP47 modulates IRE1α endoribonuclease activity by direct interaction, promoting *Xbp1* mRNA processing and cell survival under ER stress conditions”. The results presented in this thesis progress report shows that the hypothesis is valid and describe HSP47 as a novel IRE1α regulator and component of the UPRosome.

14. PUBLICATION.

Interactome screening identifies the ER luminal chaperone Hsp47 as a regulator of the unfolded protein response (UPR) transducer IRE1α. **Sepulveda D.***, Rojas-Rivera D.*, Rodriguez D.*, Groenendyk J., Köhler A., Lebeaupin C., Ito S., Urra H., Carreras-Sureda A., Hazari Y., Vasseur-Cognet M., Ali M., Chevet E., Campos G., Godoy P., Vaisar T., Bailly-Maitre B., Nagata K., Michalak M., Sierralta J., and Hetz C. Mol Cell. 2018 Jan 18; 69(2):238-252.e7. doi: 10.1016/j.molcel.2017.12.028. PMID: 29351844.

Cellular mechanisms of endoplasmic reticulum stress signaling in health and disease. 1. An overview. Dufey E, **Sepúlveda D**, Rojas-Rivera D, Hetz C. Am J Physiol Cell Physiol. 2014 Oct 1;307(7):C582-94. doi: 10.1152/ajpcell.00258.2014. Epub 2014 Aug 20. Review. PMID: 25143348.

Interplay between the oxidoreductase PDIA6 and microRNA-322 controls the response to disrupted endoplasmic reticulum calcium homeostasis. Groenendyk J, Peng Z, Dudek E, Fan X, Mizianty MJ, Dufey E, Urra H, **Sepulveda D**, Rojas-Rivera D, Lim Y, Kim do H, Baretta K, Srikanth S, Gwack Y, Ahnn J, Kaufman RJ, Lee SK, Hetz C, Kurgan L, Michalak M. Sci Signal. 2014 Jun 10;7(329):ra54. doi: 10.1126/scisignal.2004983. PMID: 24917591.

15. CONFERENCES.

XXX Annual Meeting of the Cellular Biology Society of Chile. Poster title: Interactome screening identifies the endoplasmic reticulum luminal chaperone Hsp47 as a novel regulator of the unfolded protein response transducer IRE1α. **Denisse Sepúlveda**, Diego Rojas-Rivera, Jody Groenendyk, Diego A. Rodríguez, Andres Kohler, Shinya Ito, Hery Urra, Amado Carreras-Sureda, Eric Chevet, Béatrice Bailly-Maitre, Kazuhiro Nagata, Marek Michalak, Jimena Sierralta and Claudio Hetz. November, 2016. Puerto Varas, Chile.

89th Annual Meeting of the Japanese Biochemical Society. **Denisse Sepulveda**, Diego Rojas-Rivera, Andres Kholer, Shinya Ito, Hery Urra, Amado Carreras, Kazuhiro Nagata, Jimena Sierralta and Claudio Hetz. September 25-27, 2016. Sendai International Center/ Kawauchi Campus, Tohoku University. Miyaji, Japan.

10th European Workshops on Cell Death. Defining the IRE1 interactome: Novel regulators of the UPR and ER stress-induced cell death. Diego Rojas-Rivera, Diego Rodriguez, **Denisse Sepulveda**, Hery Urra, Amado Carreras, Jimena Sierralta, Claudio Hetz. April 3-8, 2016, Fiuggi, Italy.

XXIX Annual Meeting of the Cellular Biology Society of Chile. Poster title: Functional study of the IRE1a interactome: Hsp47 regulates IRE1α. Diego Rojas-Rivera, **Sepúlveda D**, Rodriguez D, Groenendyk J, Kohler A, Urra H, Carreras A, Chevet E, Visar T, Nagata K, Michalak M, Sierralta J and Hetz C. October, 2015. Puerto Varas, Chile.

From Unfolded Proteins in the ER to Disease. Poster title: “Functional study of the IRE1 interactome: fine tuning of UPR signaling”. Diego Rojas-Rivera, **Denisse Sepúlveda**, Diego Rodriguez, Hery Urra, Christian Gonzalez, Jimena Sierralta and Claudio Hetz. June 14 -19, 2015, Saxtons River, Vermont, USA.

XXVIII Annual Meeting of the Cellular Biology Society of Chile. Oral presentation: “The IRE1α interactome: Hps47 a new modulator involved in fine tuning of UPR signaling”. **Sepúlveda D**, Rojas-Rivera D, Rodríguez D, Urra H, Dufey E, Hetz C. October 26 – 30, 2014. Puerto Varas, Chile.

16. INTERNSHIP.

Kazuhiro Nagata Laboratory. Department of Molecular Biosciences, Faculty of Life Sciences, Kyoto Sangyo University, Motoyama, Kamigamo, Kita-ku, Kyoto, Japan. From October 17th 2015 to February 19th 2016.

17. REFERENCES.

1. Berridge, M.J., *The endoplasmic reticulum: a multifunctional signaling organelle.* Cell Calcium, 2002. **32**(5-6): p. 235-49.
2. Palade, G., *Intracellular aspects of the process of protein synthesis.* Science, 1975. **189**(4206): p. 867.
3. Ellgaard, L. and A. Helenius, *Quality control in the endoplasmic reticulum.* Nat Rev Mol Cell Biol, 2003. **4**(3): p. 181-91.
4. Vembar, S.S. and J.L. Brodsky, *One step at a time: endoplasmic reticulum-associated degradation.* Nat Rev Mol Cell Biol, 2008. **9**(12): p. 944-57.
5. Hetz, C., *The unfolded protein response: controlling cell fate decisions under ER stress and beyond.* Nat Rev Mol Cell Biol, 2012. **13**(2): p. 89-102.
6. Ron, D. and P. Walter, *Signal integration in the endoplasmic reticulum unfolded protein response.* Nat Rev Mol Cell Biol, 2007. **8**(7): p. 519-29.
7. Walter, P. and D. Ron, *The unfolded protein response: from stress pathway to homeostatic regulation.* Science, 2011. **334**(6059): p. 1081-6.
8. Urra, H., et al., *When ER stress reaches a dead end.* Biochim Biophys Acta, 2013. **1833**(12): p. 3507-17.
9. Dufey, E., et al., *Cellular Mechanisms of Endoplasmic Reticulum Stress Signaling in Health and Disease. 1. An overview.* Am J Physiol Cell Physiol, 2014. **307**(7): p. C582-C594.
10. Liu, C.Y., M. Schroder, and R.J. Kaufman, *Ligand-independent dimerization activates the stress response kinases IRE1 and PERK in the lumen of the endoplasmic reticulum.* J Biol Chem, 2000. **275**(32): p. 24881-5.
11. Harding, H.P., et al., *Perk is essential for translational regulation and cell survival during the unfolded protein response.* Mol Cell, 2000. **5**(5): p. 897-904.
12. Harding, H.P., et al., *Regulated translation initiation controls stress-induced gene expression in mammalian cells.* Mol Cell, 2000. **6**(5): p. 1099-108.
13. Kimball, S.R., et al., *The double-stranded RNA-activated protein kinase PKR is dispensable for regulation of translation initiation in response to either calcium mobilization from the endoplasmic reticulum or essential amino acid starvation.* Biochem Biophys Res Commun, 2001. **280**(1): p. 293-300.
14. Kim, R., et al., *Role of the unfolded protein response in cell death.* Apoptosis, 2006. **11**(1): p. 5-13.
15. Haze, K., et al., *Mammalian transcription factor ATF6 is synthesized as a transmembrane protein and activated by proteolysis in response to endoplasmic reticulum stress.* Mol Biol Cell, 1999. **10**(11): p. 3787-99.
16. Okada, T., et al., *A serine protease inhibitor prevents endoplasmic reticulum stress-induced cleavage but not transport of the membrane-bound transcription factor ATF6.* J Biol Chem, 2003. **278**(33): p. 31024-32.
17. Schindler, A.J. and R. Schekman, *In vitro reconstitution of ER-stress induced ATF6 transport in COPII vesicles.* Proc Natl Acad Sci U S A, 2009. **106**(42): p. 17775-80.

18. Adachi, Y., et al., *ATF6 is a transcription factor specializing in the regulation of quality control proteins in the endoplasmic reticulum.* Cell Struct Funct, 2008. **33**(1): p. 75-89.
19. Imagawa, Y., et al., *RNase domains determine the functional difference between IRE1alpha and IRE1beta.* FEBS Lett, 2008. **582**(5): p. 656-60.
20. Cox, J.S., C.E. Shamu, and P. Walter, *Transcriptional induction of genes encoding endoplasmic reticulum resident proteins requires a transmembrane protein kinase.* Cell, 1993. **73**(6): p. 1197-206.
21. Calfon, M., et al., *IRE1 couples endoplasmic reticulum load to secretory capacity by processing the XBP-1 mRNA.* Nature, 2002. **415**(6867): p. 92-6.
22. Bertolotti, A., et al., *Dynamic interaction of BiP and ER stress transducers in the unfolded-protein response.* Nat Cell Biol, 2000. **2**(6): p. 326-32.
23. Lee, K.P., et al., *Structure of the dual enzyme Ire1 reveals the basis for catalysis and regulation in nonconventional RNA splicing.* Cell, 2008. **132**(1): p. 89-100.
24. Korennykh, A.V., et al., *The unfolded protein response signals through high-order assembly of Ire1.* Nature, 2009. **457**(7230): p. 687-93.
25. Ali, M.M., et al., *Structure of the Ire1 autophosphorylation complex and implications for the unfolded protein response.* EMBO J, 2011. **30**(5): p. 894-905.
26. Lee, A.H., N.N. Iwakoshi, and L.H. Glimcher, *XBP-1 regulates a subset of endoplasmic reticulum resident chaperone genes in the unfolded protein response.* Mol Cell Biol, 2003. **23**(21): p. 7448-59.
27. Yoshida, H., et al., *XBP1 mRNA is induced by ATF6 and spliced by IRE1 in response to ER stress to produce a highly active transcription factor.* Cell, 2001. **107**(7): p. 881-91.
28. Acosta-Alvear, D., et al., *XBP1 controls diverse cell type- and condition-specific transcriptional regulatory networks.* Mol Cell, 2007. **27**(1): p. 53-66.
29. Maurel, M., et al., *Getting RIDD of RNA: IRE1 in cell fate regulation.* Trends Biochem Sci, 2014. **39**(5): p. 245-54.
30. Hollien, J., et al., *Regulated Ire1-dependent decay of messenger RNAs in mammalian cells.* J Cell Biol, 2009. **186**(3): p. 323-31.
31. Oikawa, D., et al., *Identification of a consensus element recognized and cleaved by IRE1 alpha.* Nucleic Acids Res, 2010. **38**(18): p. 6265-73.
32. Kimmig, P., et al., *The unfolded protein response in fission yeast modulates stability of select mRNAs to maintain protein homeostasis.* Elife, 2012. **1**: p. e00048.
33. Mishiba, K., et al., *Defects in IRE1 enhance cell death and fail to degrade mRNAs encoding secretory pathway proteins in the Arabidopsis unfolded protein response.* Proc Natl Acad Sci U S A, 2013. **110**(14): p. 5713-8.
34. Dejeans, N., et al., *Autocrine control of glioma cells adhesion and migration through IRE1alpha-mediated cleavage of SPARC mRNA.* J Cell Sci, 2012. **125**(Pt 18): p. 4278-87.
35. Maurel, M., et al., *MicroRNA-1291-mediated silencing of IRE1alpha enhances Glypican-3 expression.* RNA, 2013. **19**(6): p. 778-88.

36. Gaddam, D., N. Stevens, and J. Hollien, *Comparison of mRNA localization and regulation during endoplasmic reticulum stress in Drosophila cells.* Mol Biol Cell, 2013. **24**(1): p. 14-20.
37. Pluquet, O., et al., *Posttranscriptional regulation of PER1 underlies the oncogenic function of IREalpha.* Cancer Res, 2013. **73**(15): p. 4732-43.
38. Maurel, M., et al., *Getting RIDD of RNA: IRE1 in cell fate regulation.* Trends Biochem Sci, 2014.
39. Upton, J.P., et al., *IRE1alpha cleaves select microRNAs during ER stress to derepress translation of proapoptotic Caspase-2.* Science, 2012. **338**(6108): p. 818-22.
40. Iwawaki, T., et al., *Translational control by the ER transmembrane kinase/ribonuclease IRE1 under ER stress.* Nat Cell Biol, 2001. **3**(2): p. 158-64.
41. Tam, A.B., A.C. Koong, and M. Niwa, *Ire1 has distinct catalytic mechanisms for XBP1/HAC1 splicing and RIDD.* Cell Rep, 2014. **9**(3): p. 850-8.
42. Urano, F., et al., *Coupling of stress in the ER to activation of JNK protein kinases by transmembrane protein kinase IRE1.* Science, 2000. **287**(5453): p. 664-6.
43. Nishitoh, H., et al., *ASK1 is essential for endoplasmic reticulum stress-induced neuronal cell death triggered by expanded polyglutamine repeats.* Genes Dev, 2002. **16**(11): p. 1345-55.
44. Nguyen, D.T., et al., *Nck-dependent activation of extracellular signal-regulated kinase-1 and regulation of cell survival during endoplasmic reticulum stress.* Mol Biol Cell, 2004. **15**(9): p. 4248-60.
45. Hu, P., et al., *Autocrine tumor necrosis factor alpha links endoplasmic reticulum stress to the membrane death receptor pathway through IRE1alpha-mediated NF-kappaB activation and down-regulation of TRAF2 expression.* Mol Cell Biol, 2006. **26**(8): p. 3071-84.
46. Hetz, C., E. Chevet, and S.A. Oakes, *Erratum: Proteostasis control by the unfolded protein response.* Nat Cell Biol, 2015. **17**(8): p. 1088.
47. Lin, J.H., et al., *IRE1 signaling affects cell fate during the unfolded protein response.* Science, 2007. **318**(5852): p. 944-9.
48. Lisbona, F. and C. Hetz, *Turning off the unfolded protein response: an interplay between the apoptosis machinery and ER stress signaling.* Cell Cycle, 2009. **8**(11): p. 1643-4.
49. Ghosh, R., et al., *Allosteric inhibition of the IRE1alpha RNase preserves cell viability and function during endoplasmic reticulum stress.* Cell, 2014. **158**(3): p. 534-48.
50. Han, D., et al., *IRE1alpha kinase activation modes control alternate endoribonuclease outputs to determine divergent cell fates.* Cell, 2009. **138**(3): p. 562-75.
51. Lu, M., et al., *Opposing unfolded-protein-response signals converge on death receptor 5 to control apoptosis.* Science, 2014. **345**(6192): p. 98-101.
52. Lerner, A.G., et al., *IRE1alpha induces thioredoxin-interacting protein to activate the NLRP3 inflammasome and promote programmed cell death under irremediable ER stress.* Cell Metab, 2012. **16**(2): p. 250-64.

53. Kimata, Y. and K. Kohno, *Endoplasmic reticulum stress-sensing mechanisms in yeast and mammalian cells.* Curr Opin Cell Biol, 2011. **23**(2): p. 135-42.
54. Okamura, K., et al., *Dissociation of Kar2p/BiP from an ER sensory molecule, Ire1p, triggers the unfolded protein response in yeast.* Biochem Biophys Res Commun, 2000. **279**(2): p. 445-50.
55. Credle, J.J., et al., *On the mechanism of sensing unfolded protein in the endoplasmic reticulum.* Proc Natl Acad Sci U S A, 2005. **102**(52): p. 18773-84.
56. Pincus, D., et al., *BiP binding to the ER-stress sensor Ire1 tunes the homeostatic behavior of the unfolded protein response.* PLoS Biol, 2010. **8**(7): p. e1000415.
57. Zhou, J., et al., *The crystal structure of human IRE1 luminal domain reveals a conserved dimerization interface required for activation of the unfolded protein response.* Proc Natl Acad Sci U S A, 2006. **103**(39): p. 14343-8.
58. Oikawa, D., et al., *Activation of mammalian IRE1alpha upon ER stress depends on dissociation of BiP rather than on direct interaction with unfolded proteins.* Exp Cell Res, 2009. **315**(15): p. 2496-504.
59. Onn, A. and D. Ron, *Modeling the endoplasmic reticulum unfolded protein response.* Nat Struct Mol Biol, 2010. **17**(8): p. 924-5.
60. Carrara, M., et al., *Noncanonical binding of BiP ATPase domain to Ire1 and Perk is dissociated by unfolded protein CH1 to initiate ER stress signaling.* Elife, 2015. **4**.
61. Woehlbier, U. and C. Hetz, *Modulating stress responses by the UPRosome: a matter of life and death.* Trends Biochem Sci, 2011. **36**(6): p. 329-37.
62. Hetz, C. and L.H. Glimcher, *Fine-tuning of the unfolded protein response: Assembling the IRE1alpha interactome.* Mol Cell, 2009. **35**(5): p. 551-61.
63. Lisbona, F., et al., *BAX inhibitor-1 is a negative regulator of the ER stress sensor IRE1alpha.* Mol Cell, 2009. **33**(6): p. 679-91.
64. Hetz, C., et al., *Proapoptotic BAX and BAK modulate the unfolded protein response by a direct interaction with IRE1alpha.* Science, 2006. **312**(5773): p. 572-6.
65. Rodriguez, D.A., et al., *BH3-only proteins are part of a regulatory network that control the sustained signalling of the unfolded protein response sensor IRE1alpha.* EMBO J, 2012. **31**(10): p. 2322-35.
66. Gu, F., et al., *Protein-tyrosine phosphatase 1B potentiates IRE1 signaling during endoplasmic reticulum stress.* J Biol Chem, 2004. **279**(48): p. 49689-93.
67. Luo, D., et al., *AIP1 is critical in transducing IRE1-mediated endoplasmic reticulum stress response.* J Biol Chem, 2008. **283**(18): p. 11905-12.
68. Hetz, C., E. Chevet, and S.A. Oakes, *Proteostasis control by the unfolded protein response.* Nat Cell Biol, 2015. **17**(7): p. 829-38.
69. He, Y., et al., *Nonmuscle myosin IIB links cytoskeleton to IRE1alpha signaling during ER stress.* Dev Cell, 2012. **23**(6): p. 1141-52.

70. Groenendyk, J., et al., *Interplay between the oxidoreductase PDIA6 and microRNA-322 controls the response to disrupted endoplasmic reticulum calcium homeostasis.* Sci Signal, 2014. **7**(329): p. ra54.
71. Eletto, D., et al., *Protein disulfide isomerase A6 controls the decay of IRE1alpha signaling via disulfide-dependent association.* Mol Cell, 2014. **53**(4): p. 562-76.
72. Gupta, S., et al., *HSP72 protects cells from ER stress-induced apoptosis via enhancement of IRE1alpha-XBP1 signaling through a physical interaction.* PLoS Biol, 2010. **8**(7): p. e1000410.
73. Li, H., et al., *Mammalian endoplasmic reticulum stress sensor IRE1 signals by dynamic clustering.* Proc Natl Acad Sci U S A, 2010. **107**(37): p. 16113-8.
74. Bailly-Maitre, B., et al., *Cytoprotective gene bi-1 is required for intrinsic protection from endoplasmic reticulum stress and ischemia-reperfusion injury.* Proc Natl Acad Sci U S A, 2006. **103**(8): p. 2809-14.
75. Bailly-Maitre, B., et al., *Hepatic Bax inhibitor-1 inhibits IRE1alpha and protects from obesity-associated insulin resistance and glucose intolerance.* J Biol Chem, 2010. **285**(9): p. 6198-207.
76. Rong, J., et al., *Bifunctional apoptosis regulator (BAR), an endoplasmic reticulum (ER)-associated E3 ubiquitin ligase, modulates BI-1 protein stability and function in ER Stress.* J Biol Chem, 2011. **286**(2): p. 1453-63.
77. Saibil, H., *Chaperone machines for protein folding, unfolding and disaggregation.* Nat Rev Mol Cell Biol, 2013. **14**(10): p. 630-42.
78. Nagata, K. and N. Hosokawa, *Regulation and function of collagen-specific molecular chaperone, HSP47.* Cell Struct Funct, 1996. **21**(5): p. 425-30.
79. Ishida, Y., et al., *Type I collagen in Hsp47-null cells is aggregated in endoplasmic reticulum and deficient in N-propeptide processing and fibrillogenesis.* Mol Biol Cell, 2006. **17**(5): p. 2346-55.
80. Satoh, M., et al., *Intracellular interaction of collagen-specific stress protein HSP47 with newly synthesized procollagen.* J Cell Biol, 1996. **133**(2): p. 469-83.
81. Natsume, T., et al., *Interactions between collagen-binding stress protein HSP47 and collagen. Analysis of kinetic parameters by surface plasmon resonance biosensor.* J Biol Chem, 1994. **269**(49): p. 31224-8.
82. Nakai, A., et al., *Involvement of the stress protein HSP47 in procollagen processing in the endoplasmic reticulum.* J Cell Biol, 1992. **117**(4): p. 903-14.
83. Groenendyk, J., et al., *Interplay between the oxidoreductase PDIA6 and microRNA-322 controls the response to disrupted endoplasmic reticulum calcium homeostasis.* Sci Signal, 2014. **7**(329): p. ra54.
84. Rojas-Rivera, D., et al., *TMBIM3/GRINA is a novel unfolded protein response (UPR) target gene that controls apoptosis through the modulation of ER calcium homeostasis.* Cell Death Differ, 2012. **19**(6): p. 1013-26.
85. Castillo, K., et al., *BAX inhibitor-1 regulates autophagy by controlling the IRE1alpha branch of the unfolded protein response.* EMBO J, 2011. **30**(21): p. 4465-78.

86. Liu, C.Y., et al., *The protein kinase/endoribonuclease IRE1alpha that signals the unfolded protein response has a luminal N-terminal ligand-independent dimerization domain.* J Biol Chem, 2002. **277**(21): p. 18346-56.
87. Masago, Y., et al., *The molecular chaperone Hsp47 is essential for cartilage and endochondral bone formation.* J Cell Sci, 2012. **125**(Pt 5): p. 1118-28.
88. Tannour-Louet, M., et al., *A tamoxifen-inducible chimeric Cre recombinase specifically effective in the fetal and adult mouse liver.* Hepatology, 2002. **35**(5): p. 1072-81.
89. Ramirez, O., et al., *Confined displacement algorithm determines true and random colocalization in fluorescence microscopy.* J Microsc, 2010. **239**(3): p. 173-83.
90. Ryoo, H.D., *Drosophila as a model for unfolded protein response research.* BMB Rep, 2015. **48**(8): p. 445-53.
91. Plongthongkum, N., et al., *Ire1 regulated XBP1 mRNA splicing is essential for the unfolded protein response (UPR) in Drosophila melanogaster.* Biochem Biophys Res Commun, 2007. **354**(3): p. 789-94.
92. Dietzl, G., et al., *A genome-wide transgenic RNAi library for conditional gene inactivation in Drosophila.* Nature, 2007. **448**(7150): p. 151-6.
93. Rubin, D.M., et al., *Genomic structure and sequence analysis of Drosophila melanogaster HSC70 genes.* Gene, 1993. **128**(2): p. 155-63.
94. Coelho, D.S., et al., *Xbp1-independent Ire1 signaling is required for photoreceptor differentiation and rhabdomere morphogenesis in Drosophila.* Cell Rep, 2013. **5**(3): p. 791-801.
95. Coelho, D.S. and P.M. Domingos, *Physiological roles of regulated Ire1 dependent decay.* Front Genet, 2014. **5**: p. 76.
96. Wang, M. and R.J. Kaufman, *Protein misfolding in the endoplasmic reticulum as a conduit to human disease.* Nature, 2016. **529**(7586): p. 326-35.
97. Maly, D.J. and F.R. Papa, *Druggable sensors of the unfolded protein response.* Nat Chem Biol, 2014. **10**(11): p. 892-901.
98. Hetz, C., E. Chevet, and H.P. Harding, *Targeting the unfolded protein response in disease.* Nat Rev Drug Discov, 2013. **12**(9): p. 703-19.
99. Oslowski, C.M., et al., *Thioredoxin-interacting protein mediates ER stress-induced beta cell death through initiation of the inflammasome.* Cell Metab, 2012. **16**(2): p. 265-73.
100. Martinon, F., et al., *TLR activation of the transcription factor XBP1 regulates innate immune responses in macrophages.* Nat Immunol, 2010. **11**(5): p. 411-8.
101. Karali, E., et al., *VEGF Signals through ATF6 and PERK to promote endothelial cell survival and angiogenesis in the absence of ER stress.* Mol Cell, 2014. **54**(4): p. 559-72.
102. Martinez, G., et al., *Regulation of Memory Formation by the Transcription Factor XBP1.* Cell Rep, 2016. **14**(6): p. 1382-94.
103. Lee, A.H., et al., *Regulation of hepatic lipogenesis by the transcription factor XBP1.* Science, 2008. **320**(5882): p. 1492-6.

104. Mardones, P., G. Martinez, and C. Hetz, *Control of systemic proteostasis by the nervous system.* Trends Cell Biol, 2015. **25**(1): p. 1-10.
105. Taylor, R.C. and A. Dillin, *XBP-1 is a cell-nonautonomous regulator of stress resistance and longevity.* Cell, 2013. **153**(7): p. 1435-47.
106. Sun, J., Y. Liu, and A. Aballay, *Organismal regulation of XBP-1-mediated unfolded protein response during development and immune activation.* EMBO Rep, 2012. **13**(9): p. 855-60.
107. Williams, B., J. Verchot, and M.B. Dickman, *When supply does not meet demand-ER stress and plant programmed cell death.* Front Plant Sci, 2014. **5**: p. 211.
108. Lee, K., et al., *IRE1-mediated unconventional mRNA splicing and S2P-mediated ATF6 cleavage merge to regulate XBP1 in signaling the unfolded protein response.* Genes Dev, 2002. **16**(4): p. 452-66.
109. Shaffer, A.L., et al., *XBP1, downstream of Blimp-1, expands the secretory apparatus and other organelles, and increases protein synthesis in plasma cell differentiation.* Immunity, 2004. **21**(1): p. 81-93.
110. Bouchecareilh, M., et al., *Peptides derived from the bifunctional kinase/RNase enzyme IRE1alpha modulate IRE1alpha activity and protect cells from endoplasmic reticulum stress.* FASEB J, 2011. **25**(9): p. 3115-29.
111. Son, S.M., et al., *Reduced IRE1alpha mediates apoptotic cell death by disrupting calcium homeostasis via the InsP3 receptor.* Cell Death Dis, 2014. **5**: p. e1188.
112. Mori, T., et al., *Sigma-1 Receptor Chaperone at the ER-Mitochondrion Interface Mediates the Mitochondrion-ER-Nucleus Signaling for Cellular Survival.* PLoS One, 2013. **8**(10).
113. Ishiwata-Kimata, Y., et al., *F-actin and a type-II myosin are required for efficient clustering of the ER stress sensor Ire1.* Cell Struct Funct, 2013. **38**(2): p. 135-43.
114. Paez-Ribes, M., et al., *Antiangiogenic therapy elicits malignant progression of tumors to increased local invasion and distant metastasis.* Cancer Cell, 2009. **15**(3): p. 220-31.
115. Hollien, J. and J.S. Weissman, *Decay of endoplasmic reticulum-localized mRNAs during the unfolded protein response.* Science, 2006. **313**(5783): p. 104-7.
116. Sakaki, K., et al., *RNA surveillance is required for endoplasmic reticulum homeostasis.* Proc Natl Acad Sci U S A, 2012. **109**(21): p. 8079-84.
117. Safra, M., et al., *The ire-1 ER stress-response pathway is required for normal secretory-protein metabolism in C. elegans.* J Cell Sci, 2013. **126**(Pt 18): p. 4136-46.
118. Ferreira, L.R., et al., *Association of Hsp47, Grp78, and Grp94 with procollagen supports the successive or coupled action of molecular chaperones.* J Cell Biochem, 1994. **56**(4): p. 518-26.
119. Sauk, J.J., et al., *Hsp47 and the translation-translocation machinery cooperate in the production of alpha 1(I) chains of type I procollagen.* J Biol Chem, 1994. **269**(6): p. 3941-6.

120. Ishida, Y. and K. Nagata, *Hsp47 as a collagen-specific molecular chaperone.* Methods Enzymol, 2011. **499**: p. 167-82.
121. Hirayoshi, K., et al., *HSP47: a tissue-specific, transformation-sensitive, collagen-binding heat shock protein of chicken embryo fibroblasts.* Mol Cell Biol, 1991. **11**(8): p. 4036-44.
122. Ishikawa, Y. and H.P. Bachinger, *A molecular ensemble in the rER for procollagen maturation.* Biochim Biophys Acta, 2013. **1833**(11): p. 2479-91.
123. Di Lullo, G.A., et al., *Mapping the ligand-binding sites and disease-associated mutations on the most abundant protein in the human, type I collagen.* J Biol Chem, 2002. **277**(6): p. 4223-31.
124. Marutani, T., et al., *Accumulation of type IV collagen in dilated ER leads to apoptosis in Hsp47-knockout mouse embryos via induction of CHOP.* J Cell Sci, 2004. **117**(Pt 24): p. 5913-22.
125. Kawasaki, K., et al., *Deletion of the collagen-specific molecular chaperone Hsp47 causes endoplasmic reticulum stress-mediated apoptosis of hepatic stellate cells.* J Biol Chem, 2015. **290**(6): p. 3639-46.
126. Ishida, Y., et al., *Autophagic elimination of misfolded procollagen aggregates in the endoplasmic reticulum as a means of cell protection.* Mol Biol Cell, 2009. **20**(11): p. 2744-54.
127. Nagai, N., et al., *Embryonic lethality of molecular chaperone hsp47 knockout mice is associated with defects in collagen biosynthesis.* J Cell Biol, 2000. **150**(6): p. 1499-506.
128. Clarke, E.P., et al., *Parallel regulation of procollagen I and colligin, a collagen-binding protein and a member of the serine protease inhibitor family.* J Cell Biol, 1993. **121**(1): p. 193-9.
129. Miyata, S., et al., *The endoplasmic reticulum-resident chaperone heat shock protein 47 protects the Golgi apparatus from the effects of O-glycosylation inhibition.* PLoS One, 2013. **8**(7): p. e69732.
130. Rutkowski, D.T., et al., *Adaptation to ER stress is mediated by differential stabilities of pro-survival and pro-apoptotic mRNAs and proteins.* PLoS Biol, 2006. **4**(11): p. e374.
131. Ishikawa, Y., Ito, S., Nagata, K., Sakai, L.Y., and Bachinger, H.P. *Intracellular mechanisms of molecular recognition and sorting for transport of large extracellular matrix molecules*. Proceedings of the National Academy of Sciences of the United States of America 2016. **113**, E6036-E6044.
132. Saito, K., Chen, M., Bard, F., Chen, S., Zhou, H., Woodley, D., Polischuk, R., Schekman, R., and Malhotra, V. *TANGO1 facilitates cargo loading at endoplasmic reticulum exit sites*. Cell, 2009. **136**, 891-902.
133. Maiers, J.L., Kostallari, E., Mushref, M., deAssuncao, T.M., Li, H., Jalan-Sakrikar, N., Huebert, R.C., Cao, S., Malhi, H., and Shah, V.H. *The unfolded protein response mediates fibrogenesis and collagen I secretion through regulating TANGO1 in mice*. Hepatology, 2017. **65**, 983-998.

Article

Molecular Cell

Interactome Screening Identifies the ER Luminal Chaperone Hsp47 as a Regulator of the Unfolded Protein Response Transducer IRE1α

Graphical Abstract

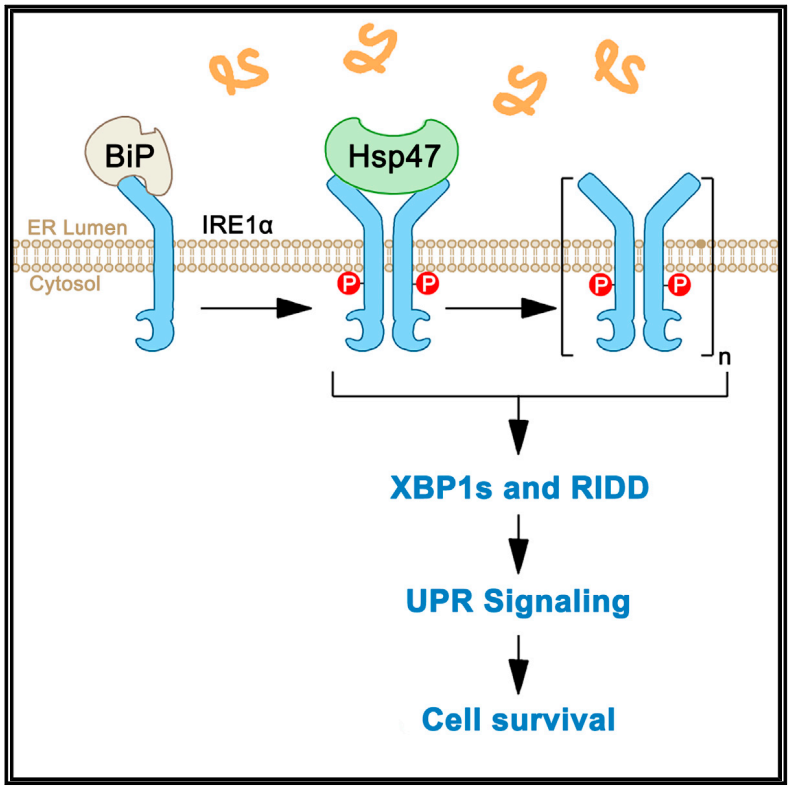

Authors

Denisse Sepulveda,
Diego Rojas-Rivera,
Diego A. Rodríguez, ...,
Marek Michalak, Jimena Sierralta,
Claudio Hetz

Correspondence

chetz@hsph.harvard.edu

In Brief

Sepulveda et al. use interactome screening and functional validation to identify a role for Hsp47 as a selective regulator of the unfolded protein response (UPR). Fine-tuning the UPR may be a useful strategy for treatment of diseases involving chronic endoplasmic reticulum stress.

Highlights

- Proteomic screening identified the ER chaperone Hsp47 as an adjustor of the UPR
- Hsp47 is a selective regulator of the ER stress transducer IRE1α
- Hsp47 displaces BiP from the IRE1 UPRosome to promote its oligomerization
- The regulation of the UPR by Hsp47 is conserved in evolution

Sepulveda et al., 2018, Molecular Cell *69*, 238–252
January 18, 2018
https://doi.org/10.1016/j.molcel.2017.12.028

CellPress

CellPress

Molecular Cell
Article

Interactome Screening Identifies the ER Luminal Chaperone Hsp47 as a Regulator of the Unfolded Protein Response Transducer IRE1α

Denisse Sepulveda,[1,2,3,17] Diego Rojas-Rivera,[1,2,3,17] Diego A. Rodríguez,[1,3,4,17] Jody Groenendyk,[5] Andres Köhler,[1,14] Cynthia Lebeaupin,[6] Shinya Ito,[7] Hery Urra,[1,2,3] Amado Carreras-Sureda,[1,2,3] Younis Hazari,[1,2,3] Mireille Vasseur-Cognet,[8] Maruf M.U. Ali,[9] Eric Chevet,[10,11] Gisela Campos,[12] Patricio Godoy,[12] Tomas Vaisar,[13] Béatrice Bailly-Maitre,[6] Kazuhiro Nagata,[7] Marek Michalak,[5] Jimena Sierralta,[1,14] and Claudio Hetz[1,2,3,15,16,18,*]

[1]Biomedical Neuroscience Institute (BNI), Faculty of Medicine, University of Chile, Santiago 8380453, Chile
[2]Center for Geroscience, Brain Health, and Metabolism (GERO), Santiago, Chile
[3]Program of Cellular and Molecular Biology, Institute of Biomedical Sciences, University of Chile, Santiago 8380453, Chile
[4]Department of Immunology, St. Jude Children's Research Hospital, Memphis, TN 38105, USA
[5]Department of Biochemistry, University of Alberta, Edmonton, Alberta T6G 2S7, Canada
[6]Inserm, Team 8, C3M, Nice 06204, France
[7]Department of Molecular Biosciences, Faculty of Life Sciences, Kyoto and Sangyo University, Motoyama, Kamigamo, Kita-ku, Kyoto 603-8555, Japan
[8]Institut d'Ecologie et des Sciences de l'Environnement de Paris, Bondy; Sorbonne Universités, and Institut National de la Santé et de la Recherche Médicale, Paris 7 113, France
[9]Department of Life Sciences, Imperial College, London SW7 2AZ, UK
[10]Inserm U1242, Chemistry, Oncogenesis, Stress, & Signaling, University of Rennes 1, F-35000 Rennes, France
[11]Centre de Lutte le Cancer Eugène Marquis, F-35000 Rennes, France
[12]IfADo-Leibniz Research Centre for Working Environment and Human Factors at the Technical University Dortmund, Dortmund 44139, Germany
[13]Division of Metabolism, Endocrinology and Nutrition, University of Washington School of Medicine, Seattle, WA 98195, USA
[14]Program of Physiology and Biophysics, Institute of Biomedical Sciences, University of Chile, Santiago 8380453, Chile
[15]Buck Institute for Research on Aging, Novato, CA 94945, USA
[16]Department of Immunology and Infectious Diseases, Harvard School of Public Health, Boston MA 02115, USA
[17]These authors contributed equally
[18]Lead Contact
*Correspondence: chetz@hsph.harvard.edu
https://doi.org/10.1016/j.molcel.2017.12.028

SUMMARY

Maintenance of endoplasmic reticulum (ER) proteostasis is controlled by a dynamic signaling network known as the unfolded protein response (UPR). IRE1α is a major UPR transducer, determining cell fate under ER stress. We used an interactome screening to unveil several regulators of the UPR, highlighting the ER chaperone Hsp47 as the major hit. Cellular and biochemical analysis indicated that Hsp47 instigates IRE1α signaling through a physical interaction. Hsp47 directly binds to the ER luminal domain of IRE1α with high affinity, displacing the negative regulator BiP from the complex to facilitate IRE1α oligomerization. The regulation of IRE1α signaling by Hsp47 is evolutionarily conserved as validated using fly and mouse models of ER stress. *Hsp47* deficiency sensitized cells and animals to experimental ER stress, revealing the significance of Hsp47 to global proteostasis maintenance. We conclude that Hsp47 adjusts IRE1α signaling by fine-tuning the threshold to engage an adaptive UPR.

INTRODUCTION

The endoplasmic reticulum (ER) is the main subcellular compartment involved in protein folding and secretion in addition to operating as a central site for calcium storage and lipid synthesis. Multiple conditions favor the accumulation of misfolded proteins in the ER lumen leading to a cellular state known as ER stress (Walter and Ron, 2011). Chronic ER stress is emerging as a relevant factor contributing to various pathological conditions, highlighting cancer, diabetes, inflammatory diseases, and neurodegeneration (Oakes and Papa, 2015; Wang and Kaufman, 2016). ER stress engages the unfolded protein response (UPR), an adaptive mechanism to cope with protein misfolding and restore proteostasis (Walter and Ron, 2011). Inositol-requiring enzyme 1 alpha (IRE1α) is a type I ER transmembrane protein with a serine and threonine protein kinase and endoribonuclease activity, representing the most conserved ER stress signal transducer. Upon activation, IRE1α catalyzes the unconventional splicing of the mRNA encoding X-box binding protein 1 (XBP1), leading to the expression of a potent and stable transcription factor termed XBP1s (Walter and Ron, 2011). XBP1s transactivates a cluster of genes involved in different aspects of the secretory pathway, including protein folding, ER-associated degradation

(ERAD), protein quality control, and phospholipid synthesis (Acosta-Alvear et al., 2007; Lee et al., 2003). The RNase activity of IRE1α also degrades selected mRNAs and microRNAs through a process known as regulated IRE1-dependent decay (RIDD), contributing to cell death, inflammation, and other biological processes (Maurel et al., 2014). Although irreversible ER stress triggers an apoptosis program involving a network of interconnected pathways (Hetz et al., 2015), the mechanisms determining the transition from prosurvival to a terminal UPR phase remain poorly defined. Sustained ER stress attenuates IRE1α signaling, which ablates the adaptive activity of XBP1s, eventually sensitizing cells to cell death (Lin et al., 2007; Lisbona et al., 2009). However, in certain experimental systems, hyperactivation of IRE1α results in apoptosis, involving changes in its oligomerization state and RIDD (Ghosh et al., 2014; Han et al., 2009). Therefore, IRE1α acts as a central adjustor of cell fate under ER stress by integrating information about the intensity and duration of the injury.

The molecular events underlying ER stress sensing are not completely defined. The binding of the ER chaperone BiP to the luminal domain of IRE1α has been proposed to maintain its monomeric inactive state. Under ER stress, BiP preferentially associates with improperly folded proteins, allowing the dimerization and auto-transphosphorylation of IRE1α in order to activate its RNase domain (Bertolotti et al., 2000; Carrara et al., 2015). In this model, BiP is the actual sensor because of its ability to directly detect misfolded proteins, whereas IRE1α operates as a signal transducer. In contrast, in yeast cells IRE1p may directly bind to misfolded proteins (Gardner and Walter, 2011) through a structure analogous to the peptide binding pocket of MHC-I (Credle et al., 2005). *In vitro* evidence suggests that the direct recognition model may not operate in mammals (Kimata and Kohno, 2011). However, a recent report indicated that unfolded proteins may bind to IRE1α, inducing allosteric changes that trigger its oligomerization (Karagöz et al., 2017). Thus, in mammals, ER stress sensing may involve BiP in addition to the binding of misfolded proteins to engage an optimal UPR reaction. Besides, other studies identified the disulfide isomerase PDIA6 as an additional ER foldase that binds to the luminal IRE1α and adjusts its signaling behavior (Eletto et al., 2014; Groenendyk et al., 2014). Overall, despite the central role of IRE1α as a master regulator of ER proteostasis, the mechanisms connecting fluctuation in protein folding efficiency and the engagement of the UPR remain poorly understood.

The amplitude and kinetics of ER stress signaling are regulated by the binding of different cofactors to the main UPR transducers, their post-translational modifications, and proteosomal degradation (Hetz et al., 2015). IRE1α can be viewed as a scaffold into which many components assemble to modulate its activity and instigate specific signaling outputs, a platform referred to as the *UPRosome* (Hetz and Glimcher, 2009). For example, several adaptor proteins bind to IRE1α and mediate the crosstalk with other alarm pathways including c-JNK (Urano et al., 2000) and NF-κB (Hu et al., 2006), among others (Hetz, 2012). The levels of IRE1α phosphorylation are modulated by several phosphatases and kinases (Lu et al., 2013; Mao et al., 2011; Qiu et al., 2010), whereas IRE1α oligomerization into large clusters is assisted by non-muscle myosin II (NMII) and the actin cytoskeleton (He et al., 2012). IRE1α signaling is also controlled by the targeting of the XBP1 mRNA to the ER membrane followed by the ligation of *Xbp1* mRNA by the RtcB ligase (reviewed in Hetz et al., 2015). Under prolonged ER stress, IRE1α is turned off, involving the physical interaction with several factors previously linked to the regulation of apoptosis (Lisbona et al., 2009; Rodriguez et al., 2012). Finally, the selectivity of the IRE1α RNase activity for RIDD substrates and the *Xbp1* mRNA may depend on its oligomerization status (Ghosh et al., 2014; Tam et al., 2014). Thus, IRE1α signaling represents a highly regulated process involving multiple checkpoints, setting up the threshold to induce an adaptive UPR or transit into a terminal proapoptotic program when ER proteostasis is irreversibly damaged.

The nature of the IRE1α interactome is not well defined, but it is essential to understanding the significance of the UPR to cell physiology. To uncover regulatory elements of the UPR, we identified IRE1α binding partners using proteomics followed by a functional genomics validation. This study allowed the identification of several interactors, highlighting heat shock protein 47 (Hsp47) as a major regulator of the UPR. Hsp47 is an ER chaperone specialized in the maturation and trafficking of collagen, the most abundant ER client in mammals (Nagata, 2003). We provide evidence indicating that Hsp47 expression enhances IRE1α activation and potentiates its downstream signaling, resulting in efficient ER stress mitigation. Using complementary approaches, we demonstrate that Hsp47 binds to the ER luminal domain of IRE1α and reduces the association of BiP to the complex, a phenomenon that may enhance its oligomerization for optimal signaling. *Hsp47* deficiency in flies and mice attenuates IRE1α signaling and sensitizes cells to experimental ER stress, revealing the significance of Hsp47 to global proteostasis maintenance. Overall, our results unravel a previously unanticipated biological function of Hsp47 as an adjustor of the UPR, setting up the threshold for IRE1α activation.

RESULTS

Functional Screening for IRE1α Regulators

To identify potential new components of the UPRosome, we immunoprecipitated HA-tagged IRE1α expressed in IRE1 (*Ern1)* null mouse embryonic fibroblasts (MEFs). This reconstitution strategy led to physiological levels of IRE1α expression and fully restored *Xbp1* mRNA splicing and RIDD activity (Figures S1A–S1D). IRE1α interacting complexes were isolated at basal conditions or in cells undergoing ER stress induced by the treatment with the N-glycosylation inhibitor tunicamycin (Tm). Immunoprecipitates (IPs) were analyzed using two-dimensional liquid chromatography along with tandem mass spectrometry followed by bioinformatic analysis. Comparison of three independent experiments led us to identify ten candidate proteins that differentially interact with IRE1α, in addition to the known regulator BiP (Table S1). These proteins are involved in different cellular functions including mitochondrial biology, collagen biosynthesis, cytoskeleton, and cell signaling, and display different subcellular distributions (Table S1). The majority of the candidates identified in IRE1α-containing complexes were present in both basal and ER stress conditions, whereas only three proteins were exclusively detected at resting conditions and two upon 6 hr of Tm treatment (Figure 1A).

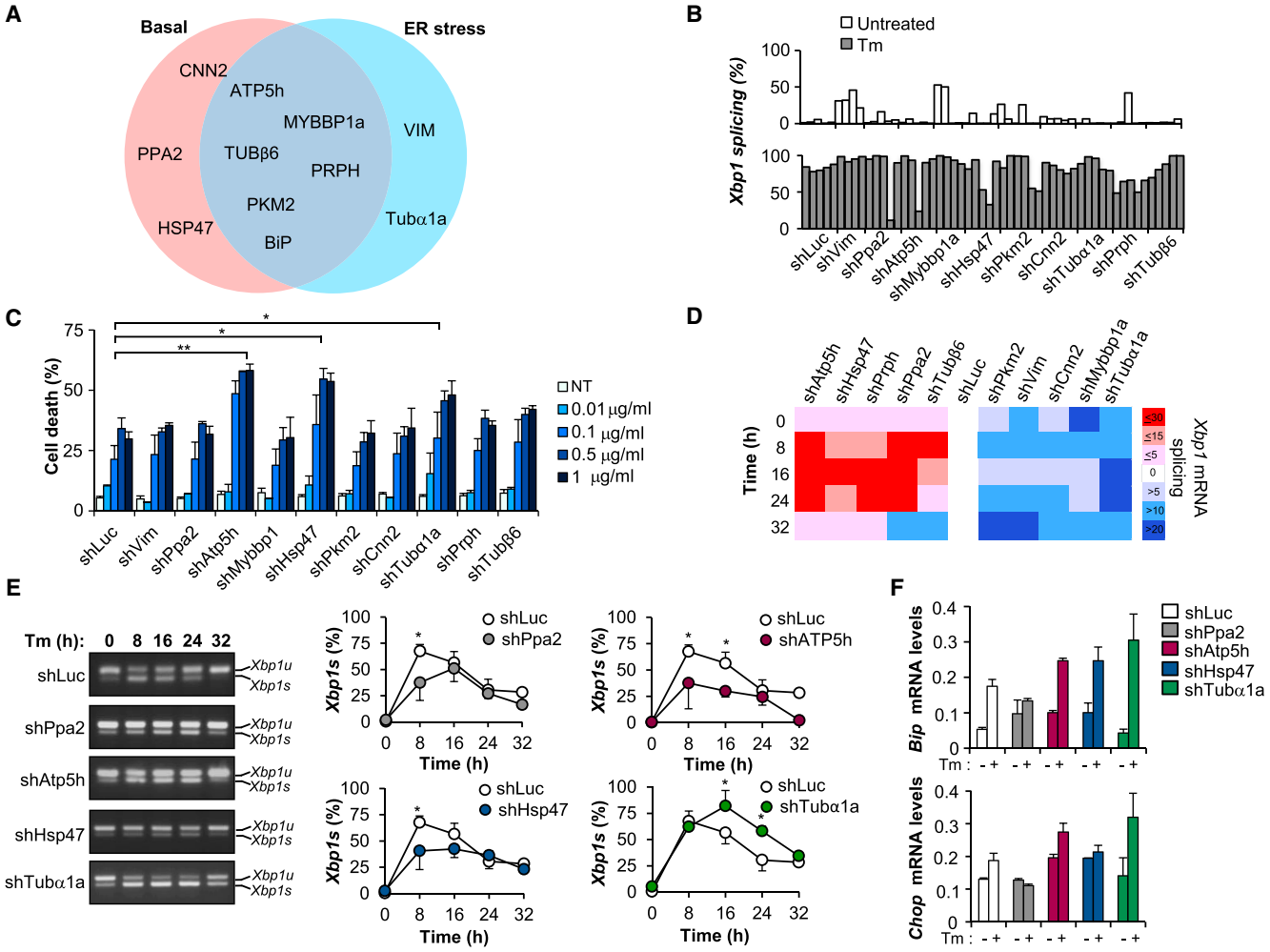

Figure 1. Functional Screening for IRE1α Interactors

(A) IRE1α-knockout MEFs were reconstituted with full-length IRE1α-HA. Immunoprecipitation of HA-tagged IRE1α was performed at basal levels or in cells treated with 250 ng/mL of tunicamycin (Tm) for 6 hr. Proteins present in complexes with purified IRE1α were then identified using mass spectrometry. IRE1α-associated proteins under basal conditions, ER stress conditions, and the intersection of both conditions are shown.

(B) The expression of ten IRE1α-binding candidates was knocked down by stably delivering different sets of individual shRNA constructs for indicated genes or shRNAs against luciferase as control. A primary screening was performed in cells treated with 10 ng/mL Tm for 24 hr followed by the analysis of *Xbp1* mRNA splicing using RT-PCR. Densitometry analysis of the *Xbp1u* and *Xbp1s* amplicons was performed to calculate the percentages of *Xbp1* mRNA splicing.

(C) Indicated shRNA cell lines were treated with increasing concentrations of Tm, and cell death was evaluated after 24 hr by propidium iodide staining and flow cytometry.

(D) Secondary validation: cells were incubated with 10 ng/mL of Tm for the indicated time, and *Xbp1* mRNA splicing was evaluated by RT-PCR. The delta of the percentage of *Xbp1* mRNA splicing relative to control cell line is represented on a hit map. Red boxes, downregulation; blue boxes, upregulation.

(E) MEFs expressing the indicated shRNA constructs were exposed to 10 ng/mL Tm for indicated time points and *Xbp1* mRNA splicing was evaluated by conventional RT-PCR. The percentage of *Xbp1* mRNA splicing was calculated after densitometric analysis (right). Of note for comparison, the curves for control shLuc cells are the same in the four graphs presented.

(F) Relative expression levels of *Bip* and *Chop* mRNA were monitored in samples presented in (E) (16 hr time point).

In (C) and (F) and in (D) and (E), respectively, average and standard error of three and four independent experiments are shown. When indicated statistical analysis was performed using Student's t test: *: $p < 0.05$, **: $p < 0.01$.

To assess the functional contribution of the putative IRE1α interactors, we knocked down their expression by the stable delivery of shRNAs (Figure S1E). To avoid saturation of the *Xbp1* mRNA splicing assay, we used low doses of Tm. Analysis of *Xbp1* mRNA splicing by RT-PCR in shRNA cells treated with Tm revealed that a subgroup of genes modulated IRE1α signaling to different extents (Figure 1B). To monitor the adaptive capacity of the cell to ER stress, we measured cell viability after Tm treatment in dose-response curves (Figure 1C). Of note, the Tm doses used to monitor UPR signaling did not result in significant apoptosis in control cells. However, at higher concentrations it was possible to detect an enhancement of ER stress-induced cell death when Atp5h, Hsp47 or Tubα1a were knocked down (Figure 1C). To define possible genes that enhance IRE1α

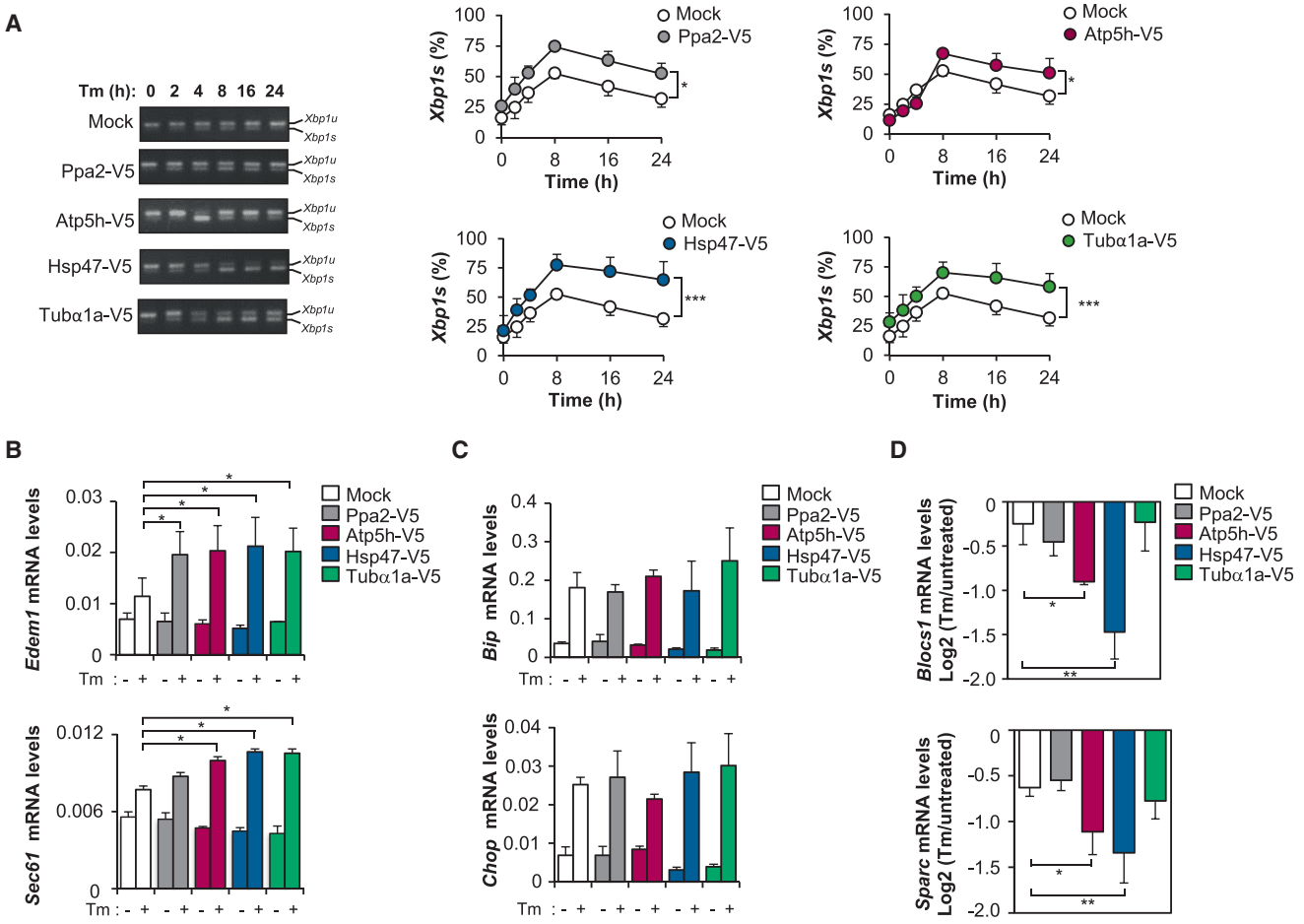

Figure 2. IRE1α Interactors Differentially Regulate RIDD and *Xbp1* mRNA Splicing

(A) Human *HSP47*, *TUBα1a*, *PPA2*, and *ATP5h* cDNA were tagged with a V5 epitope and stably expressed in MEFs. Cells were then incubated with 10 ng/mL of Tm for indicated time points and *Xbp1* mRNA splicing evaluated by RT-PCR. The percentage of *Xbp1* mRNA splicing was calculated after densitometric analysis (right). Data represent average and standard error of four independent experiments.

(B and C) *Edem1* abd *Sec61* (B) and *Bip* and *Chop* (C) mRNA levels were evaluated by real-time PCR in cells treated with 10 ng/mL of Tm for 8 hr.

(D) Cells were treated with 100 ng/mL of Tm for 16 hr, and the decay of *Sparc* and *Blocs1* mRNA was monitored by real-time PCR.

In (B), (C), and (D), average and standard error of three independent experiments are shown. Statistical analysis was performed using two-way ANOVA test: *: $p < 0.05$, **: $p < 0.01$, ***: $p < 0.001$.

signaling when they are downregulated, we performed kinetic analysis to measure *Xbp1* mRNA splicing, allowing the identification of Tubα1a as an additional regulator of the pathway (Figure 1D). The global analysis of these experiments led us to select four candidates for further functional validation, three putative activators, the phosphatase Ppa2, the ER chaperone Hsp47 and the mitochondrial ATPase Atp5h, in addition to one putative inhibitor of the pathway, Tubα1a. Secondary validation was performed with newly generated knockdown cells to monitor *Xbp1* mRNA splicing, which recapitulated the phenotypes identified in the primary screening (Figure 1E). To determine the specificity over IRE1α regulation, we measured the levels of two UPR-target genes controlled by the PERK and ATF6 branches. From this analysis, targeting Pp2a, Atp5h or Hsp47 did not affect the upregulation of *Bip* and *Chop*. In contrast, knockdown of Tubα1a increased the expression of these genes suggesting global alterations to ER physiology, resulting on ER stress (Figure 1F).

IRE1α Interactors Regulate UPR Signaling Outputs

To further validate the four selected IRE1α interacting partners, we performed gain-of-function experiments and assessed UPR signaling using different approaches. We stably expressed V5-tagged versions of human HSP47, TUBα1a, PPA2 and ATP5h in MEFs using retroviral transduction (Figure S2A). Next, we treated these cells with Tm and monitored *Xbp1* mRNA splicing in time-course experiments (Figure 2A). In agreement with our previous results, overexpression of PPA2, ATP5H and HSP47 enhanced the levels of *Xbp1* mRNA splicing (Figure 2A, right panel). Unexpectedly, TUBα1a overexpression also resulted in sustained *Xbp1* mRNA splicing after Tm treatment (Figure 2A). We confirmed these results using an alternative *Xbp1* mRNA splicing assay based on PstI digestion of RT-PCR products (Figure S2B).

To determine the activity of XBP1s in cells overexpressing IRE1α regulators, we measured the mRNA levels of *Edem1*

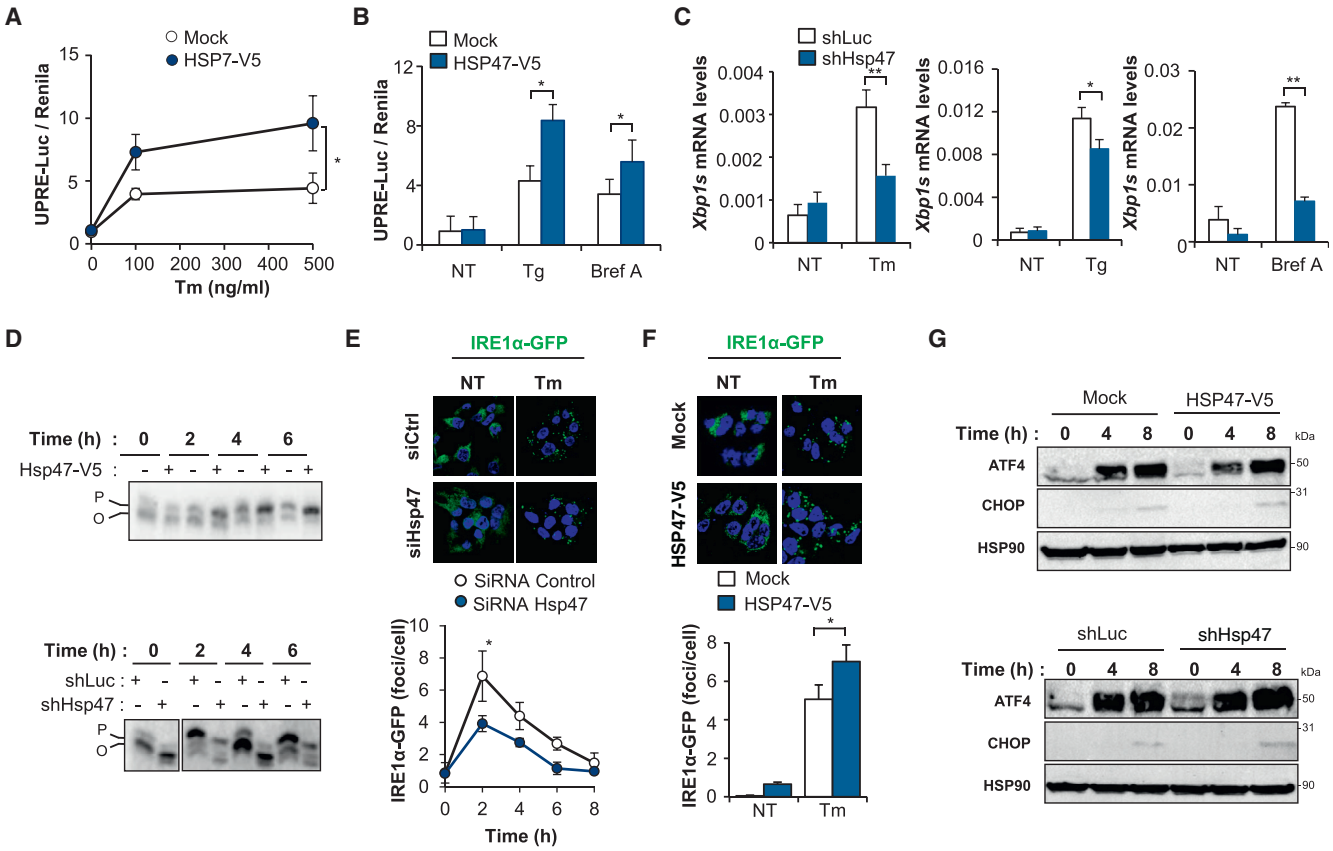

Figure 3. Hsp47 Modulates the Activation of IRE1α

(A) MEFs were transfected with a UPRE-luciferase reporter in the presence of an HSP47-V5 vector or mock. After 24 hr, cells were stimulated with indicated concentrations of Tm, and then 20 hr later, luciferase activity was determined.

(B) Similar experiments were performed after stimulating cells with 500 nM thapsigargin (Tg) and 2 μM brefeldin A (Bref A).

(C) Stable knockdown cells for Hsp47 (shHsp47) and control cells (shLuc) were treated with 25 ng/mL Tm, 10 nM thapsigargin, and 2 μM brefeldin A for indicated time points, and then *Xbp1s* mRNA levels were monitored by real-time PCR.

(D) shHsp47 and control cells (upper) or MEFs stably expressing Hsp47-V5 or empty vector (mock) (bottom) were treated with 250 ng/mL Tm for indicated time points. IRE1α phosphorylation levels were determined using Phostag assay and western blot analysis. O, non-phosphorylated; P, phosphorylated.

(E) Analysis of IRE1α oligomerization was assessed using a TREX reporter cell line expressing IRE1α-3F6H-GFP in cells either transfected with siRNA for Hsp47 or overexpressing HSP47-V5.

(F) TREX cells expressing IREIα-3F6H-GFP were transfected with HSP47-V5 expression vector or mock. Then cells were treated with 1 μg/mL of Tm for 4 hr. Quantification of GFP-positive puncta per cell was performed using ImageJ software (bottom).

(G) The expression levels of CHOP and ATF4 were determined by western blot in cells overexpressing HSP47-V5 (upper) or that were knocked down using shRNAs (lower) after stimulation with 500 ng/mL Tm for indicated time points.

In (A), (B), (C), and (F), data represent mean and standard error of three independent experiments. Statistical analysis was performed using Student's t test: *: $p < 0.05$, **: $p < 0.01$.

and *Sec61*, two classical XBP1s-target genes (Lee et al., 2003). Real time PCR analysis revealed that the overexpression of the four candidates significantly enhanced the induction of *Edem1* and *Sec61* mRNA under ER stress (Figure 2B), whereas the up-regulation of *Bip* and *Chop* was not altered in these cells (Figure 2C). We also measured RIDD activity as an additional output of the pathway. Surprisingly, analysis of two canonical RIDD substrates, *Sparc* and *Blocs1* (Hollien et al., 2009), indicated that the overexpression of HSP47-V5 or ATP5-V5 enhanced the decay of these two mRNAs, whereas the expression of PP2A-V5 or TUBα1a-V5 did not affect RIDD levels under the same conditions (Figure 2D) despite augmented *Xbp1* mRNA splicing. Based on the global analysis of our results, we decided to focus our further studies on assessing the contribution of Hsp47 to the regulation of IRE1α because (i) it is an ER-located chaperone, (ii) its modulation generated a strongest effect on cell survival, and (iii) was the greater modifier of *Xbp1* mRNA splicing and RIDD in our analysis.

HSP47 Regulates IRE1α Activation

To further explore the effects of Hsp47 on IRE1α signaling we complemented our previous analysis with a promoter reporter assay using luciferase controlled by a UPR element (UPRE) sequence (Lee et al., 2003). Expression of HSP47-V5 in MEFs led to an enhancement in the activity of the UPRE reporter after Tm treatment (Figure 3A). Similar results were observed when

cells were stimulated with other ER stressors, including thapsigargin and brefeldin A (Figure 3B). This assay was highly dependent on IRE1α expression since no signal was observed when experiments were performed in IRE1α null MEFs (Figure S2C). We confirmed these results using real time PCR to measure *Xbp1s* levels in MEFs with manipulated levels of Hsp47, observing that its expression enhanced IRE1α signaling (Figures 3C and S2D).

IRE1α activation involves its dimerization and auto-transphosphorylation, leading to a conformational change in the cytosolic region that engages the RNase domain. We used a Phostag assay to assess the phosphorylation status of IRE1α in MEFs. Treatment of Hsp47 silenced cells with Tm revealed a delay in the appearance of the electrophoretic shift associated with its activation (Figure 3D, upper panel). In agreement with these results, overexpression of HSP47-V5 accelerated the activation process, reflected by an almost complete phosphorylation of IRE1α that was sustained over time (Figure 3D, bottom panel). Importantly, total IRE1α levels were not altered when the expression of Hsp47 was modulated in MEFs (Figures S3A and S3B).

IRE1α phosphorylation leads to its oligomerization into large clusters. We took advantage of a stable TREX293 cell line overexpressing mammalian IRE1α tagged with GFP controlled by doxycycline to visualize IRE1α oligomerization (Li et al., 2010). We knocked down HSP47 in TREX293 cells using siRNA and monitored the generation of GFP-positive foci. Downregulation of HSP47 reduced the number of IRE1α clusters per cell, leading to a faster attenuation (Figure 3E). In agreement with this, increased number of IRE1α-GFP puncta was observed in HSP47-V5 overexpressing cells after Tm treatment (Figure 3F, see controls in Figures S4A and S4B).

We then further explored the specificity of Hsp47 over the regulation of IRE1α signaling. The overexpression or the knockdown of Hsp47 in MEFs did not alter the upregulation of ATF4 and CHOP under ER stress, as determined using western blot analysis (Figure 3G). Thus, Hsp47 expression specifically enhances molecular events related to IRE1α activation.

Hsp47 Physically Interacts with the Luminal Domain of IRE1α

Our initial IP-mass spectrometry analysis suggested that Hsp47 associates with IRE1α-containing protein complexes. To validate this interaction, we first determined the subcellular distribution of IRE1α and Hsp47 using immunofluorescence and then used a sensitive method based on a confined displacement analysis algorithm to calculate colocalization coefficients (Ramírez et al., 2010). Quantification of Manders coefficients M1 and M2 indicated an average 0.32 and 0.35 index of colocalization, respectively, under basal conditions (Figure 4A, right). Stimulation of ER stress for 6 hr slightly reduced the colocalization index, consistent with our proteomic data (Figure 4A, right). We moved forward to validate this interaction in living cells using an *in situ* proximal ligation assay (Duolink), a method that is predicted to have sensitivity for protein complexes in the range of 40 nm. As control, we knocked down Hsp47 with an shRNA construct (Figure S4C). This experiment corroborated a close proximity between Hsp47 and IRE1α (Figure 4B).

We then performed co-IP assays by analyzing the interaction of endogenous Hsp47 with IRE1α-HA expressed at physiological levels in an *Ern1*-null background (Figure 4C and Figure S1). We also detected a reduced interaction in cells treated with Tm for 4 hr (Figure 4C). Similarly, induction of ER stress with brefeldin A, DTT, and thapsigargin resulted in the release of Hsp47 from the IRE1α complex after prolonged treatment (Figure 4D). Since Hsp47 expression enhances IRE1α signaling and the activation of the pathway occurs very fast after stimulation of ER stress, we then monitored the interaction of Hsp47 with IRE1α during shorter time points. Treatment of cells with Tm revealed a fast and progressive release of BiP from the complex, starting at 1 hr after stimulation (Figure 4E). Interestingly, the binding of endogenous Hsp47 to IRE1α-HA was enhanced at 1 hr after ER stress induction, correlating with the release of BiP from IRE1α (Figure 4E). We also confirmed the formation of a protein complex between the endogenous proteins that was enhanced by ER stress (Figure 4F). Based on the subcellular distribution of Hsp47, we expressed an IRE1α-deletion mutant containing only the N-terminal luminal domain (NLD). Again, our co-IP experiments supported the establishment of a complex between Hsp47 and IRE1α, restricting this association to the ER lumen (Figure 4G). In addition, we also detected the interaction by pull-down assays in COS-1 cells transfected with vectors encoding the NLD of IRE1α fused with a polyhistidine sequence (His-IRE1α-NLD) (Figure 4H).

To determine if Hsp47 directly binds to IRE1α, we used two sensitive *in vitro* assays. MicroScale Thermophoresis (MST) was performed using recombinant HSP47 and IRE1α-NLD produced in *E. coli* and COS-1 cells, respectively. We incubated RED-labeled IRE1α-NLD protein with increasing concentrations of purified HSP47 (Figure 4I). Calculation of the dissociation constant (KD) revealed a high affinity between HSP47 and IRE1α-NLD in the nanomolar range (Table 1). These data were further confirmed using surface plasmon resonance to determine that the biophysical parameters of the interaction were in the nanomolar range (Table 1). We then compared the strength of the interaction between HSP47 and IRE1α-NLD with its affinity for BiP or PDIA6. In this experimental setting, recombinant BiP associated with the luminal domain of IRE1α with a KD value of 39.7 nM, in the same range as recombinant HSP47. In contrast, PDIA6 displayed a lower binding affinity to IRE1α-NLD under the same experimental conditions (Table 1). As control for the specificity of this binding, we tested the association of the ER luminal domain of PERK to recombinant Hsp47. Using MST, very low binding was observed between PERK-NLD and Hsp47 close to the background signal when compared to binding of IRE1α-NLD under the same conditions (Figure S4D). In summary, our combinatorial approaches indicate that HSP47 forms a complex with the luminal domain of IRE1α through a direct interaction.

Hsp47 Reduces the Binding of BiP to the Luminal Domain of IRE1α

Since Hsp47 is an ER-located chaperone that enhances IRE1α activation, we decided to explore possible modulatory effects on the binding of BiP to IRE1α. We transiently expressed His-IRE1α-NLD in COS-1 cells followed by His pull-down and

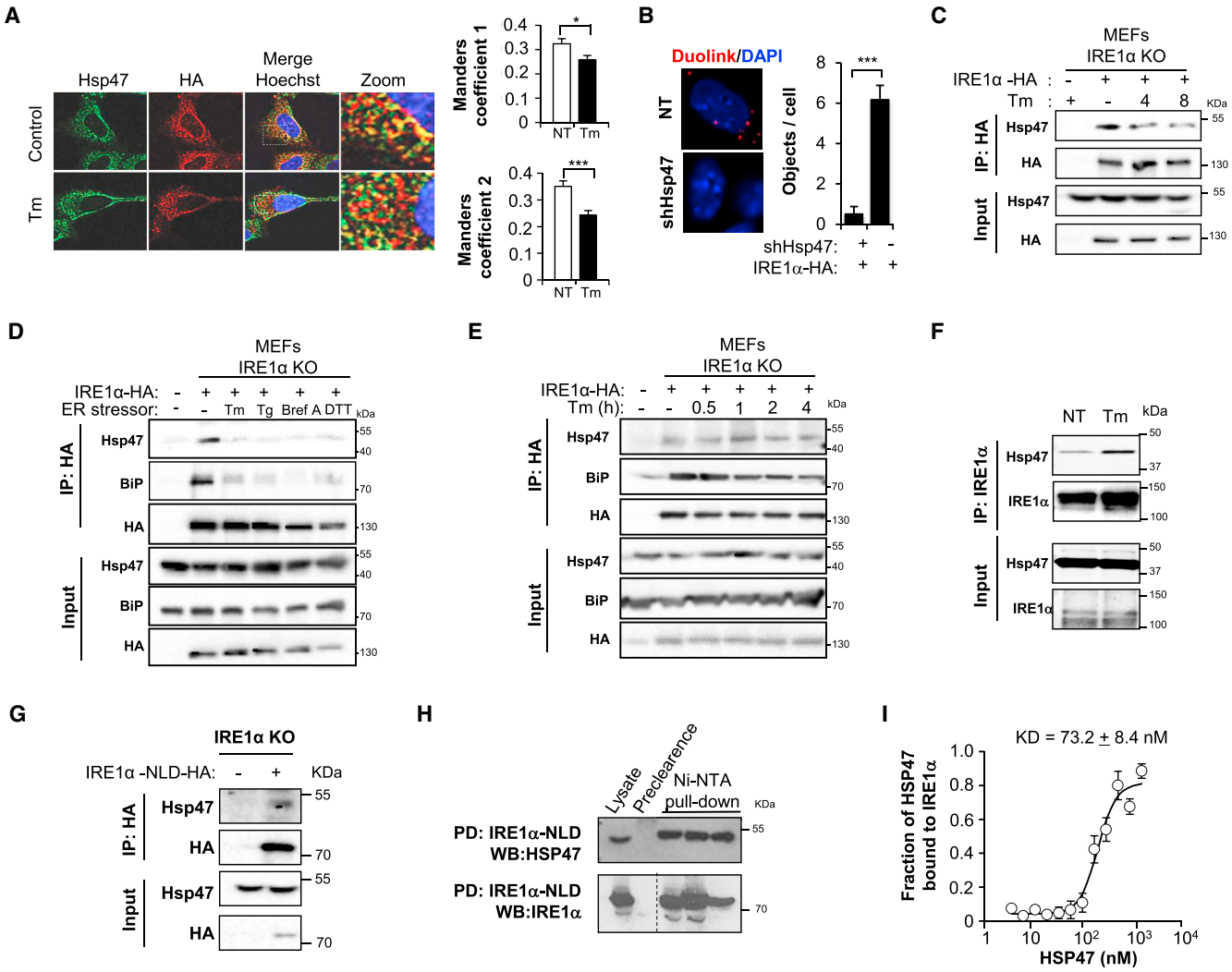

Figure 4. Hsp47 Physically Interacts with IRE1α

(A) Cells expressing IRE1α-HA were treated with 250 ng/mL of Tm for 6 hr and then fixed. The distribution of endogenous Hsp47 and IRE1α-HA was assessed by indirect immunofluorescence and visualized using a confocal microscope. Nuclei were stained with Hoechst (left). Colocalization index between Hsp47 and IRE1α-HA was calculated. Data represent the average and standard error of three independent experiments.

(B) IRE1α-KO cells expressing IRE1α-HA were fixed, and endogenous Hsp47 and HA epitopes were detected using Proximity Ligation assay (Duolink). As control, Hsp47 was knocked down using an shRNA (See Figure S4C). Confocal images were quantified using ImageJ software. (n = 13 untreated cells, n = 18 treated cells).

(C) IRE1α-KO mock or reconstituted MEF cells were treated with 250 ng/mL of Tm for indicated time points. IRE1α-HA was immunoprecipitated followed by western blot analysis of endogenous Hsp47. Total extracts (input) are shown as control.

(D) Similar experiments as described in (C) were performed after stimulating cells with 500 ng/mL Tm, 500 nM thapsigargin (Tg), 1 μM brefeldin A (BfA), or 1 mM DTT for 4 hr.

(E) Cells were stimulated with 100 ng/mL Tm for indicated time points, and then the binding of endogenous BiP and Hsp47 to IRE1α-HA was monitored over time.

(F) The interaction between endogenous IRE1α and Hsp47 was evaluated in MEF cells under resting conditions or after the stimulation with 125 ng/mL Tm for 1 hr.

(G) A deletion mutant of IRE1α-HA in the cytosolic region (IRE1α-NLD-HA) was expressed in IRE1α-KO cells and HA-tag immunoprecipitated; this was followed by western blot analysis of Hsp47.

(H) COS-1 cells were transiently transfected with a HIS-tagged version of the ER luminal domain of IRE1α (IRE1α-NLD); this was followed by a pull-down with Ni-NTA-agarose beads. The presence of HSP47 was assessed by western blot. Each lane represents an independent experiment. Dotted line indicates splicing of images from the same gel and film exposure.

(I) MicroScale thermophoresis was used to evaluate HSP47 binding to Red-labeled-IRE1α-NLD. Increasing concentrations of purified human HSP47 protein (0–10^4 nM) were incubated with 200 nM RED-labeled IRE1-NLD protein. Unlabeled HSP47 protein bound to Red-labeled IRE1α-NLD was measured as a fraction of HSP47 bound to IRE1α.

Data represent the average and standard error of 6 and 12 independent experiments, respectively. Statistical analysis was performed using Student's t test: *: $p < 0.05$, **: $p < 0.01$, ***: $p < 0.001$.

Table 1. HSP47 Interacts with High Affinity with the ER Luminal Domain of IRE1α

SPR			MST
Ka (1/Ms)	Kd (1/s)	KD (nM)	KD (nM)
BIP			
$2.09 \times 10^{12} \pm 1.47 \times 10^{12}$	$7.75 \times 10^{4} \pm 5.46 \times 10^{4}$	39.7 ± 1.6	ND
PDIA6			
$4.29 \times 10^{3} \pm 5.48 \times 10^{1}$	$7.21 \times 10^{-4} \pm 3.53 \times 10^{-6}$	168 ± 1.6	ND
HSP47			
$5.74 \times 10^{3} \pm 5.18 \times 10^{2}$	$4.15 \times 10^{-4} \pm 3.15 \times 10^{-6}$	74.9 ± 7.33	73.2 ± 8.4

Surface plasmon resonance (SPR) or MicroScale thermophoresis (MST) was employed to monitor the interaction between recombinant HSP47 with purified IRE1α-NLD protein from COS-1 cells. For the SPR assay, binding affinity was also compared with the binding of recombinant BiP or PDIA6 to IRE1α-NLD. For SPR, experimental results were corrected against the control surface response to remove any refractive index deviations. Kinetic analyses were carried out with the BiaEvaluation software (GE) using a 1:1 Langmuir binding model and were performed in triplicate. Association and dissociation rates and affinity (KD) were calculated for each experiment and averaged. Ka, equilibrium association constant; Kd, equilibrium dissociation constant; KD, affinity constant; SPR, surface plasmon resonance; MTS, microscale thermophoresis; ND, no data.

western blot analysis. Overexpression of HSP47-V5 significantly reduced the association of BiP to His-IRE1α-NLD (Figure 5A), whereas the binding of PDIA6 was not affected (Figure S4E). We confirmed the consequences of HSP47 to the stability of the BiP and IRE1α complex using MST. We incubated increasing concentrations of recombinant BiP with RED-labeled His-IRE1α-NLD in the presence or absence of recombinant HSP47. Using this approach, we observed a strong reduction in the binding of BiP to the luminal domain of IRE1α when HSP47 was included in the assay (Figure 5B). Similarly, the addition of BiP to the test tube reduced the binding of HSP47 to the luminal domain of IRE1α (Figure 5C; compare with control in Figure 4I).

We then tested the possible impact of HSP47 on the oligomerization status of IRE1α-NLD. We incubated RED-labeled IRE1α-NLD with increasing concentrations of unlabeled IRE1α-NLD in the presence or absence of recombinant HSP47 and performed MST. In these experiments, IRE1α-NLD underwent spontaneous oligomerization after augmenting its concentration (Figure 5D, left), a phenomenon that was enhanced when HSP47 was present in the reaction (Figure 5D, right). Finally, we tested the functional relationship between BiP and Hsp47 in the control of IRE1α activation. Using the UPRE luciferase reporter, we overexpressed BiP in 293T cells to repress IRE1α activation and then tested the effects of increasing the amount of HSP47-V5 in the system. Remarkably, expression of HSP47-V5 was able to repress the inhibitory activity of BiP over IRE1α signaling (Figure 5E). Taken together, these results suggest that HSP47 regulates IRE1α activation by favoring the release of BiP from the complex, increasing the oligomerization status of IRE1α.

Hsp47 Regulates IRE1α Signaling in *D. melanogaster*

Because the UPR machinery is highly conserved in flies, this model has been widely used to investigate regulatory genes (Ryoo, 2015). We previously set up simple bioassays to trigger ER stress *in vivo* in *D. melanogaster* larvae to monitor UPR signaling and to determine the survival of the whole organism after the exposure to Tm (Lisbona et al., 2009; Rojas-Rivera et al., 2012). *D. melanogaster* expresses collagen-like proteins (Chartier et al., 2002; Fessler and Fessler, 1989), and thus it is expected to contain an HSP47 homolog on its genome. Analysis of *D. melanogaster* DNA databases indicated the presence of a putative homolog of HSP47 identified as CG8137 (here termed dHsp47; Figure 5A, and see sequence analysis in Figure S5). We knocked down *dHsp47* by expressing RNAi using the UAS/Gal4 system under the control of the tubulin promoter (Tub-Gal4) (Dietzl et al., 2007; Figure 6B), and then exposed third-stage larvae to Tm to determine d*Xbp1s* levels. A significant reduction in d*Xbp1* mRNA splicing was observed after targeting *dHsp47* as assessed by conventional RT-PCR (Figure 6C) or real-time PCR (Figure 6D). We then performed time course experiments and confirmed that knocking down *dHsp47* using RNAi had a dramatic effect on the activation of dIRE1α signaling (Figure 6E). We also measured the expression levels of heat shock cognate 3 chaperone (*Hsc3*), a target gene of dXBP1's (Rubin et al., 1993). Consistent with our previous results, a strong attenuation of *dHsc3* mRNA was detected in *dHsp47* RNAi larvae compared to control animals (Figure 6F). We also monitored RIDD activity by quantifying the mRNA levels of *dSparc* and *dMys*, two dIRE1α substrates previously described in *D. melanogaster* (Coelho et al., 2013; Coelho and Domingos, 2014). As shown in Figure 6G, the decay of *dSparc* and *dMys* mRNA levels was fully blocked by knocking down *dHsp47*, with even increased levels observed in dHsp47-deficient animals treated with Tm.

To determine the global consequences of dHsp47 expression on the adaptive capacity of animals to ER stress, we quantified the lifespan of adult *D. melanogaster*. We exposed flies to 25 μg/mL Tm administered in lyophilized food or the equivalent concentration of the solvent and determined the number of surviving flies over time (Figure S6B). Remarkably, knocking down d*Hsp47* significantly reduced the survival of flies exposed to Tm (Figure 6H). Importantly, at basal levels, targeting *dHsp47* did not result in spontaneous defects in animal survival (Figure S6C). In summary, these results suggest that dHsp47 controls IRE1α signaling *in vivo* in a fly model of ER stress and influences the capacity of the whole organism to cope with alterations to ER proteostasis.

Hsp47 Regulates IRE1α Signaling in a Mouse Model of ER Stress

A classical paradigm of ER stress in mammals is the injection of mice with a single dose of Tm, which triggers a strong UPR reaction in the liver and kidney. We generated a conditional knockout (cKO) mouse model of *Hsp47* in the liver using the Cre-LoxP system to delete exon 6 in hepatocytes with a tamoxifen-inducible transthyretin promoter (TTR-Cre ind) (Figure 7A). We then treated adult animals with tamoxifen for 5 consecutive days and confirmed 1 week later the deletion of *Hsp47* in the liver

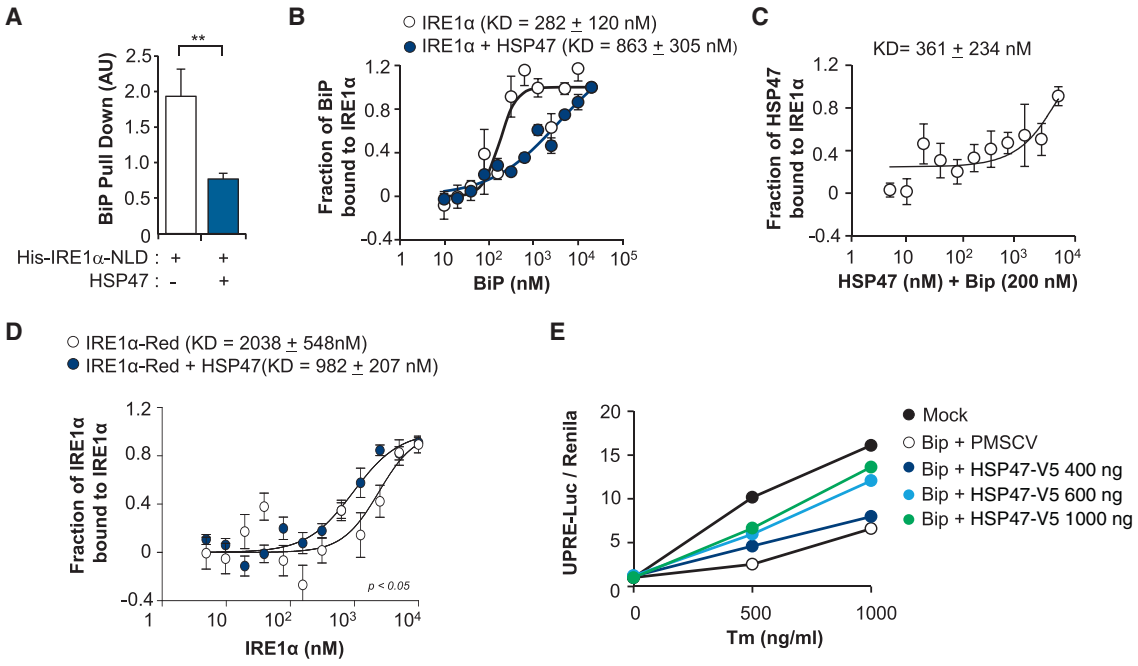

Figure 5. Hsp47 Reduces the Binding of BiP to IRE1α

(A) COS-1 cells were transfected with His-tagged IRE1-NLD expression vector in the presence or absence of an HSP47-V5 expression vector. After 72 hr, cells were lysed and pulled down using Ni-NTA-agarose beads. The presence of BiP in the complex was analyzed by western blot and quantified in three independent experiments. Normalization was performed with signal-in-total extracts and the amount of IRE1 pulled down.

(B) Increasing concentrations of recombinant BiP protein (0–10^5 nM) were incubated with Red-labeled IRE1-NLD protein in the presence or absence of 200 nM recombinant HSP47. MST was used to evaluate BiP binding to IRE1α-NLD. Data represent the average and standard error of 12 independent experiments.

(C) Increasing concentrations of recombinant HSP47 protein (0–10^4 nM) were incubated with Red-labeled IRE1-NLD protein in the presence of 200 nM recombinant BiP. MST was used to evaluate HSP47 binding to IRE1α-NLD. Data represent the average and standard error of six independent experiments.

(D) 200 nM of Red-labeled IRE1α-NLD was incubated with an increasing concentration of unlabeled-IRE1α-NLD (0–10^4 nM) in the presence or absence of 200 nM of purified human HSP47. Interaction of Red-labeled IRE1α-NLD with unlabeled IRE1α-NLD was tested using MST assay. Data represent the average and standard error of 6 and 12 independent experiments, respectively. Statistical analysis was performed using Student's t test: *: $p < 0.05$, **: $p < 0.01$, ***: $p < 0.001$.

(E) 293T cells were transfected with a UPRE-luciferase reporter in the presence of a BiP expression vector. In addition, different concentrations of a HSP47-V5 vector were included. After 16 hr, cells were stimulated with indicated concentrations of Tm, and then 24 hr later, luciferase activity was determined. Data are representative of three independent experiments.

using PCR of genomic DNA (Figure 7B). This strategy did not alter IRE1α protein levels as measured in liver extracts using western blot (Figure S4D). The quantity of Tm used for intraperitoneal injections was also calibrated to avoid saturation of the *Xbp1* mRNA splicing assay, and a concentration of 50 ng of Tm *per* gram of animal was defined for ER stress stimulation. Kinetic analysis of IRE1α signaling in the liver revealed a transient induction of *Xbp1* mRNA splicing after Tm injection (Figure 7C). A faster attenuation of *Xbp1* mRNA splicing was observed in Hsp47^{cKO} animals after 16 hr of Tm treatment compared to littermate control mice (Figure 7D). The inhibitory effects of *Hsp47* ablation were confirmed when *Xbp1s* mRNA levels were quantified by real-time PCR (Figure 7E, left). As an internal control for these experiments, we analyzed the kidney of the same animals because of the lack of *Hsp47* gene deletion in this organ by the TTR-Cre ind system (Figure 7E, right). These results indicate that Tm treatments were equally effective in inducing an ER stress response in both experimental groups.

We also measured other downstream UPR signaling events in Hsp47^{cKO} livers. Analysis of mRNA levels of *Edem1* (Figure 7F) and *Blocs1* (Figure 7G) confirmed reduced IRE1α signaling upon *Hsp47* deletion under ER stress conditions. Importantly, the upregulation of *Bip* and *Chop* was unaltered in Hsp47^{cKO} animals injected with Tm (Figure 7H). We then analyzed the extent of tissue damage triggered by Tm injections in control- and *Hsp47*-deficient livers. Hematoxylin staining indicated slight signs of hepatocyte damage in Hsp47^{cKO} mice when they were treated with Tm; this was associated with the appearance of enlarged cells and signs of inflammatory cell infiltration (Figure 7I). We also monitored the levels of apoptosis using the TUNEL assay. As expected, the low concentration of Tm used to challenge mice did not result in a clear induction of the apoptosis index in the control group, whereas a significant increase was observed in the liver of Hsp47^{cKO} animals (Figure 7J). For comparison, we also used a cKO mouse for IRE1α in the liver using the Mx-Cre system (Lee et al., 2008). Consistent with our results with Hsp47-deficient mice, targeting IRE1α also enhanced the susceptibility of liver cells to apoptosis (Figure S7A), confirming the prosurvival role of the pathway in this organ.

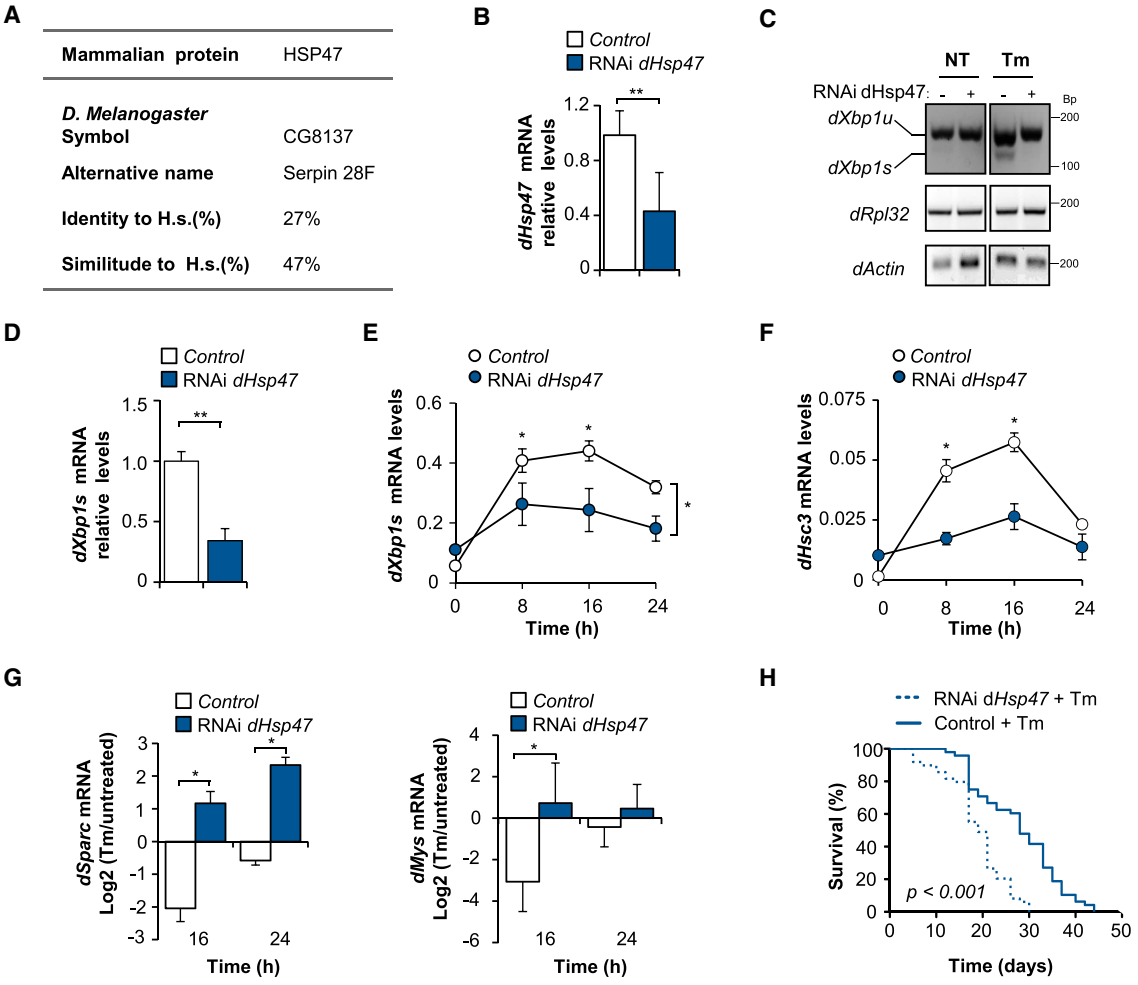

Figure 6. Hsp47 Regulates IRE1α Signaling in *D. melanogaster*, Impacting Animal Survival under ER Stress

(A) Sequence analysis of the putative homolog of Hsp47 in *D. melanogaster* (dHsp47). Accession number and percentage of sequence identity and similitude are shown.

(B) dHsp47 was knocked down *in vivo* by expressing specific RNAi constructs using the UAS-GAL4 system under the control of a tubulin driver promoter. mRNA levels of *dHsp47* were monitored by real-time PCR in total mRNA extract of early third-instar larvae. Mean and standard error are presented from three independent experiments.

(C) Early third-instar larvae of control and RNAi dHsp47 lines were grown under standard feeding conditions supplemented with 25 μg/mL of Tm. After 16 hr, larvae were collected, and *dXbp1* mRNA splicing was determined by RT-PCR. *dRpl32* and *dActin* were monitored as loading controls.

(D) Early third-instar larvae of control and dHsp47 RNAi lines were grown in food supplemented with 25 μg/mL of Tm for 8 hr, and *dXbp1s* mRNA levels were measured by real-time PCR using cDNA prepared from whole larval RNA extracts. Data represent the mean and standard error for three independent experiments.

(E and F) Control and dHsp47 RNAi and control animals were treated with 25 μg/mL of Tm for indicated time points, and the mRNA levels of *dXbp1s* (E) or *dHsc3* (F) mRNA were evaluated by real-time PCR. Statistical analysis was performed using two-way ANOVA test: *: $p < 0.05$.

(G) *dSparc* and *dMys* were also evaluated by real-time PCR from the same samples as (E). Data were normalized to non-treated larvae and the mRNA of *dRpl32* was used as housekeeping gene. Data represent the mean and standard error of three to four independent experiments. Statistical analysis was performed using Student's t test: *: $p < 0.05$, **: $p < 0.01$, ***: $p < 0.001$.

(H) A total of 50 control and 50 RNAi dHsp47 adult flies were grown in standard feeding conditions in the presence of 25 μg/mL of Tm in the food. The number of viable flies was calculated over time. Statistical analysis was performed using the Kaplan-Meyer and log-rank (Mantel-cox) tests.

Hsp47 is the major chaperone involved in the folding and secretion of collagen, and its ablation may generate deleterious effects to liver physiology. Consistent with the short period after deletion used to analyze UPR signaling here, trichrome staining did not reveal any evident collagen deposition at basal levels in Hsp47^{cKO} mice or after ER stress stimulation (Figure S7B). Analysis of the mRNA levels of genes related to fibrosis—including several collagen isoforms (*Col1α1*, *Col6α1* and *Col6α3*), *Acta2*, and the metalloproteinase inhibitor *Timp2*—revealed minor alterations under resting conditions and a slight enhancement in their expression in Hsp47-deficient livers after injection of Tm (Figures 7K and S7C). Taken together, these results indicate that Hsp47 expression modulates IRE1α signaling and the survival of hepatocytes under ER stress *in vivo* in the absence of evident signs of fibrosis.

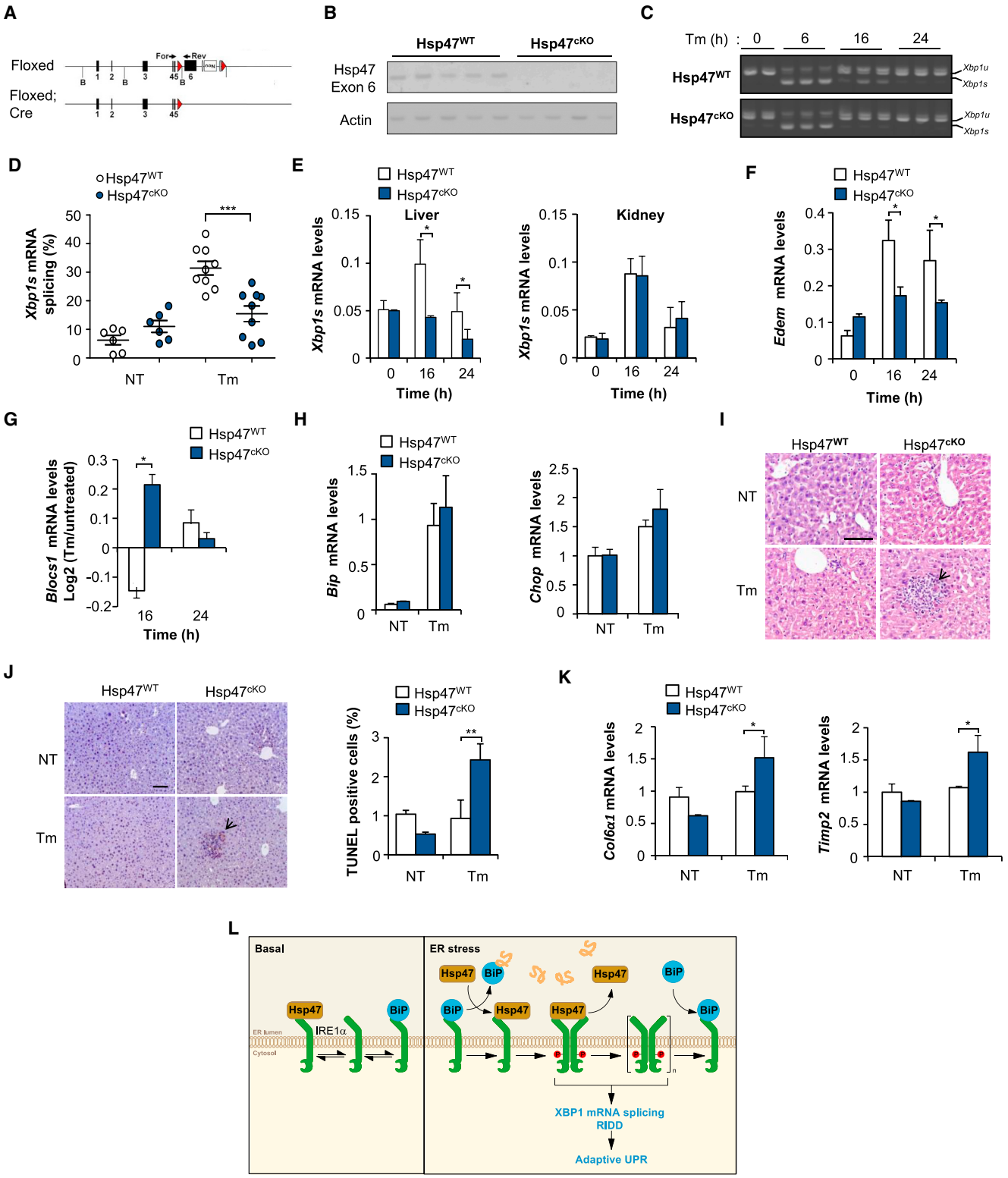

Figure 7. Conditional Deficiency of Hsp47 in the Liver Attenuates IRE1α Signaling under ER Stress *In Vivo*

(A) Conditional knockout (cKO) mice for the *Hsp47* gene was generated in hepatocytes using LoxP system and a TTR-inducible Cre line. Schematic representation of the gene targeting strategy is presented.

(B) 8-week-old animals were injected intraperitoneally (i.p.) with 1 mg of tamoxifen for 5 consecutive days and sacrificed 1 week later to confirm deletion of exon 6 of *Hsp47* using PCR of genomic DNA. Actin was amplified as the internal control.

(legend continued on next page)

DISCUSSION

IRE1α initiates the most conserved signaling branch of the UPR, determining cell fate under ER stress. Although the biology of IRE1α and its role in disease has been extensively studied for the last fifteen years, the mechanisms mediating its regulation are poorly understood. ER stress is emerging as a driver of multiple pathological conditions, ranging from cancer to neurodegeneration, inflammation, and metabolic disorders, among other diseases (Wang and Kaufman, 2016). In this context, several studies have demonstrated that targeting the activity of IRE1α with small molecules has important protective effects in various disease models (Hetz et al., 2013; Maly and Papa, 2014). Due to the implications of IRE1α in sustaining cell function under stress, a complex network of regulatory checkpoints has evolved to tightly control its signaling behavior. The concept of the UPRosome envisions IRE1α as a scaffold where many components assemble to fine-tune its activity (Hetz and Glimcher, 2009). This model has been also applied to other UPR mediators including ATF6 and PERK (Hetz et al., 2015), indicating that both the threshold of protein misfolding to engage the UPR and the amplitude of its downstream outputs depend on intrinsic and selective modifications of the UPR transducers and do not directly mirror ER stress levels (Hetz and Papa, 2017).

Here we have uncovered IRE1α interactors and identified four candidates that differentially regulate *Xbp1* mRNA splicing, RIDD, and cell survival under ER stress. From these hits, Hsp47 had a robust regulatory effect over IRE1α. Unexpectedly, PPA2 and ATP5h are localized to the mitochondria and were classified as IRE1α activators. Further studies are needed to define how PPA2 and ATP5h expression affects UPR signaling. Of note, IRE1α has been recently reported to localize to ER-mitochondrial contact sites (Mori et al., 2013; Son et al., 2014); here, the interaction with PPA2 or ATP5h may occur as part of a larger complex that may indirectly couple these internal mitochondrial proteins to IRE1α. Our studies to validate TUBα1a gave conflicting results, in that both gain and loss of function increased IRE1α signaling. Based on our results, we speculate that knocking down TUBα1a may have pleiotropic adverse effects, increasing the susceptibility of cells to ER stress, whereas its overexpression may reveal its true activity in the UPR. Since available data indicate that the actin cytoskeleton and type II myosin control the oligomerization status of IRE1α (He et al., 2012; Ishiwata-Kimata et al., 2013), it may be feasible that TUBα1a overexpression selectively regulates *Xbp1* mRNA splicing. Importantly, we also obtained data demonstrating that the corresponding homologs of PPA2, ATP5h, and TUBα1a in flies influence the survival of whole animals when exposed to ER stress, as demonstrated using loss-of-function approaches (Figure S6); this fully recapitulates the phenotypes obtained in mouse cells.

Hsp47 is an ER-resident foldase that belongs to the family of heat shock proteins and operates as a specific carrier for different types of collagen (Ishida et al., 2006; Nagata and Hosokawa, 1996; Saibil, 2013). Hsp47 assists the transport of triple-helix procollagen from the ER lumen to the *cis*-Golgi (Nakai et al., 1992; Natsume et al., 1994; Satoh et al., 1996). We provided functional evidence supporting a conserved regulation of the UPR by Hsp47 in different species as demonstrated by genetic manipulation in fly and mouse models. At the molecular level, we were able to reconstitute the interaction between Hsp47 and IRE1α using a cell-free system with purified proteins. Hsp47 associates to the ER luminal domain of IRE1α, reducing the binding of BiP to the complex, an interaction that may enhance IRE1α oligomerization or stabilize the dimeric forms. The association between Hsp47 and IRE1α is quickly enhanced upon ER stress, leading to a release of the protein after prolonged stimulation, suggesting a hit-and-run interaction. Based on our findings and previous evidence linking BiP and PDIA6 to the regulation of IRE1α, we speculate that a complex network of ER chaperones may operate as "stress sentinels" that converge into the activation of IRE1α to engage feedback mechanisms that sustain proteostasis (see model in Figure 7L).

Hsp47 has evolved as a specialized chaperone for collagen, a process that is also assisted by BiP and other ER foldases (Hirayoshi et al., 1991; Ishida and Nagata, 2011). Hsp47 guides the trafficking of the triple helix of collagen into the Golgi apparatus, operating as a quality control factor by interacting with TANGO1 (Ishikawa et al., 2016). Importantly, collagen is one of the most abundant proteins in the cell, reaching near 30% of the total proteome mass in certain cell types, and it certainly represents a main ER client. Due to the relatively high expression levels of collagens and their complex folding process, we speculate that collagen is one of the key proteins that misfold and accumulate under ER stress. In fact, complete deficiency of Hsp47 has been

(C) *Hsp47*^{WT} or *Hsp47*^{cKO} mice were injected with Tm (50 ng/g, i.p.) and sacrificed over time. The levels of *Xbp1* mRNA splicing were monitored by RT-PCR in total liver mRNA extracts. Each lane represents independent animals.

(D) The levels of *Xbp1* mRNA splicing were quantified in animals described in (C) after 16 hr of Tm injection (untreated animals, NT: n = 6; Tm treated mice: n = 9).

(E) Expression of *Xbp1s* mRNA on liver (left) and kidney (right) were measured by real-time PCR in animals presented in (C).

(F–H) *Edem1* mRNA levels (F), the decay of *Blocs1* mRNA (G), and *Bip* and *Chop* mRNA (H) were evaluated by real-time PCR on liver of the same animals as in (C) after 16 hr of Tm injection.

(I) Liver tissue from *Hsp47*^{WT} and *Hsp47*^{cKO} mice injected with 50 ng/g of Tm was fixed after 24 hr of treatment and stained with hematoxylin and eosin (magnification × 400). Immune cell infiltration is indicated with an arrowhead. Scale bars, 100 μm. At least three animals per group were analyzed.

(J) Apoptotic cells were quantified in samples described in (I) with the TUNEL assay. Data represent the average and standard error of the analysis of three animals per group. Scale bars, 100 μm.

(K) The expression levels of *Col6α1* and *Timp2* mRNAs were measured by real-time PCR in *Hsp47*^{WT} and *Hsp47*^{cKO} liver of animals treated or not treated with 50 ng/g Tm for 24 hr (untreated animals, n = 2; Tm-treated mice, n = 3). Statistical analysis was performed using Student's t test: *: $p < 0.05$, **: $p < 0.01$, ***: $p < 0.001$.

(L) Working model: under basal conditions, IRE1α is maintained in a monomeric inactive state through its interaction with the ER chaperone BiP. The ER chaperone Hsp47 binds to IRE1α and enhances its activation, in part by inducing the dissociation of BiP from the complex, which may facilitate IRE1α dimerization and oligomerization into large clusters for optimal UPR signaling. After prolonged ER stress, Hsp47 is released from the complex.

reported to result in ER-stress-mediated apoptosis in certain cellular models (Kawasaki et al., 2015; Marutani et al., 2004), engaging the activation of compensatory autophagy to eliminate misfolded collagen and sustain cell survival (Ishida et al., 2009). Thus, the molecular connection identified here between Hsp47 and IRE1α may represent a central mechanism that adjusts ER folding needs according to the production of collagen, where more collagen expression engages stronger IRE1α signals mediated by Hsp47 to improve the secretory capacity of the cell. We are currently exploring this concept. In agreement with this idea, a recent study indicated that TANGO1, a central component involved in the trafficking of the collagen triple helix to the Golgi apparatus (Saito et al., 2009), is a direct target gene of XBP1s (Maiers et al., 2017). In addition, Hsp47 is an ER stress target gene (Miyata et al., 2013; Rutkowski et al., 2006), indicating that one of the adaptive outputs of the UPR is the improvement of collagen biosynthesis and trafficking. In fact, recent studies in medaka fish indicated that misfolding of collagens is the source of physiological stress when the UPR is genetically inactivated during development (Ishikawa et al., 2013; Ishikawa et al., 2017). Interestingly, a canonical RIDD target in mammals is Collagen-6 (Hollien et al., 2009), suggesting that under ER stress, collagen levels may be rapidly reduced by the control of their mRNA stability to avoid further damage. Since the establishment of the extracellular matrix and connective tissue is an important factor to sustain multicellular organization in higher organisms, the dependency of mammalian UPR on Hsp47 expression may have evolved as an adjustor of organismal proteostasis. It remains to be determined whether the interaction between the IRE1α and Hsp47 axis has a bidirectional function influencing collagen biogenesis. To address this concept, we are currently investigating the possible contribution of the IRE1α/Hsp47 axis to fibrosis, a condition driven by abnormal collagen deposition. Overall, the current study has uncovered a previously unanticipated point of control of IRE1α signaling, contributing to our understanding of how fluctuations in the ER folding capacity are monitored and adjusted to maintain proteostasis.

STAR★METHODS

Detailed methods are provided in the online version of this paper and include the following:

- KEY RESOURCES TABLE
- CONTACT FOR REAGENT AND RESOURCE SHARING
- EXPERIMENTAL MODEL AND SUBJECT DETAILS
  - Cell lines
  - Drosophila melanogaster
  - Hsp47 conditional-knockout mice
- METHOD DETAILS
  - Viability assay
  - shRNA production, overexpression, and virus transduction
  - RNA isolation, RT-PCR, and real-time PCR
  - LTQ analysis of IRE1α-HA immunoprecipitation and identification of IRE1α-interacting proteins
  - Immunoprecipitations and pull-down assays
  - Immunoblot analysis and phostag gels
  - Luciferase assay
  - Recombinant proteins
  - Surface plasmon resonance (SPR)
  - MicroScale thermophoresis (MST)
  - Immunofluorescence, duo link assay, and IRE1-GFP clustering
  - Histological evaluation and TUNEL assay
- QUANTIFICATION AND STATISTICAL ANALYSIS

SUPPLEMENTAL INFORMATION

Supplemental Information includes seven figures and three tables and can be found with this article online at https://doi.org/10.1016/j.molcel.2017.12.028.

ACKNOWLEDGMENTS

We thank Megan Kopp for generating PERK recombinant protein. This work was primarily funded by FONDECYT 1140549, FONDAP program 15150012, Millennium Institute P09-015-F, and European Commission R&D MSCA-RISE 734749 (C.H.). We are grateful for the support from Michael J. Fox Foundation for Parkinson's Research Target Validation grant 9277, FONDEF ID16I10223, FONDEF D11E1007, US Office of Naval Research Global N62909-16-1-2003, U.S. Air Force Office of Scientific Research FA9550-16-1-0384, ALSRP Therapeutic Idea Award AL150111, Muscular Dystrophy Association 382453, and CONICYT-Brazil 441921/2016-7 (C.H.). We also thank FONDECYT 3130365 (to D.R.-R.), 3150113 (to A.C.-S), and 3160461 (to H.U.); CONICYT Ph.D. fellowship 21130169 (to D.S.); Canadian Institutes of Health research grants MOP-15291, MOP-15415, and MOP-53050 (J.G. and M.M.); INSERM and the Société Francophone du Diabète (SFD/MSD); Société Française d'Hépatologie (AFEF/Aptalis); La Ligue contre le Cancer (BMM); the French government (National Research Agency, ANR) "Investments for the Future" LABEX SIGNALIFE, program reference ANR-11-LABX-002801 (C.L.); The German Research Foundation (DFG) GO 1987/2-1 (P.G. and G.C.); and BNI-P09015F (C.H. and J.S.).

AUTHOR CONTRIBUTIONS

C.H., D.S., D.R.-R., and D.A.R. designed the study. D.S., D.R.-R., D.A.R., J.G., A.K., C.L., S.I., H.U., A.C.-S., Y.H., M.V.-C., E.C., and G.C. participated in experimental design, performed experiments, and analyzed the data. P.G., T.V., M.M.U.A., B.B.-M., K.N., M.M., and J.S. supervised experiments and participated in the designs. C.H., D.S., and D.R.-R., wrote or contributed to writing the manuscript. All authors read and approved the final version of the manuscript.

Received: April 27, 2017
Revised: October 5, 2017
Accepted: December 27, 2017
Published: January 18, 2018

REFERENCES

Acosta-Alvear, D., Zhou, Y., Blais, A., Tsikitis, M., Lents, N.H., Arias, C., Lennon, C.J., Kluger, Y., and Dynlacht, B.D. (2007). XBP1 controls diverse cell type- and condition-specific transcriptional regulatory networks. Mol. Cell *27*, 53–66.

Bertolotti, A., Zhang, Y., Hendershot, L.M., Harding, H.P., and Ron, D. (2000). Dynamic interaction of BiP and ER stress transducers in the unfolded-protein response. Nat. Cell Biol. *2*, 326–332.

Carrara, M., Prischi, F., Nowak, P.R., Kopp, M.C., and Ali, M.M. (2015). Noncanonical binding of BiP ATPase domain to Ire1 and Perk is dissociated by unfolded protein CH1 to initiate ER stress signaling. eLife *4*, https://doi.org/10.7554/eLife.03522.

Castillo, K., Rojas-Rivera, D., Lisbona, F., Caballero, B., Nassif, M., Court, F.A., Schuck, S., Ibar, C., Walter, P., Sierralta, J., et al. (2011). BAX inhibitor-1

regulates autophagy by controlling the IRE1α branch of the unfolded protein response. EMBO J. *30*, 4465–4478.

Chartier, A., Zaffran, S., Astier, M., Sémériva, M., and Gratecos, D. (2002). Pericardin, a *Drosophila* type IV collagen-like protein is involved in the morphogenesis and maintenance of the heart epithelium during dorsal ectoderm closure. Development *129*, 3241–3253.

Coelho, D.S., and Domingos, P.M. (2014). Physiological roles of regulated Ire1 dependent decay. Front. Genet. *5*, 76.

Coelho, D.S., Cairrão, F., Zeng, X., Pires, E., Coelho, A.V., Ron, D., Ryoo, H.D., and Domingos, P.M. (2013). Xbp1-independent Ire1 signaling is required for photoreceptor differentiation and rhabdomere morphogenesis in *Drosophila*. Cell Rep. *5*, 791–801.

Credle, J.J., Finer-Moore, J.S., Papa, F.R., Stroud, R.M., and Walter, P. (2005). On the mechanism of sensing unfolded protein in the endoplasmic reticulum. Proc. Natl. Acad. Sci. USA *102*, 18773–18784.

Dietzl, G., Chen, D., Schnorrer, F., Su, K.C., Barinova, Y., Fellner, M., Gasser, B., Kinsey, K., Oppel, S., Scheiblauer, S., et al. (2007). A genome-wide transgenic RNAi library for conditional gene inactivation in *Drosophila*. Nature *448*, 151–156.

Eletto, D., Eletto, D., Dersh, D., Gidalevitz, T., and Argon, Y. (2014). Protein disulfide isomerase A6 controls the decay of IRE1α signaling via disulfide-dependent association. Mol. Cell *53*, 562–576.

Fessler, J.H., and Fessler, L.I. (1989). *Drosophila* extracellular matrix. Annu. Rev. Cell Biol. *5*, 309–339.

Gardner, B.M., and Walter, P. (2011). Unfolded proteins are Ire1-activating ligands that directly induce the unfolded protein response. Science *333*, 1891–1894.

Ghosh, R., Wang, L., Wang, E.S., Perera, B.G., Igbaria, A., Morita, S., Prado, K., Thamsen, M., Caswell, D., Macias, H., et al. (2014). Allosteric inhibition of the IRE1α RNase preserves cell viability and function during endoplasmic reticulum stress. Cell *158*, 534–548.

Groenendyk, J., Peng, Z., Dudek, E., Fan, X., Mizianty, M.J., Dufey, E., Urra, H., Sepulveda, D., Rojas-Rivera, D., Lim, Y., et al. (2014). Interplay between the oxidoreductase PDIA6 and microRNA-322 controls the response to disrupted endoplasmic reticulum calcium homeostasis. Sci. Signal. *7*, ra54.

Han, D., Lerner, A.G., Vande Walle, L., Upton, J.P., Xu, W., Hagen, A., Backes, B.J., Oakes, S.A., and Papa, F.R. (2009). IRE1alpha kinase activation modes control alternate endoribonuclease outputs to determine divergent cell fates. Cell *138*, 562–575.

He, Y., Beatty, A., Han, X., Ji, Y., Ma, X., Adelstein, R.S., Yates, J.R., 3rd, Kemphues, K., and Qi, L. (2012). Nonmuscle myosin IIB links cytoskeleton to IRE1α signaling during ER stress. Dev. Cell *23*, 1141–1152.

Hetz, C. (2012). The unfolded protein response: controlling cell fate decisions under ER stress and beyond. Nat. Rev. Mol. Cell Biol. *13*, 89–102.

Hetz, C., and Glimcher, L.H. (2009). Fine-tuning of the unfolded protein response: assembling the IRE1alpha interactome. Mol. Cell *35*, 551–561.

Hetz, C., and Papa, F.R. (2017). The unfolded protein response and cell fate control. Mol. Cell *69*, this issue, 169–181.

Hetz, C., Chevet, E., and Harding, H.P. (2013). Targeting the unfolded protein response in disease. Nat. Rev. Drug Discov. *12*, 703–719.

Hetz, C., Chevet, E., and Oakes, S.A. (2015). Proteostasis control by the unfolded protein response. Nat. Cell Biol. *17*, 829–838.

Hirayoshi, K., Kudo, H., Takechi, H., Nakai, A., Iwamatsu, A., Yamada, K.M., and Nagata, K. (1991). HSP47: a tissue-specific, transformation-sensitive, collagen-binding heat shock protein of chicken embryo fibroblasts. Mol. Cell. Biol. *11*, 4036–4044.

Hollien, J., Lin, J.H., Li, H., Stevens, N., Walter, P., and Weissman, J.S. (2009). Regulated Ire1-dependent decay of messenger RNAs in mammalian cells. J. Cell Biol. *186*, 323–331.

Hoofnagle, A.N., Becker, J.O., Oda, M.N., Cavigiolio, G., Mayer, P., and Vaisar, T. (2012). Multiple-reaction monitoring-mass spectrometric assays can accurately measure the relative protein abundance in complex mixtures. Clin. Chem. *58*, 777–781.

Hu, P., Han, Z., Couvillon, A.D., Kaufman, R.J., and Exton, J.H. (2006). Autocrine tumor necrosis factor alpha links endoplasmic reticulum stress to the membrane death receptor pathway through IRE1alpha-mediated NF-kappaB activation and down-regulation of TRAF2 expression. Mol. Cell. Biol. *26*, 3071–3084.

Ishida, Y., and Nagata, K. (2011). Hsp47 as a collagen-specific molecular chaperone. Methods Enzymol. *499*, 167–182.

Ishida, Y., Kubota, H., Yamamoto, A., Kitamura, A., Bächinger, H.P., and Nagata, K. (2006). Type I collagen in Hsp47-null cells is aggregated in endoplasmic reticulum and deficient in N-propeptide processing and fibrillogenesis. Mol. Biol. Cell *17*, 2346–2355.

Ishida, Y., Yamamoto, A., Kitamura, A., Lamandé, S.R., Yoshimori, T., Bateman, J.F., Kubota, H., and Nagata, K. (2009). Autophagic elimination of misfolded procollagen aggregates in the endoplasmic reticulum as a means of cell protection. Mol. Biol. Cell *20*, 2744–2754.

Ishikawa, T., Okada, T., Ishikawa-Fujiwara, T., Todo, T., Kamei, Y., Shigenobu, S., Tanaka, M., Saito, T.L., Yoshimura, J., Morishita, S., et al. (2013). ATF6α/β-mediated adjustment of ER chaperone levels is essential for development of the notochord in medaka fish. Mol. Biol. Cell *24*, 1387–1395.

Ishikawa, Y., Ito, S., Nagata, K., Sakai, L.Y., and Bächinger, H.P. (2016). Intracellular mechanisms of molecular recognition and sorting for transport of large extracellular matrix molecules. Proc. Natl. Acad. Sci. USA *113*, E6036–E6044.

Ishikawa, T., Toyama, T., Nakamura, Y., Tamada, K., Shimizu, H., Ninagawa, S., Okada, T., Kamei, Y., Ishikawa-Fujiwara, T., Todo, T., et al. (2017). UPR transducer BBF2H7 allows export of type II collagen in a cargo- and developmental stage-specific manner. J. Cell Biol. *216*, 1761–1774.

Ishiwata-Kimata, Y., Yamamoto, Y.H., Takizawa, K., Kohno, K., and Kimata, Y. (2013). F-actin and a type-II myosin are required for efficient clustering of the ER stress sensor Ire1. Cell Struct. Funct. *38*, 135–143.

Karagöz, G.E., Acosta-Alvear, D., Nguyen, H.T., Lee, C.P., Chu, F., and Walter, P. (2017). An unfolded protein-induced conformational switch activates mammalian IRE1. eLife *6*, e30700.

Kawasaki, K., Ushioda, R., Ito, S., Ikeda, K., Masago, Y., and Nagata, K. (2015). Deletion of the collagen-specific molecular chaperone Hsp47 causes endoplasmic reticulum stress-mediated apoptosis of hepatic stellate cells. J. Biol. Chem. *290*, 3639–3646.

Kimata, Y., and Kohno, K. (2011). Endoplasmic reticulum stress-sensing mechanisms in yeast and mammalian cells. Curr. Opin. Cell Biol. *23*, 135–142.

Lai, C.W., Aronson, D.E., and Snapp, E.L. (2010). BiP availability distinguishes states of homeostasis and stress in the endoplasmic reticulum of living cells. Mol. Biol. Cell *21*, 1909–1921.

Lee, A.H., Iwakoshi, N.N., and Glimcher, L.H. (2003). XBP-1 regulates a subset of endoplasmic reticulum resident chaperone genes in the unfolded protein response. Mol. Cell. Biol. *23*, 7448–7459.

Lee, A.H., Scapa, E.F., Cohen, D.E., and Glimcher, L.H. (2008). Regulation of hepatic lipogenesis by the transcription factor XBP1. Science *320*, 1492–1496.

Li, H., Korennykh, A.V., Behrman, S.L., and Walter, P. (2010). Mammalian endoplasmic reticulum stress sensor IRE1 signals by dynamic clustering. Proc. Natl. Acad. Sci. USA *107*, 16113–16118.

Lin, J.H., Li, H., Yasumura, D., Cohen, H.R., Zhang, C., Panning, B., Shokat, K.M., Lavail, M.M., and Walter, P. (2007). IRE1 signaling affects cell fate during the unfolded protein response. Science *318*, 944–949.

Lisbona, F., Rojas-Rivera, D., Thielen, P., Zamorano, S., Todd, D., Martinon, F., Glavic, A., Kress, C., Lin, J.H., Walter, P., et al. (2009). BAX inhibitor-1 is a negative regulator of the ER stress sensor IRE1alpha. Mol. Cell *33*, 679–691.

Liu, C.Y., Wong, H.N., Schauerte, J.A., and Kaufman, R.J. (2002). The protein kinase/endoribonuclease IRE1alpha that signals the unfolded protein response has a luminal N-terminal ligand-independent dimerization domain. J. Biol. Chem. *277*, 18346–18356.

Lu, G., Ota, A., Ren, S., Franklin, S., Rau, C.D., Ping, P., Lane, T.F., Zhou, Z.H., Reue, K., Lusis, A.J., et al. (2013). PPM1l encodes an inositol requiring-protein 1 (IRE1) specific phosphatase that regulates the functional outcome of the ER stress response. Mol. Metab. *2*, 405–416.

Maiers, J.L., Kostallari, E., Mushref, M., deAssuncao, T.M., Li, H., Jalan-Sakrikar, N., Huebert, R.C., Cao, S., Malhi, H., and Shah, V.H. (2017). The unfolded protein response mediates fibrogenesis and collagen I secretion through regulating TANGO1 in mice. Hepatology *65*, 983–998.

Maly, D.J., and Papa, F.R. (2014). Druggable sensors of the unfolded protein response. Nat. Chem. Biol. *10*, 892–901.

Mao, T., Shao, M., Qiu, Y., Huang, J., Zhang, Y., Song, B., Wang, Q., Jiang, L., Liu, Y., Han, J.D., et al. (2011). PKA phosphorylation couples hepatic inositol-requiring enzyme 1alpha to glucagon signaling in glucose metabolism. Proc. Natl. Acad. Sci. USA *108*, 15852–15857.

Marutani, T., Yamamoto, A., Nagai, N., Kubota, H., and Nagata, K. (2004). Accumulation of type IV collagen in dilated ER leads to apoptosis in Hsp47-knockout mouse embryos via induction of CHOP. J. Cell Sci. *117*, 5913–5922.

Masago, Y., Hosoya, A., Kawasaki, K., Kawano, S., Nasu, A., Toguchida, J., Fujita, K., Nakamura, H., Kondoh, G., and Nagata, K. (2012). The molecular chaperone Hsp47 is essential for cartilage and endochondral bone formation. J. Cell Sci. *125*, 1118–1128.

Maurel, M., Chevet, E., Tavernier, J., and Gerlo, S. (2014). Getting RIDD of RNA: IRE1 in cell fate regulation. Trends Biochem. Sci. *39*, 245–254.

Miyata, S., Mizuno, T., Koyama, Y., Katayama, T., and Tohyama, M. (2013). The endoplasmic reticulum-resident chaperone heat shock protein 47 protects the Golgi apparatus from the effects of O-glycosylation inhibition. PLoS ONE *8*, e69732.

Mori, T., Hayashi, T., Hayashi, E., and Su, T.P. (2013). Sigma-1 receptor chaperone at the ER-mitochondrion interface mediates the mitochondrion-ER-nucleus signaling for cellular survival. PLoS ONE *8*, e76941.

Nagata, K. (2003). HSP47 as a collagen-specific molecular chaperone: function and expression in normal mouse development. Semin. Cell Dev. Biol. *14*, 275–282.

Nagata, K., and Hosokawa, N. (1996). Regulation and function of collagen-specific molecular chaperone, HSP47. Cell Struct. Funct. *21*, 425–430.

Nakai, A., Satoh, M., Hirayoshi, K., and Nagata, K. (1992). Involvement of the stress protein HSP47 in procollagen processing in the endoplasmic reticulum. J. Cell Biol. *117*, 903–914.

Natsume, T., Koide, T., Yokota, S., Hirayoshi, K., and Nagata, K. (1994). Interactions between collagen-binding stress protein HSP47 and collagen. Analysis of kinetic parameters by surface plasmon resonance biosensor. J. Biol. Chem. *269*, 31224–31228.

Neely, G.G., Hess, A., Costigan, M., Keene, A.C., Goulas, S., Langeslag, M., Griffin, R.S., Belfer, I., Dai, F., Smith, S.B., et al. (2010). A genome-wide *Drosophila* screen for heat nociception identifies $\alpha 2\beta 3$ as an evolutionarily conserved pain gene. Cell *143*, 628–638.

Oakes, S.A., and Papa, F.R. (2015). The role of endoplasmic reticulum stress in human pathology. Annu. Rev. Pathol. *10*, 173–194.

Qiu, Y., Mao, T., Zhang, Y., Shao, M., You, J., Ding, Q., Chen, Y., Wu, D., Xie, D., Lin, X., et al. (2010). A crucial role for RACK1 in the regulation of glucose-stimulated IRE1alpha activation in pancreatic beta cells. Sci. Signal. *3*, ra7.

Ramírez, O., García, A., Rojas, R., Couve, A., and Härtel, S. (2010). Confined displacement algorithm determines true and random colocalization in fluorescence microscopy. J. Microsc. *239*, 173–183.

Rodriguez, D.A., Zamorano, S., Lisbona, F., Rojas-Rivera, D., Urra, H., Cubillos-Ruiz, J.R., Armisen, R., Henriquez, D.R., Cheng, E.H., Letek, M., et al. (2012). BH3-only proteins are part of a regulatory network that control the sustained signalling of the unfolded protein response sensor IRE1α. EMBO J. *31*, 2322–2335.

Rodriguez, D.A., Weinlich, R., Brown, S., Guy, C., Fitzgerald, P., Dillon, C.P., Oberst, A., Quarato, G., Low, J., Cripps, J.G., et al. (2016). Characterization of RIPK3-mediated phosphorylation of the activation loop of MLKL during necroptosis. Cell Death Differ. *23*, 76–88.

Rojas-Rivera, D., Armisén, R., Colombo, A., Martínez, G., Eguiguren, A.L., Díaz, A., Kiviluoto, S., Rodríguez, D., Patron, M., Rizzuto, R., et al. (2012). TMBIM3/GRINA is a novel unfolded protein response (UPR) target gene that controls apoptosis through the modulation of ER calcium homeostasis. Cell Death Differ. *19*, 1013–1026.

Rubin, D.M., Mehta, A.D., Zhu, J., Shoham, S., Chen, X., Wells, Q.R., and Palter, K.B. (1993). Genomic structure and sequence analysis of *Drosophila melanogaster* HSC70 genes. Gene *128*, 155–163.

Rutkowski, D.T., Arnold, S.M., Miller, C.N., Wu, J., Li, J., Gunnison, K.M., Mori, K., Sadighi Akha, A.A., Raden, D., and Kaufman, R.J. (2006). Adaptation to ER stress is mediated by differential stabilities of pro-survival and pro-apoptotic mRNAs and proteins. PLoS Biol. *4*, e374.

Ryoo, H.D. (2015). *Drosophila* as a model for unfolded protein response research. BMB Rep. *48*, 445–453.

Saibil, H. (2013). Chaperone machines for protein folding, unfolding and disaggregation. Nat. Rev. Mol. Cell Biol. *14*, 630–642.

Saito, K., Chen, M., Bard, F., Chen, S., Zhou, H., Woodley, D., Polischuk, R., Schekman, R., and Malhotra, V. (2009). TANGO1 facilitates cargo loading at endoplasmic reticulum exit sites. Cell *136*, 891–902.

Satoh, M., Hirayoshi, K., Yokota, S., Hosokawa, N., and Nagata, K. (1996). Intracellular interaction of collagen-specific stress protein HSP47 with newly synthesized procollagen. J. Cell Biol. *133*, 469–483.

Son, S.M., Byun, J., Roh, S.E., Kim, S.J., and Mook-Jung, I. (2014). Reduced IRE1α mediates apoptotic cell death by disrupting calcium homeostasis via the InsP3 receptor. Cell Death Dis. *5*, e1188.

Tam, A.B., Koong, A.C., and Niwa, M. (2014). Ire1 has distinct catalytic mechanisms for XBP1/HAC1 splicing and RIDD. Cell Rep. *9*, 850–858.

Tannour-Louet, M., Porteu, A., Vaulont, S., Kahn, A., and Vasseur-Cognet, M. (2002). A tamoxifen-inducible chimeric Cre recombinase specifically effective in the fetal and adult mouse liver. Hepatology *35*, 1072–1081.

Urano, F., Wang, X., Bertolotti, A., Zhang, Y., Chung, P., Harding, H.P., and Ron, D. (2000). Coupling of stress in the ER to activation of JNK protein kinases by transmembrane protein kinase IRE1. Science *287*, 664–666.

Vaisar, T., Pennathur, S., Green, P.S., Gharib, S.A., Hoofnagle, A.N., Cheung, M.C., Byun, J., Vuletic, S., Kassim, S., Singh, P., et al. (2007). Shotgun proteomics implicates protease inhibition and complement activation in the antiinflammatory properties of HDL. J. Clin. Invest. *117*, 746–756.

Walter, P., and Ron, D. (2011). The unfolded protein response: from stress pathway to homeostatic regulation. Science *334*, 1081–1086.

Wang, M., and Kaufman, R.J. (2016). Protein misfolding in the endoplasmic reticulum as a conduit to human disease. Nature *529*, 326–335.

STAR★METHODS

KEY RESOURCES TABLE

REAGENT or RESOURCE	SOURCE	IDENTIFIER
Antibodies		
Anti-HA	Roche	Cat #11867431001; RRID:AB_390919
Anti-HSP47	Enzo Lifesciences	Cat #ADI-SPA-470; RRID:AB_10618557
Anti- EPR4217 (anti-HSP47)	Abcam	Cat #ab109117; RRID: AB_10888995
Anti-BiP	Enzo Lifesciences	Cat #ADI-SPA-826-D; RRID:AB_2039169
Anti-His	Santa Cruz	Cat #sc-803; RRID:AB_631655
Anti-HSP90α/β (H-114)	Santa Cruz	Cat #sc-7947; RRID:AB_2121235
Anti-CHOP	Abcam	Cat #ab11419; RRID:AB_298023
Anti-IRE1	Cell Signaling Technology	Cat #3294; RRID:AB_2055392
Anti-CREB-2 (Anti-ATF4)	Santa Cruz	Cat #sc-200; RRID:AB_2058752
Anti-GAPDH	Santa Cruz	Cay #sc-365062; AB_10847862
Anti-V5	Invitrogen	Cat #R960-25; RRID:AB_2556564
Anti-Rabbit-Alexa488	Thermo Fisher	Cat #A-11034; RRID:AB_2576217
Anti-Mouse-Alexa594	Thermo Fisher	Cat #A-11020; RRID:AB_141974
Anti-mouse-HRP	Invitrogen	Cat #62-6520; RRID:AB_2533947
Anti-Rabbit-HRP	Invitrogen	Cat #65-6120; RRID:AB_88384
Anti-HA-Agarose	Roche	Cat #11815016001; RRID:AB_88384
Anti-GFP	Santa Cruz	Cat #sc-9996; RRID: AB_627695
SureBeads Protein A Magnetic Beads, 3 mL	Bio-Rad	Cat #1614013
Bacterial and Virus Strains		
LEMO21 *E. coli* cells	Laboratory Marek Michalak	N/A
Rosetta2 (DE3)	Millipore/Merck	Cat #71397
Chemicals, Peptides, and Recombinant Proteins		
Thapsigargin	Calbiochem	Cat #586005
Tunicamycin	Merck	Cat #654380-10
Brefeldine A	Sigma	Cat #20350-15-6
DMSO	Sigma	Cat #41640-1L
Trizol	Invitrogen	Cat #15596018
Nutri-Fly Instant, White	Nutri-Fly	Cat #66-118
Tamoxifen	Sigma	Cat #T6548
sunflower oil	Sigma-Aldrich	Cat #8001-21-6
Ethanol	Merck	Cat #1070172511
formalin	Sigma-Aldrich	Cat #HT501128-4L
Paraffin	Sigma-Aldrich	Cat #8002-74-2
Hematoxylin solution modified acc. to Gill II	EMD MILLIPORE	Cat #1.05175
DMEM	GIBCO	Cat #12100046
Opti-MEM	GIBCO	Cat #31985062
Propidium iodide	Sigma	Cat #P4170-25MG
ammonium bicarbonate	Sigma	Cat #A6141
1:20, w/w, trypsin/protein	Promega	Cat #V5111
Acetonitrile	Sigma	Cat # 271004
Formic acid	EQULAB	Cat #07ACIDFORM0007
Random primers p(dN)6	Appliedbiosystems	Cat #4319979
Maxima SYBR green/Rox qPCR master mix (2x)	Fermentas	Cat #k0221

(*Continued on next page*)

Continued

REAGENT or RESOURCE	SOURCE	IDENTIFIER
5x HOT FIREPol Eva Green qPCR Mix Plus (ROX)	Solis Bio Dyne	Cat #08-24-00020
Puromycin	Merck	Cat #540222-25
Rapigest	Waters corp	Cat #186001861
DNase	Sigma	Cat #DN25
PreScission Protease	Sigma	Cat #GE27-0843-01
siRNA Hsp47	QIAGEN	Cat #SI02777131
siRNA Hsp47	QIAGEN	Cat #SI02777138
siRNA Negative control	QIAGEN	Cat #1027310
HiLoad 16/600 Superdex 200 pg	GE Healthcare	Cat # 28989335
5-mL HiTrap Q HP column	GE Healthcare	Cat #17-1154-01
TCPE	Sigma	Cat #51805-45-9
cOmplete Protease Inhibitor Cocktail	Roche	Cat #11836153001
PhosSTOP	Roche	Cat #04906845001
HSP47	This study	N/A
BiP	Laboratory of Marek Michalak (Groenendyk et al., 2014)	N/A
His-IRE1α-NLD	Laboratory of Marek Michalak (Groenendyk et al., 2014)	N/A
PDIA6	Laboratory of Marek Michalak (Groenendyk et al., 2014)	N/A
Actin	Laboratory of Marek Michalak (Groenendyk et al., 2014)	N/A
His-PERK-NLD	Laboratory of Maruf Mu Ali (Carrara et al., 2015)	N/A
Critical Commercial Assays		
Trichrome Stain (Masson) Kit	Sigma	Cat #HT15-1KT
Phos-tag	Wako Pure Chemical industries	Cat #304-93521
Duolink	Sigma-Aldrich	Cat #DUO92101
SuperScript III	Invitrogen	Cat #18080093
Tunel	Promega	Cat #G3250
Dual-Luciferase® Reporter Assay System	Promega	Cat #E1910
Lipofectamine RNAiMAX	Invitrogen	Cat #13778150
Dynabeads Co-Immunoprecipitation Kit	Invitrogen	Cat #14321D
Effectene Transfection Reagent	Quiagen	Cat #301427
RECOMBINANT DNA		
pED-IRE1α-NLD-6His-KDEL	Laboratory of R. Kaufman	N/A
pMSCV HSP47-V5puro	Genewiz, This study	N/A
pMSCV Ppa2-V5puro	Genewiz, This study	N/A
pMSCV Tubα1a-V5puro	Genewiz, This study	N/A
pMSCV ATP5h-V5puro	Genewiz, This study	N/A
pMSCV IRE1α-HA-Hygro	(Rodriguez et al., 2012)	N/A
pMSCV MOCK-Puro	(Rodriguez et al., 2012)	N/A
pMSCV MOCK-Hygro	(Rodriguez et al., 2012)	N/A
pLKO.1 shLuc-Puro	(Rodriguez et al., 2012)	N/A
pLKO.1 shHsp47-Puro	This study	N/A
pLKO.1 shPpa2-Puro	This study	N/A
pLKO.1 shTuba1a-Puro	This study	N/A
pLKO.1 shATP5h-Puro	This study	N/A
pET-21a HSP47-6His	This study	N/A

(*Continued on next page*)

Continued

REAGENT or RESOURCE	SOURCE	IDENTIFIER
pGL3 2xUPRE-Luc	(Lee et al., 2003)	N/A
pRL-SV40 Renilla-Luc	(Lee et al., 2003)	N/A
pEGFP-N1 BiP	(Lai et al., 2010)	N/A
Experimental Models: Cell Lines		
COS-1 cells	Laboratory Marek Michalak	N/A
293T	ATCC	Cat #CRL-3216; RRID:CVCL_0063
T-Rex293T::IRE1α-GFP	Laboratory Peter Walter (Li et al., 2010)	N/A
IRE1α$^{-/-}$::IRE1α-HA	Laboraory of David Ron	N/A
IRE1α$^{-/-}$::EV	Laboraory of David Ron	N/A
MEF cells (for stable cell lines)	(Rodriguez et al., 2012)	N/A
MEF cells-shRNA Luc	This study	N/A
MEF cells- shHsp47	This study	N/A
MEF cells- shPPA2	This study	N/A
MEF cells-shTUBa1a	This study	N/A
MEF cells-shATP5h	This study	N/A
MEF cells-shVim	This study	N/A
MEF cells-shMybbp1	This study	N/A
MEF cells-shPkm2	This study	N/A
MEF cells-shCnn2	This study	N/A
MEF cells-shPrph	This study	N/A
MEF cells-shTubb6	This study	N/A
MEF cells-Mock	This study	N/A
MEF cells-Hsp47-V5	This study	N/A
MEF cells-Ppa2-V5	This study	N/A
MEF cells-Tubα1a-V5	This study	N/A
MEF cells-ATP5h-V5	This study	N/A
MEF cells (for endogenous co-immunoprecipitations)	Laboratory Douglas Green (Rodriguez et al., 2016)	N/A
Experimental Models: Organisms/Strains		
Tub-Gal4/TM3-GFP (y[1] w[*];;P{w[+mC] = tubP-GAL4}LL7/TM3, Sb[1])	Bloomington Drosophila Stock Center	cat #5138; RRID:BDSC_5138
UAS-RNAi Alpha tub (CG1913)	Vienna Drosophila RNAi Center	Cat #33427
UAS-RNAi p38/NURF38 CG4634)	Vienna Drosophila RNAi Center	Cat #103776
UAS-RNAi ATPsynth (CG6030)	Vienna Drosophila RNAi Center	Cat #104353
UAS-RNAi SRP2 (CG8137)	Vienna Drosophila RNAi Center	Cat #100958
Hsp47 floxed C57BL/6 mice	(Masago et al., 2012)	N/A
TTR-Cre C57BL/6 mice	(Tannour-Louet et al., 2002)	N/A
Software and Algorithms		
Graphpad Prism 7	https://www.graphpad.com/scientific-software/prism/	RRID:SCR_015807
ImageJ	https://imagej.nih.gov/ij/	RRID:SCR_003070
Primer-Blast	https://www.ncbi.nlm.nih.gov/tools/primer-blast/	RRID:SCR_003095
Applied Biosystems 7500 Fast Real-Time PCR System	https://www.thermofisher.com/us/en/home/technical-resources/software-downloads/applied-biosystems-7500-fast-real-time-pcr-system.html	RRID:SCR_014596
BiaEvaluation	GE Healthcare	N/A
Monolith	https://nanotempertech.com/monolith/	N/A

(*Continued on next page*)

Continued

REAGENT or RESOURCE	SOURCE	IDENTIFIER
Origin graphing & Analysis	https://www.originlab.com/	RRID:SCR_014212
Olympus Fluo View FV1000 confocal laser-scanning microscope	Olympus	N/A
Trans-Proteomic Pipeline	http://tools.proteomecenter.org/TPP	N/A

CONTACT FOR REAGENT AND RESOURCE SHARING

Further information and requests for resources and reagents should be directed to, and will be fulfilled by Claudio Hetz (chetz@hsph.harvard.edu).

EXPERIMENTAL MODEL AND SUBJECT DETAILS

Cell lines

MEF cells used here were described in (Rojas-Rivera et al., 2012), and maintained in Dulbecco's modified Eagles medium supplemented with 5% fetal bovine serum, non-essential amino acids. The pMSCV-Hygro retrovirus vector expressing IRE1α-HA was previously described (Rodriguez et al., 2012). IRE1α contains two tandem HA sequences at the C-terminal domain and a precision enzyme site before the HA tag. COS-1 cells were maintained under standard tissue culture conditions using 10% fetal bovine serum in Dulbecco's modified Eagles medium (DMEM) (Sigma). HEK cells were maintained in DMEM supplemented with 5% fetal bovine serum.

Drosophila melanogaster

Flies were kept at 25°C on standard medium with a 12–12 dark-light cycle. The line Tub-Gal4/TM3-GFP was obtained from the Bloomington *Drosophila* Stock Center (Bloomington, In, USA). UAS-RNAi lines were obtained from the Vienna *Drosophila* RNAi Center (VDRC): UAS- RNAi AlphaTub (GC1913), UAS- RNAi p38/NURF38 (CG4634), UAS-RNAi ATPsynth (CG6030) and UAS-RNAi SRP2 (CG8137). For the RNAi experiments, males UAS-RNAi were crossed to females Tub-Gal4/TM3-GFP flies. Second instar GFP-positive larvae (not expressing the RNAi) were separated from GFP-negative larvae (expressing the RNAi) and fed separately with Tm or the vehicle (DMSO). After the treatments, total RNA was obtained from larvae using Trizol (Invitrogen, Carlsbad, CA, USA), and cDNA was synthesized with SuperScript III (Invitrogen) (Castillo et al., 2011; Rojas-Rivera et al., 2012). In survival experiments, the indicated number of flies was fed with 25 μg/mL Tm or DMSO in instant *Drosophila* food (Carolina Biological Supply 2700 York Burlington, NC, USA). The total number of flies alive each 2-3 days was counted. Oversight was from the University of Chile Committee for Bioethics, CBA 0511.

Hsp47 conditional-knockout mice

Generation of conditional Hsp47 knockout mice was performed by crossing Hsp47 floxed mice (Masago et al., 2012) with TTR-Cre inducible (liver-specific promoter) transgenic animals (Tannour-Louet et al., 2002). The Cre-*loxP* system was used to disrupt the *Hsp47* gene in a tissue-specific manner using a transgenic mouse harboring a floxed *Hsp47* gene in which the exon-6-containing region was flanked by *loxP* sites (Masago et al., 2012). Exon 6 is the last exon that encodes approximately 24% of the amino acid sequence of Hsp47, including a region essential for binding to collagen and a poly(A) signal. Correct targeting by homologous recombination and germline transmission was previously confirmed by Southern blotting (Masago et al., 2012). Breeding homozygous *Hsp47* floxed and TTR-Cre ind mice resulted in double-heterozygous animals. Then, animals were mated with Hsp47 floxed homozygous mice to obtain animals with the TTR–Cre in transgene with two Hsp47 floxed alleles. Mice were used for experiments after backcrossing with C57BL/6 mice for at least seven generations. Routine mouse genotyping was performed by PCR. The following primer pairs were used for floxed Hsp47 alleles and the Cre transgene: 5′-GAGTGGGCTGAGCCCTCTCAAGAAAATCC-3′, 5′-CTTCGGTCAGGCCCAGTCCTGC CAGATG-3′; and 5′-CTGCATTACCGGTCGATGCA-3′, 5′-ACGTTCACCGGCATCAACGT-3′, respectively. Tamoxifen (Sigma T6548) was dissolved in sunflower oil/ethanol (10:1) mixture. 18 weeks old TTR-Cre ind/Hsp47 flox/flox male mice or Hsp47 flox/flox male mice were injected intraperitoneally for five consecutive days with 1 mg Tamoxifen or with sunflower oil (control). These mice were housed in groups and weighed on average 27 g. One week after the last injection, the mice were injected with Tm or DMSO for different times and sacrificed using CO_2 narcosis. The liver and kidney were frozen at –80°C for biochemical analysis and the right major lobe of the liver was placed in a Petri dish (on ice). The liver was washed in PBS to remove the blood and then, it was fixed in 4% paraformaldehyde (72 hr) for histological analyses. Oversight was from the Kyoto Sangyo University Committee for Animal Care and Welfare: 2014-43, 2015-45, and 2016-42.

METHOD DETAILS

Viability assay

In all, 1.0 × 10^4 cells were seeded in 48-well plate and the maintained by 24ch in DMEM cell culture media supplemented with 5% bovine fetal serum and non-essential amino acids. ER stress was induced by adding ER stress agents to the cells at different concentrations, and maintained for 24ch. Then, cell viability was monitored using propidium iodide staining and flow cytometry (BD FACS Canto, Biosciences).

shRNA production, overexpression, and virus transduction

We generated stable MEFs with reduced levels of selected mRNAs using methods previously described and the lentiviral expression vector pLKO.1 (Castillo et al., 2011; Lisbona et al., 2009; Rodriguez et al., 2012; Rojas-Rivera et al., 2012). As a control, an shRNA construct against the luciferase gene was employed. All shRNA constructs were generated by the Broad Institute (Boston, MA, USA) based on different criteria for shRNA design (https://www.broad.mit.edu/genome_bio/trc/rnai.html). BiP was excluded from the shRNA screening because it was previously shown to regulate IRE1α. The pMSCV retroviral vectors were generated by DNA synthesis to stably express mouse HSP47-, PPA2-, ATP5h- and TUBα1a-V5 tagged protein by Genewiz (South Plainfield, New Jersey, United States).

RNA isolation, RT-PCR, and real-time PCR

Total RNA was prepared from cells and tissues using Trizol (Invitrogen, Carlsbad, CA, USA), and cDNA was synthesized with SuperScript III (Invitrogen) using random primers p(dN)6 (Roche). Quantitative real-time PCR reactions employing SYBRgreen fluorescent reagent and/or EvaGreen™ were performed in the Stratagene Mx3000P system (Agilent Technologies, Santa Clara, CA 95051, United States). The relative amounts of mRNAs were calculated from the values of comparative threshold cycle by using *Actin* as a control and *Rpl19* or *Rpl32* for RIDD in mouse or *D. melanogaster* samples, respectively. All methods for the *Xbp1* mRNA splicing assay used here were previously described (Lisbona et al., 2009; Rodriguez et al., 2012; Rojas-Rivera et al., 2012). Real time PCR primers are described in KEY RESOURSCES TABLE.

LTQ analysis of IRE1α-HA immunoprecipitation and identification of IRE1α-interacting proteins

IRE1α-deficient MEFs cells were stably transduced with retroviral expression vectors for IRE1α -HA or empty vector, and incubated for 6 hr in presence or absence of 250 ng/mL of Tm. Cell cultures were scaled-up and started with four 250 mm plates of semi-confluent cells. Then, cell lysates were prepared for immunoprecipitation. As control, to dissect non-specific background binding, experiments were performed in parallel in IRE1α KO cells. Protein complexes were eluted from anti-HA antibody-agarose (Roche) by heating the samples at 95°C for 5 minutes in presence of 0.1% Rapigest (Waters Corp.) and 100 mM ammonium bicarbonate. Eluted proteins were reduced, alkylated and digested overnight at 37°C with sequencing grade trypsin (1:20, w/w, trypsin/protein; Promega). Tryptic digests were dried, resuspended in 5% acetonitrile and 0.1% formic acid and injected into an analytical reverse-phase column (0.150 × 150 mm, 5 mm beads; Magic C18AQ, Michrom Bioresources, Inc.) and separated at a flow rate of 1 mL/min over 60 min. Mass spectra were acquired in a linear ion trap mass spectrometer (LTQ, Thermo Electron Corp.) with data-dependent acquisition (Vaisar et al., 2007). Peptide and protein identification were assessed using the database and parameters as described (Hoofnagle et al., 2012). The specific IRE1α interactors were identified using the following criteria. (i) Non-specific binding proteins were identified by performing an immunoprecipitation with beads coupled to anti-HA antibodies in MEFs IRE1α KO treated or not with Tm. All protein peptides found in this condition were discarded by subtracting the protein peptides found in immunoprecipitations on MEFs IREα KO cells reconstituted with the IRE1α -HA construct. (ii). Statistically significant peptides: We first confirmed that liquid chromatography–electrospray ionization–tandem MS (LC-ESI-MS/MS) analysis reproducibly identifies the same IRE1α-associated proteins in at least two or three independent immunoprecipitations. (iii) The filtering for each list was further validated using PeptideProphet and ProteinProphet (http://tools.proteomecenter.org/TPP), using an adjusted probability of greater than 0.90 for pep- tides and greater than 0.95 for proteins (Vaisar et al., 2007). iv) For each list of three independent immunoprecipitations, proteins identified peptides were confirmed by manual inspection for both cases under basal or ER stress conditions.

Immunoprecipitations and pull-down assays

Immunoprecipitations were performed using IRE1α-deficient MEFs cells stably transduced with retroviral expression vectors for IRE1α -HA or empty vector. Cells were incubated or not with different ER stressors. Protein extracts were prepared in CHAPS buffer (1% CHAPS, 100 mM KCl, 50 mM Tris [pH 7.5], PhosSTOP and complete Protease Inhibitor Cocktail) or NP40 buffer (0.2 or 0.5% NP40, 150 or 250 mM NaCl, 50 mM Tris [pH 7.5], 5% Glycerol, PhosSTOP and cOmplete Protease Inhibitor Cocktail). Immunoprecipitations were performed as described (Lisbona et al., 2009; Rodriguez et al., 2012; Rojas-Rivera et al., 2012). In brief, for immunoprecipitation of IRE1α -HA, ~700 μg of protein extracts were incubated with anti-HA antibody (Roche), for 16 hr at 4°C and then extracts were incubation with Protein A/G magnetic beads (Roche). Beads were washed 3 times with 1 mL of CHAPS or NP40 buffer. Protein complexes were eluted by heating at 95°C, for 16 hr in loading buffer. Endogenous IRE1α or HSP47 immunoprecipitations were performed from untreated wild-type MEFs (Rodriguez et al., 2016) or stimulated by 6 hr with Tm (250 ng/mL) or thapsigargin (100 nM), using anti-IRE1α (Cell signaling) or Hsp47 (Enzo lifesciences) primary antibodies covalently conjugated to magnetic beads

(Dynabeads®). Cell pellets were lysed with 1x extraction buffer containing PhosSTOP and complete Protease Inhibitor Cocktail. Co-immunoprecipitation was performed according manufacturer instructions (Dynabeads® Co-immunoprecipitation kit).

For pull-down experiments, COS-1 cells were transfected with the pED-IRE1α -NLD-His6-KDEL mammalian expression vector and/or human HSP47 pCAGGS mammalian expression vector, grown for 72 h, followed by treatment with 0.5 μM Tg, 5 μg/mL Tm or control conditions for 24 hr. Transfected cells were harvested by washing with cold Tris-buffered saline followed by scraping into 1 mL cold lysis buffer (25 mM Tris-Cl, pH 8.0, 150 mM NaCl, 0.5% NP-40, and 0.5% sodium deoxycholate). The lysate was incubated on ice for 30 min followed by centrifugation to pellet insoluble material and the supernatant was incubated 4 hr at 4°C with 100 μL of 10% slurry of Ni-NTA-Agarose beads (QIAGEN). Beads were then centrifuged briefly to pellet, and washed five times with 1 mL cold lysis buffer. Beads were pelleted, resuspended in 100 μL SDS-PAGE sample buffer, with 20 μL separated on SDS-PAGE (10% acrylamide), and followed by immunoblot analysis using anti-HSP47 (Enzo Lifesciences), anti-BiP (Enzo Lifesciences) or anti-His (Santa Cruz) antibodies.

Immunoblot analysis and phostag gels

Immunoblot analysis was performed using standard conditions (Rojas-Rivera et al., 2012). The following antibodies and dilutions were used: anti-HSP90 1:3000 (Santa Cruz, CA), anti-HA 1:2000 (Roche), anti-BiP 1:10000 (Enzo Lifesciences), Anti-V5 1:2000 (Invitrogen), Anti-HSP47 1:5000 (Enzo Lifesciences), Anti-EPR421 1:2000 (Abcam), Anti-HIS 1:2000 (ThermoScientific), Anti-CHOP 1:2000 (Abcam), Anti-IRE1α 1:1000 (Cell Signaling), Anti-CREB-2 (ATF4) 1:2000 (Santa Cruz), Anti-GAPDH 1:5000 (Santa Cruz) antibodies. Detection of the phosphorylated IRE1α form was performed using the Phostag™ assay loading 15 μg of total protein onto 4% SDS-PAGE minigels containing 80 μM of Phostag™ in the presence of 25 mM $MnCl_2$.

Luciferase assay

HEK293T and MEF cells were cultured in DMEM supplemented with 5% bovine serum and antibiotics (10000 U/mL Penicillin, 10 μg/mL streptomycin), at 37°C and 5% CO_2. Luciferase assays were performed using either MEF or HEK293T cells (depending on the experiment) co-transfected with the pRL-SV40 (Renilla luciferase), UPRE-Luc and/or pMSCV MOCK-Puro or/and pMSCV HSP47-V5-puro constructs using Effectene (QIAGEN). After 48 hr of transfection, cells were exposed to Tm (0.1 or 0.5 μg/mL), Tg (500 nM) or Bref (2 μM) for 20h and harvested to perform the Dual-Luciferase Reporter Assay (Promega) to quantify relative light units (RLU). Normalized luciferase activity was expressed as fold-increase over the non-treated conditions for each transfection condition. Alternatively, HSP47-V5 (pMSCV) or/and Bip sfGFP-KDEL (pCDNA.3) and vector controls using Calcium Phosphate. After 24 hr of transfection, cells were exposed to ER stress agents for 18 hr and harvested to perform the Dual-Luciferase Reporter Assay (Promega) to quantify relative light units (RLU). Normalized luciferase activity was expressed as fold-increase over the control cells transfected with the pMSCV empty vector.

Recombinant proteins

COS-1 cells were transfected with the pED-IRE1α-NLD-His6-KDEL expression vector and purified by Ni-NTA-Agarose(Liu et al., 2002). Briefly, COS-1 cells were transfected with His-IRE1α-NLD expression vector, grown for 72 hours, harvested and lysed into a buffer containing 25 mM Tris-Cl, pH 8.0, 150 mM NaCl, 0.5% NP-40, and 0.5% sodium deoxycholate. Cell lysates were incubated on ice for 30 min and centrifuged at 20,000 xg for 15 min, with the supernatant used for protein purification. Ni-NTA-Agarose chromatography was carried out using a buffer containing 50 mM Tris-Cl, pH 8.0, 300 mM NaCl, and 10 mM imidazole. His-IRE1α-NLD protein was eluted with 300 mM imidazole and concentrated. Human HSP47 was cloned into pET-21a containing a 6HIS tag for expression in LEMO21 *E. coli* cells. Transformed *E. coli* were grown at 37°C. Human HSP47 was cloned into pET-21a and proteins purified with a Ni-NTA-Agarose column using FPLC and eluted with 300 mM imidazole. Fractions were combined, concentrated and buffer exchanged for further purification using a Resource-Q column. Purified HSP47 protein was eluted using a high salt gradient, with fractions combined and concentrated. Purified proteins were buffer exchanged to the MST buffer system. Recombinant PDIA6 was previously described (Groenendyk et al., 2014).

PERK-NLD protein was expressed overnight at 22°C in Rosetta2 (DE3) *E. coli* cells (Merck). Cell pellet was lysed by sonication in 50 mM HEPES (pH 7.8), 400 mM NaCl, 10% glycerol buffer supplemented with 25 μg/mL DNase (Sigma-Aldrich), and Complete EDTA-free Protease Inhibitor tablets (Roche). Lysed cells were centrifuged at 40,000 g for 1 h, and the soluble fraction containing PERK-NLD was further purified by Co^{2+} affinity using pre-packed 5 mL HiTrap TALON crude columns (GE Healthcare). PERK-NLD was eluted with 250 mM imidazole. PERK-NLD protein was expredialyzed against 2 L of 50 mM HEPES (pH 7.8) and 10% glycerol overnight at 4°C. Samples were passed through a second TALON column to remove any residual tagged proteins. Hereon, all buffers were supplemented with 2 mM TCEP. PERK-NLD protein was further purified by anion-exchange chromatography using a 5 mL HiTrap Q HP column (GE Healthcare) and by size exclusion chromatography (SEC) on Haealthcare). PERK-NLD was eluted with 250 mM imidazol equilibrated with 50 mM HEPES (pH 7.8), 400 mM NaCl, 10% glycerol, and 2 mM TCEP.

Surface plasmon resonance (SPR)

SPR technology was employed to monitor the interaction of HSP47 or BiP with purified His-IRE1α-NLD protein (BIACore T200, GE). For BIACore analysis of HSP47, BiP, PDIA6 or actin interaction with His-IRE1α-NLD, the carboxymethylated dextran surface of a CM5 chip was activated using *N*-hydroxysuccinimide (NHS)/1-ethyl-3(3-dimethylaminopropyl)-carbodiimide hydrochloride. Purified

His-IRE1α-NLD protein was diluted in 10 mM NaAc, pH 5 at a concentration of 1 μM and injected over the activated CM5 chip at a flow rate of 5 μL/min to a total of ~1.5x10^3 Response Units (RU) followed by the blocking solution of 1 M ethanolamine, pH 9. A reference lane with no protein coupled was also generated to subtract background interactions. The CM5 chip was normalized and prepared for kinetic analysis. HSP47 and BiP, PDIA6 and ACTIN controls were diluted in a buffer containing 10 mM HEPES, pH 7.4, 150 mM KCl, and 0.005% P20 at concentrations from 0 to 1 × 10^5 nM and passed over the sensor surface. The experimental flow rate was performed at 30μL/min. The experimental results were corrected against the control surface response to remove any refractive index deviations. Kinetic analyses were carried out with the BiaEvaluation software using a 1:1 Langmuir binding model and were performed in triplicate. Association and dissociation rates and affinity (K_D) were calculated for each experiment and averaged. The binding response signals in RUs were continuously recorded and presented graphically as a function of time.

MicroScale thermophoresis (MST)

MST was carried out using a Monolith NT.115 instrument (NanoTemper Technologies GmbH). To evaluate HSP47 binding to His-IRE1α-NLD or His-PERK-NLD, an increasing concentration of purified HSP47 protein (0-20 μM) was incubated with 200 nM RED-labeled His-IRE1α-NLD protein (NanoTemper Technologies GmbH). The reverse was also performed, with 200 nM RED-labeled HSP47 incubated with an increasing concentration of purified IRE1-NLD (0-10 μM). To evaluate HSP47 competition with BiP binding to His-IRE1α-NLD, an increasing concentration of BiP (0-20 μM) was incubated with RED-labeled His-IRE1α-NLD protein in the absence of HSP47 or with a constant concentration of 500 nM HSP47 included in the buffer. To evaluate His-IRE1α-NLD dimerization ability *in vitro*, 200 nM of RED-labeled His-IRE1α-NLD was incubated with unlabeled His-IRE1α-NLD (0-10 μM) in the absence or presence of 500 nM HSP47. Experiments were carried out in a buffer containing 10 mM HEPES, pH 7.4, 125 mM KCl, 1 mM EGTA, 2 mM $CaCl_2$, 1 mM $MgCl_2$ and 0.005% P20. Experiments were done using hydrophobic capillaries and were performed independently more than three times. Data evaluation was performed using the Monolith software as well as Origin graphing software.

Immunofluorescence, duo link assay, and IRE1-GFP clustering

Cells were fixed for 30 min with 4% paraformaldehyde and permeabilized 0.5% NP-40 in PBS containing 0.5% BSA (Bovine serum albumin) for 10 min. After blocking for 1 hr with 10% FBS in PBS containing 0.5% BSA, cells were subsequently incubated with anti-HA and anti-Hsp47 antibodies overnight at 4°C followed by staining with Alexa-conjugated secondary antibodies (Molecular Probes). Images were acquired in Olympus FluoView FV1000 microscope with a 60x oil immersion objective. The Duolink assay was developed in *Ern1* null cells reconstituted with IRE1α-HA following manufacturer's instructions, (Duolink®, Sigma-Aldrich). TREX293 IRE1-3F6HGFP cells (Neely et al., 2010) were transiently transfected with pcDNA3.1-HSP47-V5 or pcDNA3.1 as a control for 24 hr. Additionally, cells were transfected using Lipofectamine RNAiMAX Transfection Reagent with 30 pmol of siRNA for HSP47 or control for 48 hr. After transfection, cells were split and reseeded on 25-mm-diameter coverslips in DMEM with 5% FBS and treated with doxycycline (5 μg/mL) for 48 hr to induce IRE1α-GFP expression, followed by the addition of 1 μg/mL Tm for the indicated times. Images were acquired using an Olympus Fluo View FV1000 confocal laser-scanning microscope. Image stacks were captured using a 63/X/1.4 objective with constant parameters for all conditions of each type of experiment. Twenty different fields were analyzed with a total of 150 to 200 cells per group in three independent experiments.

Histological evaluation and TUNEL assay

Liver tissue specimens were fixed in 10% buffered formalin, embedded in paraffin, sectioned (5 μm thick), stained with hematoxylin-eosin or Masson's trichrome. Liver tissue specimens were embedded in paraffin and sectioned at 5 μm for processing by the TUNEL method using a commercial kit, using DAB peroxidase substrate (Roche Molecular Biochemicals, Meylan, France) and counter-stained with hematoxylin. Specimens were evaluated by microscopy using a Zeiss PALM MicroBeam at high power magnification (x100) in a blinded manner. At least 10 random fields were counted for each TUNEL-stained tissue sample. Inflammatory infiltration sites were excluded from the quantification.

QUANTIFICATION AND STATISTICAL ANALYSIS

Throughout the manuscript, the data are represented as average ± SEM of pooled experiments unless otherwise stated. n values represent the number of independent experiments performed. For each independent *in vitro* experiment, three or two technical replicates were used (unless otherwise stated). The statistical significance between different groups in time courses measurement was calculated using two-way anova and tukey posttest. GraphPad software was used for statistical analysis. For all other experiments statistical analyses were performed using Prism software (GraphPad Software, La Jolla, CA, USA). Unpaired Student's t test or 2-way ANOVA was used for statistical analysis. A p value < 0.05 was considered statistically significant.

Molecular Cell, Volume *69*

Supplemental Information

Interactome Screening Identifies the ER Luminal Chaperone Hsp47 as a Regulator of the Unfolded Protein Response Transducer IRE1α

Denisse Sepulveda, Diego Rojas-Rivera, Diego A. Rodríguez, Jody Groenendyk, Andres Köhler, Cynthia Lebeaupin, Shinya Ito, Hery Urra, Amado Carreras-Sureda, Younis Hazari, Mireille Vasseur-Cognet, Maruf M.U. Ali, Eric Chevet, Gisela Campos, Patricio Godoy, Tomas Vaisar, Béatrice Bailly-Maitre, Kazuhiro Nagata, Marek Michalak, Jimena Sierralta, and Claudio Hetz

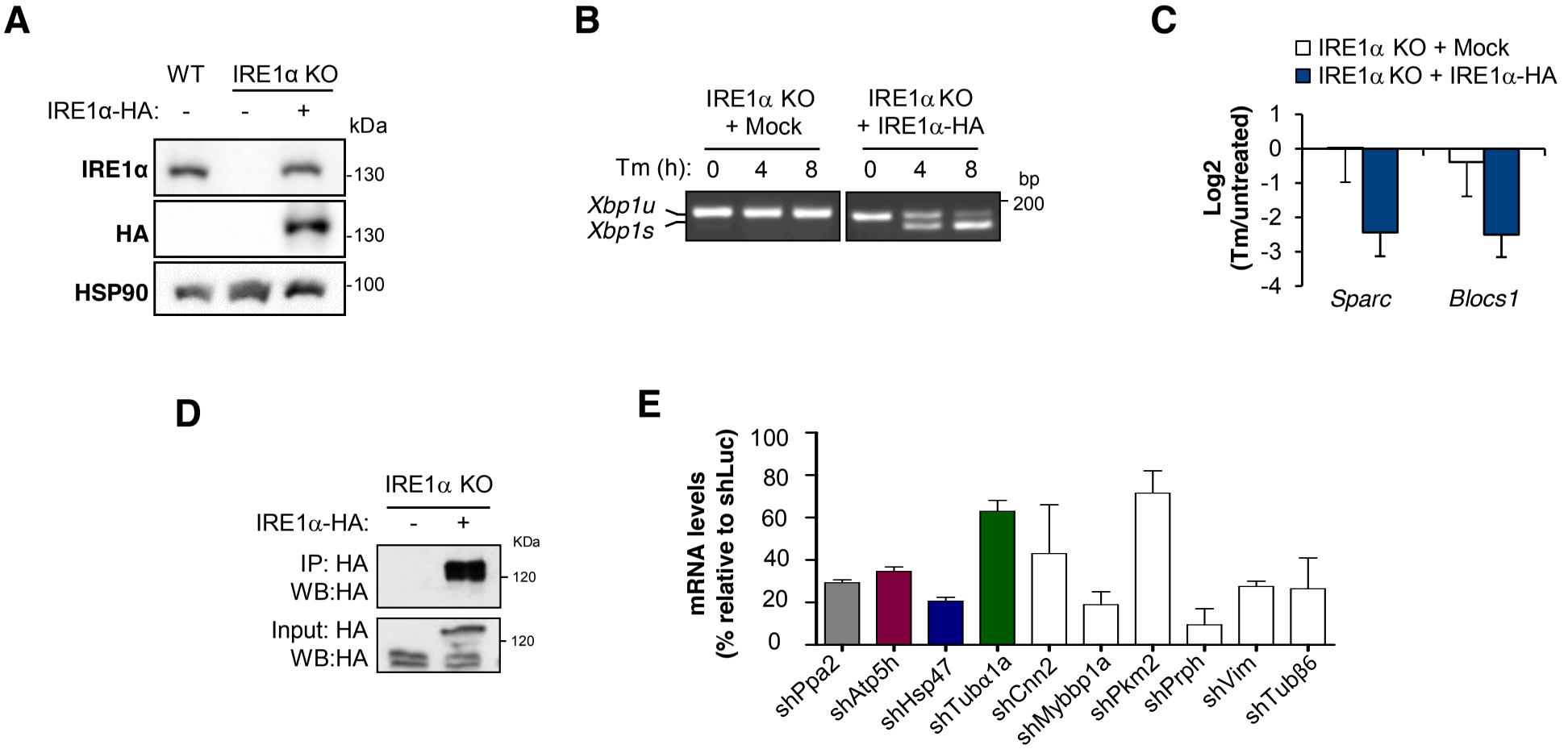
A
WT
IRE1α KO
IRE1α-HA: - - +
kDa
IRE1α
HA
HSP90
130
130
100
B
IRE1α KO + Mock
IRE1α KO + IRE1α-HA
Tm (h): 0 4 8 0 4 8
bp
Xbp1u
Xbp1s
200
C
IRE1α KO + Mock
IRE1α KO + IRE1α-HA
Log2 (Tm/untreated)
1
0
-1
-2
-3
-4
Sparc
Blocs1
D
IRE1α KO
IRE1α-HA: - +
KDa
IP: HA
WB:HA
Input: HA
WB:HA
120
120
E
mRNA levels (% relative to shLuc)
100
80
60
40
20
0
shPpa2
shAtp5h
shHsp47
shTubα1a
shCnn2
shMybbp1a
shPkm2
shPrph
shVim
shTubβ6

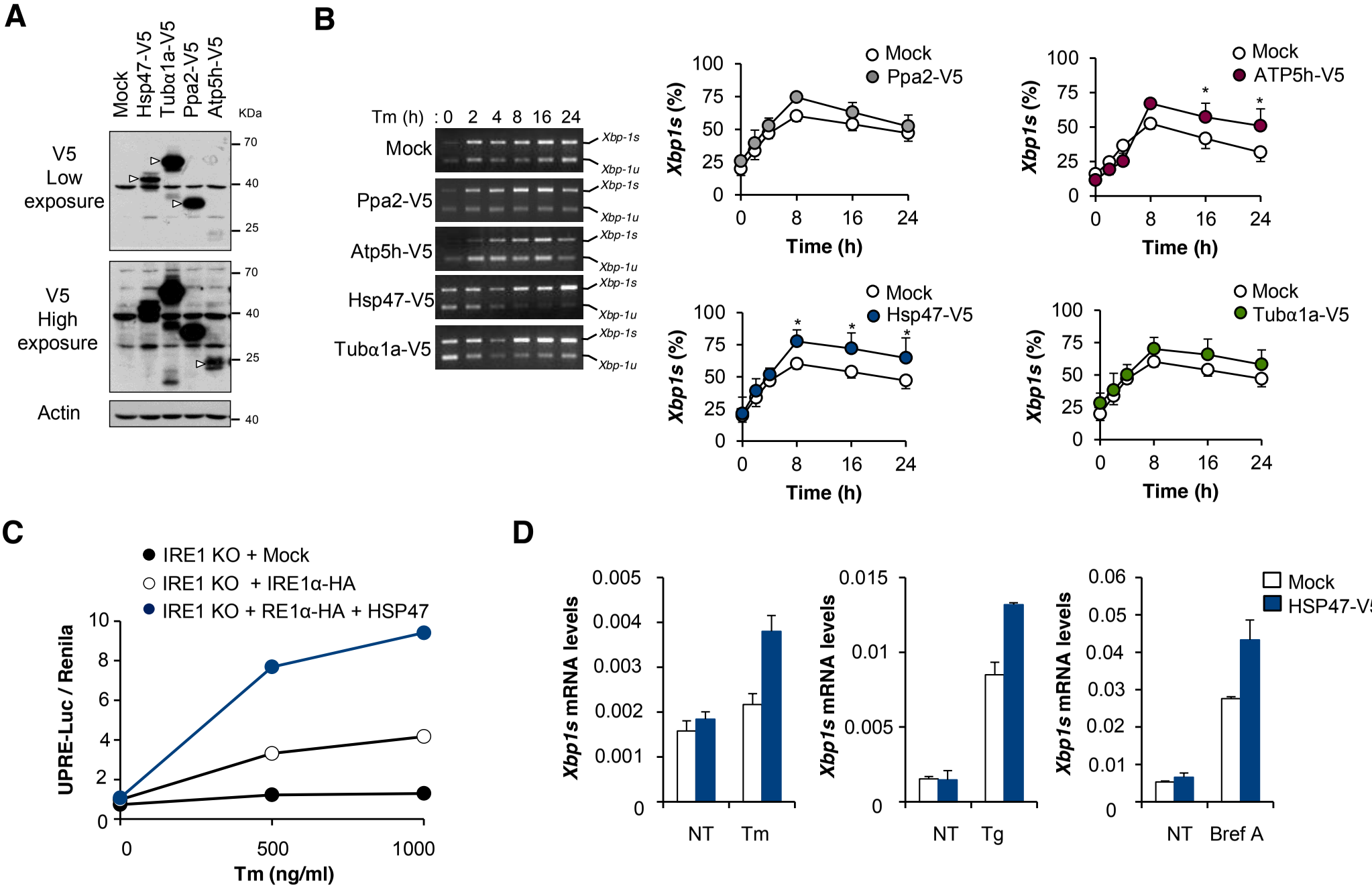
A
Mock
Hsp47-V5
Tubα1a-V5
Ppa2-V5
Atp5h-V5
KDa
V5
Low
exposure
V5
High
exposure
Actin
70
40
25
B
Tm (h) : 0 2 4 8 16 24
Mock
Ppa2-V5
Atp5h-V5
Hsp47-V5
Tubα1a-V5
Xbp-1s
Xbp-1u
Xbp1s (%)
Time (h)
Mock
Ppa2-V5
ATP5h-V5
Hsp47-V5
Tubα1a-V5
C
IRE1 KO + Mock
IRE1 KO + IRE1α-HA
IRE1 KO + RE1α-HA + HSP47
UPRE-Luc / Renila
Tm (ng/ml)
D
Xbp1s mRNA levels
NT
Tm
Tg
Bref A
Mock
HSP47-V5

A

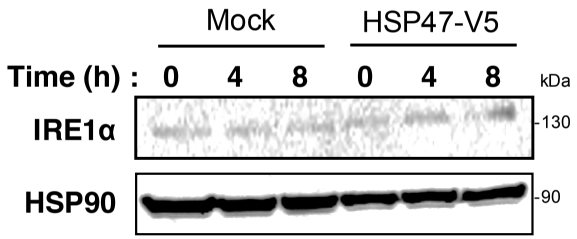
Mock
HSP47-V5
Time (h) : 0 4 8 0 4 8
kDa
IRE1α
130
HSP90
90

B

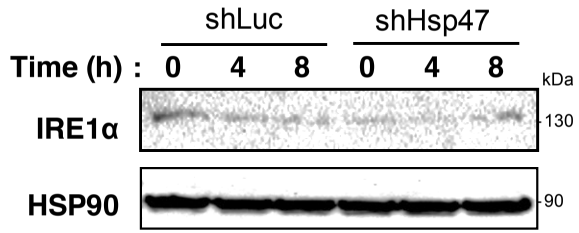
shLuc
shHsp47
Time (h) : 0 4 8 0 4 8
kDa
IRE1α
130
HSP90
90

C

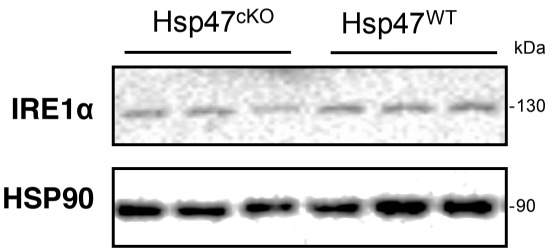
Hsp47cKO
Hsp47WT
kDa
IRE1α
130
HSP90
90

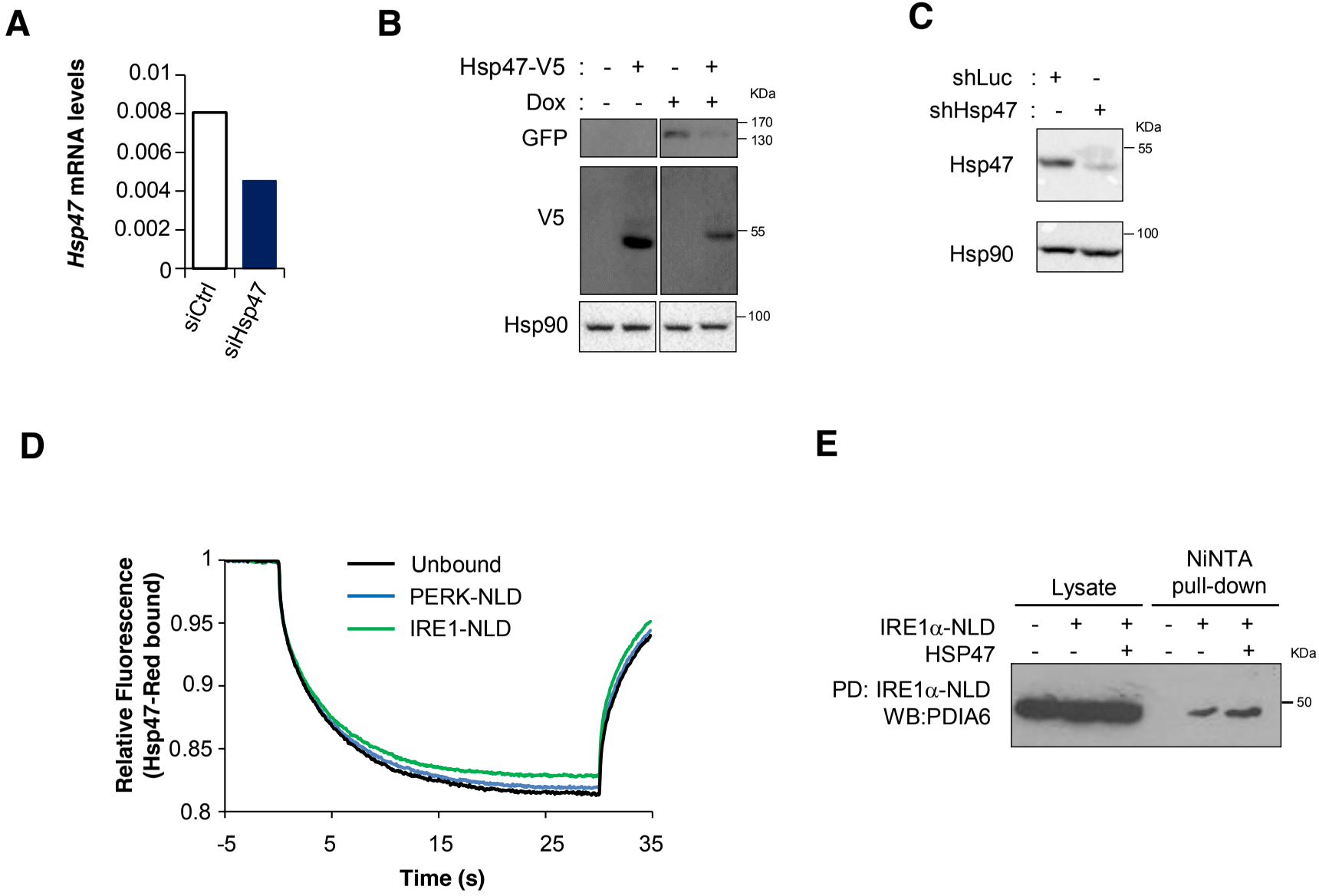
A
Hsp47 mRNA levels
0.01
0.008
0.006
0.004
0.002
0
siCtrl
siHsp47
B
Hsp47-V5 : - + - +
Dox : - - + +
KDa
GFP
170
130
V5
55
Hsp90
100
C
shLuc : + -
shHsp47 : - +
KDa
Hsp47
55
Hsp90
100
D
Relative Fluorescence (Hsp47-Red bound)
1
0.95
0.9
0.85
0.8
-5
5
15
25
35
Time (s)
Unbound
PERK-NLD
IRE1-NLD
E
Lysate
NiNTA pull-down
IRE1α-NLD - + + - + +
HSP47 - - + - - +
KDa
PD: IRE1α-NLD
WB:PDIA6
50

Figure S5

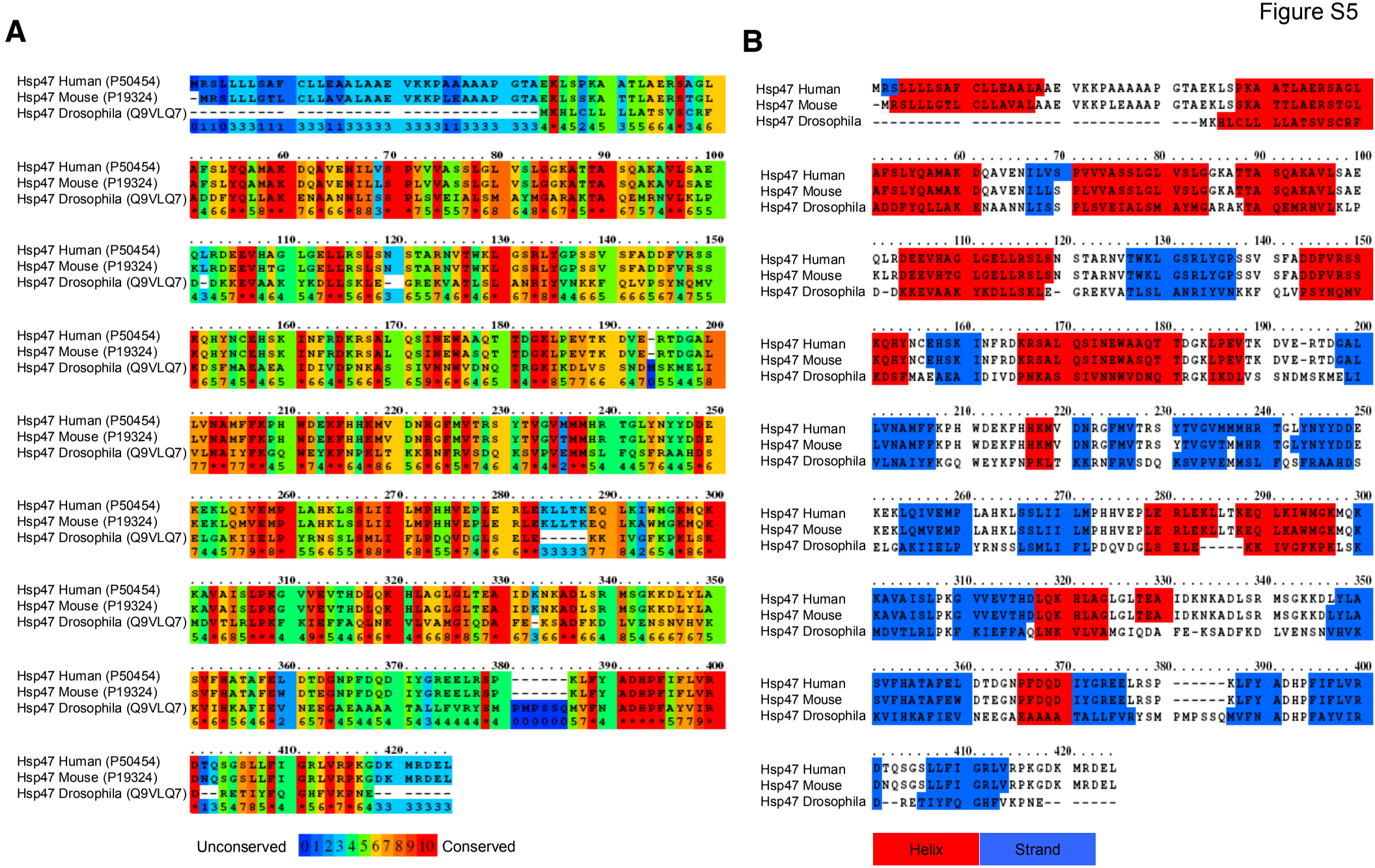
A
B
Hsp47 Human (P50454)
Hsp47 Mouse (P19324)
Hsp47 Drosophila (Q9VLQ7)
Unconserved
Conserved
Helix
Strand

A

Mammalian protein	Symbol (*D. melanogaster*)	Name (*D. melanogaster*)	Identity to H.s.(%)	Similitude To H.s.(%)
PPA2	CG4636	Nurf-38	51%	65%
ATPsynD	CG6030	ATPsynD	45%	64%
TUBα1a	CG1913	αTub84B	97%	98%

B

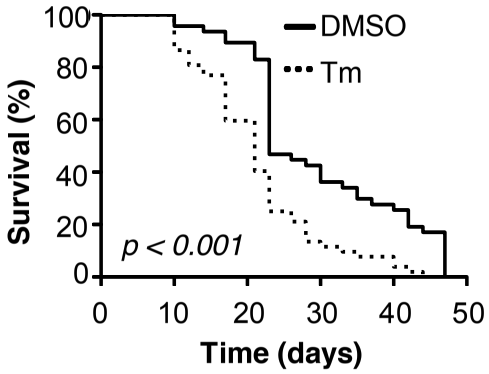

C

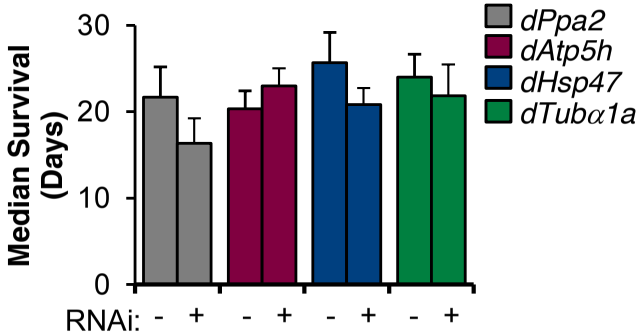

D

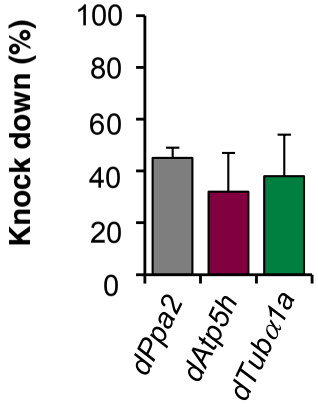

E

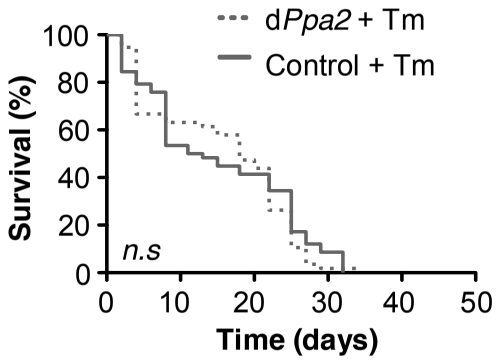

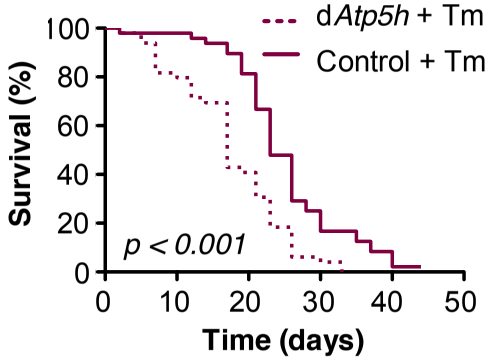

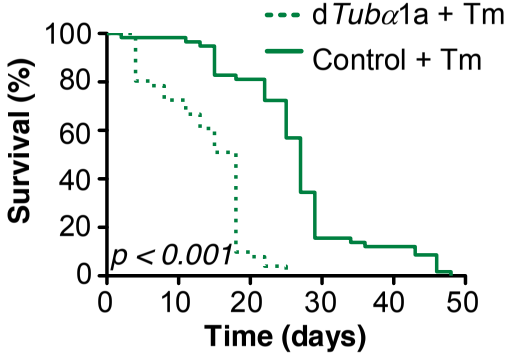

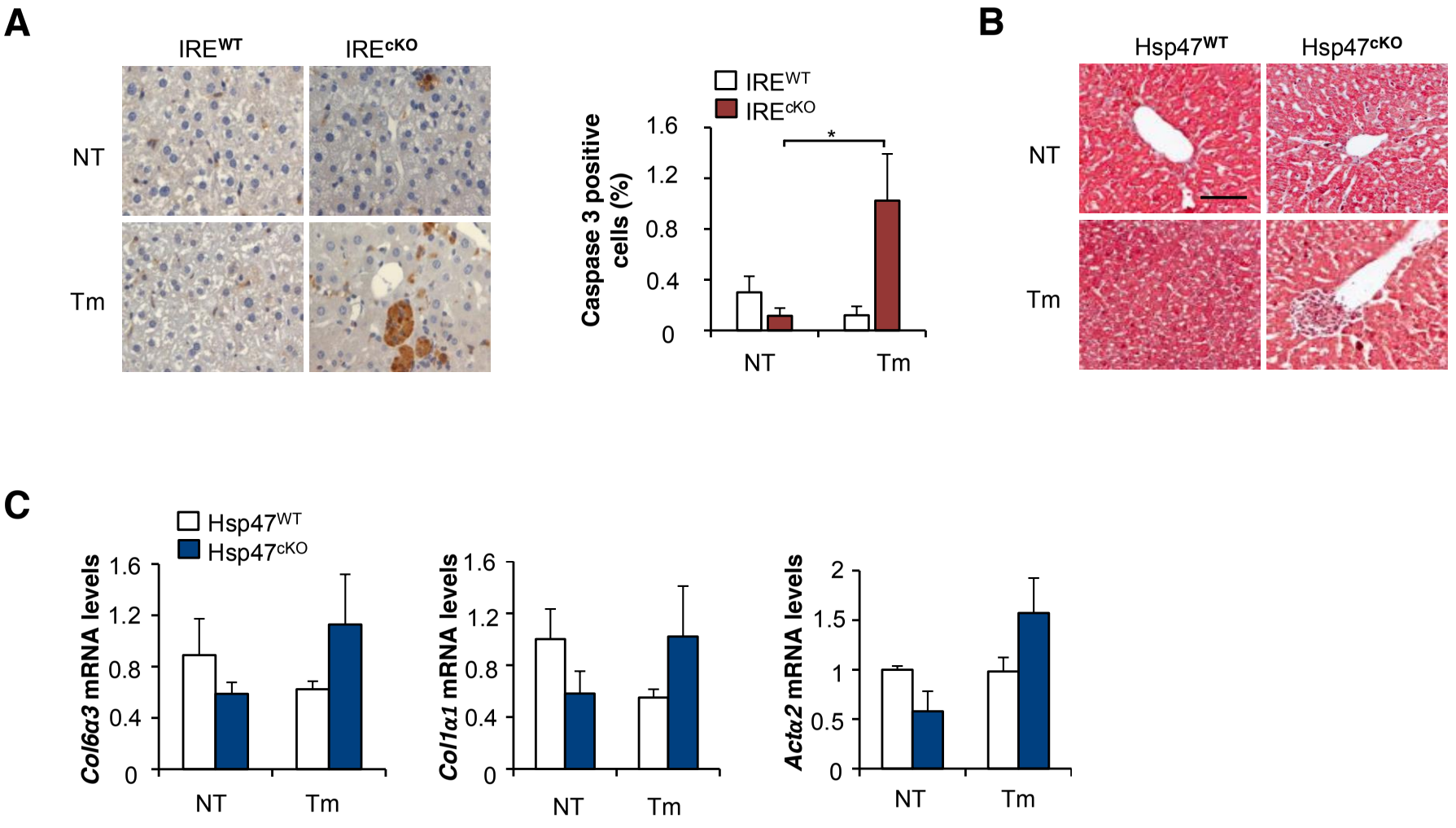
A
IRE^WT
IRE^cKO
NT
Tm
IRE^WT
IRE^cKO
Caspase 3 positive cells (%)
1.6
1.2
0.8
0.4
0
*
NT
Tm
B
Hsp47^WT
Hsp47^cKO
NT
Tm
C
Hsp47^WT
Hsp47^cKO
Col6α3 mRNA levels
1.6
1.2
0.8
0.4
0
NT
Tm
Col1α1 mRNA levels
1.6
1.2
0.8
0.4
0
NT
Tm
Actα2 mRNA levels
2
1.5
1
0.5
0
NT
Tm

Table S1. Related to Figure 1. Identification of putative IRE1α binding partners. IRE1a knockout (IRE1$\alpha^{-/-}$) MEF cells were reconstituted using retrovirus coding for full length IRE1α-HA. Immunoprecipitation of IRE1α-HA was done at basal conditions or in cells treated with 250 ng/mL of tunicamycin (Tm) for 6 h. Protein complexes were then analyzed using mass spectrometer. Analysis was performed in three independent experiments. Unique peptide sequences found are indicated, in addition to predicted protein function and cellular localization. Of note, one peptide corresponded for two putative protein candidates (PRPH and VIM).

.

Protein ID	Protein	Peptide	Treatment	Function	Cellular localization
Q08093	Calponin-2, CNN2	CASQVGMTAPGTR SMQNWHQLENLSNFIK SWIEGLTGLSIGPDFQK LGTDKCDNSSMSLQMGYTQGANQSGQVFGLGR GLQSGVDIGVK GPSYGLSAEVK TKGLQSGVDIGVK	Basal Conditions	Thin filament-associated protein that is implicated in the regulation and modulation of smooth muscle contraction. It is capable of binding to actin, calmodulin, troponin C and tropomyosin.	Extracellular exosome, focal adhesion, membrane, stress fiber.
D3Z636	Inorganic pyrophosphatase 2, PPA2	ILGTLALIDQSETDWK FKPGYLEATLNWFR		Catalyzes the hydrolysis of pyrophosphate to inorganic phosphate	Mitochondria
P19324	47 kDa heat shock protein, HSP47	STGLAFSLYQAMAK		Molecular chaperone essential for the correct folding of collagen. .	Endoplasmic reticulum, Cis-Golgi
Q3UMM1	Tubulin betha-6 chain, TUBβ6	SGPFGQLFRPDNFIFGQTGAGNNWAK FWEVISDEHGIDQAGGYVGDSALQLER	Basal conditions / ER stress	Subunit of tubulin, the major constituent of microtubules	Cytoplasm, cytoeskeleton
P52480	Pyruvate kinase, PKM2	KGDVVIVLTGWRPGSGFTNTMR GDLGIEIPAEK AGKPVICATQMLESMIK RFDEILEASDGIMVAR		Glycolytic enzyme that catalyzes the transfer of a phosphoryl group from phosphoenolpyruvate to ADP, generating ATP.	Cytoplasm, nucleus
P15331	Peripherin, PRPH.	MALDIEIATYR		Class-III intermediate filament protein.	Cytoplasm, cytoeskeleton
Q7TPV4	Myb-binding protein 1A, MYBBP1A	LYDLYWQAMR		Activate or repress transcription via interactions with sequence specific DNA-binding proteins.	Cytoplasm, nucleus, nucleolus
Q9DCX2	ATP synthase subunit d, ATP5h	LASLSEKPPAIDWAYYR		Subunit of mitochondrial membrane ATP synthase, that produces ATP from ADP in the presence of a proton gradient across the membrane.	Mitochondria
P20029	78 kDa glucose-regulated protein, GRP78,BIP	AKFEELNMDLFR TFAPEEISAMVLTK DAGTIAGLNVMR IEIESFFEGEDFSETLTR TFAPEEISAMVLTK		Involved in the correct folding of proteins, facilitating the assembly of multimeric protein complexes inside the endoplasmic reticulum	Endoplasmic reticulum lumen
P20152	Vimentin, VIM	MALDIEIATYR	ER stress	Class-III intermediate filaments attached to the nucleus, endoplasmic reticulum, and mitochondria.	Cytoplasm, cytoeskeleton
P68369	Tubulin alpha-1A chain, TUBα1A	AVFVDLEPTVIDEVR IHFPLATYAPVISAEK		Subunit of tubulin, the major constituent of microtubules.	Cytoplasm, cytoeskeleton

Table S2. Related to Figure 1. Functional genomic screening for novel regulators of *Xbp1* mRNA splicing. The sequences of each shRNAs used in the study is indicated.

Gene name	Clone name	Target Sequence
Cnn2	NM_007725.1-366s1c1	CTCCAACTTCATCAAGGCCAT
	NM_007725.1-1324s1c1	CCAATGGGCTTCCTGTTTCTT
	NM_007725.1-528s1c1	TGGAGTTAAGTATTCGGAGAA
	NM_007725.1-783s1c1	GAGGCACATCTATGACACCAA
	NM_007725.1-900s1c1	GCAGATCTACGATCCCAAGTA
Tubb6	NM_026473.2-170s1c1	GCGTCTACTACAATGAGTCAT
	NM_026473.2-1330s1c1	GAGGCATTTGAAGACGAGGAT
	NM_026473.2-732s1c1	TGTCACCACATCACTGCGTTT
	NM_026473.2-1375s1c1	GCCATAAGATGCTACAGTGAA
	NM_026473.2-177s1c1	CTACAATGAGTCATCCTCTAA
Mtap	NM_024433.2-867s21c1	AGTTTACTCCTCACTACTATA
	NM_024433.2-1173s21c1	TGTCTCACTTTCCCTATTAAA
	NM_024433.2-178s21c1	GCTTGGATGATCCCGAAATTT
	NM_024433.2-575s21c1	CCTCATAGAAACTGCTAAGAA
	NM_024433.2-266s21c1	GAAGATAAAGAACGTTGATTG
Ppa2	NM_146141.1-516s1c1	CGTCTGTGAAATAGGCTCAAA
	NM_146141.1-805s1c1	GACGTTATTAACTCTGCACAT
	NM_146141.1-804s1c1	CGACGTTATTAACTCTGCACA
	NM_146141.1-573s1c1	CCTTGGGACTTTGGCACTTAT
	NM_146141.1-363s1c1	GCAAGATATAAAGAACGGAAA
Hist1h2af	NM_175659.1-104s21c1	TCCGCAAGGGCAACTACTCGG
	NM_175659.1-160s21c1	GCCGTGCTGGAGTACCTGACG
	NM_175659.1-174s21c1	CCTGACGGCCGAGATCCTGGA
	NM_175659.1-27s21c1	CAAGGCTCGCGCCAAGGCCAA
	NM_175659.1-212s21c1	CCCGCGACAACAAGAAGACGC
Hsp47	NM_009825.1-1707s1c1	CCAGATACTATGATACCAAAT
	NM_009825.1-721s1c1	CGAACACTCCAAGATCAACTT
	NM_009825.1-1244s1c1	GACAAGAACAAGGCAGACCTA
	NM_009825.1-406s1c1	CTTCAGCCTATATCAGGCGAT
	NM_009825.2-1701s21c1	TGAGACACATGGGTGCTATTG
Rplp0	NM_007475.2-985s1c1	CGGAGGAATCAGATGAGGATA
	NM_007475.2-356s1c1	CCTCACTGAGATTCGGGATAT
	NM_007475.2-960s1c1	GCCAAAGCTGAAGCAAAGGAA
	NM_007475.2-551s1c1	GCTGATAAAGACTGGAGACAA
	NM_007475.2-1052s1c	CCTGCTTAATTTGAGAAAGAT
Atp5b	NM_016774.2-1633s1c1	CTGCAACTGATCTCTCCATAT
	NM_016774.2-1526s1c1	CCCAGAACAAGCCTTCTACAT
	NM_016774.2-337s1c1	GCACGGTCAGAACTATTGCTA
	NM_016774.2-1095s1c1	GCTATCTATGTGCCTGCTGAT
	NM_016774.3-674s21c1	GCTAATCAACAATGTCGCCAA

Gene name	Clone name	Target Sequence
Prph	NM_013639.1-1346s1c1	CCTTTGCCTCTCTAAGTTTAA
	NM_013639.1-667s1c1	GAGTCTCTGATGGATGAAATT
	NM_013639.1-862s1c1	GAGGAGTGGTATAAGTCGAAA
	NM_013639.2-859s21c1	TACGAGAACATCGCGGCAAAG
	NM_013639.2-1077s21c1	GAACGAGTCTCGACGTCAGAT
Vim	NM_011701.3-1860s1c1	GCATCACGATGACCTTGAATA
	NM_011701.3-1150s1c1	GTGGAATCCTTGCAGGAAGAA
	NM_011701.3-1987s1c1	GCGCAAGATAGATTTGGAATA
	NM_011701.3-717s1c1	GCTTCAAGACTCGGTGGACTT
	NM_011701.3-747s1c1	CGACGCCATCAACACTGAGTT
Tubα1a	NM_011653.1-332s1c1	GCAAGGAGGATGCTGCCAATA
	NM_011653.1-711s1c1	CCCAACCTACACTAACCTAAA
	NM_011653.1-868s1c1	CCTGTCATCTCTGCTGAGAAA
	NM_011653.1-1324s1c1	GCTGCCCTAGAGAAGGATTAT
	NM_011653.1-1430s1c1	CACAGGGATGTTTATTGTGTT
Pkm2	NM_011099.2-1403s21c1	ATCATTGCCGTGACTCGAAAT
	NM_011099.2-1508s21c1	GATGTCGACCTTCGTGTAAAC
	NM_011099.2-1861s21c1	GACTGGAAACCCTGACTTTAT
	NM_011099.2-231s21c1	AGATGCTGAAGGAGATGATTA
	NM_011099.2-767s21c1	GACATGGTGTTTGCATCTTTC
Gcat	NM_013847.2-299s1c1	GACTCAGTTCTACTCGATTTA
	NM_013847.2-1115s1c1	GTATCTTTGTCATCGGATTTA
	NM_013847.2-297s1c1	TGGACTCAGTTCTACTCGATT
	NM_013847.2-351s1c1	AGAAGCCAAGATAGCCCACTT
	NM_013847.2-1747s1c1	CCCAGAAAGAAGAAAGCAGAT
Mybbp1a	NM_016776.2-2010s1c1	CCGGAGTGTATTTGGTCATAT
	NM_016776.2-2951s1c1	CCAAGCGTAACAGCTCACTTA
	NM_016776.2-193s1c1	CCCAATGATTCGGAGATGAAA
	NM_016776.2-465s1c1	CCTGATGAAGTCCGTGCAATT
	NM_016776.2-4060s1c1	CCTGCCCTAGAGACTCCTATT
Atp5h	NM_027862.1-416s1c1	CCCTTTGACCAGATGACCATT
	NM_027862.1-424s1c1	CCAGATGACCATTGATGACTT
	NM_027862.1-416s21c1	CCCTTTGACCAGATGACCATT
	NM_027862.1-160s1c1	GTTGGCTAGTCTGTCTGAGAA
	NM_027862.1-253s1c1	GAAGTATAATGCCCTGAAGAT

Table S3. Related to Figure 1; Figure 2; Figure 3; Figure 6; Figure 7. . The sequences of each primers used in the study is indicated.

Mus musculus

mRNA	Primer sequences
Xbp1 splicing	Fwd - ACA CGC TTG GGA ATG GAC AC Rev - CCA TGG GAA GAT GTT CTG GG
Xbp1s	Fwd - TGC TGA GTC GGC AGC AGG TG Rev - GAC TAG CAG ACT CTG GGG AAG
Xbp1T	Fwd - CCA TGG AAG ATG TTC TGG G Rev - TCC AGA ATG CCC AAA AGG AT
Blocs1	Fwd - AAC ACC AAG CCA AGC AGA ACG A Rev - TCA CCT CAT GGT CCA GCT TTC TCT
Sparc	Fwd - GTG GAA ATG GGA GAA TTT GAG GA Rev - CTC ACA CAC CTT GCC ATG TTT
Rpl19	Fwd - ACC GCC ATA TGT ATC ACA GCC TGT A Rev - CGC TTT CGT GTC TCC TTG GTC TTA
Edem	Fwd – AAG CCC TCT GGA ACT TGC G Rev – AAC CCA ATG GCC TGT CTG G
Sec61	Fwd - CTATTTCCAGGGCTTCCGAGT Rev - AGGTGTTGTACTGGCCTCGGT
Chop	Fwd - TGG AGA GCG AGG GCT TTG Rev - CCG CTC GTT CTC CTG CTC
BiP	Fwd - TCA TCG GAC GCA CTT GGA A Rev - CAA CCA CCT TGA ATG GCA AGA
Actin	Fwd - TACCACCATGTACCCAGGCA Rev - CTCAGGAGGAGCAATGATCTTGAT
Hsp47	Fwd - GCG AGA TAA TCA GAG CGG GT Rev - CCA CGC CCA CTC TTG GAC T
Tuba1a	Fwd - CTG TGG AAA ACC AAG AAG CC Rev - CAC TAC ACC ATT GGC AAG GA
Ppa2	Fwd - ATG TGA ATG ATC CTG AGG CTG Rev - ACC AAT TGA GAG TGG CTT CC
Atp5h	Fwd - GAA ACC ACC TGC GAT TGA CT Rev - CAC AGG AAT CTT GGC AT

Drosophila melanogaster

mRNA	Primer sequences
dXbp1 splicing	Fwd - CAG ATG CAT CAG CCA ATC CAA Rev - CAG GCT CTT GCT GCT CTT CA
dXbp1s	Fwd - CCT TGG ATC TGC CGC AGG GTA TAC Rev - AGA GGG CCA CAA CTT TCC AGA GTG A
dXbp1T	Fwd - GGA TCT GCC GCA GGG TAT Rev - TAT CTG CGA GCA GAC TTT CG
dHsc3	Fwd - AGA ACC AGA TCG GTG ACA AGG ACA Rev - TTA GCA ATC ACG GGC TGA ACG ATG
dSparc	Fwd - ATT GAG CGC GAG AAT GAG ATT GCC Rev - ACT CCG GAA TGC ACA CGC ATT T
dMys	Fwd - TCG CAA AAT CTC CTC TTC GG Rev - GGG ACA CTT GAG CAA CTG AA
dHsp47	Fwd - AAC TCG AAG GAC GCG AGA AG Rev - AAT GTC GAT TGC CTC CGC TT
dTuba	Fwd - TTC GTC CAC TGG TAC GTT GG Rev - TTG AAG TGG CGT GAC GCT TA
dPpa2	Fwd - AGA AGG GTA AGC TGC GGT TC Rev - AGG GCT CCG TAG TTC CAG AT
dAtp5h	Fwd - TGT GAC ACT TTG TTG GAT GGA Rev - CTG CAA GGA CCG GCT ATC AT
dRpl32	Fwd - AGC GCA CCA AGC ACT TCA TA Rev - GTG CGC TTG TTC GAT CCG TAA

SUPPLEMENTARY FIGURES

Figure S1. Related to Figure 1; Figure 4. Control experiments in MEFs. (A) Reconstitution of IRE1α deficient cells with retroviruses expressing IRE1α-HA. Expression levels of IRE1α were then monitored by western blot using indicated antibodies. For comparison, wild-type cells expressing endogenous levels of IRE1α are shown. (B) IRE1α KO Mock MEFs or cells expressing IRE1α-HA MEF cells were treated with 100 ng/mL Tunicamycin (Tm) for indicated time points. *Xbp1* mRNA splicing was then evaluated by RT-PCR. PCR fragments corresponding to the unspliced (*Xbp1u*) or spliced (*Xbp1s*) forms are indicated. (C) The same cells as described in **a** were incubated with 100 ng/mL Tm for 16 h. Then, RIDD activity was evaluated by monitoring the decay of *Sparc* and *Blocs1* mRNA using real time PCR. Data represents average and standard error of 3 independent experiments. (D) IRE1α-HA was immunoprecipated using anti-HA covalently beads and IRE1α binding proteins were eluted using HA peptide. Immunoprecipitation efficiency was determined by Western blot using anti-HA antibody. (E) The efficiency of the knockdown of indicated stable cell lines expressing specific shRNAs (shPpa2, shAtph5h, shHsp47, shTubα1a was validated by real time PCR.

Figure S2. Related to Figure 2; Figure 3. Gain-of-function experiments to assess the impact of IRE1α interactors on XBP1 mRNA splicing (A) Mouse *Ppa2*, *Atp5h*, *Hsp47* and *Tubα1a* cDNA were tagged with a V5 epitope and stably expressed in MEFs using retroviruses and then expression levels assessed by western blot analysis. (B) Cells were then incubated with 10 ng/mL of Tm for indicated time points and *Xbp1* mRNA splicing evaluated using an RT-PCR assay based on PstI digestion. Spliced mRNA is resistant to PstI digestion. The percentage of *Xbp1* mRNA splicing was calculated after densitometric analysis of PCR fragments corresponding to *Xbp1u* or *Xbp1s* forms (right panel). Data represents average and standard error of 4 independent experiments. Statistical analysis was performed using Student's t-test: *: $p < 0.05$, **: $p < 0.01$, ***: $p < 0.001$. (C) IRE1α expression was ablated using a double nickase CRISPR system and then transfected with a UPRE-luciferase reporter. In addition, an expression vector for IRE1α-HA was introduced in the presence or absence of an HSP47-V5 expression vector. Cells were stimulated with 500 and 1000 ng/ml Tm for 20 h and then luciferase activity determined as indicated in material and methods. (D) Stable cells overexpressing HSP47-

V5 and control cells (Mock) were treated with 25 ng/ml Tm, 10n M thapsigargin and 2 μM brefeldin A for 16, 8 and 8 hours, respectively and then *Xbp1s* mRNA levels monitored by real time PCR. Data is representative of three independent experiment. Average and standard deviation of duplicates is shown.

Figure S3. Related to Figure 3. Hsp47 expression does not affect IRE1α levels. (A) MEFs stably expressing Hsp47-V5 or empty vector (Mock) were lysed and total levels of IRE1α were determined using western blot analysis. (B) Similar experiments were performed in shHsp47 and shLuc cells. (C) Hepatocyte specific *Hsp47* gene conditional knockout (cKO) mice were generated using LoxP system and a TTR-inducible Cre line. 8 weeks-old animals were injected intraperitoneal (i.p.) with 1 mg of tamoxifen for 5 consecutive days and sacrificed 1 week later to monitor IRE1α levels using western blot analysis. Each well represents an independent animal. Hsp90 levels were monitored as loading control.

Figure S4. Related to Figure 3; Figure 4; Figure 5. Control experiment for the IRE1α-GFP clustering (A) TREX cells expressing IRE1α-3F6H-GFP were transfected with siHsp47 constructs. The levels of *Hsp47* mRNA levels were evaluated by real-time PCR. (B) TREX cells expressing IRE1α-3F6H-GFP were stably transduced with retroviruses expressing the HSP47-V5. The levels of IRE1α-GFP and HSP47-V5 proteins were evaluated as control by western blot. Hsp90 levels were monitored as loading control. (C) Control experiment for the Duolink assay: Knockdown Hsp47 was confirmed in MEFs after western blot analysis. (D) MicroScale Thermophoresis (MST) was used to evaluate HSP47 binding to Red-labeled-IRE1α- NLD or PERK-NLD. Red-labeled HSP47 (200 nM) was incubated with an increasing concentration of IRE1-NLD or PERK-NLD (0-10 mM), with graph showing an average of a minimum of 8 individual experiments. (E) Control experiment for pull-down assays: COS-1 cells were transiently transfected with a HIS-tagged version of the ER luminal domain of IRE1α (IRE1α-NLD-His6-KDEL) in the presence or absence of Hsp47 followed by a pull-down with Ni-NTA-agarose beads. The presence of PDIA6 was assessed in the pull-down using western blot analysis.

Figure S5. Related to Figure 6. Identification of an HSP47 homologue in *D. melanogaster* (A) Amino acid sequence alignment of Hsp47 from *H. sapiens*, *M.*

musculus and *Drosophila melanogaster* using PRALINE with BLOSUM62 scoring matrix (Pirovano et al., 2008; Simossis et al., 2005). (B) Predicted secondary structure alignment of Hsp47 from *H. sapiens*, *M. musculus* and *D. melanogaster* using PRALINE (Jones, 1999; Kabsch and Sander, 1983).

Figure S6. Related to Figure 6. Effects of Ppa2, Atp5h and Tubα1a in whole animal survival in *D. melanogaster* (A) Putative homologues of Ppa2, Atp5h and Tubα1a were identified in *D. melanogaster* using bioinformatics analysis. The table indicates the name and accession code, in addition to the percentage of identity and similarity of the fly protein sequence with *H. sapiens*. (B) Control experiments for survival of wild type flies to ER stress conditions: 50 adult flies were grown in standard feeding conditions in presence of DMSO 0.2% as vehicle or 25 μg/mL of Tm (dotted line). The percentage of animal survival was calculated over time. Lifespan statistics were evaluated using log-rank test *p* values. (C) Basal survival of all RNAi lines tested: Median survival of fly lines expressing RNAis against dHsp47, dPpa2, dAtp5h and dTubα1a and the corresponding control fly lines were monitored over time. The ratio of the median survival times for control or RNAi adult fly was calculated using a 95% confidence interval. Mean and standard error is presented of 3 independent experiments. (D) *D. melanogaster* dPpa2, dAtp5h and dTubα1a were knocked down by expressing specific RNAi constructs using the UAS-GAL4 system under the control of a tubulin promoter. mRNA levels of *dppa2*, *dAtp5h* and *dTubα*1a were monitored by real time PCR in total extracts prepared from second stage larvae. mRNA levels of RNAi line (Tub<Gal4/UAS<RNAi) were normalized to the respective control line. Mean and standard error is presented from three independent experiments. (E) 50 control and 50 RNAi flies for dPpa2, dAtp5h and dTubα1a were grown in standard feeding conditions in presence of 25 μg/mL of Tm. The number of viable flies was calculated over time by counting dead flies and the percentage of survival was obtained. Statistical analysis was performed using the Kaplan-Meyer and log-rank (Mantel-cox) test.

Figure S7. Related to Figure 7. Conditional deficiency of Hsp47 in the liver does not result in spontaneous fibrosis in the short term (A) A conditionally knockout (cKO) mouse for *Ire1α* gene was generated using the MxCre system. Then animals were injected with Tm (1 ug/g, i.p.) and sacrificed after 72 h. Liver from animals were collected and apoptosis measured by cleaved caspase 3 staining. Data represents the average and

standard deviation (untreated animals n = 2; Tm treated mice n = 3). (B) The possible occurrence of fibrosis was analyzed in the liver of *Hsp47*^{WT} and *Hsp47*^{cKO} mice after trichrome staining (untreated animals n = 2; Tm treated mice n = 3). Scale bars, 100 μm. (C) mRNA levels of *Col1α1*, *Col6α3* and *Actα2* mRNAs were measured by real time PCR in *Hsp47*^{WT} and *Hsp47*^{cKO} liver mice at basal levels (NT) or treated with Tm for 24 h (untreated animals n = 2; Tm treated mice n = 3). When indicated statistical analysis was performed using Student's t-test: *: $p < 0.05$, **: $p < 0.01$, ***: $p < 0.001$.